

12-17-2017

Preparation and In Vitro Characterization of an Integrated Graft System for Regenerative Engineering

Mohammed Barajaa
mohammed.barajaa@uconn.edu

Recommended Citation

Barajaa, Mohammed, "Preparation and In Vitro Characterization of an Integrated Graft System for Regenerative Engineering" (2017). *Master's Theses*. 1158.
https://opencommons.uconn.edu/gs_theses/1158

This work is brought to you for free and open access by the University of Connecticut Graduate School at OpenCommons@UConn. It has been accepted for inclusion in Master's Theses by an authorized administrator of OpenCommons@UConn. For more information, please contact opencommons@uconn.edu.

Preparation and In Vitro Characterization of an Integrated Graft System for Regenerative Engineering

Mohammed A. Barajaa

B.S., University of Hartford, 2014

A Thesis

Submitted in Partial Fulfillment of the
Requirements for the Degree of
Master of Science

At the
University of Connecticut

2017

Copyright by
Mohammed A. Barajaa

2017

APPROVAL PAGE

Master of Science Thesis

Preparation and In Vitro Characterization of an Integrated Graft System for Regenerative Engineering

Presented By

Mohammed A. Barajaa, B.S.

Major Advisor_____

Cato T. Laurencin

Associate Advisor_____

Lakshmi Nair

Associate Advisor_____

Kevin Lo

University of Connecticut 2017

DEDICATIONS

I dedicate this thesis to “**Allah**”, the Almighty Creator,
my strong pillar, my source of inspiration, wisdom, knowledge and understanding,
on him only have I soared.

ACKNOWLEDGEMENTS

At the first place, I would like to deeply acknowledge whom without I would not have been existed in this life, my parents **Mr. Amin Barajaa** and **Mrs. Aminah Alradhi**, for all the love, support, prayers and care throughout my entire life.

I would like to acknowledge my lovely wife **Ms. Farah Omar** for her the love and support. Thank you for your patience and understanding when I was mostly away from you conducting my research.

I am also grateful to many individuals for their support, kindness and loving guidance through my academic journey at the Institute of Regenerative Engineering.

First, I would like to acknowledge **Dr. Cato T. Laurencin** for believing in me and giving me the opportunity to work in his great Institute, where I learned what I wouldn't have learned in any other lab. I thank him for being a source of inspiration, motivation, and encouragement throughout my entire Master's journey at the institute. I will never forget the lovely quote he inspired me with "**To stumble is not to fall, but to move forward**" when he was talking about the struggles he has been through throughout his academic journey, as to motivate me to never give up and to keep the hard work. I have always been proud to have him as my major advisor and I will always be. His ambition towards regenerating an entire limb has become an ambition of mine, and I will put the best of my effort to move this dream closer towards reality, throughout the rest of my journey at the institute.

I would also like to acknowledge **Dr. Lakshmi Nair**, the brilliant spark of life whose boundless energy, intelligence and curiosity have served as a constant inspiration and source of knowledge for me. When I started working in her lab, she never blinked an eye, and has constantly made herself available to me for guidance along this intellectual path, as well as moral support when I doubted myself and my abilities.

Thank you so much for the tremendous amount of time and help you provided me with in order to move my research forward.

I am also grateful to **Dr. Kevin Lo**. He has always been a great support of mine and has always expressed a high confidence in my abilities. I thank him so much for motivating me with the work I have conducted to develop the tri-culture system, and for advising me with the experimental design of my tri-culture experiment.

I am also thankful to many other individuals within and outside the Institute for Regenerative Engineering whose participation and contribution were part of my success. **Dr. Yousuf Khan** has been a constant source of knowledge, support, and compassion throughout my journey. **Eva Kan** is the most selfless and helpful person I have ever met. She has always opened her doors for me whenever I have had any question about me lab techniques or experimental designs. **Dr. Jorge Escobar** was a great source of motivation and inspiration for me, he has always believed in my abilities and frequently repeated “**you’re smart I know you can do it**” as to motivate me and encourage me to do better. **Dr. Maumita Bhattacharjee** has helped at the beginning as well as throughout my journey at the institute with clarifying some scientific concepts that helped me making future decisions. **Dr. Emmanuel Kuyinu** is acknowledged for helping me learning the surgical techniques. I am also grateful to **Dr. Naveen Nagiah** for helping me with electrospinning, it was great working with him to develop the electrospinning setup we have in the lab. **Dr. Sun Xuanhao** is acknowledged for his help with the scanning electron microscopy. **Dr. Mary Arico** is highly acknowledged for her help with the three-dimensional printing.

I am also grateful to many friends within and outside the Institute for Regenerative Engineering who have, supported me constantly, cheered me on wholeheartedly and have been my family away from home, my laughter in times of sadness, and my inspiration in loss of sight. These individuals: **Guleid Awale, Hyun Kim, Paulos Mengsteab, Soliman Alhudaithy, Aundrya Montgomery, Leila Daneshmandi,**

Xiaoyan Tang, Deborah Dorcemus, Faye Assanah, and Anupama Prabhath have truly blessed my life and for that I am lucky.

My cousin Dr. **Baker Omear**, who has always been a great source of inspiration for me since I was in high school, and my brother **Muath** and my two beautiful sisters **Malak** and **Mead**, I thank you for your love and support.

I thank God again for all He's done for me, and for that, **I am grateful.**

Table of Contents

List of Figures and Tables	xviii
Chapter 1: INTRODUCTION	1
1.1.Biomimetic Scaffolds.....	1
1.1.1. General Scaffold Requirements.....	4
1.1.1.1.Biocompatibility.....	4
1.1.1.2.Biodegradability.....	4
1.1.1.3.Porosity.....	5
1.1.1.4.Mechanical Properties.....	6
1.1.1.5.Architecture.....	6
1.1.2. Biomaterials and Fabrication Techniques for Biomimetic Scaffolds.....	7
1.1.2.1.Biomaterials.....	8
1.1.2.2.Fabrication Techniques for Biomimetic Scaffolds.....	9
1.1.2.2.1. Sintered Microsphere.....	10
1.1.2.2.2. Solvent Casting and Particle Leaching.....	11
1.1.2.2.3. Gas Foaming and Particle Leaching.....	13
1.1.2.2.4. Electrospinning.....	14
1.1.3. Biomimetic Bone Tissue Regeneration.....	16
1.1.3.1.Bone Structure and Function.....	16
1.1.3.2.Materials for Biomimetic Bone Tissue Regeneration.....	18
1.1.3.3.Scaffold Requirements for Biomimetic Bone Tissue Regeneration.....	19
1.1.3.4.Biomimetic Bone Tissue Regeneration Approaches.....	20
1.1.4. Biomimetic Ligament Tissue Regeneration.....	28

1.1.4.1.Ligament Structure and Function.....	28
1.1.4.2.Materials for Biomimetic Ligament Tissue Regeneration.....	31
1.1.4.3.Scaffold Requirements for Biomimetic Ligament Tissue Regeneratio.....	35
1.1.4.4.Biomimetic Ligament Tissue Regeneration Approaches.....	38
1.1.5. Biomimetic Skin Tissue Regeneration.....	46
1.1.5.1.Skin Structure and Function.....	46
1.1.5.2.Materials for Biomimetic Skin Tissue Regeneration.....	49
1.1.5.3.Scaffold Requirements for Biomimetic Skin Tissue Regeneration.....	56
1.1.5.4.Biomimetic Skin Tissue Regeneration Approaches.....	56
1.2.Complex Tissue Regeneration.....	67
1.2.1. The Complex Bone-Ligament-Bone Junction Regeneration.....	74
1.2.1.1.Ligament-Interface-Bone Junction Structure and Function.....	74
1.2.1.2.Ligament-Interface-Bone Junction Tissue Regeneration Approaches.....	75
1.2.2. The Complex Muscle-Interface-Tendon and Tendon-Interface-Bone Junction Regeneration.....	83
1.2.2.1.Muscle-Interface-Tendon Junction Structure and Function.....	83
1.2.2.2.Tendon-Interface-Bone Junction Structure and Function.....	84
1.2.2.3.Current Clinical Treatment for Tendon-Interface-Bone Junction Injures..	86
1.2.2.4. Tendon-Interface-Bone Junction Tissue Regeneration Approaches.....	86
1.2.2.5.Current Clinical Treatment for Muscle-Interface-Tendon Junction Injuries.....	91
1.2.2.6.Muscle-Interface-Tendon Junction Tissue Regeneration Approaches.....	93
1.2.3. The Complex Cartilage-Interface-Bone Regeneration.....	96

1.2.3.1. Cartilage-Interface-Bone Complex Structure and Function.....	96
1.2.3.1.1. Cartilage Zones Structure and Function.....	96
1.2.3.1.2. Subchondral Bone Structure and Function.....	98
1.2.3.2. Osteochondral Defect.....	99
1.2.3.3. Current Clinical Treatment for Osteochondral Defects.....	99
1.2.3.4. Cartilage-Interface-Bone Tissue Regeneration Approaches.....	101
1.2.4. Cell-Cell Interactions to Form Interfaces in Ligament/Tendon-Bone Junctions.....	108
1.2.5. Cell-Cell Interactions to Form Interfaces in muscle-Tendon Junction.....	110
1.2.6. Cell-Cell Interaction to Form Interfaces in Cartilage-Bone Junction.....	112
1.3. Coaxial and Uniaxial Electrospinning.....	114
1.3.1. Electrospinning Technique.....	117
1.3.2. General Electrospinning Parameters.....	119
1.3.3. Electrospinning Strategies for Drug Delivery.....	121
1.3.3.1. Uniaxial Electrospinning for Drug Delivery.....	122
1.3.3.2. Coaxial Electrospinning for Drug Delivery.....	126
1.3.3.3. Coaxial and Uniaxial Electrospinning for Drug Delivery.....	129
1.3.4. Techniques and Potential Applications for Coaxial Electrospinning.....	131
1.4. Research Objectives and Specific Aims.....	133
1.5. References.....	135

**Chapter 2: SYNTHESIS, CHARACTERIZATION AND IN VITRO DEGRADATION OF
THE DIFFERENT PHASES WITHIN THE INTEGRATED GRAFT SYSTEM.....185**

2.1.Introduction.....	185
2.1.1. Microsphere Fabrication Technique.....	188
2.1.2. Uniaxial Electrospinning Technique.....	189
2.1.3. Coaxial Electrospinning Technique.....	190
2.2.Materials and Methods.....	193
2.2.1. Fabrication of PLGA-Gelatin Coaxial Electrospun Nanofibers Scaffolds.....	193
2.2.2. Fabrication of PLGA Uniaxial Electrospun Nanofibers Scaffolds.....	194
2.2.3. Fabrication of PLGA Microspheres.....	194
2.2.4. Fabrication of Gelatin-mTG Hydrogel.....	194
2.2.5. Fabrication of PLGA-Gelatin-mTG Microspheres Scaffolds.....	195
2.2.6. Scanning Electron Microscopy (SEM).....	195
2.2.7. Particle Size Distribution and Pore Size Analysis.....	196
2.2.8. Transmission Electron Microcopy (TEM).....	196
2.2.9. Degradation of PLGA Coaxial, Uniaxial Electrospun Nanofiber Scaffolds and Sintered Microsphere Scaffolds.....	196
2.2.10. Statistical Analysis.....	198
2.3. Results.....	198
2.3.1. PLGA-Gelatin Coaxial and PLGA Uniaxial Electrospun nanofiber Scaffolds.....	198
2.3.1.1.Scanning Electron Microscopy (SEM).....	198
2.3.1.2.Transmission Electron Microscopy (TEM).....	204
2.3.2. PLGA-Gelatin-mTG and PLGA-Gelatin-mTG Free Sintered Microspheres Scaffolds 2.3.2.1.Scanning Electron Microscopy (SEM).....	205
2.3.3. PLGA Coaxial-Gelatin and PLGA Uniaxial Electrospun Nanofibers Scaffolds	

Degradation Behavior.....	210
2.3.3.1.Weight Loss.....	210
2.3.3.2.Swelling.....	211
2.3.3.3.pH Change.....	212
2.3.4. PLGA-Gelatin-mTG and PLGA-Gelatin-mTG Free Sintered Microsphere Scaffolds	
Degradation Behaviors.....	213
2.3.4.1.Weight Loss.....	213
2.3.4.2.Water Uptake.....	214
2.3.4.3.pH Change.....	215
2.4.Discussion.....	216
2.5.Conclusion.....	221
2.6.References.....	222
 Chapter 3: IN VITRO EVALUATION OF PDGF-BB AND IGF-I RELEASE FROM COAXIAL-GELATIN, UNIAXIAL NANOFIBER SCAFFOLDS, AND BMP-2 FROM PLGA-GELATIN-MTG INCROPORATED MICROPSERE SCAFFOLD.....	227
3.1.Introduction.....	227
3.2.Materials and Methods.....	232
3.2.1. Fabrication of PLGA-Gelatin-PDGF and IGF-I Coaxial Nanofiber Scaffolds....	232
3.2.2. Transmission Electron Microcopy (TEM).....	233
3.2.3. Fabrication of PLGA-PDGF-BB and IGF-I Uniaxial Nanofiber Scaffolds.....	233
3.2.4. Fabrication of PLGA Microspheres.....	234
3.2.5. Incorporation of BMP-2 in Gelatin-mTG Hydrogel.....	234
3.2.6. Fabrication of PLGA Microsphere Scaffolds Incorporated	
Gelatin-mTG/BMP-2.....	235

3.2.7. In Vitro PDGF-BB and IGF-I Release from Coaxial and Uniaxial PLGA Electrospun Nanofiber Scaffolds.....	235
3.2.8. In Vitro BMP-2 Release From PLGA-Gelatin-mTG Scaffolds.....	236
3.2.9. Extraction of BMP-2 from Gelatin-mTG Hydrogel.....	236
3.2.10. Alkaline Phosphate Activity Assay.....	237
3.2.11. Statistical Analysis.....	238
3.3. Results.....	238
3.3.1. PDGF-BB and IGF-I Release from Coaxial and Uniaxial PLGA Electrospun Nanofiber Scaffolds.....	238
3.3.2. BMP-2 Release from Gelatin-mTG Incorporated Microsphere Scaffolds.....	239
3.3.3. Alkaline Phosphate Activity of MC3T3 Seeded on PLGA-Gelatin-mTG/ BMP-2 Microsphere Scaffolds.....	240
3.4. Discussion.....	242
3.5. Conclusion.....	248
3.6. References.....	249
Chapter 4: PRIMARY CELL ISOLATION, AND IN VITRO BIOCOMPATIBILITY AND CHARACTERIZATION OF THE THREE DIFFERENT CELLS CULTURED WITH THE RELEVANT PHASES.....	253
4.1. Introduction.....	253
4.1.1. Cells.....	253
4.1.1.1. Primary Dermal Fibroblasts.....	254
4.1.1.2. Primary Ligament Fibroblasts.....	256
4.1.1.3. Primary Osteoblasts.....	256

4.1.1.4.Primary Cells Characterization.....	258
4.1.1.5.Morphological Characterization and Specific Markers of Primary Dermal Fibroblasts.....	259
4.1.1.5.1. Morphological Characterization.....	259
4.1.1.5.2. Dermal Fibroblasts Specific Markers.....	259
4.1.1.5.2.1.Vimentin.....	259
4.1.1.5.2.2.TE-7.....	260
4.1.1.6.Morphological Characterization and Specific Markers of Primary Ligament Fibroblasts.....	261
4.1.1.6.1. Morphological Characterization.....	261
4.1.1.6.2. Ligament Fibroblasts Specific Markers	261
4.1.1.6.2.1.Scleraxis.....	262
4.1.1.6.2.2.Tenomodulin.....	262
4.1.1.7.Morphological Characterization and Specific Markers of Primary Osteoblasts.....	263
4.1.1.7.1. Morphological Characterization.....	263
4.1.1.7.2. Osteoblasts Specific Markers.....	263
4.1.1.7.2.1.Alkaline Phosphate (ALP).....	264
4.1.1.7.2.2.Osteocalcin (OCN).....	264
4.1.2. Scaffolds.....	265
4.1.2.1.General Scaffold Requirements.....	265
4.1.2.2.Scaffold Materials.....	266
4.1.3. Growth Factors Delivery.....	268

4.1.3.1. Platelet-Derived Growth Factor-BB (PDGF-BB).....	280
4.1.3.2. Insulin-Like Growth Factor-I (IGF-I).....	280
4.1.3.3. Bone Morphogenetic Protein 2 (BMP-2).....	271
4.2. Materials and Methods.....	273
4.2.1. Fabrication of PLGA-Gelatin Coaxial Nanofiber Scaffolds.....	274
4.2.2. Fabrication of PLGA Uniaxial Nanofiber Scaffolds.....	275
4.2.3. Fabrication of PLGA Microspheres.....	275
4.2.4. Incorporation of BMP-2 in Gelatin-mTG Hydrogel.....	276
4.2.5. Fabrication of PLGA Microspheres Scaffolds Incorporated Gelatin-mTG/BMP-2	276
4.2.6. Primary Cells Isolations.....	277
4.2.6.1. Primary Dermal Fibroblasts Isolation and Culture Maintenance.....	277
4.2.6.2. Primary Ligament Fibroblasts Isolation and Culture Maintenance.....	278
4.2.6.3. Primary Osteoblasts Isolation and Culture Maintenance.....	280
4.2.7. Morphological and Immunofluorescence Phenotypic Characterization of the Isolated Primary Cells.....	281
4.2.7.1. Morphological Catheterization of the Isolated Primary Cells.....	282
4.2.7.2. Immunofluorescence Phenotypic Characterization of the Isolated Primary Cells.....	282
4.2.8. LIVE/DEAD Viability Assay.....	284
4.2.9. Proliferation Assay.....	285
4.2.10. Statistical Analysis.....	286
4.3. Results.....	286

4.3.1. Morphological and Immunofluorescence Phenotypic of the Isolated Primary Cells.....	286
4.3.2. LIVE/DEAD Viability and Proliferation Assays.....	292
4.4.Discussion.....	300
4.5.Conclusion.....	306
4.6.References.....	308
Chapter 5. DEVELOPMENT AND CHARACTERIZATION OF A TRI-CULTURE SYSTEM AND EVALUATING THE CAPABILITY OF THE INTEGRATED GRAFT SYSTEM TO SUPPORT HETEROGENIC CELLULAR INTERACTIONS.....	319
5.1.Introduction.....	319
5.2.Materials and Methods.....	325
5.2.1. Tri-Culture Design Concept.....	326
5.2.2. Mold Design Development and Three-Dimensional Printing.....	327
5.2.3. Polydimethylsiloxane Segments Fabrication.....	327
5.2.4. Testing the Functionality of the Tri-Culture System.....	327
5.2.4.1.Liquids Penetration.....	328
5.2.4.2. Cell Migration.....	328
5.2.5. Fabrication of PLGA-Gelatin Coaxial Nanofiber Scaffolds.....	328
5.2.6. Fabrication of PLGA Microspheres.....	329
5.2.7. Incorporation of BMP-2 in Gelatin-mTG Hydrogel.....	330
5.2.8. Fabrication of PLGA Microsphere Scaffolds Incorporated Gelatin-mTG/ BMP-2.....	330
5.2.9. Primary Cells Isolations.....	331

5.2.9.1.Primary Dermal Fibroblasts Isolation and in Culture Maintenance.....	331
5.2.9.2.Primary Ligament Fibroblasts Isolation and in Culture Maintenance.....	331
5.2.9.3.Primary Osteoblasts Isolation and in Culture Maintenance.....	331
5.2.10. In vitro Tri-Culture Study for the Determination of a Heterogenic Culture Medium.....	332
5.2.11. <i>In vitro</i> Evaluations of the Integrated Graft System.....	333
5.2.11.1. LIVE/DEAD ASSAY.....	333
5.2.11.2. Proliferation Assay.....	335
5.2.11.3. Cell Localization and Phenotypic Maintenance of the Three Different Cellular Populations Within the Integrated Graft System.....	335
5.2.11.4. Cell Migration Within the Integrated Graft System.....	337
5.2.12. Statistical Analysis.....	337
5.3. Results.....	338
5.3.1. Development and Testing the Functionality of the Tri-Culture System.....	338
5.3.2. In vitro Tri-Culture Study for the Determination of a Heterogenic Culture Medium.....	346
5.3.3. LIVE/DEAD and Proliferation Assays.....	351
5.3.4. Localization, Migration and Phenotypic Maintenance.....	353
5.4.Discussion	355
5.5.Conclusion	367
5.6.References	368
Chapter 6. Future Direction	376
6.1.Conclusion and Future Work.....	376

List of Figures and Tables

Figure 1.1. Schematics of regenerative engineering approach to create complex functional tissues and organs.

Figure 1.2. Fabrication process of Polymeric Microsphere through the single water/oil emulsion technique.

Figure 1.3. Schematic of solvent casting and particle leaching scaffold fabrication technique

Figure 1.4. Schematic of gas foaming and particle leaching scaffold fabrication technique

Figure 1.5. Schematic of the most extensively used tissue engineering fabrication technique, electrospinning set up.

Figure 1.6: Cortical and Cancellous bone

Figure 1.7: (a) A chitosan/PLAGA composite microsphere; (b) a 3D chitosan/PLAGA scaffold fabricated by heat sintering (c) Chitosan/PLAGA scaffold immobilized with heparin as evidenced by them green fluorescence; (d)–(f) MC3T3-E1 osteoblast-like cell proliferation at days 4, 7, and 11 on the heparinized chitosan/PLAGA scaffolds as illustrated by dual staining of cell nuclei (blue) and cytoskeletal protein actin (red); (g) The surgical procedure showing a 15 mm segment of ulna was removed and a sintered microsphere scaffold was implanted into the defect site; (h) Three-dimensional micro-CT reconstruction of the bone regeneration in the ulnar defect from the animals with the most amount of new bone formation (HP-CS-PLAGA-BMP2 12 weeks); (i) A radiograph showing new bone formation bridging the critical-sized defect at 12 weeks after operation using chitosan/PLAGA scaffolds loaded with heparin and bone morphogenetic protein—2 using a rabbit ulnar model; (j) VonKossa staining of implanted scaffold showing new bone formation adjacent to the scaffold (M: microsphere, NB: new bone); (k) trichrome staining showing dense connective tissue formation in the void space among microspheres (CT: connective tissue); (i) . Parallel images of new bone formation sections stained with both Trichrome staining

Figure 1.8. Schematic illustration of the fabrication of BMP-2-loaded BSA nanoparticles stabilized with chitosan

Figure 1.9: Anterior Cruciate Ligament (ACL)

Figure 1.10. ACL fibroblast growth and matrix formation on different synthetic braided scaffolds visualized with SEM. Images were taken after 14 days of *in vitro* culture in 10% fetal bovine serum. (Left) Culture with PGA resulted in substantial matrix degradation from acidic byproducts. (Middle) PLA and PGA in an 82:18 mass ratio showed more sustainable matrix formation, particularly with the addition of fibronectin (Fn). (Right) PLLA scaffolds also displayed considerable matrix formation, which again was amplified by the addition of Fn

Figure 1.11. Representative image of the three-dimensional braided scaffold developed by Laurencin et al. with distinct fiber organizations in the bony attachment ends and central intra-articular zone. [215]

Figure 1.12. (top) Schematic diagram showing the fabrication process of a pore size gradient in

PCL scaffolds by a centrifugation method and (bottom) SEM photographs of the top surfaces of the PCL scaffold sections along the longitudinal direction ($\times 100$; *, average pore size) [64]

Figure 1.13. Aligned nanofibers (A), nanofiber bundle (B), scaffold composed of *20 nanofiber bundles (C), and small scaffold composed of 4 nanofiber bundles (D)

Figure 1.14. Anatomy of the skin. Skin is composed of three layers, starting with the outermost layer: the epidermis, dermis, and hypodermis. Epidermis is a stratified squamous epithelium that is divided into four layers, starting with the outermost layer: stratum corneum (SC), stratum granulosum (SG), stratum spinosum (SS), and stratum basale (SB). Outer root sheath of the hair follicle is contiguous with the basal epidermal layer. Stem cell niches include the basal epidermal layer, base of sebaceous gland, hair follicle bulge, dermal papillae, and dermis

Figure 1.15. Electrospun nanofibers, (A) Polycaprolactone, (B) PCL/collagen nanofibers (NUS), and scanning electron microscopy morphology of fibroblast culture on nanofibrous scaffolds. (C) Polycaprolactone, (D) PCL/collagen nanofibers, and (C) cultured dermal substitute (Fibroblast cultured on PCL/Collagen nanofibrous membrane)

Figure 1.16. Appearances of wounds in different groups on days 0 and 10

Figure 1.17 Schematic of coaxial electrospinning setup, and the conventional uniaxial electrospinning setup.

Figure 1.18. (A) Schematic presentation of the multi-layer skin substitute, (B) Immunohistochemical staining with antibodies against collagen IV. Extracellular matrix is produced by keratinocytes on the scaffold surface (20-fold magnification). Scale bar: 10 μm , (C) Immunofluorescence labeling with DAPI. Cytoblasts appear blue, matrix green. Keratinocytes form epithelial-like layers on the surface of the matrix (20-fold magnification). Confocal Laser Scan. Scale bar: 10 μm , (D) Simultaneous growth of keratinocytes (*) and preadipocytes (>). Preadipocytes penetrate into deeper layers of the scaffold whereas keratinocytes build a confluent layered epidermis-like sheet on the surface of the matrix (20-fold magnification). Confocal Laser Scan. Scale bar: 10 μm , and (E) Proliferation of keratinocytes. Strong staining with anti-Ki67 antibody (brown) was observed, indicating proliferation of the seeded cells on the matrix. Scale bar: 10 μm

Figure 1.19 Common orthopedic tissue-tissue interfaces. Ligaments, such as the anterior cruciate ligament (ACL) in the knee (Modified Goldner's Masson Trichrome),¹²⁶ and tendons, such as the supraspinatus tendon in the shoulder (Toluidine blue),⁷⁰ connect to bone via a fibrocartilaginous (FC) transition, which can be further subdivided into non-mineralized (NFC) and mineralized (MFC) regions (Von Kossa). The muscle-tendon junction (Modified Goldner's Masson Trichrome) consists of an interdigitating band of connective tissue.⁶⁰ Articular cartilage (AC), which can be subdivided into surface (SZC), middle (MZC), and deep (DZC) zones (Modified Goldner's Masson Trichrome), connects to subchondral bone via a transitional calcified cartilage (CC) region (Von Kossa)

Figure 1.20 Scaffold design for ligament-interface-bone regeneration. Mimicking the stratified structure (Modified Goldner's Masson Trichrome) and composition (FTIR-I: Fourier Transform infrared spectroscopy)⁸⁹ of the native insertion, a tri-phasic scaffold (Phase A: PLGA mesh, Phase

B: PLGA microspheres, Phase C: PLGA-BG microspheres) was designed for ACL-bone interface regeneration.^{110,111} This design allowed for spatial control over cell distribution (Fb: fibroblasts on Phase A, Ob: osteoblasts on Phase C, along with chondrocytes in a hydrogel in Phase B) enabled the formation of compositionally distinct yet structurally continuous tissue regions *In vivo* (Modified Goldner's Masson Trichrome)

Figure 1.21. (Top) Schematic diagram showing the fabrication process of a pore size gradient in PCL scaffolds by a centrifugation method and (bottom) SEM photographs of the top surfaces of the PCL scaffold sections along the longitudinal direction ($\times 100$; *, average pore size) [64]

Figure 1.22 Picture depicting tendon structure and the junctions at muscle and bone

Figure 1.23 Scaffold design for *tendon-interface-bone* regeneration. A biphasic scaffold comprised of layered aligned PLGA and PLGA-HA nanofibers was fabricated by electrospinning, which led to phase-specific mineral deposition *in vivo* (Von Kossa, subcutaneous athymic rat model). The bilayer scaffold was subsequently tested in a rat rotator cuff repair model, disorganized scar tissue was observed in the single-phased controls (PLGA, PLGA-HA only). Interestingly, tendon-bone integration via an organized bilayer fibrocartilage interface was only observed with the biphasic design (Picrosirius red, Alcian blue)

Figure 1.24 Immunostaining for paxillin indicating its upregulation at the MTJ of a scaffoldless muscle construct created by co-culturing a heterogeneous muscle “sarcolemma” and tendon “fibroblasts” isolations

Figure 1.25 Osteochondral tissue structure. Cross section of the long bone and its zonal cartilage including (A) articular surface, (B) the superficial zone, (C) the middle zone, (D) the deep zone (E) tidemark (the interface), (F) calcified cartilage, (G) subchondral bone, and (H) trabecular bone

Figure 1.26 *In vivo* repair. Photographs of an osteochondral defect site in the lateral trochlear sulcus (A) immediately after and (B) 26 weeks after implantation of a collagen-GAG scaffold along with the (C) H&E and (D) Safranin-O with fast green histological stains of the explants

Figure 1.27 (Ai) *In vitro* co-culture model to evaluate the interactions of interface-relevant cells of fibroblasts and osteoblast permit heterotypic and homotypic cell-cell interactions [99]. (Aii) Co-culture models to evaluate interaction of interface-relevant cells. (A-i) *In vitro* coculture model of fibroblasts (Fb) and osteoblasts (Ob) permit heterotypic and homotypic cell-cell interactions. (A-ii) Fibroblast (CFDA-SE, green) and osteoblast (CM-DiI, orange-red) distribution at day 7, bar = 100 μm

Figure.1.28. Schematic picture of the MTJ structural development from early embryonic and neonatal to adult stages. MTJ: myotendinous junctions; Tnb: tenoblasts; Mbl: myoblasts; Ten: tenocytes; MF: muscle fibers

Figure 1.29: Extracellular (interstitial) matrix

Figure 1.30: Schematic representation of electrospinning basic set up. a) Image of Taylor cone forming at the spinneret during the electrospinning process. b) Image of polymeric filament forming from Taylor cone and moving toward the collector

Figure 1.31: Porous electrospun fibers. 28 wt% polystyrene in tetrahydrofuran (15kV).

Figure 1.32. Schematic representation of coaxial electrospinning setup. [419]

Figure 1.33. A schematic showing the three steps involved in establishing the integrated graft system.

Figure 2.1 Chemical structure of poly(lactic-*co*-glycolic acid) and its monomers [6].

Figure 2.2 Fabrication process of PLGA Microsphere through the single water/oil emulsion technique.

Figure 2.3 Schematic of coaxial electrospinning setup, and the conventional uniaxial electrospinning setup.

Figure 2.4 PLGA-Gelatin coaxial electrospun nanofiber mat (A) a uniform deposition during electrospinning (B) the resultant 9 x 9 cm coaxial electrospun mat, and (C) coaxial electrospun mat thickness (400 μ m); and PLGA uniaxial electrospun nanofiber mat (D), uninform deposition of nanofibers during electrospinning that can be noticed from the bigger mat area when compared to the coaxial group (E), the resultant un-uniformly deposited mat, and (F) uniaxial electrospun mat thickness of \sim 80 μ m when electrospun for 1.5, which is the same duration used for electrospinning PLGA-Gelatin that results in a mat with a thickness of \sim 400 μ m .

Figure 2.5 SEM images of PLGA-Gelatin Coaxial electrospun nanofibers showing (A) overall morphology of the electrospun (Scale bar 100 μ m), (B) morphology of nanofibers showing the smooth fibers surface (Scale bar 5 μ m), and (C) PLGA-Gelatin Coaxial electrospun nanofibers size distribution (400 nm – 1100 nm).

Figure 2.6 SEM images of PLGA Uniaxial electrospun nanofibers showing (A) overall morphology of the electrospun (Scale bar 100 μ m), (B) morphology of nanofibers showing the smooth fibers surface (Scale bar 5 μ m), and (C) PLGA Uniaxial electrospun nanofibers size distribution (100 nm – 1100 nm).

Figure 2.7 SEM images showing the morphological change of coaxial electrospun nanofibers after incubation In PBS at 37 C over 8 weeks period of time. (A) weeks 0, original morphology of nanofibers, (B) 1 week after incubation, (C) 2 weeks after incubation, (D) 3 weeks after incubation, (E) 4 weeks after incubation, (F) 5 weeks after incubation, (G) 6 weeks after incubation showing the beginning of sever surface degradation, (H) 7 weeks after incubation, and (I) 8 weeks after incubation showing a significant swelling and sever surface degradation when compared to week 0. White arrows indicate some of the pores created at the surface of the fibers.

Figure 2.8 SEM images showing the morphological change of uniaxial electrospun nanofibers after incubation In PBS at 37 C over 8 weeks period of time. (A) weeks 0, original morphology of nanofibers, (B) 1 week after incubation, (C) 2 weeks after incubation, (D) 3 weeks after incubation, (E) 4 weeks after incubation, (F) 5 weeks after incubation, (G) 6 weeks after incubation, (H) 7 weeks after incubation, and (I) 8 weeks after incubation showing a significant swelling when compared to week 0.

Figure 2.9. TEM images. (a) PLGA-Gelatin Coaxial nanofiber with a core-sheath of \sim 781 nm, a fiber diameter of 1000 nm and a sheath thickness of 219 nm, and (b) Uniaxial nanofiber.

Figure 2.10 SEM images of PLGA-mTG Free sintered microspheres showing (A) overall

morphology of the sintered microspheres (Scale bar 500 μm), (B) high magnification image of the interconnectivity between microspheres (Scale bar 100 μm), and (C) PLGA-mTG Free sintered microspheres (300 μm – 600 μm).

Figure 2.11 SEM images of PLGA-mTG sintered microspheres showing (A) overall morphology of the sintered microspheres (Scale bar 500 μm), (B) high magnification image of the interconnectivity between microspheres (Scale bar 100 μm), and (C) PLGA-mTG sintered microspheres (300 μm – 600 μm).

Figure 2.12 SEM images showing the morphological change of sintered PLGA-Gelatin-mTG Free microspheres after incubation In PBS at 37 C over 8 weeks period of time. (A) weeks 0, original morphology of sintered microspheres, (B) 1 week after incubation, (C) 2 weeks after incubation, (D) 3 weeks after incubation, (E) 4 weeks after incubation, (F) 5 weeks after incubation, (G) 6 weeks after incubation, (H) 7 weeks after incubation, and (I) 8 weeks after incubation showing a significant change in morphology at the interconnected pore comparing to week 0. White arrows indicate cracks between the adjacent microspheres.

Figure 2.13 SEM images showing the morphological change of sintered PLGA-Gelatin-mTG microspheres after incubation In PBS at 37 C over 8 weeks period of time. (A) weeks 0, original morphology of sintered microspheres, (B) 1 week after incubation, (C) 2 weeks after incubation, (D) 3 weeks after incubation, (E) 4 weeks after incubation, (F) 5 weeks after incubation, (G) 6 weeks after incubation, (H) 7 weeks after incubation, and (I) 8 weeks after incubation showing a significant change in morphology at the interconnected pore comparing to week 0. White arrows indicate cracks between the adjacent microspheres, and blue arrows indicate presence of the lyophilized gelatin

Figure 2.14 Weight loss of PLGA-Gelatin Coaxial nanofibers and PLGA Uniaxial nanofibers curve over 8 weeks after incubation in PBS at 37C.

Figure 2.15 Swelling Rate of PLGA-Gelatin Coaxial nanofibers and PLGA Uniaxial nanofibers curve over 8 weeks after incubation in PBS at 37C.

Figure 2.16 pH change of PLGA-Gelatin Coaxial nanofibers and PLGA Uniaxial nanofibers curve over 8 weeks after incubation in PBS at 37C.

Figure 2.17 Weight loss of PLGA-Gelatin-mTG microsphere scaffold and PLGA-Gelatin-mTG Free microsphere scaffold curve over 8 weeks after incubation in PBS at 37 C.

Figure 2.18 Water uptake of PLGA-Gelatin-mTG microsphere scaffold and PLGA-Gelatin-mTG Free microsphere scaffold curve over 8 weeks after incubation in PBS at 37 C.

Figure 2.19 pH change of PLGA-Gelatin-mTG microsphere scaffold and PLGA-Gelatin-mTG Free microsphere scaffold curve over 8 weeks after incubation in PBS at 37C.

Figure 3.1 Schematic of coaxial electrospinning setup, and the conventional uniaxial electrospinning setup.

Figure 3.2 PDGF-BB and IGF-I release profiles from coaxial and uniaxial PLGA electrospun nanofibers. (A) PDGF-BB release profile from coaxial nanofibers and uniaxial nanofibers, (B)

TEM image showing PDGF-BB in the core sheath of PLGA nanofiber with a sheath thickness of 284 nm, (C) IGF-I release profile from coaxial nanofibers and uniaxial nanofibers and (D) TEM image showing IGF-I in the core sheath of PLGA nanofiber with a sheath thickness of 137 nm.

Figure 3.3. (A) The average of the retained BMP-2 in the enzymatically cross-lined geatin-mTG hydrogel, and (B) ALP activates

Of MC3T3 cell lines seeded on PLGA-Gelatin-mTG scaffold in the three different experimental groups shown in the figure.

Figure 3.4 TEM images of PLGA coaxial electrospun nanofibers with growth factors incorporated at the core-shell of the nanofiber (A) TEM image showing PDGF-BB in the core sheath of PLGA nanofiber with a sheath thickness of 284 nm, (B) TEM image showing IGF-I in the core sheath of PLGA nanofiber with a sheath thickness of 137 nm.

Figure 4.1 Morphological characterization of primary dermal fibroblasts (A) Primary Dermal Fibroblasts (10X), (B) Primary Dermal Fibroblasts (40X)

Figure 4.2 Morphological characterization of primary ligament fibroblasts (A) Primary Ligament Fibroblasts (10X), (B) Primary Ligament Fibroblasts (40X)

Figure 4.3 Morphological characterization of primary osteoblasts (A) Primary Osteoblasts (10X), (B) Primary Osteoblasts (40X)

Figure 4.4 Detection of dermal fibroblastic markers expression by Immunofluorescence (A) ALP stain DAPI channel, (B) ALP expression, (C) merged between DAPI and ALP expression, (D) OCL DAPI channel, (E) OCL expression, (F) merged between DAPI and OCL, (G) SCXA DAPI channel, (H) SCXA expression, (I) merged between DAPI and SCXA

Figure 4.5 Detection of ligament fibroblastic markers expression by Immunofluorescence (A) SCXA stain DAPI channel, (B) SCXA expression, (C) merged between DAPI and SCXA expression, (D) Temd DAPI channel, (E) Temd expression, (F) merged between DAPI and Temd, (G) TE-7 DAPI channel, (H) TE-7 expression, (I) merged between DAPI and TE-7

Figure 4.6 Detection of osteoblastic markers expression by Immunofluorescence (A) ALP stain DAPI channel, (B) ALP expression, (C) merged between DAPI and ALP expression, (D) OCL DAPI channel, (E) OCL expression, (F) merged between DAPI and OCL, (G) SCXA DAPI channel, (H) SCXA expression, (I) merged between DAPI and SCXA

Figure 4.7 Viability and proliferation of dermal fibroblasts on different PLGA nanofibers scaffolds (A) Uniaxial PLGA at day 3, (B) Uniaxial PLGA at day 7, (C) Coaxial PLGA at day 3, (D) Coaxial PLGA-Gelatin at day7, and (E) proliferation of primary dermal fibroblasts cultured on Uniaxial PLGA, and Coaxial PLGA-Gelatin. $n=3$ $P < 0.05^*$, $P < 0.001^{***}$

Figure 4.8 Viability of dermal fibroblasts on different PLGA coaxial or uniaxial elctrospun nanofibers scaffolds (A) PLGA-Gelatin-PDGF-BB at day 3, (B) PLGA-Gelatin-PDGF-BB at day 7, (C) PLGA-Gelatin at day 3, (D) PLGA- Gelatin at day7, (E) PLGA/PDGF-BB at day 3, (F)

PLGA/PDGF-BB at day 7, (G) PLGA at day 3, (H) PLGA at day 7.

Figure 4.9 Proliferation Assay. Primary Dermal fibroblasts were cultured on PLGA-Gelatin PDGF-BB, PLGA-Gelatin (negative control), PLGA-PDGF-BB (positive control), PLGA (negative control), then assayed for cell proliferation on day 3 and 7. $n = 3$ $P < 0.05^*$, $P < 0.0^{**}$, $P < 0.001^{***}$

Figure 4.10 Viability and proliferation of ligament fibroblasts on different PLGA nanofibers scaffolds (A) Uniaxial PLGA at day 3, (B) Uniaxial PLGA at day 7, (C) Coaxial PLGA at day 3, (D) Coaxial PLGA-Gelatin at day 7, and (E) proliferation of primary ligament fibroblasts cultured on Uniaxial PLGA, and Coaxial PLGA-Gelatin. $n = 3$ $P < 0.05^*$, $P < 0.0^{**}$, $P < 0.001^{***}$

Figure 4.11 Viability of ligament fibroblasts on different PLGA coaxial or uniaxial electrospun nanofibers scaffolds (A) PLGA-Gelatin-IGF-I at day 3, (B) PLGA-Gelatin-IGF-I at day 7, (C) PLGA-Gelatin at day 3, (D) PLGA-Gelatin at day 7, (E) PLGA/IGF-I at day 3, (F) PLGA/IGF-I at day 7, (G) PLGA at day 3, (H) PLGA at day 7.

Figure 4.12 Proliferation Assay. Primary ligament fibroblasts were cultured on PLGA-Gelatin IGF-I, PLGA-Gelatin (negative control), PLGA-IGF-I (positive control), PLGA (negative control), then assayed for cell proliferation on day 3 and 7. $n = 3$ $P < 0.05^*$, $P < 0.0^{**}$, $P < 0.001^{***}$

Figure 4.13 Viability and proliferation of osteoblasts on different PLGA microsphere scaffolds (A) PLGA-Gelatin-mTG free at day 3, (B) PLGA-Gelatin-mTG free at day 7, (C) PLGA-Gelatin-mTG at day 3, (D) PLGA-Gelatin-mTG at day 7, and (E) proliferation primary osteoblasts cultured on PLGA-Gelatin-mTG free, and PLGA-Gelatin-mTG. $n = 3$ $P < 0.05^*$, $P < 0.0^{**}$, $P < 0.001^{***}$

Figure 4.14 Viability of osteoblasts on different PLGA microsphere scaffolds (A) PLGA-Gelatin-mTG/BMP-2 at day 3, (B) PLGA-Gelatin-mTG/BMP-2 at day 7, (C) PLGA-Gelatin-mTG at day 3, (D) PLGA-Gelatin-mTG at day 7, (E) PLGA/BMP-2 at day 3, (F) PLGA/BMP-2 at day 7, (G) PLGA-Gelatin-mTG Free at day 3, (H) PLGA-Gelatin-mTG Free at day 7.

Figure 4.15 Proliferation Assay. Primary osteoblasts were cultured on PLGA-Gelatin-mTG/BMP-2, PLGA-Gelatin-mTG (negative control), PLGA/BMP-2 (positive control), PLGA-Gelatin-mTG Free (negative control), then assayed for cell proliferation on day 3 and 7. $n = 3$ $P < 0.05^*$, $P < 0.0^{**}$, $P < 0.001^{***}$

Figure 5.1. A three-dimensional representation of the mold used for the devolvment of the tri-culture model. (A) 3D view of the mold design showing the disc inserted in the provided hole, (B) the actual 3D printed mold and the PDMS elastomer filling the cavity within the disc, (C) the morphology of the cured PDMS segment after incubation at 37 C, and (D) the PDMS segment placed inside of the well of the 24-well plate and separating the well into three different cambers, the three different phases are shown occupying the different chambers. Blue arrow indicates the PDMS elastomer.

Figure 5.2. Dimensions of the plate that was used as the platform for the disc. (A) 3D view showing the dimensions of the plate from different planes, (B) top view showing the width 8 mm and the length 13 mm of the plate, and (C) side view Showing the height of the plate 2 mm.

Figure 5.3. Dimensions of the disc. (A) 3D view showing the dimensions of the disc from different planes, (B) top view showing the diameter of the disc 17 mm, and (C) side view Showing the thickness of the disc 5 mm.

Figure 5.4. Three different water-based dyes were added to the different chambers to examine the permeability of these dyes to the neighboring chambers. (A) top view of the well showing the three different dyes, each in a different chamber at day 0, and (B) bottom view of the same well showing no evidence for water penetration after incubation at 37 C for 7 days.

Figure 5.5. Three different cell types, dermal fibroblasts, ligament fibroblasts and osteoblasts were seeded and cultured in the well of a 24-well plate, each in a different chamber after placing the PDMS segment to examine cell migration to the neighboring chambers. At day 3, the PDMS segment was removed and different wells were visualized under a normal light microscopy to examine the cell migration, as seen in the figure, no evidence for cell migration was observed between the neighboring chambers after Day 3. Scale bars 4X and 10 X.

Figure 5.6. Three different cell types, dermal fibroblasts, ligament fibroblasts and osteoblasts were seeded and cultured in the well of a 24-well plate, each in a different chamber after placing the PDMS segment to examine cell migration to the neighboring chambers. At day 7, the PDMS segment was removed and different wells were visualized under a normal light microscopy to examine the cell migration, as seen in the figure, no evidence for cell migration was observed between the neighboring chambers after Day 7. Scale bars 4X and 10 X.

Figure 5.7. The three different cell types were seeded in their relevant phases and each phase was cultured in different medium and medium compositions in a single and tri-culture environment in order to determine what medium would best sustain their growth in the tri-culture environment. Numbers indicate the increase in fold between day 3 and 7.

Figure 5.8. Proliferation Assay. Dermal fibroblasts cultured in different medium and medium compositions in a single and tri-culture environment. Numbers on top of the bars indicate the increase in fold between day 3 and 7. $n = 3$ $P < 0.05^*$, $P < 0.0^{**}$, $P < 0.001^{***}$

Figure 5.9. Proliferation Assay Ligament fibroblasts cultured in different medium and medium compositions in a single and tri-culture environment. Numbers on top of the bars indicate the increase in fold between day 3 and 7. $n = 3$ $P < 0.05^*$, $P < 0.0^{**}$, $P < 0.001^{***}$

Figure 5.10. Proliferation Assay. Osteoblasts cultured in different medium and medium compositions in a single and tri-culture environment. Numbers on top of the bars indicate the increase in fold between day 3 and 7. $n = 3$ $P < 0.05^*$, $P < 0.0^{**}$, $P < 0.001^{***}$

Figure 5.11 Viability Assay. Dermal fibroblasts, ligament fibroblasts and osteoblasts were seeded

in phases A, B and C respectively and cultured for 2 days. 2 days post initial culture, they were assembled in which, Phase B was placed on top of Phase C and both phases were covered by Phase A and cultured for further 3 and 7 days. After 3 and 7 days, phases were separated and assayed for cell Viability using LIVE/DEAD assay. $n=3$ $P < 0.05^*$, $P < 0.0^{**}$, $P < 0.001^{***}$

Figure 5.12 Proliferation Assay. Dermal fibroblasts, ligament fibroblasts and osteoblasts were seeded in phases A, B and C respectively and cultured for 2 days. 2 days post initial culture, they were assembled in which, Phase B was placed on top of Phase C and both phases were covered by Phase A and cultured for further 3 and 7 days. After 3 and 7 days, phases were separated and assayed for cell proliferation. $n=3$ $P < 0.05^*$, $P < 0.0^{**}$, $P < 0.001^{***}$

Figure 5.13 Immunofluorescence Staining. The three different phases within the IGS were immunostained with cell-specific markers to examine the localization and phenotypic maintenance of the cells cultured within every phase. Cell migration between the phases was examined too by immunostaining. As seen in the figure, the three different cell types remained localized in their relevant phases and as well as maintained their phenotype in the heterogenic cellular population for up to 7 days. Cell migration between all phases was observed after 3 and 7 days. However, no cell migration was observed between Phase A and B after 3 days.

Table 1: A list of *in vitro* **Endogenously** secreted growth factors by dermal fibroblasts, ligament fibroblasts and osteoblasts and the *in vitro* responses of the three cell types to the secreted growth factors.

CAHAPTER 1

1. INTRODUCTION

1.1.Biomimetic Scaffolds

Tissues within the human body are prone to injuries or trauma that can lead to tissue damage or degeneration. These traumas require treatments to facilitate their restoration, replacement or regeneration to enhance the overall quality of life. Currently, the use of biological grafts is considered the only viable clinical strategy for treating damaged tissues or organs. Biological grafts include autografts known as the transplantation of tissue within an individual from a donor site to the injury site, or allografts known as the transplantation of a tissue or a whole organ from another individual or a cadaver. Autografts demonstrate high biocompatibility and healing potential compared to allografts, making them the gold standard among all the biological grafts [9]. The poor biocompatibility and integration of allografts to the host tissues, and the limited availability and high price demand of autograft led to the necessity of finding alternatives that mostly focus on regenerating the damaged tissues rather than repairing or replacing them [10]. [110-113]. Hence, clinical limitations associated with the treatment of several traumatic injuries led to the emergence of an interdisciplinary known as “tissue engineering.” Tissue engineering has been defined as “the application of biological, chemical and engineering principles toward the repair, restoration and regeneration of tissues using biomaterials, cells, and factors alone or in combination” [86, 110]. Tissue engineering is proposed to repair, restore or regenerate damaged tissues or organs by combining cells, genes, or biologically active molecules with a 3D porous matrix known as a scaffold [17]. Scaffold serve as a structural support for tissue formation where cells interact and behave according to the physiochemical cues embedded in the scaffold itself. [114]. Despite the fact that enormous progress has been made in the past two decades in designing

and engineering scaffolds, tissue engineering scaffolds lack many physiochemical cues that are essential for tissue regeneration and do not truly mimic the in vivo cellular microenvironment of the natural extracellular matrix (ECM) [115]. The limitations of the current biological and engineering approaches towards effective tissue regeneration made it clear that a paradigm shift is required to successfully create technologies that can address the grand clinical challenges [6]. Developing a new interdisciplinary approach that utilizes the most advanced technologies currently available in different fields such as developmental biology, bioengineering, biomaterials science, stem cell biology, and clinical medicine along with full understanding of the different tissues specific topographies may hold the key toward effective tissue regeneration [6, 15]. The efforts of scientists from these various fields led to the emergence of a new paradigm we term “Regenerative Engineering”. Regenerative Engineering has been defined as “*the Convergence of Advanced Materials Sciences, Stem Cell Sciences, Physics, Developmental Biology and Clinical Translation for the regeneration of complex tissues and organ systems*”. Distinct from the tissue engineering, regenerative engineering more focuses on the subsequent response of cells to biomaterials through the utilization of appropriate materials that exhibit suitable properties and surface chemistry as well as providing the appropriate topographical and physiochemical cues that could potentially influence cell differentiation and fate towards a particular tendency for effective tissue development and regeneration (Figure 1.1) [164]. Scaffolds with such characteristics are referred to as “biomimetic scaffolds” [116]. Biomimetic scaffolds have recently emerged as a promising strategy for effective tissue regeneration. A biomimetic scaffold represents a synthetic ECM niche that determines cell migration, proliferation, and differentiation to ensure proper regulation of tissue/organ formation, maintenance of tissue integrity and repair, and regeneration [116]. Ideally, a biomimetic scaffold should provide cells with a variety of physical, chemical, and

biological cues that are naturally inherited by the native ECM to facilitate cell growth and function [123]. *In vivo*, cells are found entrapped within an ECM, in which they are provided with all the necessary physical and chemical cues that guide their development, arrangement and regenerative abilities by molecular interactions between specific cell membrane receptors and signaling cues from surrounding ECM material [123]. To duplicate the *in vivo* environment, the biomimetic scaffold should exhibit controllable physical, chemical and mechanical properties, cell adhesion properties and growth factor release kinetics [115]. Generally, an ideal tissue engineering scaffold should be biocompatible that do not elicit an immune response, biodegradable to be replaced with newly formed tissue, highly porous to facilitate cell migration, proliferation, nutrition diffusion and waste removal, and exhibits topographical mechanical and architectural properties resembling those found at the native tissue [116]. Therefore, a basic understanding of the entire spectrum of biomimetic scaffolds provides insight into how they can potentially be used in diverse tissue engineering, regenerative medicine, and drug delivery applications.

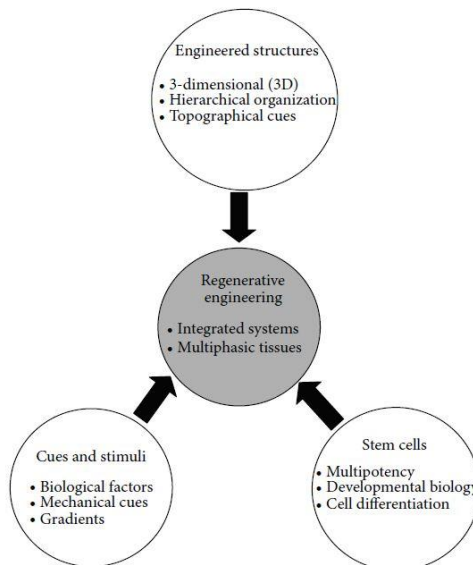


Figure 1.1. Schematics of regenerative engineering approach to create complex functional tissues and organs [164].

1.1.1. General Scaffold Requirement

1.1.1.1. Biocompatibility

Biocompatibility is one important criteria of any tissue engineering scaffold that must be considered as the first priority when choosing any biomaterials. Tissue engineering scaffold must be biocompatible and allow cells to function normally, adhere, migrate throughout the scaffold, proliferate and produce ECM [116]. In addition, tissue engineering scaffold must not elicit any immune response upon implantation as this can result in inflammatory reaction, which in turn can initiate fibrous encapsulation that prevents tissue formation [116].

1.1.1.2. Biodegradability

Tissue engineering scaffold should not permanently stay within the host body, as the whole purpose of using a biodegradable construct is to allow it to be replaced with the body's own tissues over time as it degrades, and also to limit the chance of a secondary surgery [251]. The degradation by-products should not be toxic and be able to be eliminated out of the body without any interference with other tissues. Incorporation of anti-inflammatory agents within the tissue engineering scaffold is recommended to prevent any chance of inflammatory response. In addition, depending on the application needs, the scaffold degradation rate must be tailored by selecting the appropriate biomaterial in order to achieve a tandem degradation with the neo-tissue formation. Due to the increase in the number of biodegradable tissue engineering products entering clinical practice, the number of the immunological studies examining the body response to the degradation by-products of many materials has also increased as a result, which lies lots of promises in the research area [118, 119].

1.1.1.3.Porosity

Tissue engineering scaffold should be highly porous with an open porous geometry and well interconnected channels to achieve high density cell growth within the engineered construct, as well as high mass transport of oxygen, nutrition and metabolic waste in addition to supporting neovascularization within the construct. All, high cell density, mass transport, and neovascularization contribute to cell viability, proliferation, and ultimately regeneration of a functional tissue [120]. Average pore size, pore size distributions, pore volume and pore interconnectivity are all important parameters that have to be considered when designing the tissue engineering scaffold. Several reports have emphasized the effect of the pore size on tissue regeneration to determine the optimum pore size for every scenario, revealing that the optimum pore size for neovascularization is 5 μm [244], 5-15 μm for fibroblasts ingrowth [245], 20 μm for hepatocytes ingrowth [246], 200-350 μm for osteoconduction [247], and 20-125 μm for the regeneration of mammalian adult skin [248]. These pore sizes were found to be the optimal for these specific tissue types, as they may differ with other tissues [249]. In general, pore volume and size should be a few times larger than the size of the cells intended to be seeded or recruited to the scaffolds to provide extra space for sufficient entry and exit of nutrition and waste removal, neovascularization and thus, tissue ingrowth [250]. When designing the tissue engineering scaffold, it has to be taken into consideration that a subsequent balance between the pore size, volume and mechanical property is required, as increase in the pore volume leads to decrease in the mechanical integrity of the engineered construct, whereas decreasing the porosity can have negative effects on the cellular performance.

1.1.1.4.Mechanical property

Tissue engineering scaffolds should be fabricated from biomaterials that exhibits intrinsic properties mimicking those found in the native tissue and should be mechanically compatible with the anatomical location. The human body is composed of hard and soft tissues with different mechanical properties and these tissues contain cells that are tuned to the specific mechanical environments in which they reside. Therefore, scaffold with biomimetic mechanical property can act as a cue to guide cellular behaviors and fate. Many mechanobiology studies demonstrated the role of the construct mechanical property in guiding cellular differentiation. These studies revealed that an appropriate scaffold stiffness and mechanical properties to guide cellular differentiation into a specific tendency can be achieved [121]. Thus, providing the appropriate mechanical properties is a key role for effective tissue regeneration.

1.1.1.5.Architecture

The scaffold architecture plays an active role in tissue regeneration and remodeling. Scaffold architecture mainly contributes to how a cell transduces input from the external physical environment into biochemical signals that dictate cell response [122]. The cell response to the surrounding architecture is a phenomenon known as “contact guidance”, which can be used to regulate cytoskeletal organization, cell shape, migration, and differentiation [123, 125-128]. Therefore, scaffolds with defined topological patterns have been studied based on the hypothesis that topographic patterns can be employed as instructive cues to direct cellular responses [123]. A wealth of evidence has shown that cells grown on different architectures demonstrate altered cell morphologies and gene expressions [122]. Thus, providing a biomimetic ECM architecture may be used to ultimately control cell behavior and fate.

Successful tissue regeneration is highly dependent on the aforementioned requirements. These are the general tissue engineering scaffold requirements that have to be taken into accounts when designing the tissue engineering scaffold. However, the choice of the biomaterials in which the tissue engineering scaffold should be fabricated is the one important criteria that all the above-mentioned criteria depend on, as different materials exhibit different surface properties, degradation rates, mechanical strengths, biocompatibility, all in which contribute to the overall quality and integrity of the engineered scaffold. Tissue engineering scaffolds have been produced using a wide variety of biomaterials through well-developed processing conditions, thus; choosing the appropriate biomaterial and fabrication technique is critical for successful regeneration of the target tissue.

1.1.2. Biomaterials and Fabrication Techniques for Biomimetic Scaffolds

For a successful tissue regeneration, the scaffold should emulate certain advantages of the native ECM while temporarily act as a cell template that allows for tissue ingrowth and infiltration as it degrades [131]. Surprisingly, a biomimetic scaffold does not have to entirely duplicate the native ECM, due to the fact that the neo-tissue genesis in tissue engineering is not exactly the same as a developmental or a wound healing process [131]. In fact, a native ECM may not be the ideal scaffold for tissue regeneration, because tissue regeneration is an accelerated process compared to the native development process. Natural ECMs do not possess the basic tissue engineering scaffold requirements such as porosity and interconnected macro- or micro pore structure, that are essential in order to allow for quick and uniform cell population throughout. Therefore, for optimal and accelerated tissue regeneration, some important and necessary features such as porosity, pore size and interpore connectivity have to be provided, which can only be obtained through artificially

designed scaffolds. However, artificially designed scaffold that mimics the structural aspects of the native ECM with tailored porosity and interconnectivity may be the best option to achieve a functional biomimicry tissue regeneration. Thus, providing a proper niche for cell adhesion, migration, and proliferation will be based on the material choice.

1.1.2.1.Biomaterials

In tissue engineering applications, materials are selected based on their chemistry, molecular weight, solubility, shape and structure, hydrophilicity/hydrophobicity, lubricity, surface energy, water absorption degradation, and erosion mechanism [129]. All of these are essential properties that can influence the scaffold's overall quality and the degree of biomimicry. Biomaterials used for tissue engineering scaffold are mainly classified into two categories, naturally derived and synthetic biomaterials. Natural biomaterials can be further classified into proteins (silk, collagen, gelatin, fibrinogen, elastin, keratin, actin, and myosin), polysaccharides (cellulose, amylose, dextran, chitin, and glycosaminoglycan), or polynucleotides (DNA, RNA). Natural biomaterials are known for their excellent biocompatibility, bioactive properties, and good interactions with cells, owing an enhanced cellular performance in biological systems [129]. Despite all of their advantages, natural biomaterials possess poor physical and mechanical properties, which limit their use for load-bearing applications. Synthetic biomaterials on the other hand, are further characterized into degradable and non-degradable synthetic polymers. Biodegradable synthetic polymers are preferred over the non-degradable polymers due to their degradability nature, which in turn facilitate a faster neo-tissue ingrowth and better tissue infiltration, in addition to minimizing the chance for a secondary surgery after implantation [129]. A wide range of synthetic biodegradable polymers such as, poly(lactic acid) (PLA), poly(glycolic acid) (PGA), poly(lactic-

co-glycolic acid) (PLGA), poly-L-lactic acid (PLLA), and polycaprolactone PCL, have been used for many musculoskeletal tissues and skin tissue engineering due to their intrinsic tailored properties [129]. Although synthetic polymers have the advantages of tailoring their properties such as, porosity, degradation rate, physical and mechanical characteristics for specific applications and needs, they possess poor biocompatibility and lack all the ligands required for cell attachments and proliferation, which can result in poor cell adaption to the matrix and thus, poor tissue formation. Limitations associated with both natural and synthetic biomaterials limit their use on their own in many tissue engineering applications where both mechanical and biocompatibility are highly required, or as materials for a biomimetic scaffold. The native ECM resembles some properties that are found in synthetic materials only or natural materials only, therefore, composite scaffolds are the best solution to address the disadvantages of both natural and synthetic scaffolds, as it helps in the mutual enhancement of the scaffold properties and thereby allowing controlled degradation and mechanical properties as well as improving the biocompatibility, and providing cells with all the necessary physical and chemical cues that are naturally inherited by the natural ECM, to achieve the best possible biomimicry of the native ECM [130].

1.1.2.2.Fabrication Techniques for Biomimetic Scaffolds

Scaffold's fabrication techniques play key role in emulating the architecture of the natural ECM. The degree of emulation is highly effected by which fabrication technique is applied. Generally, the scaffold's architecture should mimic the natural ECM in a way that it should act as an instructive tool that instruct and guide cellular behaviors while adequately housing the cells [131,132] Biomimetic tissue engineering scaffolds have been produced using a wide variety of

different materials and well-developed fabrication techniques to achieve the most possible close biomimicry to the native ECM; considering the appropriate fabrication method is critical for successful tissue regeneration of the target tissue. Some of the most extensively used fabrication techniques for musculoskeletal tissues and skin tissue engineering include; sintered microsphere method, solvent casting and particle leaching, gas foaming and particle leaching, and electrospinning.

1.1.2.2.1. Sintered Microsphere

Microspheres-based tissue engineering scaffolds have attracted a significant interest in the research field in recent years [242]. Microsphere scaffolds demonstrate several benefits, including ease of fabrication, control over morphology, physicochemical characteristics, and its versatility of controlling the release kinetics of encapsulated factors [243]. The Fabrication of microsphere scaffolds was first established in 1998 by Laurencin et al. Microspheres are fabricated using the single emulsion technique, briefly, a solution of organic polymer in Dichloromethane (DCM) is generally added to an aqueous polyvinyl alcohol (PVA) surfactant (Figure 1.2). The mixture is let to stir under a certain speed inside a chemical hood to allow the solvent to evaporate. The end product of this process is a pellet of solidified microspheres, which are collected, rinsed, freeze or air dried and sieved to the desired diameter size range.

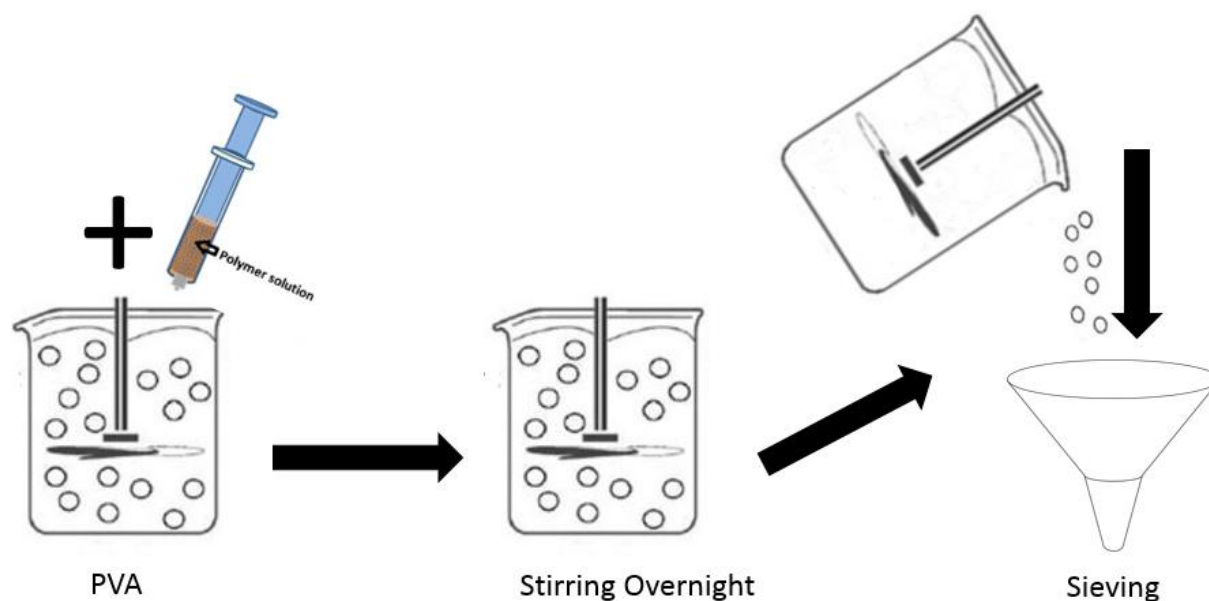


Figure 1.2. Fabrication process of polymeric microsphere through the single water/oil emulsion technique.

To construct scaffolds, microspheres with the desired particle size distribution are poured into a mold, generally stainless-steel mold, then heated above the glass transition temperature of PLGA ($T_g \sim 58^\circ\text{C}$) until they are thermally fused into the desired three-dimensional shape and morphology [10,11]. The advantages of using PLGA to develop 3D sintered microsphere scaffolds with a porous interconnected structure for bone tissue engineering has been demonstrated. These scaffolds were shown to possess mechanical properties controllable pore size and pore volume that are relatively close to the native tissue ECM, which makes them ultimately ideal for bone regeneration [12, 13].

1.1.2.2.2. Solvent Casting and Particle Leaching:

Solvent casting and particle leaching (SCPL) is a very simple technique that does not require specialized equipment. The main idea behind this technique is to create a highly porous three-

dimensional construct that mechanically and structurally resembles the native bone ECM (Figure 1.3). Briefly, the polymer is dissolved in a solvent until a homogenous and viscous polymer solution is obtained. The polymer solution is then casted in a mold of the desired geometry along with porogen particles (usually NaCl). The solvent then evaporates leaving behind a solidified polymeric scaffold with the porogen particles embedded throughout. To leach out the porogen particles, the structure is normally submerged in water, causing all particles to dissolve, leaving behind a highly porous structure suitable for use in tissue engineering applications. By controlling the shape, size, orientation and the amount of porogen added, different pore volumes, sizes and different pore gradients can be obtained. Some drawbacks associated with the use of solvent casting is that the majority of solvents used to dissolve polymers are very toxic. In addition, depending on the pore volume and the scaffold geometry, it is sometimes very difficult to completely leach out all porogen particles from the core of the scaffolds. The only way to overcome this problem is by applying the principle, where multiple porous thin sheets are glued into a thick 3D architecture. However, this method is very time consuming [255].

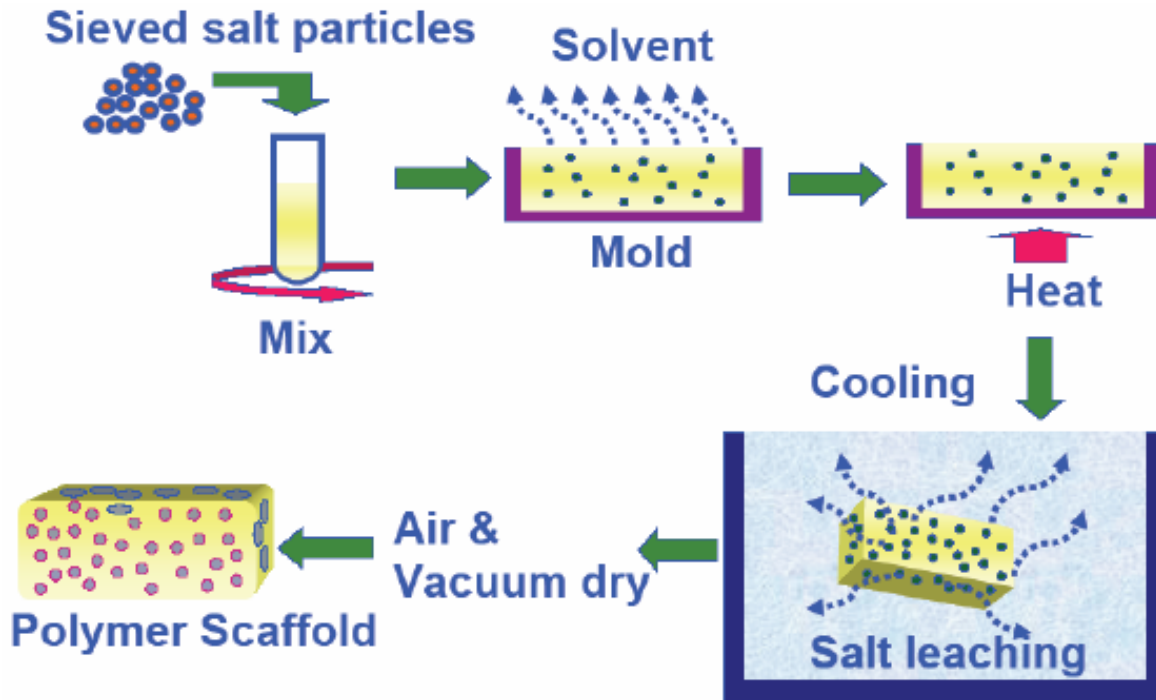


Figure 1.3. Schematic of solvent casting and particle leaching scaffold fabrication technique [256].

1.1.2.2.3. Gas Foaming and Particle Leaching:

Gas foaming and particle leaching (GFPL) is the modified version of the previously discussed technique addressing the problem of using toxic solvents. In this method, solvents are completely dismissed, and very high pressure is used instead to guide the fabrication process (Figure 1.4). Briefly, polymer granules are grinded and mixed with porogen particles (usually NaCl) at the desired ratio, and then sieved to yield particles with the desired diameter. Polymer/ porogen particles are then loaded into a mold of the desired geometry for compression with a very high pressure. This step allows the polymer particles and the porogen particles to fuse together under the effect of the high pressure applied, resulting in the formation of a solid polymer/porogen composite structure resembling the geometry of the used mold. The resultant structure is then exposed to CO₂ for some time to create surface porosity throughout the structure. Exposure

duration with CO₂ and other parameters can be tailored to achieve different surface pore volumes. Once porosity is created, the structure is then immersed in distilled water to leach out the porogen (NaCl). The process results in highly porous structure with enhanced interconnectivity throughout comparing to the SCPL method. Kim et al. [147] developed PLGA/HA scaffolds by gas foaming and particulate leaching technique and emphasized that PLGA/HA scaffolds produced with GFPL were found to significantly enhance bone regeneration when compared to SCPL fabricated scaffolds, owing their ability to enhance bone tissue engineering.

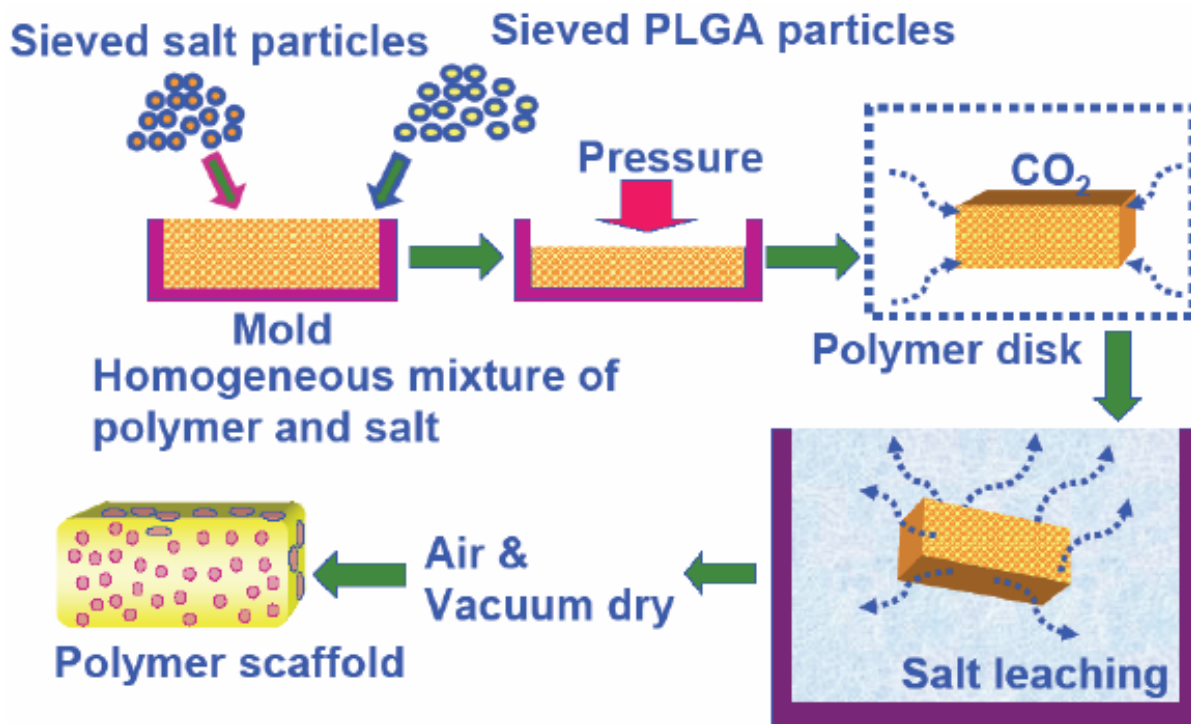


Figure 1.4. Schematic of gas foaming and particle leaching scaffold fabrication technique [256].

1.1.2.2.4. Electrospinning:

Electrospinning is currently one of the most extensively used technique for tissue engineering scaffold fabrication due to its resemblance to the native ECM, and its ability to process a wide

range of different natural and synthetic materials with different fibers orientations and diameters that can range from the sub-microns down to the nanometer scale depending on the applications needs [252]. Briefly, polymer granules or powder are dissolved in the appropriate solvent until a viscous, homogeneous and completely dissolved polymer solution is obtained. A complete dissolution of the polymer is very important for a successful bead-free production of electrospun fibers. The polymer solution is then loaded into a syringe, and placed in an apparatus pump for electrospinning (Figure 1.5). During electrospinning, an electrical field of high voltage is applied at the syringe needle tip that creates large enough forces at the surface of the polymer solution to overcome the surface tension, resulting in the ejection of an electrically charged jet that solidifies into electrically charged fibers. The needle tip is normally placed some distance away from the collection unit to allow branching and drawing of the fibers to occur. Polymer solution viscosity, flow rate, applied voltage, distance between the needle tip to the collecting unit are all important electrospinning parameters that mainly affect the fiber diameter, mechanical properties and the overall morphology of the electrospun fibrous scaffold [253, 254].

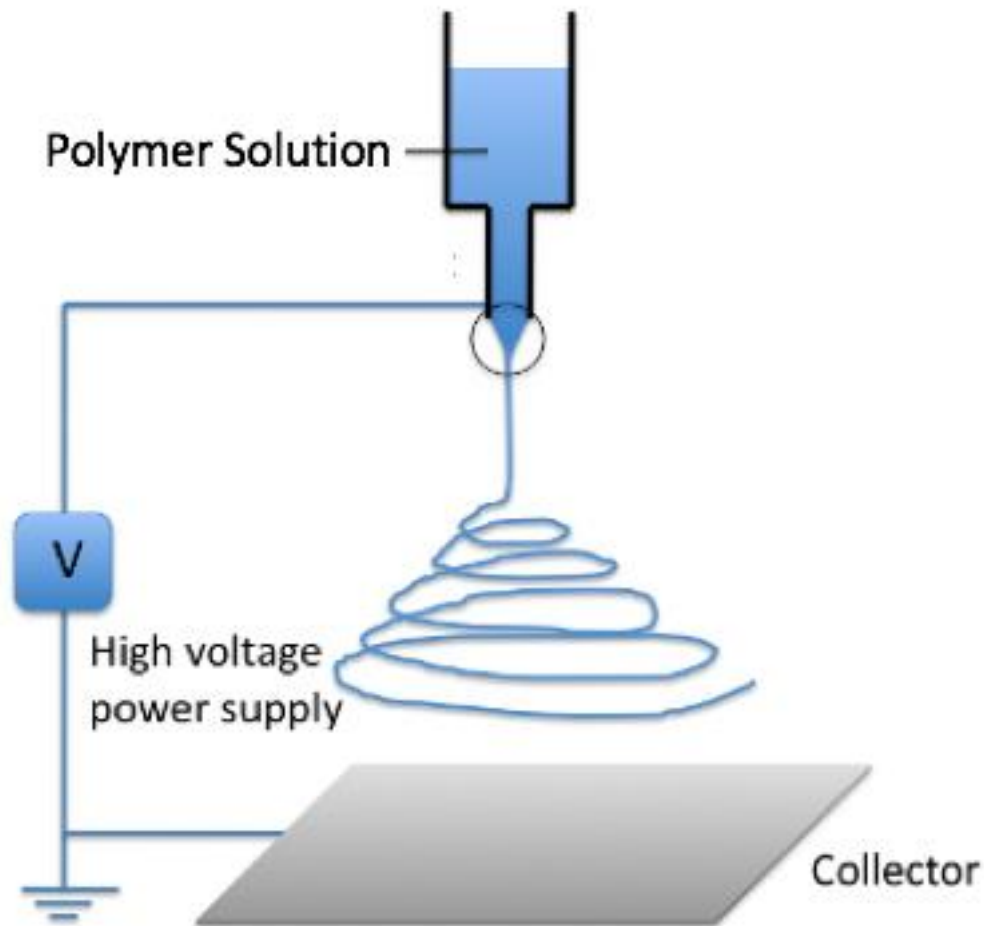


Figure 1.5. Schematic of the most extensively used tissue engineering fabrication technique, electrospinning set up.

1.1.3. Biomimetic Bone Tissue Regeneration:

1.1.3.1. Bone Structure and Function:

Bone is a mineralized connective tissue that serves to provide the structural support to the entire body [158]. Bone total mass is occupied by 8% water, 22% protein, and 70% mineral [158]. Bone consists of organic and inorganic portions, where the organic portion of bone is collagen type 1, and the inorganic portion is primarily hydroxyapatite (HA) and calcium phosphate (CaP) [158]. Bone tissue is characterized according to its macroscopic structure into either trabecular (spongy)

or cortical (compact) (Figure 1.6) [158]. Cortical bone is an extremely dense tissue that forms the outside layer of the bone, or cortex. It is formed and organized into concentric rings of sheets or “lamellae” of densely packed collagen fibrils [158]. Cortical bone is known for its high mineralization content and few pores, giving it the rigidity that allows it to maintain the body’s mechanical strength and structure [158]. Human cortical bone has compressive modulus and compressive strength of 12 – 20 GPa, and 150 MPa, whereas trabecular bone has a compressive modulus and compressive strength of 0.04 – 1.0 GPa, and 1.0 – 7.0 MPa, respectively [159]. Trabecular bone is found forming the inner shell of the cortex with a low mineralization content when compared to the cortex bone. Trabecular bone exhibits a highly porous structure with sufficient amount of vascularity, connective tissues and bone marrow [158]. Bone marrow is a great source of pluripotent stem cells, which contribute in the replenishment of the body’s connective tissues, including bone [158]. Three different primary cell type that make up bone and contribute in bone remodeling are Osteoclasts, Osteoblasts and Osteocytes. Osteoclasts and Osteoblasts are fully differentiated cells that are present at the surface of the bone, while osteocytes permeate the mineralized interior [163]. Osteoblast work in synthesizing the bone matrix in the bone forming surfaces in addition to regulating the matrix mineralization. Osteocytes are terminally differentiated osteoblasts that are entrapped within the mineralized matrix and serve to support the overall bone tissue [163]. Osteoclasts on the other side are larger than osteoblasts in size, and are multinucleated cells that are derived from different cellular precursors. They work on reabsorbing the synthesized bone by osteoblasts for bone remodeling [163]. These cells however, are regulated by growth factors within the bone that stimulate their proliferation, differentiation for continuous bone remodeling and healing upon fracture.

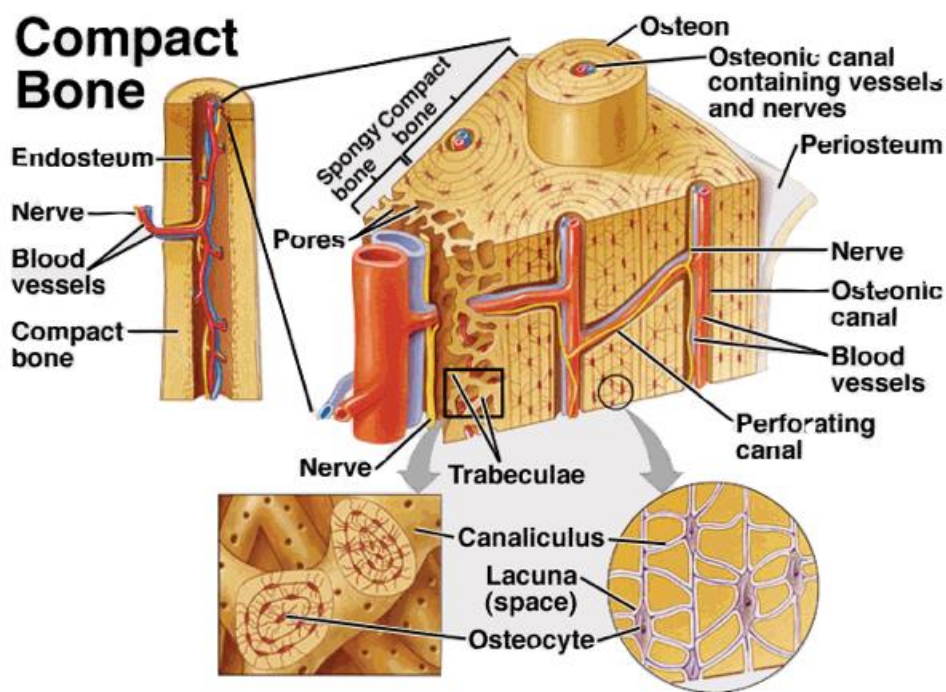


Figure 1.6: Cortical and Cancellous bone [220].

1.1.3.2. Materials for Biomimetic Bone Tissue Regeneration:

Materials choice for bone tissue engineering is essential, as differences in the materials properties may largely affect the overall quality of bone formation. Bone tissue engineering (BTE) scaffold material can be optimized to achieve the possible closest biomimicry to the natural ECM and to develop a clinically relevant engineered bone. Regardless of the material type, the ideal BTE scaffold should be biodegradable to be replaced with newly formed bone, as the permanent presence of the graft substitute could potentially alter bone formation or limit the tissue ingrowth within the substrate. Certain inorganic/ceramic materials such as hydroxyapatites (HAP) or bioactive glasses are used for their great osteoconductivity and mineralization content; but their use is limited due to the poor solubility and resorption profile as well as poor processability into highly porous structures, and brittleness [133].

Synthetic polymers such as PLA, PGA, PLGA, PLLA, and PCL have been widely used for BTE due to their degradability nature, tuned mechanical properties and the ease processability into a variety of different fabrication techniques such as gas foaming, porogen leaching, phase separation, electrospinning, microsphere sintering, and 3D printing to generate a wide range of three-dimensional scaffolds with different properties and surface characteristics [133-138]. However, the poor biocompatibility and lack of supportive cell attachment cues in the synthetic polymers limit their use on their own for BTE. In contrast, composite materials such as inorganic-organic, synthetic-organic composition are widely used aiming to mimic the properties of the native bone by combining toughness and bioactivity of the inorganic materials, biocompatibility of the organic materials, and degradability of the synthetic polymers, to generate bioactive materials with tuned mechanical and degradation profiles and surface properties.

1.1.3.3.Scaffold Requirements for Biomimetic Bone Tissue Regeneration:

In bone tissue engineering (BTE), scaffolds should possess osteoconductive, osteoinductive and oteointegrative properties to promote bone regeneration. However, osteoconductivity is the ability of a scaffold, or a physical matrix to provide a suitable environment for the deposition of new bone from the surrounding bone or encourage differentiated mesenchymal cells to grow along the graft surface, osteoinductivity is the ability of the scaffold to promote osteoblastic differentiation of progenitor cells through growth factors induction, and osteointegrivity is the ability of the scaffold to anchor and integrate into the surrounding bone [164]. BTE scaffolds should also be designed to fill the structure of the defect cavity, maintain it and restore bone function. It should also mimic the mechanical and structural properties of the native bone with a sufficient amount of porosity throughout the construct to allow cell infiltration, proliferation, neovascularization and nutrient

transport [164]. In addition, the scaffold should also serve as a reservoir for growth factors delivery such as, morphogenetic proteins (BMPs), insulin-like growth factors (IGFs) and transforming growth factors (TGFs), all of which help induce the transformation of host precursor cells into bone matrix producing cells [165].

1.1.3.4. Biomimetic Bone Tissue Engineering Approaches:

Bone is a living tissue that undergoes constant remodeling and self-renewal to maintain its hemostasis, comprising the ability to repair its self [116]. Due to this fact, restorative surgical intervention, after surgery for instance, usually requires not more than alignment and stable fixation. However, if self-repair mechanisms are overstrained, in case of non-unions or critical size defects, bone losses the ability to repair its self, which necessities the development of biomimetic bone grafts that mimic all the different aspects found at the native ECM for effective and functional bone restoration. In an attempt to mimic the native bone mechanically and structurally, Borden et al. developed a scaffold for BTE using a heat sintering technique to fabricate sintered microsphere scaffold with sufficient porosity throughout to support cellular migration and movement within the substrate. The microsphere scaffold was fabricated from PLGA (85:15) ratio between lactic-to-glycolic acid [140, 141]. By orderly pouring and the fabricated microsphere in a predefined mold with heat applied, the neighboring individual microspheres fuse together resulting in a highly porous 3D structure that resembles the native human trabecular bone mechanically and structurally. The resultant scaffold had a compressive modulus of 232 MPa, and approximately ~ 35% pore volume with a median pore size of 100-300 μm that allows for bone cells and tissue ingrowth. During bone formation, the pore volume would be occupied by the newly forming bone while the microsphere matrix slowly degraded leaving voids that will resemble the pore structure

found in the human trabecular bone. When the polymeric scaffold completely degrades, the regenerated bone tissue possesses approximately 65% void volume resembling that of human trabecular bone. The author demonstrated the feasibility towards developing a mechanically and structurally biomimetic bone tissue engineering scaffold that resembles the trabecular bone mechanical and structural properties. However, the scaffold will need to be optimized in order to in order to increase its biocompatibility for supportive cellular performance.

To enhance the biocompatibility and cellular performance of the sintered PLGA microsphere scaffold having the same mechanical and structural properties as well as the pore volume, the same group modified this technique to fabricate a composite microsphere scaffold prepared from chitosan/PLGA [142]. Milled chitosan microparticles were mixed with PLGA solution to fabricate the chitosan/PLGA microspheres. The resultant chitosan/PLGA microsphere were poured in predefined mold and heat sintered to achieve bonding between adjacent microspheres. The 3D chitosan/PLGA microsphere scaffold presented a rough surface morphology (Figure 1.7a), even distribution of microsphere surface with excellent interconnected porous structure and appropriate mechanical properties suitable for load-bearing applications (Figure 1.7b). The composite scaffold was able to support MC3T3-E1 cells proliferation. In addition, the presence of chitosan contributed to the enhancement of the differentiation and the maturation of MC3T3-E1 osteoblastic-like cells over time when compared to the raw PLGA microspheres. Findings from this study revealed that composite scaffolds seem to combine multiple properties and increase the scaffold biocompatibilities, which in turn leads to enhanced cellular performance.

Scaffold bioactivity play an important role in tissue regeneration as it largely influences, directs, or manipulates cellular responses. To further enhance the bioactivity of the chitosan/PLGA sintered microsphere scaffold, the scaffold was surface functionalized with the biomolecule heparin sulfate immobilization through ionic interaction between oppositely charged chitosan and heparin molecules resulting in a bioactive scaffold mimicking the natural bone environment (Figure 1.7c) [144]. Treatment with heparin sulfate did not alter the mechanical properties and pores structure. Characterization experiments revealed that the heparinized chitosan/PLGA scaffolds possessed a compressive modulus of 403.98 ± 19.53 MPa, and a compressive strength of 9.83 ± 0.94 MPa, which were in the range of the human trabecular bone. Furthermore, the scaffold resulted in a highly porous interconnected structure with a total pore volume of $30.93 \pm 0.90\%$ and a median pore size of 172.33 ± 5.89 μm . MC3T3-E1 cells were pre-seeded on the heparinized chitosan/PLGA microsphere scaffold to evaluate the effect of the immobilized heparin. In vitro results revealed that the cell number has increased significantly over time, and MC3T3-E1 cells showed elevated osteocalcin expression when compared to the non-heparinized chitosan/PLGA scaffolds (Figure 1.7d, e, f). In addition to the modification that has been done in order to enhance the biocompatibility of the mechanically and structurally biomimetic PLGA sintered microsphere scaffold, this study also demonstrated the potential of enhancing the bioactivities of the scaffold through the surface functionalization with heparin sulfate, resulting in a possibly close biomimicry to the native bone mechanically, structurally and chemically.

The heparinized chitosan/PLGA sintered microsphere scaffold's ability to support bone formation has been evaluated in an ulnar bone critical-sized-defect model *in vivo* (Figure 1.7 g). *In vivo* assessments revealed that Heparinized chitosan/PLGA scaffold was able to guide bone formation.

μ CT analysis demonstrated that a successful bridging between the two ends of the defects was achieved through the heparinized chitosan/PLGA scaffold with a complete bridging and enhanced mechanical properties when compared to the chitosan/PLGA scaffold alone (Figure 1.7h). Further histological analysis suggested that heparinized chitosan/PLGA scaffold supported normal bone formation via intramembranous formation (Figure 1.7i).

These studies demonstrated series of different approaches attempting to generate a possibly close biomimetic bone tissue engineering scaffold that resembles the native bone mechanically, structurally and chemically. Despite the multitude scaffolds that have been studied, scaffold optimization continuous to be an active area of research to find the most optimal scaffold design for bone tissue engineering.

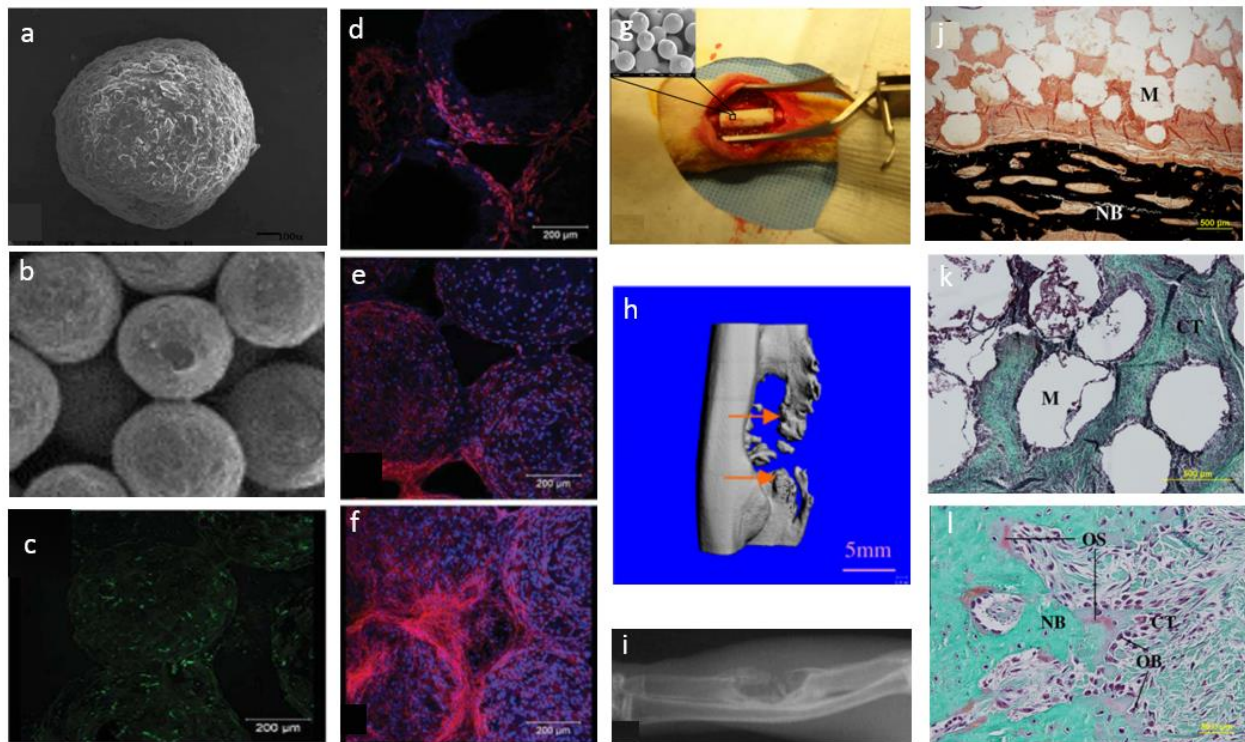


Figure 1.7: (a) A chitosan/PLAGA composite microsphere; (b) a 3D chitosan/PLAGA scaffold fabricated by heat sintering (c) Chitosan/PLAGA scaffold immobilized with heparin as evidenced by them green fluorescence; (d)–(f) MC3T3-E1 osteoblast-like cell proliferation at days 4, 7, and 11 on the heparinized

chitosan/PLAGA scaffolds as illustrated by dual staining of cell nuclei (blue) and cytoskeletal protein actin (red); (g) The surgical procedure showing a 15 mm segment of ulna was removed and a sintered microsphere scaffold was implanted into the defect site; (h) Three-dimensional microCT reconstruction of the bone regeneration in the ulnar defect from the animals with the most amount of new bone formation (HP-CS-PLAGA-BMP2 12 weeks); (i) A radiograph showing new bone formation bridging the critical-sized defect at 12 weeks after operation using chitosan/PLAGA scaffolds loaded with heparin and bone morphogenetic protein—2 using a rabbit ulnar model; (j) VonKossa staining of implanted scaffold showing new bone formation adjacent to the scaffold (M: microsphere, NB: new bone); (k) trichrome staining showing dense connective tissue formation in the void space among microspheres (CT: connective tissue); (l) . Parallel images of new bone formation sections stained with both Trichrome staining [144].

Hydroxyapatite is an important inorganic bone mineral that gives it its rigidity. It possesses high compressive strength and its osteoconductivity allows for bone cell attachment, migration, and growth [145, 146]. Several studies have revealed that the induction of hydroxyapatite increases the scaffold's osteoconductivity, resulting in a scaffold with a functional biomimicry to the native matrix, making it a suitable environment for cell housing that can facilitate cellular migration, proliferation and differentiation. In an attempt to reinforce the osteoconductivity of the matrix, Levi et al. developed sintered microsphere scaffold prepared from PLGA/ HA nanocrystals for matrix reinforcement and osteoconduction, and salt crystals for macroporosity and control of matrix pore size [143]. Characterization studies revealed that the resultant PLGA/ HA scaffold had Young's modulus and an ultimate strength values ranged between 168-265 MPa and 6-17 MPa, respectively, which was within the range for human trabecular bone. In addition, the microspheres diameter size distribution was between 80 – 300 μm . The scaffold was pre-seeded with human fibroblasts to evaluate its biocompatibility for 14 days. *In vitro* biocompatibility studies revealed that cells were well maintained within the matrix and cell number has significantly increased by day 14 comparing to PLGA alone. In this work, the PLGA scaffold was reinforced with HA to increase its osteoconductivity, resulting in an increase in cell number and enhanced biocompatibility. Despite the advantageous of HA, introducing them in larger amounts could result

in a poorly soluble scaffold that can alter tissue ingrowth and neovascularization during osteogenesis.

To address the solubility issue, a recent and a novel approach was developed in order to increase the osteoconductivity of the scaffold with less HA content by functionalizing the surface of the scaffold with appetite for more efficient bone tissue engineering aiming to produce a biomimetic uniform distribution of appetite on the surface of the scaffold. Soo et al. developed a PLGA/ HA composite scaffold by gas foaming and particulate leaching (GF/PL) method without the use of organic solvents [147]. This study not only attempted to find better alternatives in order to increase the osteocunductivity of the scaffold, but also addressed the limitations associated with solvent-based technique. Briefly, PLGA granules are grinded and mixed with Sodium Chloride particles and sieved to yield particles with a 100-200 Pm diameter. PLGA/NaCl particles are then mixed with HA nanoparticles in a mass ratio of 1:9:1, respectively, and loaded into a disk mold for compression with a very high pressure. The resultant PLGA/HA/NaCl disk is then exposed to CO₂ to create the porosity throughout the structure. Once porosity is created, the disk is then immersed in distilled water to leach out the salt (NaCl). To create a uniform mineral coating of apatite on the surface of the PLGA/hydroxyapatite scaffold, the disk is then incubated in an ion rich simulated body fluid (SBF) solution. Incubation in an ion rich SBF helps creating a sufficient layer of apatite on the surface of the scaffold. The novelty in this work lies behind the addition of the nano-HA particle to the scaffold structure prior to incubation in the SBF, as the presence of the nano-HA particles within the scaffold structure helps inducing a sufficient layer of apatite on the surface of the scaffold compared to PLGA scaffold alone with no nano-HA particles in its structure. It was hypothesized that functionalizing the surface with appetite would enhance the osteogenic potential

of the biomaterial scaffold. SEM images revealed that the appetite layer was uniformly created on the surface of the PLGA/HA scaffold when compared to the PLGA scaffold alone, which showed very poor and not uniform deposition of appetite. In vitro characterization showed improved human osteoblast adhesion, proliferation, alkaline phosphatase expression, and mineralized matrix synthesis on these scaffolds, which were evidenced as compared to that on PLGA scaffolds. In vivo implantation of the scaffolds in a subcutaneous model for 5 and 8 weeks showed enhanced osteogenesis, calcium deposition and extensive amount of mineralization on the PLGA/HA group when compared to PLGA alone, confirming their potential for bone regeneration

This study demonstrated a novel way of increasing the osteoconductivity of a composite PLGA/HA scaffold by exposing appetite on the surface of the scaffold without the interference of any solvents. The resultant scaffold exhibited less ceramic content (HA) comparing to the previous methods [143] and high content of uniformly distributed appetite on the surface. This biomimetic approach of uniformly distributing the appetite on the surface enhanced osteoblasts growth and mineralization *in vitro*, and osteogenesis *in vivo*. Findings from these studies demonstrate the potential of biomimicking the natural bone matrix by introducing HA in efficient amounts that do not alter tissue ingrowth or effect the scaffold's solubility, for more efficient bone tissue engineering.

In addition to the architecture and inherit properties of a polymer based scaffold, the use growth factors to stimulate bone formation is an established approach to treat musculoskeletal disease and trauma. However, spatial control over the release of growth factors is essential in order to eliminate the unwanted side effect and improve tissue repair. Bone formation has been proven to be enhanced

in many reports under the osteoinductive influence of BMP-2. However, this portion may lose bioactivities over a short period of time due to its short half-life, which can result in poor bone defect repair *in vivo* [148]. Using very high doses of proteins to maintain the therapeutic effect is expensive and can lead to undesirable side effects [149-151]. Dexamethasone (DEX) is a bioactive molecule that has extensively been used in bone tissue engineering due to its ability in guiding the differentiation of mesenchymal stem cells (MSCs) toward the osteogenic tendency [152-156]. The direct use of DEX, however, has been limited due to its toxic side effects [157]. Therefore, developing a system capable of exhibiting a spatial deliver over these bioactive molecules in a controlled and sustained fashion and simultaneously is indeed required to eliminate their side effects for effective biomimetic bone regeneration.

In an attempt to address these limitation, Li et al, introduced a biomimetic bone tissue engineering scaffold by developing a new nanoparticles-embedded coaxial electrospun nanofiber scaffold for controlled dual delivery of BMP-2 and dexamethasone (DEX) [157]. BMP-2 was encapsulated into bovine serum albumin in order to maintain the bioactivity of BMP-2 and it was coaxially electrospun with a blend of BSA nanoparticles, DEX and the poly(ϵ -caprolactone)-co-poly(ethylene glycol) (PCE) copolymer having the BSA encapsulated BMP-2 in the core-shell of the nanofibers (Figure 1.8). *In vitro* studies revealed that the bioactivities of both DEX and BMP-2 have been well maintained in the dual-drug-loaded nanofiber system, and a sequential release pattern has been obtained in which DEX expressed a fast release and BMP-2 release lasted for up to 35 days. In addition, further *in vitro* studies demonstrated the ability of the system to induce differentiation toward osteoblastic tendency when compared to the non-loaded group. *In vivo* analysis revealed that the loaded-drug groups exhibited a significantly higher degree of

osteogenesis when compared to the non-loaded group in a rat caldaria model, confirming the synergistic effect of BMP-2 and DEX. Thus, data show that the dual-drug-loaded nanofiber scaffold may have the strong potential in bone tissue engineering application.

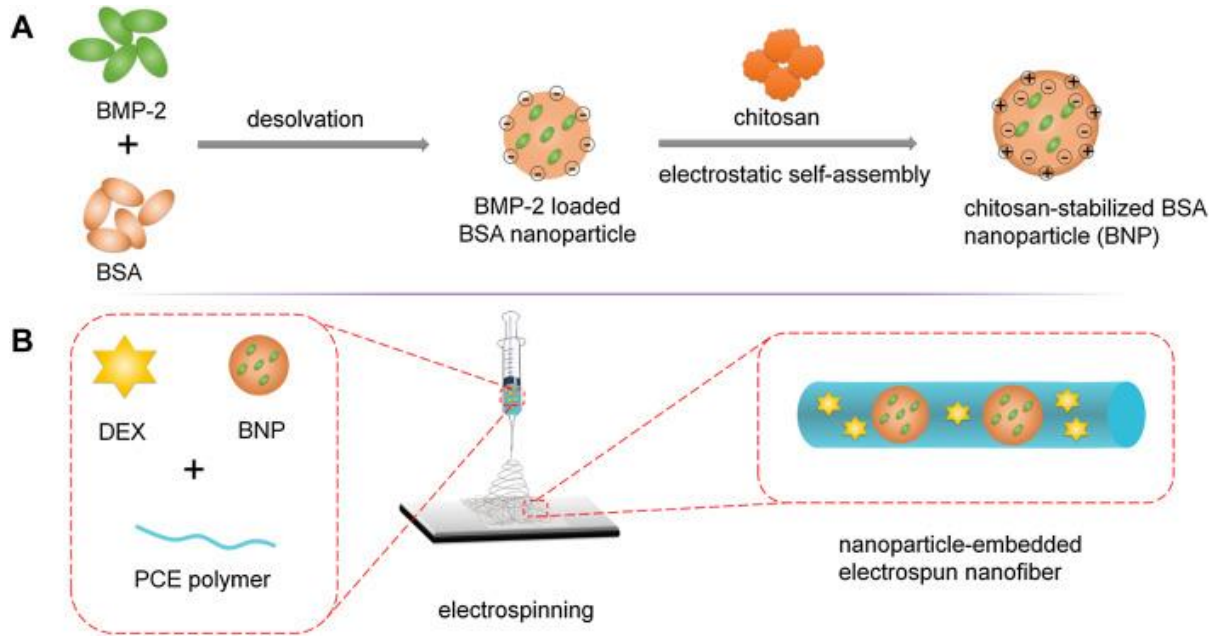


Figure 1.8. Schematic illustration of the fabrication of BMP-2-loaded BSA nanoparticles stabilized with chitosan [157].

1.1.4. Biomimetic Ligament Tissue Regeneration:

1.1.4.1. Ligament Structure and Function:

Ligament is a dense fibrous connective tissue that connects bones together to achieve joint stability [160]. Ligament consists of very complex hierarchically interconnected organized groups of parallel fibers, known as bundles [160]. At the microscopic level, fibroblasts are found entrapped in the matrix. These cells are responsible for the matrix synthesis and they are relatively low in number representing a small percentage of the ligament total volume [161]. Ligament matrix is composed of aligned nano-micro-fibers oriented along the axis displaying a wavy or crimp structure [162]. This complex structure, however, plays a vital biomechanical role in transferring

the loads along the matrix axis allowing the ligament to elongate without sustaining damage upon movement [162]. Differences in the waviness or crimp structure can largely affect the ligament's mechanical properties as fibers with small crimp angle are mechanically weaker than fibers with a wider crimp angle [166]. Biochemically, 75% of the total dry weight of ligament is occupied by different types of collagen such as collagen type I (made up 85% of the total collagen found in the ligament), and types III, VI, V, XI and XIV, whereas the rest is occupied by watery components that are responsible for the viscoelastic behavior of the ligament such as, proteoglycans, and other glycoproteins such as fibronectin and tenascin-C [162]. Proteoglycans is found in various concentrations depending on the mechanical loading to which the ligament is exposed [167]. The higher proteoglycans concentration is found in areas that are subjected to compression, giving the role for proteoglycans in resisting compression loads [168, 169]. Fibronectin is found on the surface of the collagen and it acts as an adhesive glycoprotein that supports cell attachment, in addition to its involvement in the regeneration and the repair of the ligament [170, 171]. Tenascin-C is another glycoprotein that is extensively found during the early stages of the ligament development, which mainly contributes in the ECM network formation to achieve mechanical stability [172].

Ultrastructural studies have revealed that collagen fibers (1 – 20 μm in diameter) found within the ligament are further composed of fibrils (20 – 150 nm in diameter). During ligament development, ligament fibroblasts secrete a molecule known as “procollagen” into the extra cellular space, which is a primary molecule responsible for collagen synthesis. Once it is secreted, a transitional modification takes place allowing the triple helical collagen molecule to line up and start forming fibrils and then fibers to form the extra cellular matrix. This process is promoted by an enzyme

known as lysyl oxide, which promotes the crosslinking between the collagen fiber molecules. The crosslinking reaction is an essential step as it reinforces the matrix and gives collagen fibers such incredible strength [162].

Ligament acts as a connection that connects bones together, for example, anterior cruciate ligament (ACL) connects the femur to the tibia through collagen fibers that are anchored into the bone structure (Figure 1.9) [173]. The change between the flexible ligament to the hard bone is mediated by a transitional zone known as “fibrocartilage”. Fibrocartilage is further divided into two regions, mineralized and nonmineralized. Nonmineralized fibrocartilage is directly anchored to ligament, whereas the mineralized fibrocartilage is directly anchored to the bone matrix. This transitional fibrocartilage zone with its unique gradual transition in structure and mineralization content allows for gradual change in even distribution of stress [174].

From a mechanical point of view, human ACL is exposed to tensile forces ranging from 67 N to 630 N during normal daily activities. However, the maximum tensile load that a human's ACL can withstand before failure was found to be 1730 N, 182 N/mm for linear stiffness, and 12.8 N m for energy absorbed. The Young's modulus of human ACL was found to be 111 MPa and the ultimate tensile stress is 38 MPa [175]. These values increase during ACL development and diminish as the person ages [176].

To this end, understanding the anatomy, orientation, the attachment sites of the normal ligament, mechanical properties and the kinematics is indeed necessary not only for surgeons performing the

reconstruction, but also for scientist in order to achieve a possibly closer biomimetic design for successful ligament tissue engineering.

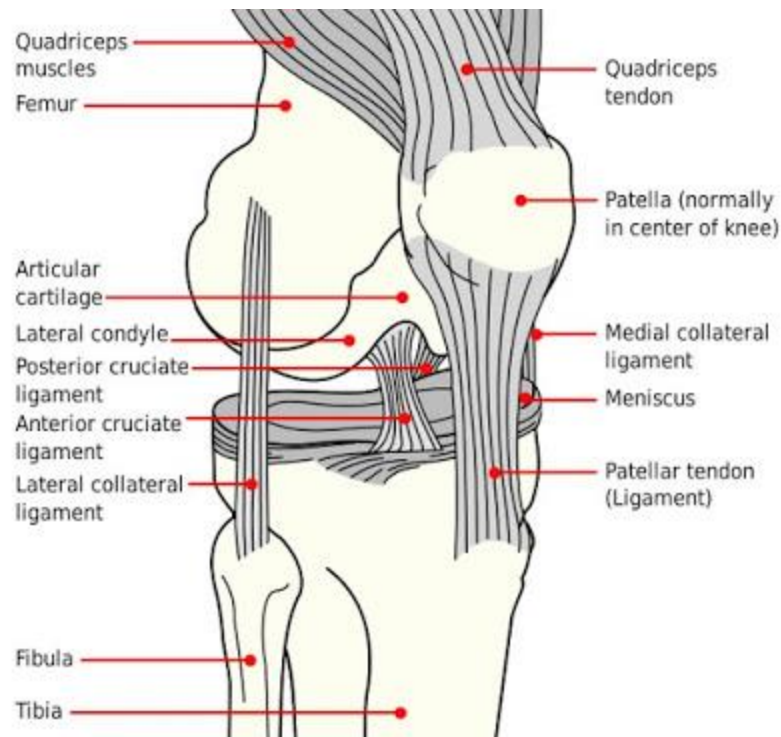


Figure 1.9: Anterior Cruciate Ligament (ACL) [396].

1.1.4.2. Materials for Biomimetic Ligament Tissue Regeneration:

One of the most important preliminary steps for designing any ACL graft is to choose the appropriate material that would achieve the design of a mechanically, physically, chemically and structurally biomimetic ACL graft that resembles the native ACL ECM. All materials with their degradation by-products should be biocompatible that do not elicit any immune response upon implantation or degradation, and should also be biodegradable to allow for collagen bundle formation and tissue ingrowth [177]. The material degradation rate should be comparable with that of the tissue ingrowth, in which a complete degradation to the biomaterial should take place after several months to allow for replacement by the regenerated ligament matrix [182]. In addition, the

materials should be capable of supporting cell adhesion, proliferation and differentiation.

The current ongoing research on ligament tissue engineering, specifically ACL, mainly uses polymers-based materials for graft fabrication such as, natural and synthetic polymers. Natural polymers mainly include collagen, and silk fibroin, while synthetic polymers used for ligament tissue engineering include PLA, PGA, PLLA, and PLGA [178]. The majority of these materials have found a great interest for use in ligament tissue engineering application due to the easy processability of these materials into wide variety of different structures with tailored mechanical and degradation properties that meet the applications needs [178].

Collagen-based scaffolds have been used for ligament tissue engineering due to their biocompatibility, ability to provide functional chemical groups for cellular binding, and due to their prevalence. Using collagen in its simplest form as a graft for ACL reconstruction may not meet the requirements for successful ligament tissue engineering due to its poor mechanical and degradation properties. However, for mechanical reinforcement; collagen can be crosslinked through one of the most common crosslinking methods such as hydroxylsiononleucine (HLNL), dihydroxylsiononleucine (DHLNL), histidinohydroxymeresmosine (HHMD), and nordihydroguaiaretic acid (NDGA). It was reported that crosslinking collagen with NDGA method achieved much improved mechanical properties that matched with the normal ACL, when compared to the other crosslinking methods [179, 180]. Although collagen-based scaffolds are biocompatible, easily modifiable, hemostatic and synergic with bioactive molecules and not toxic, limitations are still present such as, high cost, high level of hydrophilicity, patch-to-patch variation,

complex handling, and the potential of disease transmission, which limit their use for ligament tissue engineering [181].

Silk fibroin is another natural polymer that has been widely used for ligament tissue engineering due to its unique mechanical properties, biocompatibility, slow degradation rate, the ability to genetically control it as well as the easy processability into multiple structures such as gels, films, braided fibers and nanofibers [182]. The elegant mechanical properties and stability of silk fibers are due to the homogeneity of the polymeric back-bone structure, extensive hydrogen bonding, as well as the hydrophobic nature of silk and its crystallinity [178]. The primary advantageous of silk fibroin lies in its noteworthy tensile strength, which is unmatched for other natural polymers [183]. It was reported that silk has an elastic modulus that ranges between 5-9 GPa, a tensile strength of 250-400 MPa, and failure strain values of 23-26% [183]. Another remarkable property about silk fibroin is that it displays surface amino acids, which mainly support cell attachment [184]. Silk fibroin is barely degraded *in vitro*, and slowly degraded *in vivo* (weeks-months) through proteolysis [185]. Silk fibroin-based scaffolds have been reported to exhibit similar mechanical properties to the natural ECM, and biocompatibility both *in vitro* and *in vivo* [185, 186]. These unique characteristics make silk fibroin one of the best natural polymers for ligament tissue engineering.

On the other hand, the tailored mechanical and degradation properties, the easy processability into a variety of different structures and morphologies as well as into specific structures for ligament-like geometries with tuned pore frequencies has established an interest in the use of synthetic polymers for ligament tissue engineering [187]. Several poly- α -hydroxy esters are FDA approved,

and the most common synthetic polymers used for ligament tissue engineering include PLA, PGA, PLLA, and PLGA, [188].

PLA is an aliphatic polyester that is more amorphous and hydrophobic than PGA [189]. PLA usually has two isoform (L- and D-) forms because of the extra methyl group compared to PGA. This, however, slows the degradation rate of PLA when compared to PGA. PLA degrades through desertification, and degrades completely within 10 months to 4 years depending on the molecular weight, crystallinity, shape of the device and implantation site [189].

PLGA is a linear copolymer that can be synthesized at different ratios between its constituent monomers, lactic (LA) and glycolic acid (GA). Depending on the ratio of lactide to glycolide used for the polymerization, different forms, degradation and mechanical properties of PLGA can be obtained, where the higher the lactic content to glycolic generally exhibits prolonged degradation rates, and higher mechanical integrity. These are usually identified in regard to the monomers' ratio used (*i.e.*, PLGA 85:15 identifies a copolymer consisted of 85% lactic acid and 15% glycolic acid) [190]. PLGA undergoes degradation by hydrolysis of its ester linkages, through bulk or surface erosion, in aqueous environments, and it completely degrades within a period of between 6 – 9 months depending on the molecular weight, purity and the shape of the device [191]. PLGA

It was proven that both PLGA and PLLA fibers enhance the overall cellular performance as well as matrix formation of ligament fibroblasts comparing to other biomaterials. Braided PLLA, PLGA and PGA three dimensional scaffolds have been fabricated by Lu et al. Scaffolds were immersed in a solution of human recombinant fibronectin (Fn) to improve cell adhesion [192].

After 14 days of culture with rabbit ACL fibroblasts, scanning electron microscopy (SEM) analysis found that cells seeded on PLLA-Fn and PLGA-Fn scaffolds produced the most matrix, and that PGA was detrimental to matrix formation, thought to be from rapidly produced acidic byproducts (Figure 1.10).

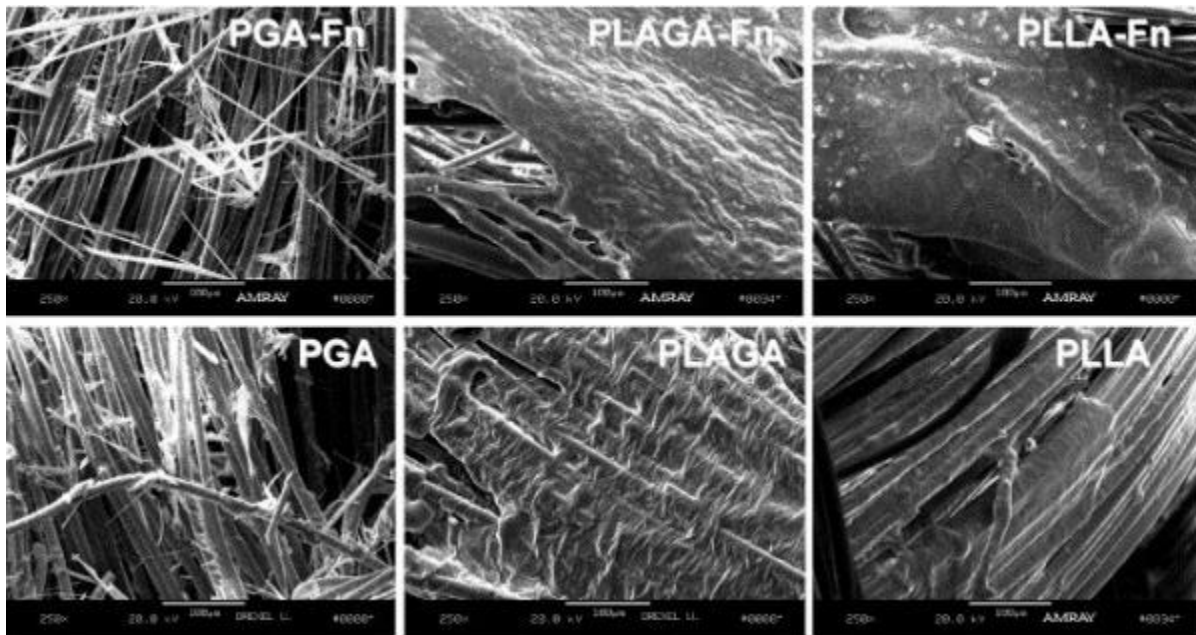


Figure 1.10. ACL fibroblast growth and matrix formation on different synthetic braided scaffolds visualized with SEM. Images were taken after 14 days of *in vitro* culture in 10% fetal bovine serum. (Left) Culture with PGA resulted in substantial matrix degradation from acidic byproducts. (Middle) PLA and PGA in an 82:18 mass ratio showed more sustainable matrix formation, particularly with the addition of fibronectin (Fn). (Right) PLLA scaffolds also displayed considerable matrix formation, which again was amplified by the addition of Fn [192].

1.1.4.3. Scaffold Requirements for Biomimetic Ligament Tissue Regeneration:

Scaffolds are important components of ligament tissue engineering strategy as they define the ultimate shape of the construct while providing the required mechanical strength during regeneration and proper cell attachment sites, in addition to the delivery of regulatory growth factors that stimulate cellular behaviors [195]. Regenerative engineering aims to use scaffolds to produce a functional tissue replacement *in vitro*, which can be then implanted into the body to

induce self-regeneration in vivo [193]. Anatomical location, poor vascularity, volume of the tissue loss, the elegant mechanical and structural properties of the natural ligament and the mediated fibrocartilage zone, are all factors that have to be taken into consideration to achieve a successful and a biomimetic ligament tissue engineering graft [194].

Scaffolds for ligament tissue engineering should mimic all the specific characteristics of the native ligament such as strength, compliance, elasticity and durability without causing any side effects [178]. In addition, they should be biocompatible that do not elicit any inflammatory response or demonstrate any immunogenicity or cytotoxicity when implanted [196]. They should also be biodegradable that demonstrate a compatible degradation rate with the growth rate of the neo-tissue, in which the scaffold is totally degraded by the time the tissue is healed [197]. Degradation rate can be tuned by tailoring many factors such as, device structure, porosity, material crystallinity, molecular weight [198]. The graft material should be bio-resorbable and all of its degradation by-products should be totally eliminated out of the body through natural metabolic pathways with no residual side effects [199]. Appropriate surface chemistry and efficient amount of porosity are indeed important features that ligament tissue engineering grafts have to exhibit in order to enable cellular attachment, proliferation, differentiations, and to permit the diffusion of nutrition throughout the graft [200]. In addition, the scaffold should be capable of osteointegration to the bone matrix to increase the degree of successful ligament tissue engineering and to achieve knee stability.

From a mechanical point of view, ligament is a load-bearing tissue that plays a crucial role in providing joint stability and load transfer during movement such as extension and flexion [178].

The natural ligament inherits its incredible mechanical strength from the unique crimp structure of its bundles, reinforcing its mechanical properties and giving it such incredible stability [162]. Due to the complexity associated with the ligament mechanical properties, many complex biomimetic structures have been adopted for ligament reconstruction such as woven, knitted and braided fibers [178]. Woven and knitted fibers exhibit great porosity throughout the structure, but they are mechanically weak. On the other hand, braided fibers are mechanically and dimensionally very stable, but they are less extensible and porous when compared to the other structures [178]. However, pore size of the braided fibers structures can be regulated by both yarn bundle size and braiding angles [201]. Previous studies have shown that the optimal porosity for ligament scaffolds should be above 50% to create the optimal pore diameter of 100-300 μm , which is needed for *in vivo* tissue ingrowth [214]. Therefore, subsequent balance between fibers structure and porosity is a key role for providing mechanical stability and thus, successful tissue restoration and reconstruction

In addition to the mechanical and structural biomimicry, the scaffold should also serve as a reservoir for local, sustained, and controlled growth factors delivery to regulate cellular activates in order help induce neovascularity and promote ligament tissue regeneration. Several growth factors were shown to be effective in the healing of ligament repair, including, insulin like growth factor I (IGF-I), transforming growth factor- β (TGF- β), vascular endothelial growth factor (VEGF), basic fibroblast growth factor (bFGF), epidermal growth factor (EGF), and platelet derived growth factor (PDGF). Both *in vitro* and *in vivo* data have revealed that these growth factors have the capability to enhance ligament fibroblasts proliferation and matrix production alone or in combine [202-210]. For example, VEGF and PDGF were shown to promote vascularity

within the regenerating matrix [211]. IGF was shown to modify the metabolic activity of cells during ligament healing [212]. In addition, it was shown that TGF- β 1, alone or in combination with EGF, have the potential to strengthen the ligament through increasing matrix production during the healing process in vivo [213]. Therefore, growth factors introduction may serve as a promising tool for regulatory ligament tissue engineering.

1.1.4.4. Biomimetic Ligament Tissue Regeneration Approaches.

One of the major challenges in ligament tissue engineering is to mimic the inherited mechanical and the structural properties of the native ACL, which are crucial for a functional ACL repair or regeneration. Current grafts for ACL tissue replacement do not duplicate the native tissue structurally and lack sufficient flexibility and tensile strength. One of the earliest attempts to engineer a mechanically and structurally biomimetic graft for ACL reconstruction was adopted by Cooper et al. In this study, a PLLA three-dimensional braided fibrous tissue engineered anterior cruciate ligament (ACL) graft has been developed for use in ACL reconstruction [215]. The graft structure was based on the hierarchical complexity found in the native ligament. To construct the graft, PLLA fibers were woven into circular and rectangular braids with different branding patterns and yarn densities to achieve mechanical properties that best resemble the native ligament. The author has evaluated the tensile testing of different shapes and yarn configurations in order to determine configuration that best matches the triphasic nature of the natural ligament. In addition to evaluating the implant's capability to maintain mechanical function, the effect of porosity and pore interconnectivity on cell and collagen infiltration, the capability of the implant to allow for vascularization as well as the *in vivo* response of the ACL cell-seeded/ unseeded graft in a rabbit ACL model for 4 and 12 weeks have been evaluated. Mechanical evaluation of the implant resulted

in stress/strain curves that matched the triphasic nature of the native ligament, with initial low modulus followed by a linear region of increased modulus, and ending with plateaued curves at failure. *In vitro* biocompatibility tests showed good viability of the rabbit ACL cells seeded on the PLLA graft. *In vivo* evaluation revealed that both cell-seeded/ unseeded PLLA graft showed collagen infiltration, blood vessels formation and vascularity throughout the implant, however, the cell-seeded groups (Figure b) showed more organized collagen orientation tissue formation, enhanced vascularity with no fibrous encapsulation when compared to the unseeded group (Figure c). Although the *in vitro* biocompatibility testing showed positive results, a thin layer of fibrous capsule in the unseeded group was evidence as compared to the cell-seeded group. Data from this study suggest the importance of biomimicking the structural and mechanical aspects of the natural ligament tissue, as mechanically and structurally biomimicking the native ACL resulted in enhanced matrix production and scaffold's mechanical integrity. In addition, scaffold's porosity largely contributed in the vascularity found within the engineered graft. Data suggest that a biomimetic ACL graft may lead to promising ligament replacement technology.

In a different attempt to mimic the viscoelastic properties of the ACL graft to resemble those found in the native tissue, Laurencin et al. developed a novel PLLA braided-twist scaffold for use in ACL reconstruction [216]. The graft was evaluated for stress relaxation, cell viability and scanning electron microscopy SEM. In addition, the graft's viscoelastic properties were tested using Maxwell and quasi-linear viscoelastic (QLV) models. Stress relaxation experiments revealed that the braided twist graft showed similar behavior to the native ACL, with final normalized stresses of 87% and 83% after an 8 N load when compared to the braided, twisted fiber and aligned fiber scaffolds. Maxwell study demonstrated that the braided-twist had the most favorable viscoelastic

properties. *In vitro* cell proliferation study showed that there was no significant difference in cell proliferation between the braided-twist and the braided scaffolds. Data from this study suggest that the braided-twist scaffold design may be effective in scaffolds for ACL tissue regeneration as they not only achieved a mechanical and structural biomimicry, but also mimicked the viscoelastic aspects of the natural ACL.

Although these studies showed great mechanical, structural and viscoelastic properties that resemble those found in the native tissue, they do not mimic the mechanical, and structural gradual transition found along the ligament to bone junction, which can lead to the formation of a fibrous scar tissue at the insertion site that lacks all the mechanical and structural properties of the native one. Therefore, mimicking the complexity found at the native tissue is a key role for functional tissue regeneration.

More recently, there has been a serious shift towards the fabrication of gradient scaffolds aiming to mimic the complex properties transition found along the ligament to bone junction for more functional tissue restoration. Laurencin et al. developed a multi-region polymeric based scaffold system for use in ACL reconstruction. The graft system is specifically designed in order to promote ligament regeneration and proper fixation to the bone at the implantation site [217]. The three-dimensional graft system consists of quickly-degrading biocompatible polymeric fiber (17% PLLA), and slowly-degrading biocompatible polymeric fiber (83% PLLA). The middle region of the scaffold is formed from the quickly-degrading polymeric fiber to support ligament fibroblasts ingrowth, whereas the slowly-degrading polymeric fiber forms the two ends of the braided scaffold, which is intended to promote bone ingrowth after being secured into drilled bone tunnels

to serve as bony attachment ends of the scaffold. The degradation rates of the quickly-degrading and the slowly-degrading polymeric fibers are 9 – 12 months, and 1 year respectively. The uniqueness of the design lies on the inclusion of three different region, each with specific pore size, in which the pore size at the bony regions is designed to allow for bone cell ingrowth, whereas the pore size at the middle region is designed to allow for ligament cell ingrowth. This structural gradual transition plays a vital role in supporting the formation of a fibrocartilage-like tissue at the interface. The graft system exhibits porosity at the range of between 50 – 70 %, and pore size between 177 μm – 250 μm . The graft system has been mechanically evaluated resulting in a peak load strength of 500 – 3200 N, with an initial stiffness range of 200 – 700 N/mm. These values were based on a number of 10 – 60 fibers per bundle, and a number of 36 bundles per braid. To evaluate the graft's ability on supporting ligament regeneration and osteointegration, the graft was implanted in a sheep ACL reconstruction model for 12 weeks. In vivo evaluations revealed that there was a significant tissue ingrowth within the ligament region, with a complete osteointegration at the bone tunnels along with the presence of a fibrocartilage-like tissue at the insertion site. An early representative version of the braided graft can be shown in (Figure 1.11).

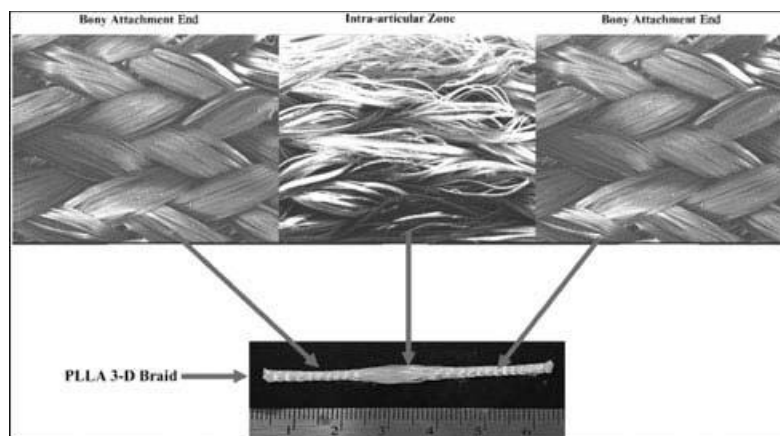


Figure 1.11. Representative image of the three-dimensional braided scaffold developed by Laurencin et al. with distinct fiber organizations in the bony attachment ends and central intra-articular zone. [215]

Considering the scaffold physical properties such as cross-link density, pore size, stiffness and material composition is a key element in guiding the cell behavior, especially musculoskeletal cells. In another gradient study by Oh et al, a scaffold with different pore size gradient was fabricated using PCL for ACL reconstruction following a centrifugation method (Figure 1.12) [64]. The scaffold exhibits different pore size gradients along the three regions, starting from 405 μm at the bony region, with a gradual decrease to 186 μm at the end of the ligament region. Osteoblasts, chondrocytes and fibroblasts were seeded in the three graft regions, respectively. Cell counting was performed along the graft, and it was found that both osteoblasts and chondrocytes showed increased in cell number at the regions with pore size 380-405 μm , while fibroblasts were more localized at areas with pore size of 186-200 μm . These findings suggest that different pore sizes can strongly affect cell behavior such as proliferation and cell fate. Thus, providing the appropriate gradient in pore size, may act as a useful tool that can guide cell differentiation and proliferation during complex tissue regeneration [64].

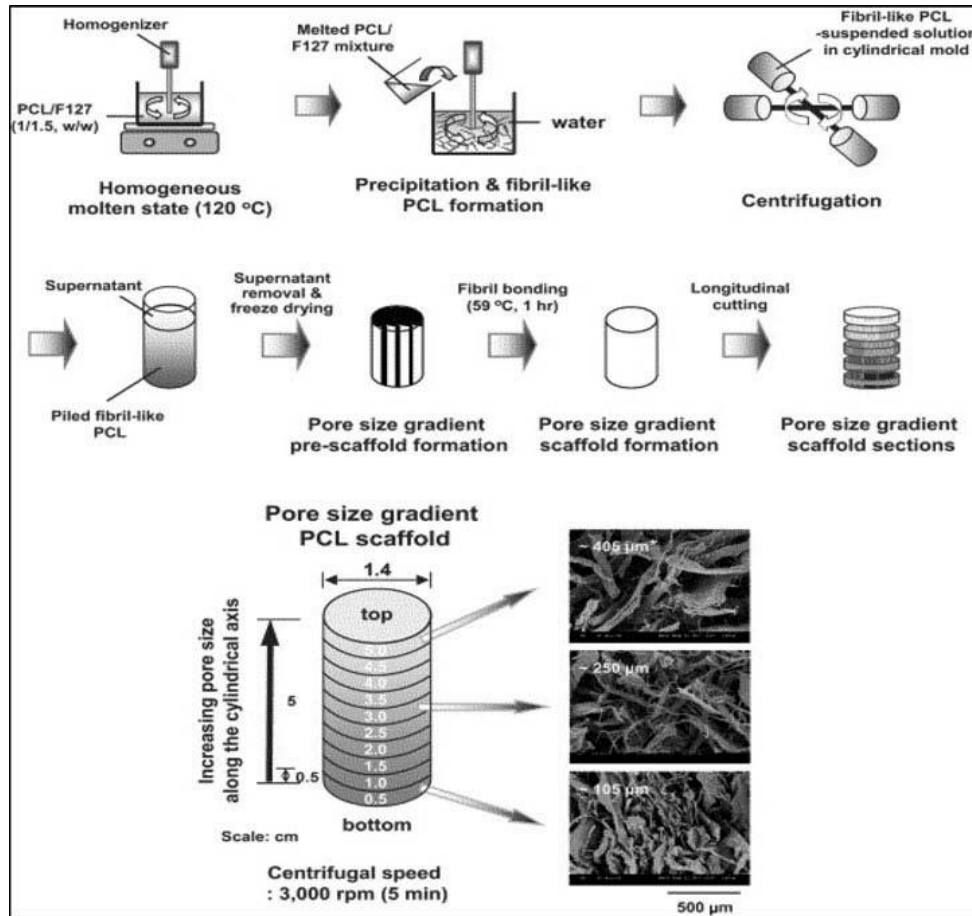


Figure 1.12. (top) Schematic diagram showing the fabrication process of a pore size gradient in PCL scaffolds by a centrifugation method and (bottom) SEM photographs of the top surfaces of the PCL scaffold sections along the longitudinal direction ($\times 100$; *, average pore size) [64]

A wealth of evidence has shown that cells grown on surfaces with different architectures and stiffness demonstrate altered cell morphologies and gene expressions [122]. Thus, providing a biomimicry ECM architecture may be used to ultimately control cell behavior and fate. In a study by Thayer et al. a thin (~ 5 fiber thick) layers of aligned electrospun microfibers ($0.7 \mu\text{m}$) were embedded within collagen hydrogels containing mesenchymal stem cells (MSCs), which were cultured for up to 14 days [218]. Electrospun microfibers were fabricated from polycaprolactone (PCL), poly(ester-urethane) (PEUR), or a 75/25 PEUR/PCL blend, with elastic moduli of 31, 15, and 5.6 MPa, respectively. It was hypothesized that mimicking the mechanical and structural aspects of the native ACL can work as a cue to guide cell fate. However, *in vitro* gene expression

assay showed significantly higher expression of the specific ligament marker (scleraxis) in MSCs seeded on the composite containing 5.6 MPa fibers along with high expression of the contractile phenotype marker α -smooth muscle actin when compared to the stiffer fiber composites. In addition, further structural studies revealed that cells within the 5.6 MPa microfibers composite exhibited more organized orientation along the aligned axis of the microfibers when compared to the 15 and 31 MPa microfiber composites.

Confirming the findings from the aforementioned study, degradable PLGA nanofibers-based scaffold has been in vitro evaluated by Moffat et al [79]. The effect of fibroblasts attachment, alignment, and gene expression has been tested as a function of nanofibers organization (aligned vs randomly aligned). It was found that underlying orientation primarily guided ligament fibroblasts morphology, alignment and gene expression. In addition, it was found that the deposition of collagen types I and III as well as mechanical properties were directly related to the underlying nanofibers orientation. Findings from these studies indicate that nanofibers organization and stiffness play crucial role in guiding cell response, which clearly highlight biomimetic potential of nanofibers to the ligament native tissue.

Growth factors have been also used to support ligament tissue engineering for their active roles in establishing the complex structure of the enthesis, healing the tissue after injury, and maintaining tissue homeostasis. In a study by Hannah et al. a hierarchical bioactive scaffold for ligament tissue engineering using connective tissue growth factor (CTGF)-conjugated PCL aligned nanofiber bundles was developed (Figure 1.13 a) [219]. This study not only intend to mimic the mechanical and the complexity found within the ACL structure, but also introduced a biochemical factor in

order to provide a biomimetic biological environment suitable for cell housing, similarly to the natural ECM. In this study, three different scaffold geometries were fabricated as follows; (1) individual nanofiber bundles (Figure 1.13b), (2) scaled-up scaffolds that are composed of 20 nanofiber bundles (Figure 1.13c), and (3) small scaffolds composed of only of 4 nanofiber bundles (Figure 1.13d). In order to introduce the growth factor to the scaffold, it was covalently bound to the surface of the individual nanofiber bundles, or on the surface of the scaffold consisting of multiple nanofiber bundles. Controls for these scaffolds were the same scaffolds but non-CTGF-conjugated. The conjugation efficiency and the release of conjugated CTGF were assessed using X-ray photoelectron spectroscopy, assays, and immunofluorescence staining. In addition, all Scaffolds were pre-seeded with MSCs, and the cellular response for these constructs was evaluated both *in vitro* and *in vivo* in a nude mouse subcutaneous model for 6 weeks. Results showed that more than 90% of the loaded growth factor has been conjugated into the surface of all scaffolds, indicating the efficiency in loading. *In vitro* release studies of the CTGF-conjugated nanofiber scaffold showed a sustained and linear release of the biochemical factor for the first 5 days with no burst release, and a complete release of the growth factor after 15 days of incubation at 37 C in PBS. In addition, further results showed that all CTGF conjugation scaffold resulted in more cell proliferation and enhanced ligament-specific tissue formation *in vitro* and *in vivo* when compared to all the other non-CTGF conjugated groups, owing the great potential for hierarchical electrospun nanofiber bundles conjugated with CTGF as scalable and bioactive scaffolds for ACL tissue engineering.

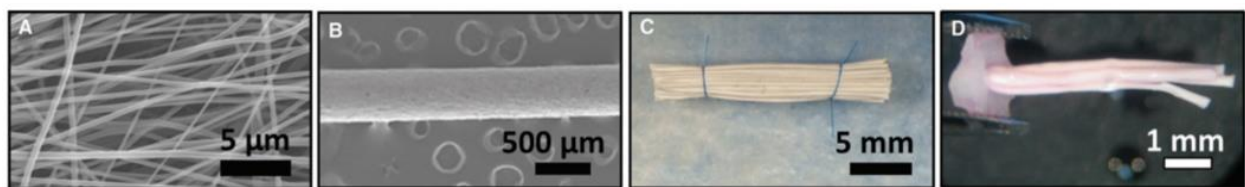


Figure 1.13. Aligned nanofibers (A), nanofiber bundle (B), scaffold composed of *20 nanofiber bundles

(C), and small scaffold composed of 4 nanofiber bundles (D) [219].

1.1.5. Biomimetic Skin Tissue Regeneration:

1.1.5.1. Skin Structure and Function:

Skin is the largest organ in the human body, covering the entire exterior of the body and forming about 8% of the total body mass, and it is necessary for the animal survival and hemostasis [257]. Skin mainly functions as a protecting interface, physically shielding internal organs and tissues from external insults and pathogens [258]. Functionally, the skin is responsible for maintaining the homeostasis of the living organism, through regulating the body temperature, hydration and Vitamin D synthesis [259]. Damages to any part of the skin will expose the individual to the risk of other health complications. Structurally, skin is composed of many cell types that are derived from three distinct embryonic origins: neurectoderm, mesoderm, and neural crest [259]. The skin is comprised of two layers that cover a third fatty layer. These three layers differ in function, thickness and strength (Figure 1.14). The outermost layer is called the epidermis, and is primarily composed of stratified squamous epithelium of keratinocytes. Keratinocytes are derived from neurectoderm and occupies almost 90% of the total epidermal cellular population. Further, keratinocytes are responsible for supporting the cohesion of the epidermal structure and the barrier function [259]. Moreover, the epidermis is comprised of other cell types such as, melanocytes of neural crest origin (contain the skin pigment), Merkel cells of the neural origin (responsible for pressure sensing), and Langerhans cells of mesoderm origin (responsible for processing antigen) [259]. Epidermis is a highly regenerative layer, due to the presence of stem cells which contribute in the process of wound healing during injury.

The middle layer is called the dermis. The dermis is a connective tissue that is responsible for providing the skin with the mechanical support and elasticity. The dermis layer is comprised of dermal fibroblasts of mesoderm origin, of which found entrapped within the extracellular specialized matrix. In this layer, collagen fibers are interwoven with proteoglycans, elastin, fibronectin, and some other components. Dermal fibroblasts are responsible for synthesizing the extracellular matrix that makes up the skin. The first two layers, the epidermis and the dermis, are connected by a basement membrane that is composed of various integrins, laminins, collagen fibers, and some other proteins that play important vital roles in regulating and maintaining epithelial-mesenchymal cross-talk [259]. In the dermis, papillary loops with candles-like structure, called the dermal papillae, contain the microvascular and neural networks and extends the surface area for these epithelial mesenchymal interactions. The dermis further contains of sebaceous glands, eccrine glands, apocrine glands and hair follicles, all of which are from a neurectoderm origin. In addition, blood vessels and lymphatic vessels of the mesoderm origin, and sensory nerve endings of the neural crest origin are all found in the dermis. The last layer is called the hypodermis. This last layer is located right beneath the dermis layer and it is primarily composed of adipose tissue of mesoderm origin, and separates the dermis from the underlying muscular fascia [259].

Human skin is a very elastic material that can be stretched to several times its original size and still maintain its original phenotypic [264-267]. This impressive feature return to its specialized matrix mechanical structure [268]. When the skin is stretched beyond its physiological limit, series of cascade of events take place to restore its hemostatic balance that include, activation of ion channels, conjugation of integrins, growth factor receptors and G-receptors with protein reactions

[269]. These series of events result in increased mitotic activity and collagen synthesis [269 - 271]. The same series of events are initiated when damages to the skin occur during injuries that also result in increased mitotic activity and the synthesis of collagen in order to restore the function of the skin damaged skin. However, massive injuries such as chronic wounds cause irreversible deformation and damage to the skin, resulting in a loss of its mechanical properties [272, 273]

Human skin is a complex living material, composed of several heterogeneous layers: epidermis, dermis and hypodermis, with different mechanical properties, and thickness variation depending on the anatomical location [274, 275, 276, 277]. Despite the complexity and the mechanical diversity found within the three different layers of the human skin, the skin is mechanically treated as a homogenous material in all induction measurements [278]. From mechanical point of view, the human's skin mechanical properties are age dependent, where measurements of mechanical parameters are normally higher in newborn children than in elderly adults. For example, the mean ultimate skin deformation before bursting is 75% for newborns and 60% for the elderly [279]. In addition, uniaxial loads and elasticity modulus have average values of 21 N/mm² and 70 (MPa) in newborn and 17 N/mm² and 60 (MPa) in elderly adults respectively. This clearly explains why elderly adults have much thinner, stiffer, less dense and less flexible of a skin when compared to newborn children [280, 281].

Due to the complexity associated with the structure and function of skin, engineering skin equivalent to the normal skin has been challenging. Current skin tissue engineering approaches primarily focus on regenerating the dermis and the epidermis layers to restore the structural integrity of the skin, rather than regeneration for a functional restoration. Mechanical properties

measurements may also differ than normal in the case of diabetic and some other more factors. A complete awareness of the skin anatomy and structure, in addition to the factors affecting the mechanical properties is indeed required for effective biomimetic skin tissue engineering.

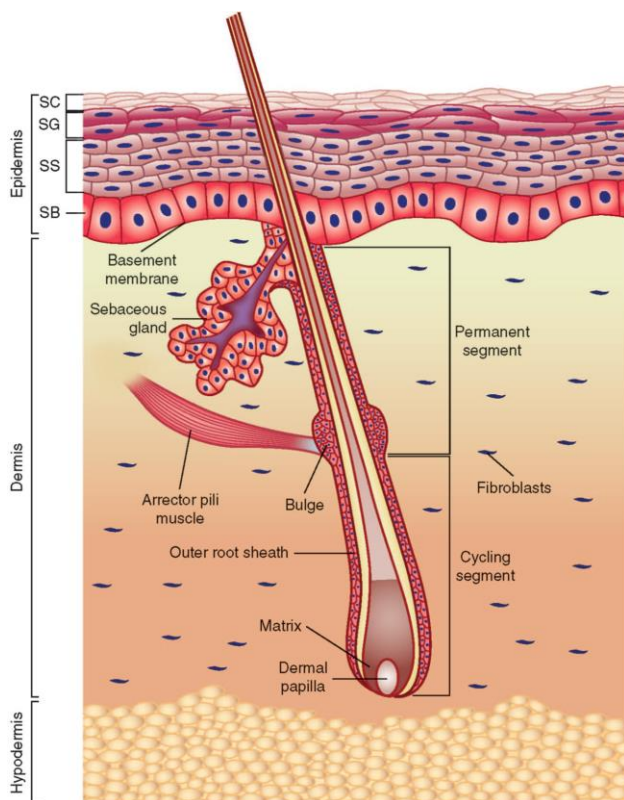


Figure 1.14. Anatomy of the skin. Skin is composed of three layers, starting with the outermost layer: the epidermis, dermis, and hypodermis. Epidermis is a stratified squamous epithelium that is divided into four layers, starting with the outermost layer: stratum corneum (SC), stratum granulosum (SG), stratum spinosum (SS), and stratum basale (SB). Outer root sheath of the hair follicle is contiguous with the basal epidermal layer. Stem cell niches include the basal epidermal layer, base of sebaceous gland, hair follicle bulge, dermal papillae, and dermis [259].

1.1.5.2. Materials for Biomimetic Skin Tissue Regeneration:

Several natural, synthetic or composite biomaterials have been utilized for effective biomimetic production of skin tissue engineering scaffolds. Composite biomaterials are used in skin tissue engineering due to the fact that they resemble the natural ECM, and can be tailored to inherit a wide variety of instructive cues that can be used to guide the attachment, proliferation and

differentiation of cells for enhanced skin tissue regeneration. Natural biomaterials used for skin tissue engineering and construction could be of protein or carbohydrate. Such materials stimulate the healing by repair of the damaged tissue and promote effective skin regeneration through providing biomimetic surface properties for better cell adhesion and thus wound repair [260]. On the other hand, synthetic polymers are used for their tailored degradation properties and architecture characteristics, all of which contribute in the process of wound repair [261-263].

In skin tissue engineering, the most commonly used natural biomaterials are protein-based such as, collagen, gelatin, silk, and fibronectin. Collagen is the most abundant naturally occurring protein in the body responsible for maintaining structural integrity, representing approximately 25% of the total dry weight of mammals [282]. The skin ECM is primarily composed of collagen fibers that provide the skin with structural integrity and tensile strength to support tissue growth. Within the skin, collagen is synthesized by the skin's fibroblasts to stimulate faster wound healing process [283]. Structurally, collagen inherit a helical polypeptide structure with repeating sequence units of the amino acids glycine, proline and hydroxyproline [284, 285, 286]. Out of the 29 different collagen types that have been already identified, skin is predominantly composed of collagen type I, where collagen type III makes up very minor portion of the skin [283]. Collagen-based skin substitutes have been reported to be effective in accelerating wound healing by providing an appropriate environment for fibroblast and keratinocyte proliferation [284]. Moreover, it has been reported that collagen can be processed into a wide variety of dressing formulation for wound and burn repair that include, collagen sponges for deep skin wounds [287, 288], collagen absorbable membrane [289], collagen composite films [290], composite of type III collagen with polysaccharides [291, 292], drug loaded collagen hydrogels [293], microfiber

collagen scaffolds [294], and electrospun collagen nanofibrous scaffolds. Amongst all, electrospinning is the most extensively used technique to fabricate collagen-based scaffolds for skin tissue engineering due to the compositional and structural resemblance to the native ECM. Gelatin, the denatured form of collagen, is another remarkable natural biomaterial for skin tissue engineering that offers many advantages over collagen as it inherits all the necessary arginine-glycine-aspartic acid (RGD) sequences that allows for enhanced cell adhesion, and it is less immunogenic [295, 296]. Many reports have demonstrated the advances of the differently formulated gelatin-based scaffolds in facilitating wound healing and tissue growth such as, gelatin electrospun nanofibers [284], gelatin-alginate sponge [297], and gelatin containing EGF [298]. Gelatin is suggested to be a great candidate for treating wound and burn skin tissue.

Silk has been utilized as a promising biomaterial for skin tissue regeneration and wound healing. Silk is extracted from silkworms and it is found as a classical fibrous protein in nature. Silk proteins are found in two different forms in nature, either fibroin (hydrophobic) or sericin (hydrophilic); however, the biodegradable silk- fibroin is the preferred over the sericin for its great biocompatibility, high permeability for nutrition, due to the fact that it has been widely used as a skin substitute for wound repair [298 - 300]. Silk fibroin-based scaffold have been prepared in the form of electrospun nanofibers, films and woven matrixes of microfibers. Out of these silk fibroin scaffold fabrication methods, silk fibroin-based scaffolds prepared by electrospinning have attracted much attention as a scaffold design and material for wound dressing as they exhibit more surface area to volume ratio of spread collagen that promoted enhanced cell adhesion and proliferation of dermal fibroblasts and keratinocytes when compared to the other fabrication methods of silk fibroin based scaffolds [301]. This demonstrated a rapid re-epithelialization and

less scar formation due to the increased proliferation of keratinocytes in the wound setting [302]. It is suggested that silk fibroin may be able to address many skin tissue engineering limitations due to its biocompatibility [303, 304], material versatility and mechanical robustness [305, 306], controllable degradability [307 - 309] and positive impact on wound healing effect.

Fibronectin is a major multifunctional component of the extracellular matrix (ECM). Fibronectin plays a crucial role in wound healing as it supports the migration and the proliferation during the recovery process [310]. Fibronectin has been used in many settings either alone or with the combination of collagen and with or without fibroblasts as a skin substitute to treat different forms of skin losses due to burn, or diabetic ulcer [311, 312]. Because of the failure to promote vascularization in vivo, and the severe stretching fibronectin-based scaffold exhibits, the number of fibronectin-based material is limited in the tissue engineering field [313]. Further studies are indeed required in order to address limitations associated with the usage of fibronectin as a biomaterial for skin tissue engineering

Synthetic biomaterials have been extensively used for skin tissue engineering due to their tailored structural, mechanical and degradation properties as well as easy processability into wide variety of different geometries which render them as great biomaterials for the development of biomimetic skin substitutes. Most of synthetic biomaterials are either degradable or non-degradable. Biodegradable synthetic biomaterials are preferred over the non-degradable biomaterials due to their degradability nature, which in turn can facilitate a faster neo-tissue ingrowth and better tissue infiltration, in addition to minimizing the chance for a secondary surgery after implantation [314]. A wide range of synthesis biodegradable polymers such as, poly(lactic acid) (PLA), poly(glycolic

acid) (PGA), poly(lactic-co-glycolic acid) (PLGA), poly-L-lactic acid (PLLA), and polycaprolactone PCL, have been used for and skin tissue engineering due to their intrinsic tailored properties, and more importantly, their non-toxic degradation [284, 315]. PLGA have been used in the form of 3D electrospun nanofibers skin graft to treat chronic wounds in a rat model *in vivo*, which resulted in a complete wound healing and re-epithelialization after 14 days [316]. Similarly, PLA and PLLA membranes as artificial skin substitute have been evaluated for their potential to treat chronic wound (2 x 3 cm) in a rat model *in vivo*. Histological analysis revealed that chronic wounds treated with PLA and PLLA membranes completely healed after 21 days with extensive collagen production [317]. Both PCL [318] and PGA [319] have been also shown to enhance re-epithelialization at the wound site. Although synthetic biomaterials have recently shown advances in many tissue engineering applications including utilizing them for substitutes, they lack all the ligands required for cell adhesion, which can result in poor cell adaption to the matrix and thus, poor tissue formation. The native ECM resembles some properties that are found in synthetic materials only or natural materials only, however, developing synthetic/natural composite scaffolds is the best solution to address the disadvantages associated with synthetic scaffolds, as it will help in the mutual enhancement of the scaffold properties and thereby allowing controlled degradation and mechanical properties as well as improving the biocompatibility, and providing cells with all the necessary physical and chemical cues that are naturally inherited by the natural ECM, to achieve the best possible biomimicry to the native ECM for effective skin regeneration [130].

The biomimicry potential of composite biomaterials to the natural ECM render them as great candidate for skin tissue regeneration and wound healing. Composites could be a mixture of

different natural biomaterials, different synthetic biomaterials, or the combination of both. The mixing of materials of different classes and different intrinsic properties to obtain composite scaffolds seems particularly promising as limitations of single material scaffolds such as poor biocompatibility, surface properties, or poor mechanical properties are often overcome by the composite nature. As an example, for synthetic/natural composite biomaterial, Neishaboor et al. developed composite microsphere system containing PLGA/Chitosan conjugated with stratafin for wound healing [320]. The scaffold served as a multifunctional product, in which chitosan provided drug binding ability and PLGA provided protection against burst release of the drug. This work has demonstrated the feasibility toward composite scaffolds and their potential to serve as multifunctional products. Synthetic/synthetic composite scaffolds have been also prepared for skin tissue engineering. Lueng et al. developed a 3D electrospun nanofiber PCL/PVA composite scaffold as a drug carrier for wound healing [321]. To fabricate the scaffold, an initial of PCL with a thickness of 200-400 μm was first electrospun, followed by electrospinning a second layer of drug loaded-PVA, and finally another layer of PCL was electrospun to sandwich the drug loaded-PVA layer. PVA crosslinking was performed by spraying sodium tetraborate solutions onto the fibers after electrospinning. In this study, the scaffold served as a multifunctional, in which PCL provided the mechanical and structural integrity of the scaffold, whereas the crosslinked PVA controlled the drug release, which was evidenced by the drug release data when compared to the non-crosslinked PVA fibers.

Findings from these studies demonstrate the potential of the composite scaffolds in enhancing wound healing for effective tissue regeneration. Composite scaffolds allow for mixing of materials of different classes and different intrinsic properties to enhance the scaffold's overall performance

and capability to support cell attachments and proliferation, while acting as a template for tissue regeneration. These optimized composite-based scaffolds were used as modular building units for skin tissue engineering.

1.1.5.3.Scaffold Requirements for Biomimetic Skin Tissue Engineering:

Skin undergoes serious of events after injury in order to restore its function that include, migration of fibroblasts to the site of injury, secretion of extracellular matrix (ECM) by fibroblasts, formation of keratinocytes followed by the differentiation of keratinocytes to form the outermost layer of epidermis; such as stratum lucidum and stratum corneum [322]. Skin injuries are either acute (small skin wounds) or chronic (large skin wounds). Acute wounds are minor wound that are more likely to self-heal through simple contraction and growth of the cells inside the wound. However, large skin wound usually take much longer to heal and are more prone to risks, such as inflammation, infection, scar formation, which results in the formation of chronic wounds. Some factors such as older age or disease conditions such as diabetes, and renal infection, etc., can largely affect the normal wound healing process thus resulting in poor tissue restoration. Therefore, it is very important to put these factors into consideration while designing skin substitutes to achieve a successful and a biomimetic skin tissue engineering graft [322 - 325]. Ideally, scaffolds for skin tissue engineering should serve as a 3D supporting framework or template for tissue regeneration while simultaneously preventing scar formation during the very first early stages of wound healing [326]. Skin tissue engineering scaffolds should be biocompatible that don not elicit any immune response upon implantation, and biodegradable with a compatible degradation rate to the rate of the neo-tissue formation. The scaffold should possess high pore volumes with interconnectivity throughout to enable cell infiltration, proliferation, nutrition exchange and waste removal. The scaffold should mechanically mimic the natural skin tissue with tailored mechanical properties and

elasticity; however, a subsequent balance between porosity and mechanical properties is indeed required in order to achieve mechanical stability. Architecturally, the scaffold should resemble the native ECM and should possess the appropriate surface chemistry to provide a niche for seeded cells for adhesion, proliferation and differentiation. The scaffold should also serve as a reservoir for controlled and spatial delivery over growth factors to stimulate cellular recruitment, proliferation and differentiation. It is anticipated that a biomimetic scaffold resembling the mechanical, physical, and structural aspects of the native ECM while acting as a delivery vehicle for cells or/and growth factors can have the potential for effective skin tissue regeneration [327 - 328].

1.1.5.4. Biomimetic Skin Tissue Regeneration Approaches

Mimicking the mechanical and structural aspects of the natural ECM is of extreme importance in order to guide cellular behavior and fate. Most skin tissue engineering scaffolds can be easily tailored in order to obtain the initially desired mechanical and structural properties. However, most of these substitutes fail to retain their mechanical and structural integrity after *in vitro* culturing, limiting their potential use *in vivo*. Skin tissue engineering scaffolds must have the ability to retain their structural and mechanical integrity after *in vitro* culture or when exposed to external forces during the process of implantation into the defect site *in vivo*. After surgery, the structure at the implant site must provide sufficient biomechanical support during the process of tissue regeneration and structure degradation. Synthetic biomaterials have been extensively used as scaffold materials for skin wound healing applications for their elegant mechanical properties and ability to be processed into fibrous structures that resemble the native ECM structure. In addition, synthetic biomaterials have been extensively used as composite with other naturally derived

biomaterials to provide the required mechanical reinforcement for more effective skin tissue regeneration. Venugopal et al. developed a biocompatible PCL/collagen electrospun nanofiber scaffold for wound healing applications that resembled the native ECM mechanically and structurally (Figure 1.15 A, B) [329]. The study not only intend to develop a skin graft that mechanically and structurally mimic that native ECM, but also able to retain its mechanical and structural integrity after *in vitro* culture for potential clinical translation. The scaffold was morphologically and mechanically characterized and the behavior of human dermal fibroblasts on both PCL/collagen and PCL electrospun nanofiber scaffolds have been examined. The fabricated scaffold had an appropriate high pore volume of 90% with pore size of $2.252 \pm 0.876 \mu\text{m}$. *In vitro* evaluations revealed that human dermal fibroblasts seeded on PCL/collagen elctrospun nanofiber scaffolds showed enhanced cell morphology and proliferation after 2, 4 and 6 days in culture when compared to the PCL alone (Figure 1.15 C, D). In addition, the scaffold's mechanical integrity was evaluated after 6 days in culture to examine the ability of the scaffold retain its mechanical integrity for its potential to be used for transplantation. Results from this test showed the mechanical stability (8.79 MPa) of the scaffold, suggesting that it can be used as an allogenic cultured dermal substitute for transplantation *in vivo* (Figure 1.15 E).

In this study, PCL/collagen was used in order to produce a mechanically, structurally, and biologically biomimetic scaffold for sufficient wound healing. The scaffold served as a multifunctional, in which PCL provided the mechanical and structural integrity to the scaffold, whereas collagen exposure influenced cell adhesion directly or indirectly through binding with other ECM molecules such as fibronectin, laminin to cell surface glycoprotein, which in turns provided the required adhesion sites that enhanced cell attachment. This study demonstrated the

feasibility toward synthetic/natural composite biomaterials and their positional to be used as scaffold materials for the production of mechanically and structurally biomimetic substitutes for wound healing.

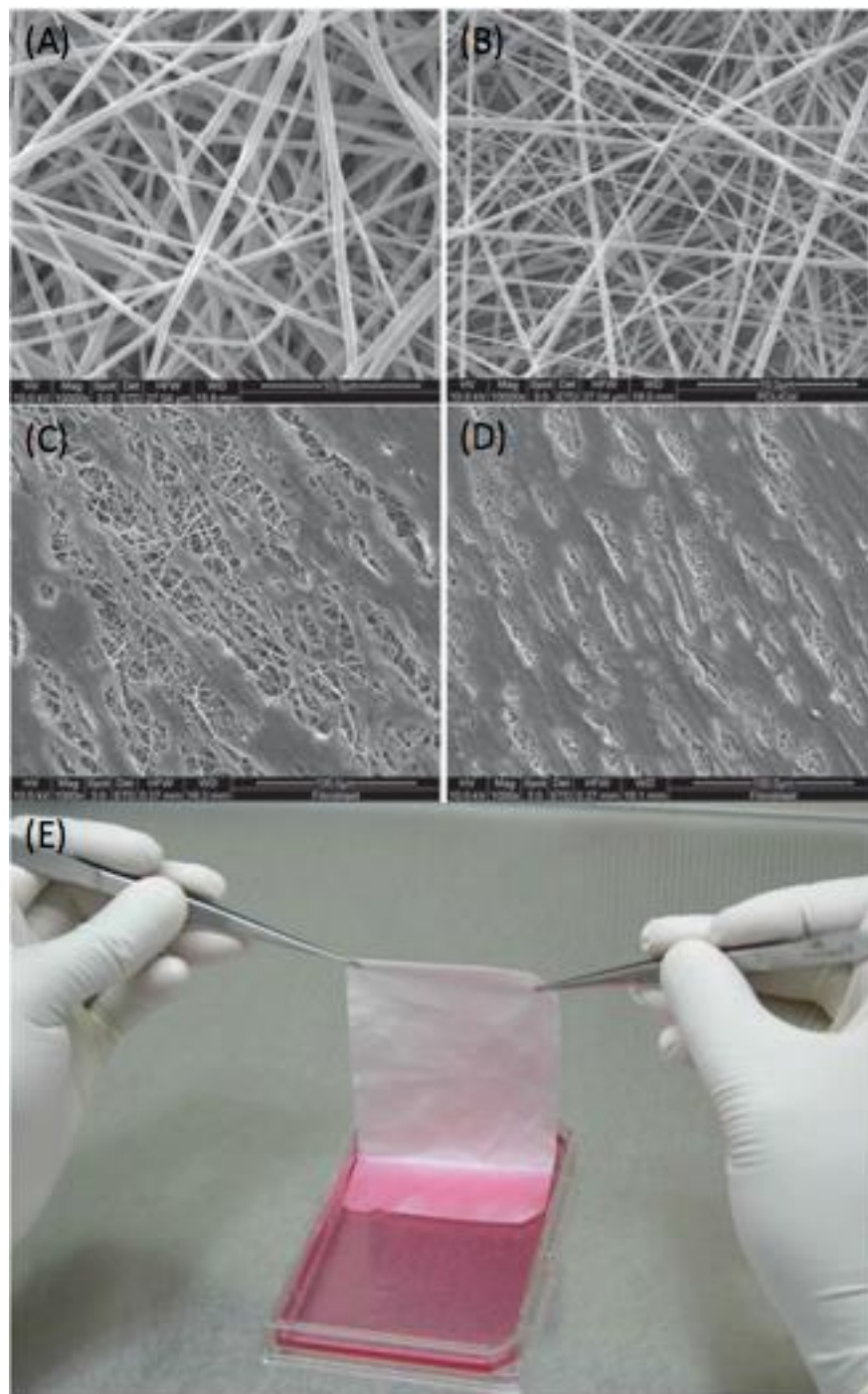


Figure 1.15. Electrospun nanofibers, (A) Polycaprolactone, (B) PCL/collagen nanofibers (NUS), and scanning electron microscopy morphology of fibroblast culture on nanofibrous scaffolds. (C) Polycaprolactone, (D) PCL/collagen nanofibers, and (E) cultured dermal substitute (Fibroblast cultured on PCL/Collagen nanofibrous membrane) [329].

Beside the use of composite biomaterials, Stem cell-based therapies are expected to have a great impact in medicine and are also thought to be a powerful tool for the treatment of a wide spectrum of lesions including skin wounds [330]. Amongst all different types of stem cells, bone marrow derived stem cells have been shown to differentiate into different tendencies including epithelial cells of the lung and liver, and into skin fibroblasts. Many promising results have shown the positive effect of MSCs on chronic wound healing through systematic or local transplantation of these cells [330]. The mechanism of which MSCs contribute to the wound healing process is by either differentiating into phenotypes of various damaged cells or by enhancing the repair process through the secretion of endogenous growth factors or cytokines that accelerate the wound healing process [331]. Wu et al. proofed that wounds treated with BM-MSCs exhibited significantly accelerated wound closure with increased re-epithelization, angiogenesis, and cellularity [332]. Paunescu et al. evaluated the ability of MSCs to differentiate into epithelial-like cells by simply culturing them in using EGF, keratinocyte growth factor (KGF), hepatocyte growth factor, and IGF-II. It has been shown that many factors including the surface chemistry, mechanical properties or even architecture of the underlying substrate can trigger MSCs to differentiate into the epithelial lineage [339]. Ma et al. developed a PLGA/collagen electrospun nanofibers composite scaffold that structurally, mechanically and biologically resembled the natural ECM, for culturing BM-MSCs, which was further transplanted into a full thickness wound bed in Sprague-Dwaley rats [340]. Four different experimental groups were involved in the study, (1) open wound bed with no scaffold which served as a negative control, (2) PLGA/collagen scaffold free of cells which served as a positive control, (3) PLGA/collagen scaffold with low cell density, and (4) PLGA/collagen

scaffolds with high cell density (Figure 1.16). Histological analysis revealed that PLGA/collagen with high MSCs resulted in a complete wound closure within 10 days when compared with the other groups. The author further revealed that the architecture, exposure of collagen and resembling the natural ECM mechanically and structurally as well as transplanting it in a wound bed environment all stimulated MSCs to differentiate into epithelial tendency, which in turn accelerated the formation of hair follicle and subcutaneous glands as well as promoted epithelial ingrowth through chemotactic interaction and therefore facilitated the delivery of follicle progenitor cells toward the center of wound during re-epithelialization.

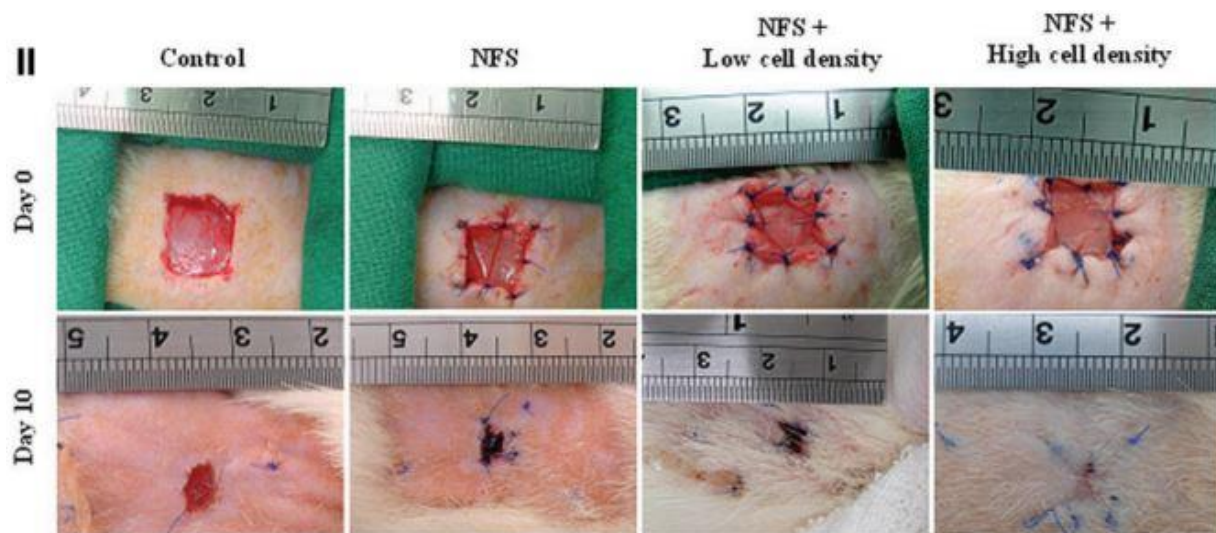


Figure 1.16. Appearances of wounds in different groups on days 0 and 10 [340].

The important role of growth factors for cell migration, proliferation, differentiation in the wounded areas has been recognized. *In vivo*, growth factors are endogenously secreted within the ECM by cells themselves in constant rates to stimulate cellular proliferation and differentiation for tissue regeneration or remodeling. Efforts in tissue engineering have focused on the incorporation of growth factors such as fibroblast growth factor (FGF), Epidermal growth factor (EGF),

Keratinocyte growth factor (KGF), Insulin-like growth factor-1 (IGF-1), Platelet-derived growth factor (PDGF), Transforming growth factor-b (TGF-b), into the matrix scaffolds [333]. Numerous growth factors incorporation methods have been developed aiming to achieve spatial release over growth factors to mimic the endogenous release environment for more effective tissue regeneration. one effective way of incorporating growth factors is by introducing them coaxially in the core shell of a polymeric nanofiber for tuned and safe delivery of the growth factor to the target sites. This has been shown to exhibit precise control over the location of the drug within the core or shell of the nanofibers [334]. The main advantage of coaxial electrospinning over the conventional uniaxial electrospinning is that it generates core and sheath fibers by physical separation between the core and the sheath through the utilization of two electrospinning tips and two solutions (Figure 1.17) [335]. The core generally contains the growth factor solution and the sheath contains the polymeric solution. This nanofiber structure will allow for more of a spatial control over growth factors delivery and will hugely minimize any possibility of burst release when compared to the conventional uniaxial nanofiber [335]. Advantages of the coaxial electrospinning made it one area of a significant interest for many researches for more effective drug delivery and thus, tissue regeneration.

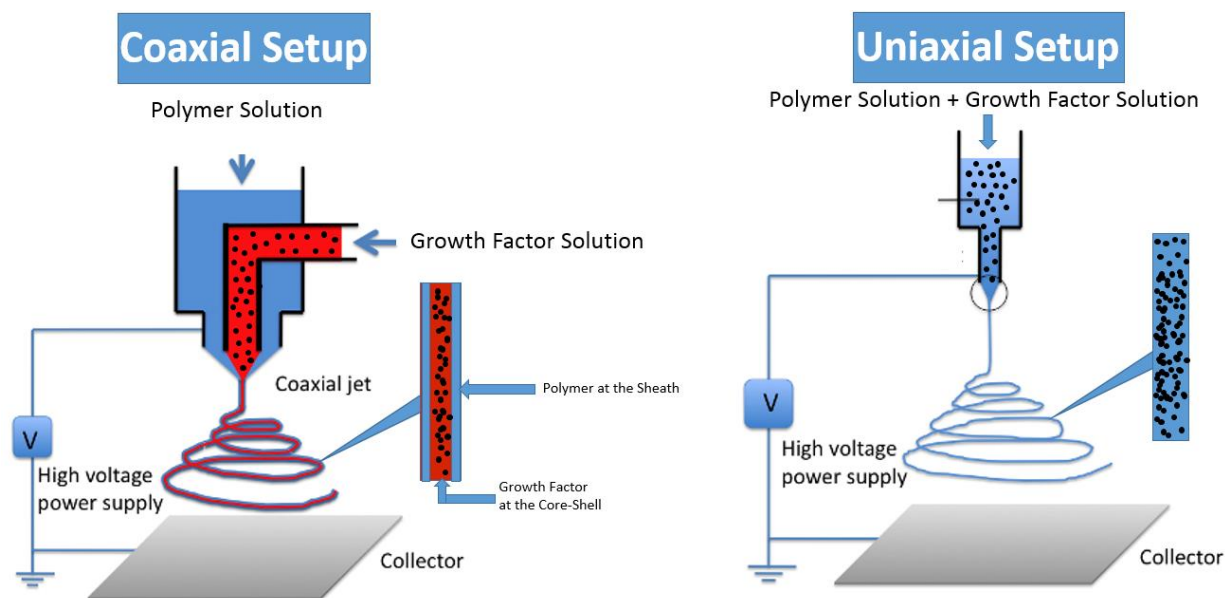


Figure 1.17 Schematic of coaxial electrospinning setup, and the conventional uniaxial electrospinning setup.

Building upon the knowledge, Choi et al. Developed a PCL/PEG Coaxial electrospun nanofibers scaffold for treatment of diabetic ulcers with binary release of multiple growth factors bFGF and EGF [336]. Two different growth factors were physically and chemically loaded into a single nanofibrous matrix to increase wound healing efficacy and to obtain bi-phasic release profiles of the loaded growth factors. To prepare the coaxial nanofibrous mesh, bFGF was physically incorporated in the core-shell of the amine-functionalized copolymer PCL/PEG by coaxial electrospinning, where the core-shell contained the growth factor and the outer sheath of the fiber consisted of the copolymers. To chemically load the other growth factor, the initially electrospun PCL/PEG-bFGF mesh was chemically modified with an EGF by conjugating surface-exposed amine groups of nanofibers to carboxylate groups of EGF. To confirm the presence of bFGF in the core-shell of the polymer and the conjugation of EGF on the surface of the fibrous mesh, X-ray photoelectron spectroscopy analysis were conducted, which confirmed the presence of a surface-immobilized EGF on the nanofiber by the distinctive peaks of nitrogen atoms shown in the data set. Release studies of both growth factors

clearly demonstrated the binary release profiles of each protein; where bFGF a high initial burst release within the first 24 hours, followed by a sustained and controlled release for 7 days, whereas EGF showed no negligible release in 7 days. *In vitro* evaluation on the effect of the binary release of both growth factors revealed that PCL/PEG-bFGF-EGF scaffold showed a significant increase in human keratinocytes and fibroblasts proliferation when compared to the scaffolds incorporated with bFGF or conjugated with EGF alone. To evaluate the capability of the scaffolds in treating wounds defects, they were *in vivo* administered in wound beds created at the dorsal of diabetic rats. Histological analysis revealed that the wound closure rates of diabetic ulcers were significantly increased in 7 days in bFGF/EGF with higher keratin 14, 5, 1 expression levels and extensive collagen and cemented matrix of keratin production when compared to bFGF, EGF and the control group. These data strongly suggest the positive effect of the bi-phasic release of bFGF and EGF in supporting tissue recovery with the similar phenotypes as the original keratinized tissues, owing its promising potential as wound dressing approach that can increase wound healing rates while reducing scar formation.

Although much progress has been made in the previously discussed approaches, most attention has been paid to develop methods that more focus on wound closure to prevent further dehydration and potential infection rather than looking for integrative and functional strategies for functional restoration. In an attempt to partially restore the function of the skin, Mahjour et al. developed a biomimetic multilayered PCL/collagen electrospun nanofiber scaffold that aimed to regenerate the epidermal and dermal layers of the skin as well as hair follicle [337]. The multilayered skin graft is composed of two distinguishable layers, with different architecture and mechanical properties mimicking those found in the native tissue, where the lower layer is engineered to support dermal

fibroblasts culture for dermal layer regeneration, and the top layer is intended to support keratinocytes culture for epidermal layer regeneration. In addition, dermal papilla cells aggregates were embedded in a predetermined arrangement at the interface between the epidermal and dermal graft for hair regeneration. These dermal papilla aggregates are thought to have the capability to differentiate into hair follicle *in vivo*. To construct the graft, isolated dermal fibroblasts were seeded on the first layer, followed by embedding dermal papilla aggregates then adding the second layer and seeding isolated keratinocytes on the top portion of the second epidermal layer. the multilayered graft was further *in vitro* cultured to differentiate the dermal papilla aggregates into hair follicles and produce proto hairs. The graft was shown to develop hair follicle-like structures *in vitro* (“proto hair”), and consequently form new hairs *in vivo* along with the formation of dermal and epidermal layers after transplantation to a full-thickness skin wounds in a rat model. It was concluded that the *in vitro* differentiation of the dermal papilla and the *in vivo* regeneration of hair was promoted by interaction between the dermis and the epidermis layer, suggesting their contribution in regenerating new hair. In this study, a multilayered skin graft was designed to provide a biomimetic environment for interactions between the dermis, epidermis, hair follicles and proto hairs for a partial restoration of the skin function.

Although the previously mentioned skin tissue engineering strategies have been shown to improve wound healing, they do not mimic the complexity found at the native skin matrix, thus limiting their potential for functional and integrative restoration. There has been a serious shift towards developing multilayered scaffolds that mimic the diversity found at the native ECM mechanically and structurally to move from survival to an improved functional as well as aesthetic outcome. Patient with severe burns suffer from irreversible loss of the skin and underlying subcutaneous

tissue. These patients would indeed benefit from the development of sufficient epidermal-dermal-hypodermal multilayered replacement. Great effort has been made in the past few years in developing epidermal-dermal replacement to treat skin wounds and to prevent scarring, but less attention has been paid to the reconstruction of the deeper hypodermis layer (subcutaneous tissue). In an attempt to regenerate the three different layers, Maïke et al. developed a bovine-derived collagen–elastin tri-layered graft to examine its ability to regenerate a full-thickness wound [338]. Human keratinocytes and preadipocytes were isolated and seeded on their relevant phases, where preadipocytes are seeded on the deeper hypodermal layer, and keratinocytes are seeded on the outermost layer of the epidermis (Figure 1.18). After 21 days in culture, the graft was histologically evaluated, using hematoxylin eosin, immunohistochemical staining with collagen IV as well as immunofluorescence labeling with anti-Ki67 antibody (proliferation marker) and DAPI (40 ,6-diamidino-2-phenylindole). Histological analysis revealed that a simultaneous growth of keratinocytes and preadipocytes could be observed on the collagen–elastin matrix with extensive production of collagen type IV on the outermost layer as evidenced by the immunohistochemical and immunofluorescence. In addition, it was shown that keratinocytes adhered well to the surface of the matrix and formed a confluent epidermis-like layer. Moreover, preadipocytes adhered well and also penetrated into the deeper layers of the matrix. These promising results suggest that the deeper layer could serve as a subcutaneous replacement. This work presented the feasibility of a simultaneous cultivation of keratinocytes as well as preadipocytes on a single matrix, with respective location of the layers mimicking the actual sequence of the natural skin, and could serve as a useful template of a three-layered skin substitute for future reconstructive surgery.

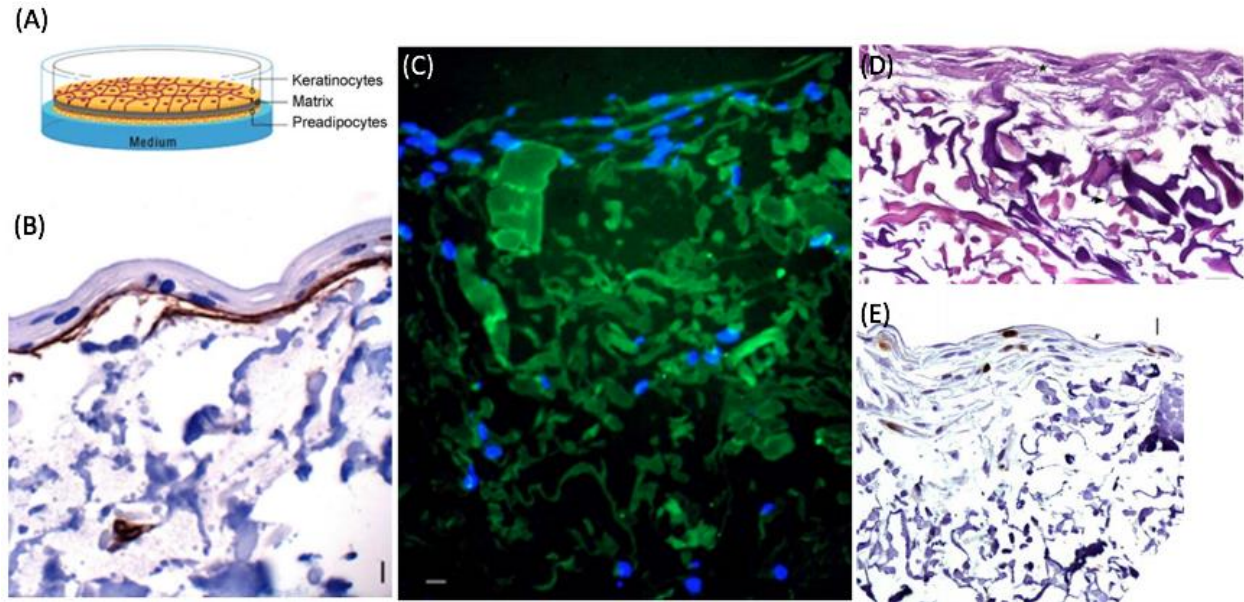


Figure 1.18. (A) Schematic presentation of the multi-layer skin substitute, (B) Immunohistochemical staining with antibodies against collagen IV. Extracellular matrix is produced by keratinocytes on the scaffold surface (20-fold magnification). Scale bar: 10 μm , (C) Immunofluorescence labeling with DAPI. Cytoblasts appear blue, matrix green. Keratinocytes form epithelial-like layers on the surface of the matrix (20-fold magnification). Confocal Laser Scan. Scale bar: 10 μm , (D) Simultaneous growth of keratinocytes (*) and preadipocytes (>). Preadipocytes penetrate into deeper layers of the scaffold whereas keratinocytes build a confluent layered epidermis-like sheet on the surface of the matrix (20-fold magnification). Confocal Laser Scan. Scale bar: 10 μm and (E) Proliferation of keratinocytes. Strong staining with anti-Ki67 antibody (brown) was observed, indicating proliferation of the seeded cells on the matrix. Scale bar: 10 μm [338].

1.2.Complex Tissue Regeneration:

The human body is surprisingly known for its regenerative capability. Blood, for instance, is continuously regenerated throughout the human's life. Several tissues also have the ability to self-regenerate upon injury to a certain extent, such as skin and bone; depending on how severe the damage is [1]. Skin injuries, for instant, can be classified into two main categories; based on the degree of trauma. Acute or Chronic. Acute wounds referred to as "Superficial Wounds" progress through the normal stages of wound healing "hemostasis, inflammation, proliferation, and tissue remodeling"; and show definite signs of tissue regeneration over time without any complications. On the other hand, Chronic wounds referred to as "Full Thickness Wounds" do not progress normally through the stages of healing and do not show evidence of healing over time, which leads to an unsuccessful wound healing and results in the formation of a scar tissue that lacks necessary functional and biological properties [2, 3, 4]. Bone injuries are also classified into either small fractures that can heal and self-regenerate undergoing the normal bone fracture healing stages "inflammation, soft callus, hard callus, tissue remodeling" in a timely manner, or into critical size defects or lost limbs beyond a certain critical size that fail to regenerate, which necessitates the clinical intervention [5].

One of the primarily grand challenges in the modern medicine is the limited availability of subsequent functional impairment to lost or damaged tissues. Historically, prosthetic devices are used to rehabilitate individuals living with joint or limb loss as a strategy to resolve this issue [6]. Artificial limbs, knees, and hips are some examples of prosthetic devices that are used. Although a great deal of advances has been accomplished in the past few decades in order to improve the functions of these prosthetic devices, serious drawbacks are still present such as the low stability

and lacking the ability to perform complex biological functions that are easily performed by the native limb, such as sensation or normal gait cycle [3, 7]. Allogenic limbs transplantations have also been attempted with disastrous outcomes [8].

The use of biological grafts is a well-sought approach that addressed the clinical challenges of restoring the function of damaged organs or tissues to certain extents. Currently available biological grafts include autografts known as the transplantation of tissue within an individual from a donor site to the injury site, or allografts known as the transplantation of tissue or a whole organ from another individual or a cadaver. Autografts demonstrate high biocompatibility and healing potential comparing to allografts, making them the gold standard among all the biological grafts [9]. The poor biocompatibility and integration of allografts to the host tissues, and the limited availability and high price demand of autograft led to the necessity of finding alternatives that mostly focus on regenerating the damaged tissues rather than repairing or replacing them [10].

The field of “Tissue engineering,” which was established to represent a new window that primarily focuses on the repair, restoration, and regeneration of neo-tissues using the three triangular general components, cells with the support of biomaterials and growth factors, evolved out of this necessity [11]. Tissue engineering utilizes scaffold matrices to fill the tissue void, provide structural support, and to deliver growth factors and/or cells that have the ability to form tissues within the body upon transplantation. Significant efforts have been made in the past few decades towards regenerating single tissues both *in vitro* and *in vivo* using the tissue engineering approaches. By utilizing the tissue engineering approaches, tissue-specific scaffolds for almost every single tissue within the

lower and the upper extremities such as bone, ligament, cartilage, muscle, and skin have been created with great potential [85].

This new engineering interdisciplinary has attracted much attention as a new therapeutic means that thought to overcome all drawbacks associated with artificial organs or organ transplantation in order to replace severely damaged tissues or organs. Despite the fact that tissue engineering demonstrated many approaches that led to understanding the feasibility toward repairing or regenerating single targeted tissues, the number of clinically translated products from this field are relatively low and do not address the grand challenges associated with engineering complex tissues such as organ systems or an entire limb.

The limitations of the current biological and engineering approaches towards complex tissue regeneration made it clear that a paradigm shift is required to successfully create translational technologies that can address the grand clinical challenges [6]. Developing a new interdisciplinary approach that utilizes the most advanced technologies currently available in different fields such as developmental biology, bioengineering, biomaterials science, stem cell biology, and clinical medicine along with a full understanding of the human's self-regenerative capacity may hold the key toward complex tissue regeneration [6, 15]. The efforts of scientists from these various fields led to the emergence of a new paradigm we term "Regenerative Engineering," which has been defined as *"the Convergence of Advanced Materials Sciences, Stem Cell Sciences, Physics, Developmental Biology and Clinical Translation for the regeneration of complex tissues and organ systems"*. Regenerative Engineering has elements of regenerative medicine, tissue engineering, and morphogenesis but is distinct from these individual disciplines in that it is less

applicable to spot the repair of injured tissues and elements and primarily focuses on the integration and the subsequent response of stem cells to biomaterials and regeneration of the interfaces between different tissue types [16]. This new interdisciplinary is proposed to regenerate damaged complex tissues, with the addressing grand challenges such as the regeneration of a total knee or a whole limb [17].

Formation of tissues simultaneously, as well as their functional assembly into complex tissues or organ systems, is one of the primary grand challenges in regenerative engineering. It is a well-known fact that increasing the levels of complexity in tissues or organs targeted for repair presuppose a concomitant increase in the complexity of the associated tissue engineering approaches or scaffold designs [19]. For example, solid organs, such as the kidney, would require multiple essential structures to restore its function, whereas tubular hollow organs, such as the urethra, are more easily tissue engineered from basic cells and biomaterials [19]. Similarly, complexity is found at the interfaces between tissues, such as the transition from cartilage to bone in the osteochondral interface in articulating joints, ligament to bone interface, tendon to bone and muscle to tendon interfaces, which also require complexity in the associated scaffold design and engineering approaches. [20, 21, 22, 23, 24].

From a structure-function perspective, the organs of the body are comprised of diverse tissue types that interface with each other and operate in synchrony to enable complex functions. Musculoskeletal tissue units, for instance, work at a very advanced level of synchrony, where all the physiological movements of the body are systematically performed through very well-organized actions of bone in conjunction with all the other musculoskeletal soft tissues, such as

ligaments, tendons, muscles, and cartilage. These tissues are well intact and integrated with each other through tissue-tissue junctions, or referred to as interfaces. These interfaces regions demonstrate well defined, spatial change in cellular phenotype, extracellular matrix deposition, as well as a change in mechanical properties (Figure 1.19) [25]. The gradual mechanical properties presented at the interface has a number of functions, starting from mediating load transfer between two distinct types of tissue to sustaining the heterotypic cellular communications required for interface function and homeostasis [25]. Due to the structural and compositional complex transition found at the tissue-to-tissue interfaces, the conventional surgical methods cannot reestablish their function upon injury, leading to high rates of re-injury due to poor integration between tissues at the reconstruction site [26]. For example, one of the clinically used approaches in restoring the function of the damaged ligament after an ACL injury is by using the patellar tendon (PT) approach. The patellar tendon is used to replace the damaged ACL and is fixed within the bone tunnel with pins and screws. Despite the fact that this approach can result in good stability to the knee joint, it does not correlate with the functional outcomes. Additionally, PT approach results in long-term postoperative pain as well as movement restrictions to the patients, which makes the advantages associated relatively low [27]. Similarly, some clinical methods followed in repairing rotator cuff tears can be associated with a high possibility of postoperative failure, which can be as high as 94% [28].

Understanding the mechanisms that derive the formation of complex tissues such as tissue-tissue interfaces, has provided us with insights on what it is required for a regenerative tissue-tissue interface to regenerate. These observations have provided invaluable clues for the design of biomimetic scaffolds for engineering the complex tissue-to-tissue interface [29]. Ideally, the

scaffold should be multi-phased to recapture the multi-tissue organization observed at the tissue-to-tissue interface. The scaffold should also exhibit phase-specific structural, compositional, material properties to stimulate cellular response such as proliferation and differentiation and with a gradual increase in mechanical properties across the scaffold phases, similar to those found at the native tissue in order to eliminate the formation of stress concentration. In addition, the scaffold should introduce a spatial control over mineral distribution across the distinct phases, which can control the mechanical heterogeneity at the interface. To better sustain the load transfer across the scaffold, the scaffold should be pre-integrated. The scaffold should also exhibit phase-specific surface properties to support the phase-specific relevant cell performance. Considering all these parameters along with employing the advanced tools that the field of regenerative engineering has provided us with will enable the creation of biomimetic scaffolds with location-specific topographies and physicochemical cues that will guide cells towards the formation of different tissue types. This, however, may hold the key towards the regeneration of intact multi-components complex tissues simultaneously [18]. Therefore, the next horizon in the field of regenerative engineering resides in how to enable the assembly of these single-tissues systems into multi-tissue units or facilitate the integration of these composite tissue grafts *in vivo* [25]. Herein, we discuss the most relevant complex tissue regeneration approaches, particularly musculoskeletal tissue interfaces.

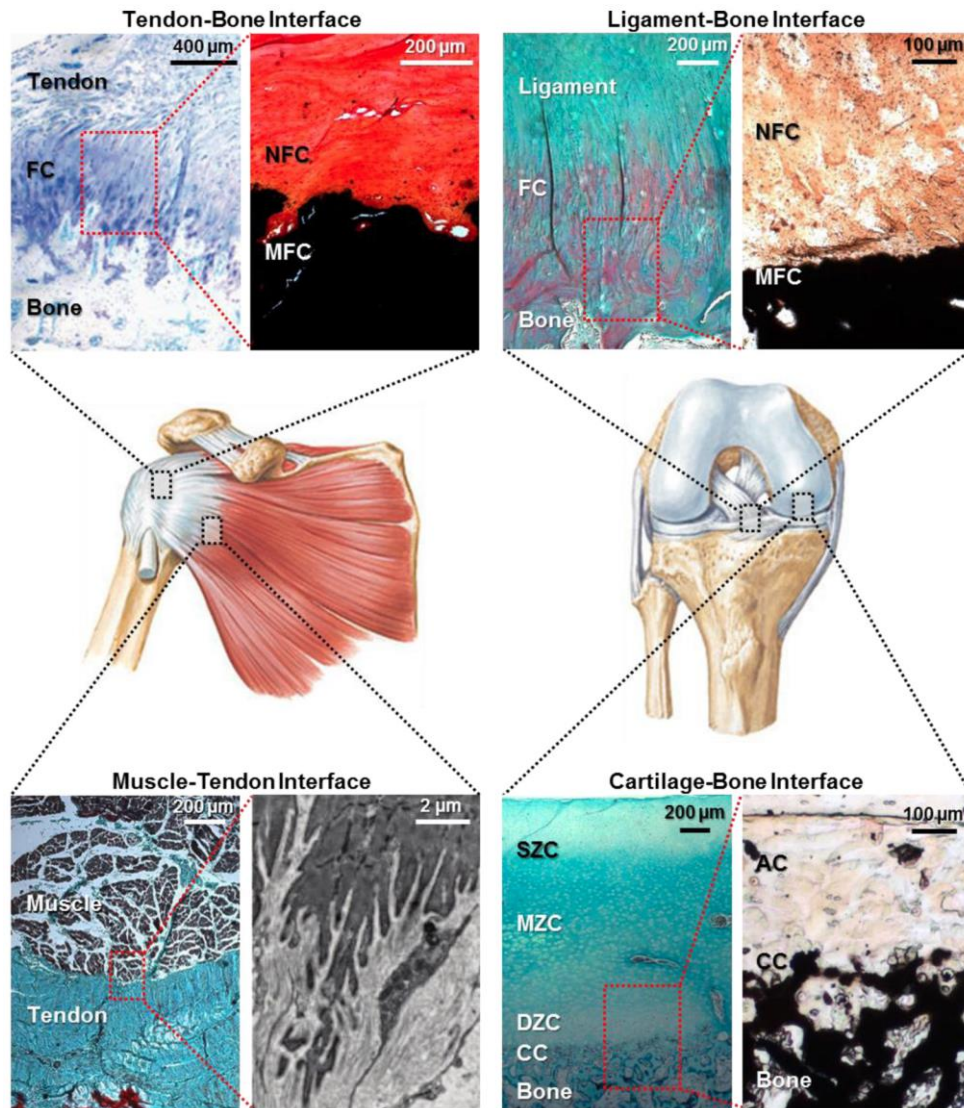


Figure 1.19 Common orthopedic tissue-tissue interfaces. Ligaments, such as the anterior cruciate ligament (ACL) in the knee (Modified Goldner's Masson Trichrome),¹²⁶ and tendons, such as the supraspinatus tendon in the shoulder (Toluidine blue),⁷⁰ connect to bone via a fibrocartilaginous (FC) transition, which can be further subdivided into non-mineralized (NFC) and mineralized (MFC) regions (Von Kossa). The muscle-tendon junction (Modified Goldner's Masson Trichrome) consists of an interdigitating band of connective tissue.⁶⁰ Articular cartilage (AC), which can be subdivided into surface (SZC), middle (MZC), and deep (DZC) zones (Modified Goldner's Masson Trichrome), connects to subchondral bone via a transitional calcified cartilage (CC) region (Von Kossa) [25].

1.2.1. The Complex Bone-Ligament-Bone Junction Regeneration:

1.2.1.1.Ligament-Interface-Bone Junction Structure and Function

Ligament is a soft tissue that connects bone to bone through a characteristic fibrocartilage interface, with controlled spatial change in cell phenotype, extracellular matrix deposition and mechanical properties. Three distinct regions are found along the bone-ligament interface: ligament, fibrocartilage, and bone. The fibrocartilage region is further divided into mineralized and nonmineralized fibrocartilage zones [29]. Where ligament is directly connected to the nonmineralized region of fibrocartilage and the mineralized region is directly connected to bone [36]. Within the ligament tissue, ligament fibroblasts are found entrapped in collagen type I and III matrix [29]. At the insertion site, more specifically, the nonmineralized region, ovoid chondrocytes are found entrapped in collagen II proteoglycan-rich matrix. Heterotrophic chondrocytes are found in the mineralized fibrocartilage region, found entrapped in collagen type X calcified matrix. Within the bony region, referred to as “subchondral”, osteoblasts, osteocytes and osteoclasts are found embedded into a mineralized collagen type I matrix. This cellular heterogeneity found along the bone-ligament insertion area is a key role in permitting the gradual transition of mechanical loads between soft tissues and bone, which decreases the concentration of stress formation [37, 38]. In addition, the complexity found along the bone-interface-ligament presuppose a concomitant increase in the complexity of the associated tissue engineering approaches or scaffold designs. However, a structurally, compositionally, and biomimicry scaffold that support the heterogenic cellular interaction while promoting the regeneration of the distinct tissues is indeed required to recapitulate the composite tissue structure across the ligament-bone junction.

1.2.1.2.Ligament-Interface-Bone Junction Tissue Regeneration Approaches

One of the initial steps that have been taken into consideration in order to address the drawbacks associated with the traditional clinical approaches in repairing ligament injuries, specifically ACL was adopted by Tien et al, when he attempts to improve ligament grafts to bone fixation by filling calcium phosphate cement at the ligament-bone-ligament junction in rabbit ACL reconstruction, which results in improved and organized bone growth at the junctions [39]. Huangfu et al, reported a similar study where tricalcium phosphate cement (TCP) was injected at the interface region in a canine ACL reconstruction model, which also results in improved and organized bone growth comparing to the control group (uncemented) [40]. A different approach was adopted by Mutsuzaki et al, when a tendon graft was soaked in different concentrations of calcium phosphate as an ex vivo step prior to implantation in a rabbit ACL reconstruction model. The surface coated graft was found to enhance healing and increase cellular integration at the junction site [41]. In a different attempt, Rodeo et al, used a different technique to improve bone tunnel osteointegration by incorporating Bone Morphogenetic Protein-2 (BMP-2) in collagen I sponge carrier, which was placed at the edge of a tendon grafts that interact with the bone prior to implantation in a dog ACL reconstruction model. BMP-2 incorporated collagen sponge carrier significantly increased osteointegration at the bone tunnel after 2 weeks comparing to the control group (collagen sponge only) [42]. Although these approaches have improved the outcomes of the ACL reconstruction surgeries to a certain extent by promoting osteointegration to the bone tunnel, these approaches do not lead to the regeneration of fibrocartilage interface due to the fact that these are single-phased grafts, which do not mimic the complexity found at the native interface. This clearly demonstrate the need for a biomimetic multi-phased stratified scaffold that mimics the complexity found in the native tissue, which in turn can guide the regeneration of multi—tissue interface.

There has been a serious shift towards forming multi-tissues as an attempt to form interfaces between musculoskeletal tissues. Cooper et al. developed a multi-phased ACL graft system composed of braided polylactide-*co*-glycolide (PLGA) microfibers at the center of the graft for ligament formation, with two denser fiber regions at either end of the graft to facilitate bone ingrowth [43]. *In vitro* evaluations demonstrated the high biocompatibility of the graft [44], in addition, *in vivo* evaluations showed a great healing potential, when collagenous tissue infiltration after 12 weeks has been observed [45]. In a similar approach, Altman et al. reported an establishment to an appropriate highly porous ACL graft system that consisted of multi-regions, silk yarns at the middle of the implant, which densely connects the knit regions at either end for the bony integration. The graft system was evaluated in a goat ACL reconstruction model, resulting in the formation of collagenous like structure with cell alignment after 12 months [46]. To enhance the osteointegration at the bone tunnel, and ligament regeneration, Kimura et al. evaluated a multi-phased PLA-Collagen braided scaffold with basic fibroblast growth factor (FGF), which was incorporated at the collagen hydrogel at either ends of the implant. *In vivo* evaluations revealed that the scaffold design supported the formation of ligament and bone at the tunnel, in addition to a significant improvement in tensile mechanical properties that was observed when compared to the single-phased controls [47]. Paxton et al. investigated the use of a poly(ethylene glycol) diacrylate (PEGDA) hydrogel incorporated with hydroxyapatite (HA) and the cell-adhesion peptide RGD (Arg-Gly-Asp) as a material for creating an *in vitro* tissue interface to engineer intact ligaments (i.e., bone-ligament-bone). Incorporating HA into PEG hydrogel decreased the swelling rate associated with the hydrogel, but increased the stiffness of the hydrogel as well as mechanical strength. In addition, HA incorporation increased the cellular growth capacity and most importantly, interface formation. On the other hand, when RGD was incorporated into the

hydrogel, it increased the swelling rate, but reduced the gel stiffness as well as mechanical strength. The study revealed that incorporation of both HA and RGD into the hydrogel resulted in optimal conditions for cell attachment, when compared to PEG alone [48]. Using a cell based approach, Ma et al. reported that it is possible to form bone–ligament–bone constructs by introducing engineered bone segments to ligament monolayers. This was achieved through co-culturing of mesenchymal stem cells (MSC)-derived on a bone construct with a (MSC)-derived ligament monolayer which was rolled between the two bony regions at the middle of the construct. *In vivo* evaluation 2 months after implantation in an ovine model showed a complete graft integration to the native bone along with presence of aligned, crimped, type 1 collagen, and elastin throughout [49, 50].

These novel approaches and scaffold designs in attempting to form the bone-ligament multi-tissue units clearly represent the advances over the single-phased unit designs. However, none of these advanced approaches or scaffold designs touched upon the necessity of engaging the formation the fibrocartilage interface between bone and ligament during the regeneration process of these two tissues. The fibrocartilage interface is optimized to withstand the tensile and compressive loading distributions at the ligament-bone interface, and thus, it plays a critical role in transitioning mechanical load between soft tissues and bone, which as a result protects the soft tissues from contact deformation and damage at high strains [51, 52, 53, 54, 55]. The next challenge will be to incorporate the fibrocartilage interface regeneration in the graft design, which is an essential step in order to achieve physiological joint function after ligament reconstruction. This can be achieved by considering the gradual transition in both mechanical properties and ECM morphology along the ligament-interface-bone in the graft design. Spalazzi et al, reported a tri-phasic scaffold design

that was hypothesized to reestablish the formation of the ligament-to-bone interface considering the mechanical transition, transition in ECM morphology and relevant cell heterogeneity along the complex tissues [56]. The tri-phasic scaffold consisted of three different pre-integrated continuous phases are each engineering for the regeneration of a specific tissue type, ligament, fibrocartilage and bone. Phase A is made from polyglactin (10:90) knitted mesh to support ligament fibroblasts culture for the regeneration of ligament, Phase B is made from PLGA (85:15) microspheres to support fibrocondrocytes culture for the regeneration of fibrocartilage interface, and Phase C is made from PLGA (85:15) sintered microspheres and 45S5 bioactive glass to support osteoblasts culture for bone regeneration [57]. The three different phases were assembled and heat sintered to pre-integrate them (Figure 1.20) [57]. Pre-integrating the scaffold to form multi-phased graft system was essential in order to allow for cellular interaction and to support the multiple tissues regions observed across the native ligament-interface-bone junction [58].

For ligament and bone formation, fibroblasts and osteoblasts were seed in phases A and C respectively. Cellular interactions in the co-cultured tri-phasic scaffold have been evaluated both *in vitro* and *In vivo*. *In vitro* cell interaction evaluations revealed that the controlled cell distribution resulted in the formation of cell type-specific matrix on each phase of scaffold. In addition, Phase C was found to be mineralized, and an extensive deposition of type I collagen was found in both Phase A and B [57]. *In vivo* evolution of the co-culture revealed that the tri-phasic scaffold supported multilineage cellular interactions as well as tissue Infiltration with abundant specific-matrix production in Phase A and C. In addition, cell migration from both phases to phase B was observed with vascularity and matrix production [58].

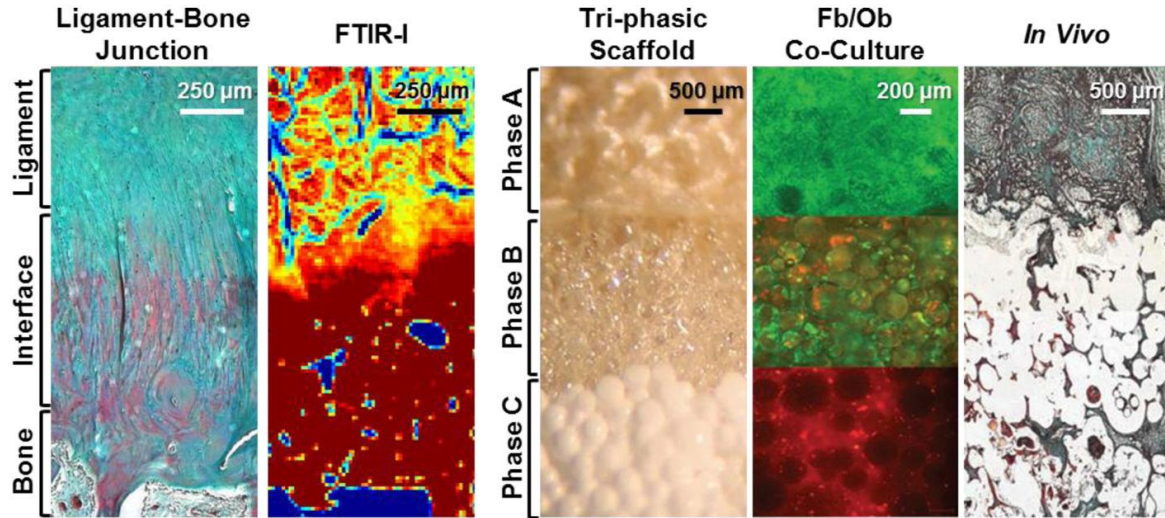


Figure 1.20 Scaffold design for ligament-interface-bone regeneration. Mimicking the stratified structure (Modified Goldner's Masson Trichrome) and composition (FTIR-I: Fourier Transform infrared spectroscopy)⁸⁹ of the native insertion, a tri-phasic scaffold (Phase A: PLGA mesh, Phase B: PLGA microspheres, Phase C: PLGA-BG microspheres) was designed for ACL-bone interface regeneration.^{110,111} This design allowed for spatial control over cell distribution (Fb: fibroblasts on Phase A, Ob: osteoblasts on Phase C, along with chondrocytes in a hydrogel in Phase B) enabled the formation of compositionally distinct yet structurally continuous tissue regions *In vivo* (Modified Goldner's Masson Trichrome) [57].

The tri-phasic scaffold system was further *In vivo* evaluated for the formation of fibrocartilage-like tissue at the interface region. This was done by tri-culturing the three different cell types, fibroblasts, chondrocytes and osteoblasts respectively along the three different phases and compare the findings to the co-culturing system. Specifically, fibroblasts were seeded on Phase A, chondrocytes were seeded on phase B and osteoblasts were seeded on phase C, respectively. Tri-culturing the three different cell types resulted in an extensive collagen rich matrix production at the three different phases comparing to the co-culture system. In addition, formation of fibrocartilage-like tissue at the interface rejoin containing type I and II collagen as well as glycosaminoglycans was observed. Mechanical properties of the tri-phasic scaffold were evaluated *In vivo* both after the co-culture and tri-culture experiments resulting in improved mechanical gradient with the highest elastic modulus and yield strength at the bone phase, mimicking that at the native ligament-interface-bone junction [57].

These encouraging findings demonstrate that a biomimetic stratified multi-phased scaffold system that exhibits spatial control over the phase-relevant cell heterogeneity can lead to the regeneration of complex tissues as well as a fibrocartilage-like interface *In vivo*, which highlighted the possibilities in regenerating complex tissues on a single scaffold.

Building upon the previous observations, Subramony et al. developed a five-phased bone-interface-ligament-interface-bone caprolactone (PCL) nanofibers gradient scaffold for ACL reconstructions [59]. To form a continuous five phases construct, mechanoactive collar were applied at either ends of the graft. MSCs were seeded in every junction along the graft and cultured for both *in vitro* and *In vivo* evaluations. *In vitro* evaluations revealed that MSCs upregulated into fibroblasts, fibrocondrocytes and osteoblasts specific markers on the ligament, interface and bone phases, respectively. *In vivo* evaluation showed more tissue regeneration in the multi-phased graft comparing to the single-phased graft. In another study, stem cells differentiation into fibroblasts and osteoblasts was guided by introducing a gradient scaffold that consisted of a region of aligned PCL fibers for ligament regeneration, contiguous with regions of unaligned PLGA nanofibers at either ends for bone regeneration [60]. These findings suggest that the gradient multi-phased scaffolds can be used to promote complex tissue regeneration for ACL reconstructions.

Moving forwards, by taking the mineral gradient distribution across the calcified fibrocartilage interface into accounts. Different groups have utilized the concept of introducing a gradient of minerals or chemical cues, such as growth factors, to induce the formation of graded calcified matrix, mimicking that found in the native ligament-interface-bone junction. In a study that was done by Samavedi et al. osteogenic differentiation of stem cells seeded on polymeric composition

and mineral content graded coaxial electrospun PCL fibrous scaffold was guided in a gradient-dependent manner [61, 62]. Another study that was done by Phillips et al, fibroblasts seeded on collagen fabricated scaffold with a compositional gradient of retroviral coating for osteogenic transcription factor (RUNX2) were induced to produce a gradient of mineralized matrix both in vitro and *In vivo* [63].

Considering the scaffold physical properties such as cross-link density, pore size, stiffness and material composition is a key element in guiding the cell behavior, especially musculoskeletal cells. In a study by Oh et al. a scaffold with different pore size gradient was fabricated using PCL for ACL reconstruction following a centrifugation method (Figure 1.21) [64]. The scaffold exhibits different pore size gradients along the three rejoins, starting from 405 μm at the bony region, with a gradual decrease to 186 μm at the end of the ligament region. Osteoblasts, chondrocytes and fibroblasts were seeded in the three graft regions, respectively. Cell counting was performed along the graft, and it was found that both osteoblasts and chondrocytes showed increased in cell number at the regions with pore size 380-405 μm , while fibroblasts were more localized at areas with pore size of 186-200 μm . These findings suggest that different pore sizes can strongly affect cell behavior such as proliferation and cell fate. Thus, providing the appropriate gradient in pore size, may act as a useful tool that can guide cell differentiation and proliferation during complex tissue regeneration [64].

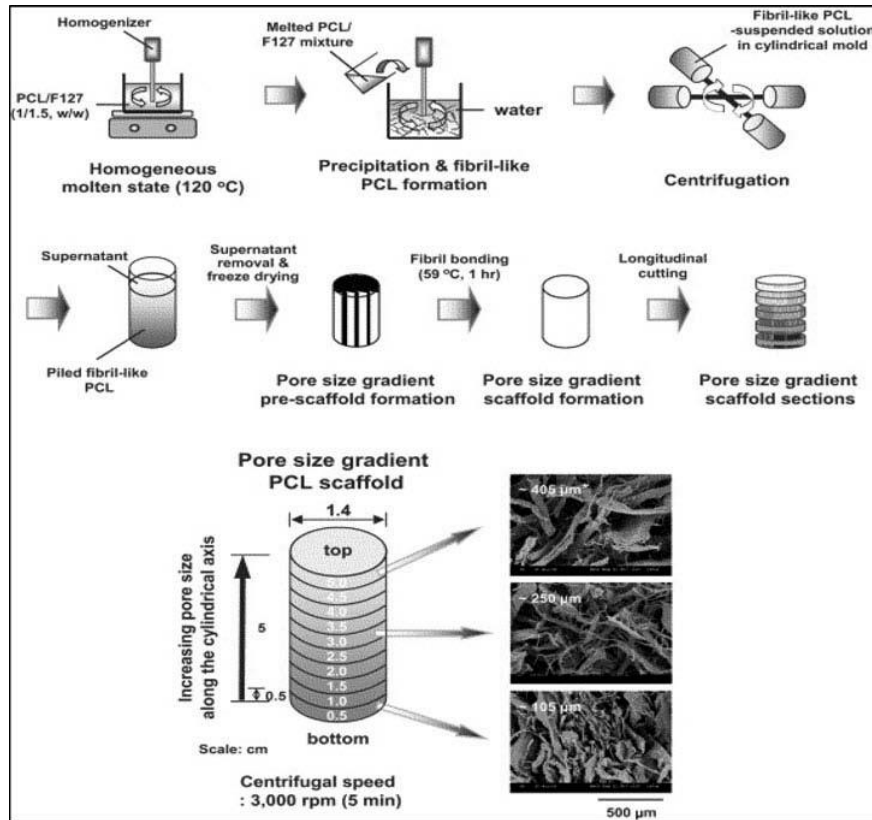


Figure 1.21. (Top) Schematic diagram showing the fabrication process of a pore size gradient in PCL scaffolds by a centrifugation method and (bottom) SEM photographs of the top surfaces of the PCL scaffold sections along the longitudinal direction ($\times 100$; *, average pore size) [64]

These results demonstrate the high potential of tissue engineering interfaces by utilizing gradient multi-phased scaffold. Gradient scaffolds exhibit continuity in the structure, which in turns can lead to improved gradual, continuous mechanical transition, cellular interactions, and gradient in mineralization across the ligament-interface-bone junction. The physical and chemical gradual transitions demonstrated in the gradient scaffold can stimulate stem cells to differentiate [64]. For example, it was shown that the fate of MSC is highly sensitive to the matrix physical properties, and they can differentiate into muscle, fibroblasts, or bone simply by changing the stiffness of the substrate [67]. In addition, pore size gradual distribution has been shown to have a large effect on guiding cell differentiation and proliferation during complex tissue regeneration [64]. Gradient scaffolds are challenging to fabricate, due to the gradual transition in properties found along the

single scaffold, which may limit gradation in fabrication from the nano-scale to the micro-scale found in the native ligament-bone junction respectively. Although both stratified and gradient scaffold designs seemed to overcome most drawbacks associated with complex ligament-interface-bone regeneration, it is strenuous to conclude which strategy is best for this application. Further studies are needed that systematical investigate and compare between stratified and gradient scaffolds in order to determine whether both or either once is optimal for complex tissue regeneration.

In summary, different approaches towards complex tissue regeneration have been attempted seeking to recapitulate the graded structural, mechanical, and biochemical properties of native interface tissue. Growth factors as well as biochemical and biomechanical stimulation can be incorporated into the scaffold design to promote the maintenance of heterotypic cell populations relevant to tissue interfaces.

1.2.2. The Complex Muscle-Interface-Tendon and Tendon-Interface-Bone Junctions

Regeneration:

1.2.2.1. Muscle-Interface-Tendon Junction Structure and Function.

Tendon is a highly organized connective tissue that connects muscles to bone through a characteristic fibrocartilage interface at either end, which plays an important role in gradually transmitting force between muscle and bone [68]. Three specialized rejoins are characterized along the muscle-tendon-bone junction, which are, the myotendinous junction (MTJ), the tendon proper with the region where tendons change direction by wrapping around bony pulleys, and the bone–tendon junction (BTJ), (Figure 1.22) [69]. The MTJ is divided into muscle and tendon rejoins

overlapping through an interface in between. At the muscle rejoin, myoblasts found, which are entrapped in collagen type IV. At the interface, muscle and tendon meet, creating a network of overlapping muscles and tendon tissues with a greater surface area for adhesion between them. At the tendon tissue, tendon fibroblasts are found entrapped in collagen type I matrix [70].

Further, four separate ultrastructural domains are found in the MTJ connecting the actin filaments of the terminal sarcomere with the collagen fibers of the tendon. (1) '*the internal lamina*', composed of actin filaments and associated crosslinking structures; (2) '*the connecting domain*', which connects the internal lamina to the external lamina; (3) '*the lamina densa of the external lamina*', with a structure similar to other laminae densa; and (4) '*the matrix*', found in the space between lamina densa and the collagen fibers [97].

1.2.2.2.Tendon-Interface-Bone Junction Structure and Function.

Tendon is found transitioning into bone through a fibrocartilage interface at the BTJ. This fibrocartilage region is further divided into mineralized and nonmineralized fibrocartilage zones [29]. At the nonmineralized fibrocartilage ovoid chondrocytes are found entrapped in collagen II proteoglycan-rich matrix. Heterotrophic chondrocytes are found in the mineralized fibrocartilage region, found entrapped in collagen type X calcified matrix. The bony region, referred to as "subchondral", osteoblasts, osteocytes and osteoclasts are found embedded into a mineralized collagen type I matrix. From a mechanical point of view, nonmineralized and mineralized fibrocartilage rejoins are half as stiff as the tendon, while bone is two orders in magnitude stiffer than tendon. Under applied compression, a gradual decrease at the interface site takes place progressing from the nonmineralized to mineralized fibrocartilage rejoins and then to the bone

rejoin, resulting in an increase in Young modulus at the interface site. This mechanical synchrony presented at the tendon-interface-bone junction minimize the formation high stress concentration and support gradual load transfer from soft to hard tissues. However, an intense load transfer between tendon and bone can lead to increase in stress concentrations, which as a result would increase the risk of failure at the interfaces. Thus, the cellular heterogeneity found along the muscle-tendon-bone junction is a key role in permitting gradual transition of mechanical load between muscle and bone, which decreased the concentration of stress formation at the insertion site [37, 38].

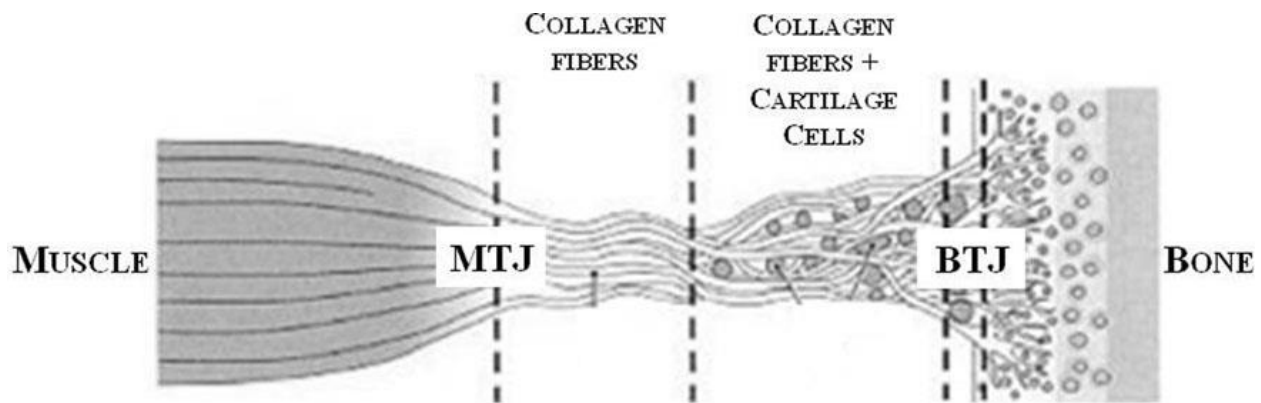


Figure 1.22 Picture depicting tendon structure and the junctions at muscle and bone [69].

Similar to the bone-ligament-bone, complexity is also found in the muscle-tendon-bone junction, which presuppose a concomitant increase in the complexity of the associated tissue engineering approach or scaffold design. Currently, scientific literature on tendon tissue engineering (TTE) shows that much work has focused on engineering the tendon proper; however, the structural complexity of the bone– tendon (BTJ) and muscle– tendon (MTJ) makes their reproduction for tissue engineering applications very difficult. Relatively few studies have investigated the characteristics of these regions from a tissue engineering point of view. In this section, BTJ and

MTJ tissue engineering will be reviewed, giving indications about the most promising approaches in this field.

1.2.2.3.Current Clinical Treatment for Tendon-Interface-Bone Junction Injuries

Rotator cuff tears is considered as one of the most common tendon injuries that an immediate require medical interveinal upon injury due to the poor self-healing potential. However, distinct from treatment strategies followed for ligament restoration, which mainly fuscous on the restoration of the ligament, tendon injuries are clinically managed by reattaching the tendon to bone via mechanical means. However, restoration of the native tendon-bone function is challenging and tendon post-operative detachment remains a primary reason for surgical failure. Although tendon-based grafts can to certain extents restore the physiological range of motion and joint function through the mechanical fixation methods, they do not result in adequate graft integration, which in turns result in the formation of a scare tissue at the insertion site that lacks all biological and mechanical functions of the native fibrocartilage tissue.

1.2.2.4.Tendon-Interface-Bone Junction Tissue Regeneration Approaches

In order to address this challenge, the feasibility of integrating tendon graft to bone has been evaluated by several groups. Fujioka et al. reported that cellular reorganization has been observed at the reattachment site, along with the formation of non-mineralized and mineralized fibrocartilage-like regions by surgically reattaching the Achilles tendon to its original attachment site [71]. Inoue et al. also reported that a supraspinatus tendon integration was successfully promoted with a metallic implant using a bone marrow-infused bone graft [72]. In an attempt to improve tendon fixation to bone, Chang et al, revealed that by surgically separating periosteum

tissue or demineralized bone matrix found between the native insertion and bone, osteointegration and the development of fibrocartilage-like matrix can be facilitated with improvement in mechanical function [73, 74]. This has been further examined by Kyung et al. when the periosteum was found to improve the integration of the tendon at the bone tunnel [96]. In this study, histological evaluation showed extensive bone growth around the tendon at the bone tunnel in the periosteum-wrapped limb than in the control limb. Kyung et al. concluded that the periosteum is able to generate all types of connective tissue and has osteogenic capacity that can support bone formation. These promising results suggest that osteointegration can be facilitated with the formation of fibrocartilage-like tissue and emphasize the need for functional grafting solutions that can promote biological fixation and true regeneration of the three distinct tissues along tendon-interface-bone junction.

Nanofibers scaffold is considered as a promising strategy that has recently been explored for tendon and tendon-bone interface tissue engineering applications [77]. The biomimicry potential of these fibrous nanofibers scaffolds makes them ideal for orthopedic tissue engineering. Porosity, permeability and fibers diameter as well as morphology can be easily modulated during fabrication process to resemble the native tendon ECM [78]. In addition, both randomly aligned and aligned nanofibers scaffold can be easily achieved during fabrication and used to guide cellular response. Moreover, structure, mineral as well as protein/growth factors content continuous gradation can be achieved on nanofibers substrates using a variety of approaches. It is anticipated that gradient nanofibers graft will enable integrative and functional repair of tendon-bone injuries due to the relatively close biomimicry to the native tissue.

Recently, degradable PLGA nanofibers-based scaffold has been *in vitro* evaluated for rotator cuff repair by Moffat et al. [79]. The effect of fibroblasts attachment, alignment, and gene expression has been tested as a function of nanofibers organization (aligned vs randomly aligned). It was found that underlying orientation primarily guided tendon fibroblasts morphology, alignment and gene expression. In addition, it was found that the deposition of collagen types I and III as well as mechanical properties were directly related to the underlying nanofibers orientation. These findings indicate that nanofibers organization play a crucial role in guiding cell response, which clearly highlight biomimetic potential of nanofibers to the tendon native tissue.

Building upon these successful based-nanofibers observations, and taking into accounts the formation of fibrocartilage tendon-bone interface, Moffat et al. also reported the development of a biomimetic biphasic electrospun nanofibers scaffold with contiguous nonmineralized (Phase A) and mineralized (Phase B) regions that are designed to facilitate the regeneration of the tendon-bone insertion. Phase A, however, is composed of aligned PLGA nanofibers, and Phase B consists of aligned PLGA-HA composite nanofibers (Figure 1.23). *In vivo* evaluations in rat [75] and sheep [76] rotator cuff models revealed the formation of fibrocartilage-like matrix at the insertion site of the graft. In addition, it was observed that mineralization distributions was highly maintained, in which calcified fibrocartilage formed only at the HA-containing phase. Further, fibrocartilage matrix maturation and enhanced collagen organization at the tendon-bone junction was promoted by pre-seeding the biphasic scaffold with bone marrow-derived cells. When comparing the findings with the single-phased PLGA or PLGA-HA, it was found that the regeneration of an organized fibrocartilage interface was not achieved. These observations indicate that biomimicking the alignment and mineral distribution found in the native tendon-bone insertion

play a crucial role in guiding cells to form a fibrocartilage-like matrix at the insertion site with promoting its integration to the tendon, and supporting calcified fibrocartilage formation and osteointegration.

Moving forwards, by taking the mineral gradient distribution across the calcified fibrocartilage interface into accounts to enhance fibrocartilage formation, different groups have utilized the concept of introducing a gradation in minerals and protein content, to induce the formation of graded calcified matrix, mimicking that found in the native tendon-interface-bone junction. Li et al. demonstrated a coating-based method to generate a linear gradation of calcium phosphate on a nonwoven mat of a polymeric electrospun nanofibers by varying the incubation time of the scaffolds in a concentrated simulated body fluid (SBF). The gradation in mineral distribution resulted in gradation in mechanical properties along the tendon-interface-bone junction [80]. To further improve the mechanical properties, the soaking solution has been optimized by increasing the concentration of bicarbonate ions, which resulted in an increase in mineral content that has improved mechanical properties along the tendon-interface-bone junction [81]. In order to evaluate the ability of the pre-coated scaffold to induce graded osteogenesis, adipose-derived MSCs were seeded along the scaffold resulting in more extensive staining of osteogenic markers that was observed on areas with higher mineral content [82]. In a similar approach, another group has evaluated the effect of fibronectin protein gradation on a polymeric electrospun nanofibers scaffold for the formation of fibrocartilage interface, which found to exhibit control over density and morphology of cultured fibroblasts [83]. These findings indicate that gradation in mineral or/and protein content along the tendon-interface-bone graft may result in spatial control over osteogenesis and may promote the formation of fibrocartilage interface.

In a separate study, both BMP-2 and IGF-I were used by absorbing different concentrations of BMP-2 and IGF-I along the tendon-bone silk construct. This was achieved by increasing BMP-2 content from the center of the scaffold towards the direction of the bone, while simultaneously decreasing IGF-I content in a gradation fashion, where the highest BMP-2 and IGF-I content were added at the boney and the interface rejoins respectively. Culturing MSCs on the growth factors graded substrate in a subchondral medium resulted in graded increases in calcium and GAG deposition and increases in collagen type I, II, and X gene transcription at the bony and interface rejoins respectively. Further results revealed that the gradations achieved closely resembled the transition from unmineralized fibrocartilage to mineralized fibrocartilage to bone, similarity resembling those found at the native tissue.

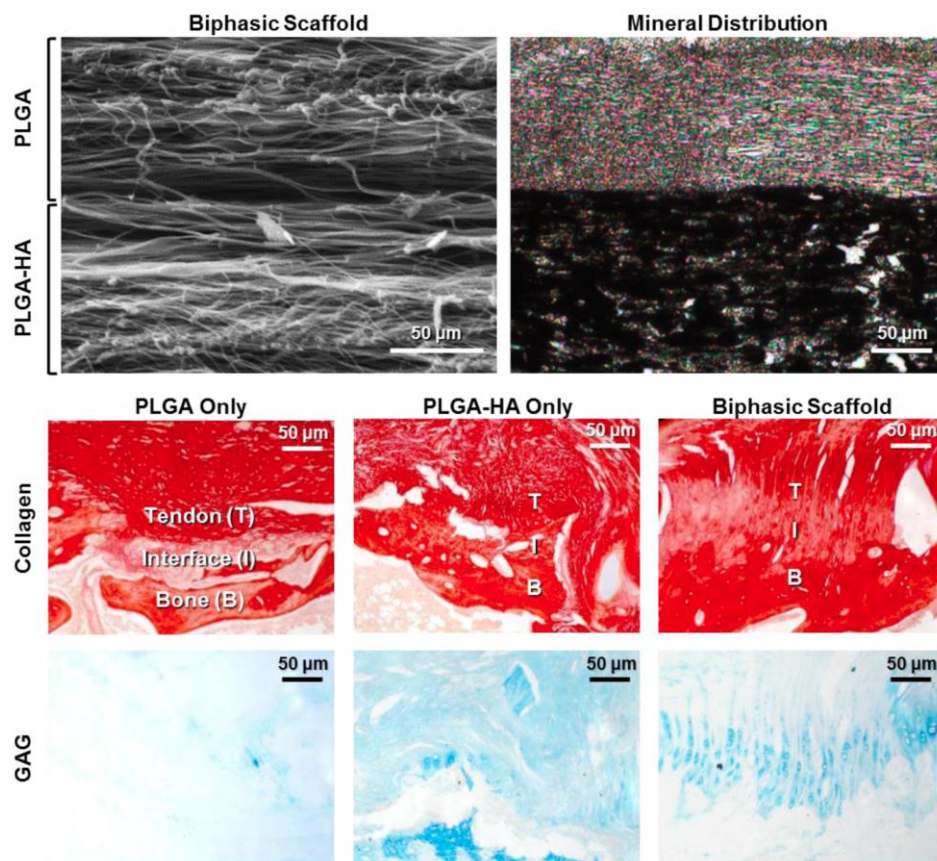


Figure 1.23 Scaffold design for *tendon-interface-bone* regeneration. A biphasic scaffold comprised of layered aligned PLGA and PLGA-HA nanofibers was fabricated by electrospinning, which led to phase-

specific mineral deposition *in vivo* (Von Kossa, subcutaneous athymic rat model). The bilayer scaffold was subsequently tested in a rat rotator cuff repair model, disorganized scar tissue was observed in the single-phased controls (PLGA, PLGA-HA only). Interestingly, tendon-bone integration via an organized bilayer fibrocartilage interface was only observed with the biphasic design (Picrosirius red, Alcian blue) [75].

To evaluate the potential of dual growth factors delivery in restoring the native tendon-interface-bone junction *In vivo*, a study by Lee et al. estimated the feasibility of the gradually immobilizing both PDGF-BB and BMP-2 in an asymmetrically porous PCL membrane as a potential strategy for effective regeneration of tendon-interface-bone junction. Both growth factors were immobilized using “heparin-intermediated interactions”, which resulted in a minimal burst release in addition to a sustained and controlled release with up to 80% of the total content has been released after 5 weeks. *In vivo* evaluation in rat patellar tendon avulsion model revealed that both PDGF-BB/BMP-2 dual release from the PCL membrane accelerated the regeneration of tendon-interface-bone respectively due to the continuous release of both factors [89]. These results demonstrate the feasibility and the potential of gradual immobilization for dual growth factor delivery from tendon-interface-bone grafts for the regeneration and the restoration of these complex tissues.

1.2.2.5.Current Clinical Treatment for Muscle-Interface-Tendon Junction Injuries

Muscle-tendon interface is another critical research area in addition to tendon-bone interface, for integrative tendon repair. As tendon connects muscle to bone, the MTJ, which connects muscle to tendon acts as a bridge to distribute mechanical load between muscles and bones [91]. However, any injury at the muscle-tendon junction will result in failure in mechanical load distribution. This will result in movement restrictions and low quality of life to the injured individual due to the extreme pain associated with the injury [91]. Current clinical treatments include conservation or surgical. In conservation treatment, the patient is normally asked to rest to relief the pain, or is

given injections of a variety of drugs, including corticosteroids and physiotherapy. However, due to the limited self-healing capacity of tendons, these types of treatments can result in prolonged treatments times, recurrent injury, weakness in the affected site, and thus partial loss of function, which can require extensive and intensive future rehabilitation [236, 237].

Surgical intervention includes the use of autografts and allograft to treat tendons injuries. However, the high price demand, pain and the donor site morbidity associated with harvesting autograft, as well as the limited availability and poor biocompatibility of allografts, in addition to the poor integration of these grafts with the surrounding tissues, are some of the drawbacks associated with the use of autografts and allografts [238].

Alternatively, the ability of cells to sense the mechanical signals can be used as another treatment option, which is referred to as Mechanotransduction. In this treatment, mechanical stimuli are applied at the injured site guiding cells to convert the mechanical stimuli into biochemical signals that can be used to aid the healing process [239]. However, many factors can either positively or negatively affect the overall outcome of tendon healing such as the duration, frequency, magnitude and type of mechanical stimulation applied to a tendon [240]. Therefore, the specific parameters of the Mechanotransduction treatment necessary to improve or accelerate the healing process without causing any damage to the tendon remains unclear [241]. Limitation associated with the current clinical treatment clearly highlight the need for more functional and integrative methods that mostly focus on effectively regenerating these tissues rather than repairing them

1.2.2.6.Muscle-Interface-Tendon Junction Tissue Regeneration Approaches

Tissue engineering approaches for muscle-tendon interface repair may include the use of scaffold-based techniques or may be associated with scaffoldless fabrication methods. Scaffold-based approaches include the use of composite, stratified and gradient scaffolds, in which the native tissue can effectively be stimulated and mimicked. On the other hand, scaffoldless approaches largely rely on the concept of cellular self-assembly or self-organization for tissue formation or repair without the use of an exogenous substrate [90]. To date, relatively very few studies have explored the feasibility to muscle-tendon interface regeneration comparing to the tendon-bone interface. This may be due to the fact that the majority of tendon injuries occur in either the tendon proper or the tendon-bone insertion, which limits the number of trails in this area. In addition, it has been reported that no single biological scaffold has been ideal for muscle and tendon regeneration, which marks them as inappropriate for developing a functional tissue engineered muscle-tendon interface [94]. However, limitations associated with the clinically applied methods for the treatment of muscle-tendon interface injuries have established an unmet clinical need for the development of new strategies to restore the function of the native muscle-interface-tendon junction.

An ideal scaffold design for muscle-tendon interface repair should mimic every single aspect in the native tissue for successful restoration of the muscle-tendon-bone junction. The engineered scaffold should consist of distinct multiple phases with different mechanical properties with the ability to withstand mechanical loads values near that undergone by the native tissue junction. In addition, the scaffold should structurally and compositionally mimic the native muscle-interface-tendon junction.

The first successful fabrication of multiphasic muscle-tendon graft with functional MTJ was adopted by Larkin et al. from a heterogeneous muscle “sarcolemma” and tendon “fibroblasts” isolations, a scaffoldless substrate has been fabricated by co-culturing both cell types. Specifically, cylindrical scaffoldless multiphasic tissue construct was created with robust interfaces. The contractile and structural characteristics of the muscle constructs co-cultured with (1) engineered self-organized tendon constructs, or (2) segments of adult or (3) fetal rat-tail tendon have been evaluated in vitro. In addition, the construct diameter (1 m) and maximum isometric force (microN) were measured, and specific force (kPa) was determined. In vitro evaluations revealed that the neo-interface region exhibited upregulated expression of muscle-tendon junction-specific paxillin (Figure 1.24), and was able to maintain tensile loading at super-physiologic strain rates [92]. However, when extended to the point of rupture, they failed at the mid substance of the engineered muscle, with the muscle-tendon interface intact. When implanted *In vivo*, it resulted in complete maturation and integration to the native tissue [93]. This, however, resulted in increased in force production, which in turns strengthened the MTJ. This successful initial step towards the regeneration of the muscle-interface-tendon junction clearly outlines the feasibility of the engineering MTJ.

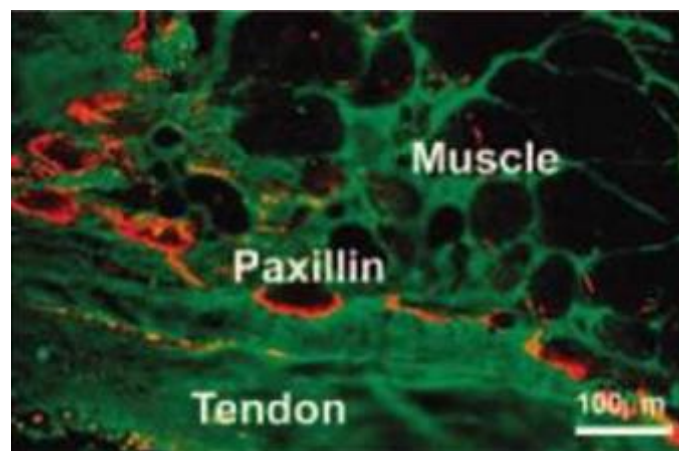


Figure 1.24 Immunostaining for paxillin indicating its upregulation at the MTJ of a scaffoldless muscle construct created by co-culturing a heterogeneous muscle “sarcolemma” and tendon “fibroblasts” isolations [92].

Larkin et al. has further investigated another possibility of restoring the MTJ by developing an in vitro model of three-dimensional (3-D) skeletal muscle-tendon constructs to address mechanisms of the MTJs development. In this study, it was hypothesized that engineered in vitro 3-D skeletal muscle-tendon constructs would develop MTJs ultrastructurally resembling those found during fetal development *In vivo* [100]. MTJs structures *In vivo* has been compared to those developed in 3-D skeletal muscle constructs co-cultured with engineered self-organized tendon constructs (SOT), or segments of adult (ART) or fetal rat tail (FRT) by means of electron microscopy. In vitro evaluations revealed that some of the myofibers of the engineered 3-D skeletal muscle-FRT and -SOT constructs only displayed emerging finger-like sarcolemma projections surrounded by collagen fibers, which structurally resemble fetal MTJs *In vivo*. In addition, a complete muscle-interface-tendon junction was developed on the muscle-FRT constructs. These findings suggest that the muscle-FRT constructs model could be used for studies of developmental mechanisms involved in the establishment of interfaces among all four muscular-skeletal tissues: muscle, tendon and cartilage/bone.

Recently, Ladd et al. developed a tri-phasic PC-collagen and PLA-collagen co-electrospun nanofibers scaffold onto opposite ends of a mandrel to create a scaffold with three regions for engineering muscle-interface-tendon junction [95]. *In vitro* evaluation demonstrated that the scaffold exhibited regional variations in mechanical properties with moduli from 4.490-27.62 MPa, similar to the native muscle-tendon junction and generally withstood cyclic testing. In addition, further results revealed that the scaffold facilitated both myoblasts and fibroblasts attachment at the relevant-cell rejoins.

To this end, different approaches have been demonstrated for the regeneration of the complex muscle-interface-tendon and tendon-interface-bone junctions starting by using biological grafts to the use of gradient scaffolds that exhibited continuity in the structure, which in turn led to improved gradual, continuous mechanical transition, cellular interactions, and gradient in mineralization across the muscle-tendon-bone junction in addition to supporting the formation of fibrocartilage interface. Muscle-tendon interface regeneration is a critical research area for integrative tendon repair that has not been explored enough yet. Further studies in this area are indeed required in order to overcome many limitations associated with muscle-tendon regeneration.

In summary, the aforementioned studies demonstrate the promise of the complex gradient scaffold system for tendon-to-bone interface tissue engineering as well as the potential of utilizing cellular interaction for engineering both tendon-to-bone and muscle-to-tendon interface and ultimately, functional and integrative tendon repair.

1.2.3. The Complex Cartilage-Interface-Bone Regeneration:

1.2.3.1. Cartilage-Interface-Bone Junction Complex Structure

1.2.3.1.1. Cartilage Zones Structure and Function

Osteochondral (OC) is a uniquely structured tissue that is comprised of articular cartilage, the subchondral bone and the central cartilage-bone interface (Figure 1.25) [102]. This unique hierarchical structure plays an important role in maintaining the tissue homeostasis as well as providing the synchrony in physiological movement. The articular cartilage is further divided into three distinguishable well-organized articular cartilage zones from top to bottom [103]. The first top is the superficial or tangential zone, which occupies 10-20% of the articular cartilage [124].

The next is the middle zone, which occupies the following 40-60% of the articular cartilage, and the remaining thickness is occupied by the deep zone and the calcified cartilage which is believed to be 30% of the total articular cartilage thickness.

Cells within the superficial zone or “articulating surface” are known to secrete special types of proteins that facilitate the wear and frictional properties of the tissue during movement [106]. The middle zone, the largest zone, has the most abundant content of proteoglycans (GAC) with the least number of cells. This zone is known for its arch shaped, and obliquely oriented collagen fibrils, which inherits its high compressive modulus that allows recovery from impacts undergone by the articular surface [107, 125]. In the deep zone, where the fibrils are anchored in the underlying subchondral bone, cells and the collagen fibrils are oriented perpendicularly to the articular cartilage’s surface [108]. This zone is known for its high compressive modulus, less proteoglycans content comparing to the middle zone, and less cellular content comparing to the previous two zones [109]. However, the GAC nature of the two last layers enables the extracellular

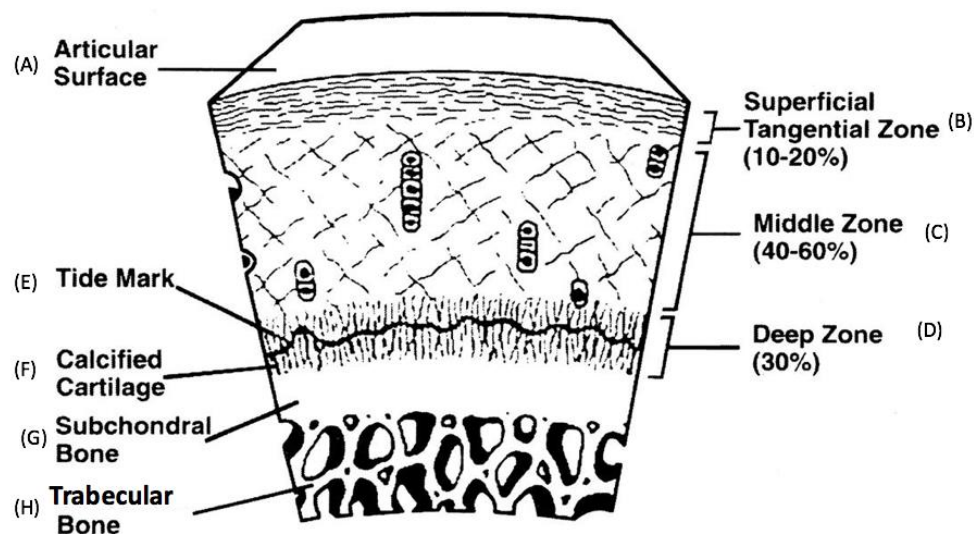


Figure 1.25 Osteochondral tissue structure. Cross section of the long bone and its zonal cartilage including (A) articular surface, (B) the superficial zone, (C) the middle zone, (D) the deep zone (E) tidemark (the interface), (F) calcified cartilage, (G) subchondral bone, and (H) trabecular bone [102].

matrix to withstand high compressive forces. At the bottom of the deep zone, a thin layer known as “tidemark”, marks the interface between the last calcified cartilage zone to the subchondral bone. This layer is known to minimize the stiffness gradient between the cartilage and subchondral bone. The cell content and the collagen fibrils are very minimal in this last layer [110].

The articular cartilage is a rich collagen tissue that is mainly composed of collagen type II, however, other collagen types V, VI, IX, and XI are also present throughout the zonal cartilage, which play a role in the intermolecular interactions and the modulation of type II collagen [104]. In addition, type X collagen is known to assist in the mineralization between the cartilage and underlying bone [105].

1.2.3.1.2. Subchondral Bone Structure and Function:

The subchondral bone is the last components of the osteochondral tissue, which is located just below the interface between the zonal cartilage and the subchondral bone. It is composed two bony zones, lamella and trabeculae. The lamella however, contains a large mass of bone with thicknesses variations between 0.2 – 0.4 mm in humans [111]. The trabecular of the subchondral bone supplies both the lamella and the adjacent articular cartilage with nutrition due to the high vasculature nature [112]. However, the three main functions of the subchondral bone are absorption, maintaining joint shape as well as providing the strength to the adjacent articular cartilage due to its large area and low modulus of elasticity [113].

1.2.3.2.Osteochondral Defect:

Articular cartilage is a connective tissue that acts as a shock absorber and facilitates joint's motion in low friction [101]. Like any other tissue, the articular cartilage is prone to lesions for many reasons, such as traumatic events, chronic repetitive microtrauma, and aging [114]. Distinct from bone, the avascular nature of articular cartilage makes it irreparable due to the consequent lack of supplementation of potentially reparative cells/bioactive factors, which makes the possibility of the cartilage to self-regenerate below minimal [115]. Thus, as the cartilage lesion progresses, it extends to the underlying subchondral bone and the osteochondral defect (OCD) appears. Not only diseases orienting from cartilage will result in OCD, in fact, other disease originating from the subchondral bone can also induce OCD when reached the cartilage layer, such as osteochondritis dissecans and osteonecrosis [116].

As a result of the OCD, the formation of fibrocartilage tissue at the defect site takes place, which only provides very poor protection to the subchondral bone [117] However, the continuous movement of the individual can cause a subsequent degradation to the formed fibrocartilage tissue following by degradation to the adjacent tissues as well, resulting in impaired joint mobility, severe pain, and low quality of life, which necessitate the clinical intervention [118, 119].

1.2.3.3.Current Clinical Treatment for Osteochondral Defects

Current clinical treatments to OCD are limited by arthroscopic debridement, bone marrow stimulation techniques, the use of osteochondral allografts, autologous chondrocyte implantation (ACI), or matrix-assisted chondrocyte implantation (MACI) [120, 221]. while debridement and marrow stimulation techniques have shown some positive results in treating OCD, these techniques are palliative, but not curative and has no significant benefits for larger OCD [121]. In addition,

the poor biocompatibility and integration of allografts to the host tissues led to the necessity of finding alternative therapies that mostly focus on regenerating the damaged tissues rather than repairing or replacing the tissues.

ACI and MACI are two clinical reparative techniques that to a certain extent have overcome most of the drawbacks associated with the discussed conventional clinical treatments. However, ACI generally involve an arthroscopic evaluation of the defect site, following by a biopsy collection from the same patient. The biopsy is then used to isolate autologous chondrocytes, expand them in culture and finally seed them back onto the affected area [223]. A similar approach is followed for the MACI with a slight difference, where the chondrocytes are first seeded on a biodegradable matrix and then implanted at the affected area [223]. Although these two approaches are considered the gold standard among all the alternative clinical treatments in the modern medicine, limitations are still presented which include; the creation of a second OCD during the biopsy, the multiple number of surgeries required, the relatively long recovery time as well as the slow regeneration of the defect [224].

The aforementioned clinical treatments are more focused on either palliating the pain associated with the OCD or repairing the damaged cartilage only. It was shown in many reports that without the support from the subchondral bone, any treatment to reestablish the cartilage layer is likely to fail [122]. Thus, the cartilage and subchondral bone should be taken into account as one unit during OC regeneration, instead of being considered separately. This comes after the fact that both the zonal cartilage and the subchondral bone are tightly connected, and no matter where the disease is orienting from, the connected tissue will always be affected, which will result in the negative contributions to the mechanical homeostasis of the whole joint [123].

In another word, OCD leads to the degeneration in bone, cartilage and the bone–cartilage interface. However, in order for OCD defect repair to be possible it is essential that each of these components be taken into account as one complex synchronized unit during OC regeneration, instead of being considered separately, as the main goal for OC regeneration is to restore its biomechanical properties, besides the regeneration of the defect.

This end, Complexity associated with the unique structure of Osteochondral tissue requires the development of a complex multi-phased biomimetic matrix that not only support regeneration of the zonal structure but also helps to establish a proper cartilage-bone interface.

1.2.3.4. Cartilage-Interface-Bone Tissue Regeneration Approaches:

One of the very early tissue engineering attempts to regenerate an osteochondral defect was adopted by Chu et al. In this study, commercially available PLLA cubes were used to fabricate a single-phased osteochondral scaffold. Peri-chondrocytes were derived from the cartilage of New Zealand white rabbits and used to pre-seed the scaffolds prior to *in vitro* and *In vivo* evaluations [225]. Both *in vitro* and *In vivo* evaluations showed an extensive production of collagen type I as high as $81 \pm 4 \%$, with very minimal production of collagen type II. Although the single-phased scaffold did not show evidence for sufficient production of collagen type II, it supported the proliferation, attachment and survival of the pre-seeded peri-chondrocytes cells.

In a different attempt, Malda et al. evaluated the effect of the scaffold's fabrication techniques on the osteochondral regeneration based on the hypothesis that the scaffold design can highly affect the regeneration of the osteochondral tissue [226]. In this study, two different fabrications

techniques, compression molding, and 3D fiber deposition were used in order to fabricate a single-phased scaffold using the biodegradable poly(ethylene glycol) terephthalate/poly(butylene terephthalate) (PEGT/PBT). Pore size analysis revealed that there was a significant pore size variation between the two scaffold designs, where the compression molding scaffolds had an average pore size of 182 μm , while the 3D fiber deposition scaffolds had an average pore size of 525 μm . To further validate the hypothesis, both scaffolds were pre-seeded with chondrocytes and *in vitro* and *In vivo* evaluations were conducted. *In vitro* evaluations showed a slight increase in the DNA content of the compression scaffold after 3 days of culture in comparison with the other scaffold, but no difference was noticed after 14 days. *In vitro* GAC production was also determined resulting in no difference between the scaffolds at all-time points. *In vivo* evaluations in a nude mice subcutaneous model showed that there was an increase in the GAC production in the 3D fiber deposition scaffolds in comparison with the compression scaffold along with a better mechanical integrity. This study suggests that porosity as well as the scaffold architecture may play a crucial key role in the osteochondral tissue regeneration.

Following a different approach, Coburn et al. developed a single-phased poly(vinyl alcohol)-methacrylate and chondroitin sulfatemethacrylate low density electrospun nanofibers scaffold that was used to aid chondrogenesis of goat MSCs *in vitro* [227]. *In vitro* results showed that the scaffold exhibited an elastic-like mechanical properties similar to that found in the hyaline cartilage. In addition, further tests showed an increase in cell proliferation and an extensive accumulation of GAC and lacunae formation. To evaluate the *in vitro* production of both collagen types I and II, Immunohistochemical assay was conducted resulting an increase in collagen type II production, with no evidence of collagen type I production. This indicated that the addition of

chondroitin sulfatemethacrylate facilitated the production of collagen type II and had no effects on collagen type I production. *In vivo* evaluations for the scaffold in a rat osteochondral model revealed that the nanofiber scaffold defect had a higher proteoglycan deposition than the empty defects but less proteoglycan deposition than normal articular cartilage. Similar to the *in vitro* study, collagen type II was observed with no evidence to collagen type I in the nanofiber scaffold. Results from this study demonstrate the potential of chondroitin sulfatemethacrylate in supporting cartilage regeneration, in addition to the potential of nanofibers matrix to serve as suitable scaffold for cartilage regeneration for osteochondral defect applications.

Although these observations suggest that the single-phased scaffolds may support the proliferation, attachments of both bone and cartilage cells as well as the production of collagen type II and GAG *In vivo*, they do not mimic the complexity found at the native osteochondral tissue. This clearly demonstrates the need for a biomimetic multi-phased scaffold that mimics the complexity found in the native tissue, which in turn can guide the regeneration of multi—tissue interface.

Based on these findings from the single-phased scaffolds, there has been a serious shift towards the production of bi-phasic and multiphasic scaffolds to facilitate the regeneration of the different components found in the native osteochondral tissue including the interface. Getgood et al. developed two bi-phasic scaffolds to evaluate their performance at healing medial femoral condyle and lateral trochlear sulcus osteochondral defects in a caprine model [228]. The first scaffold was composed of collagen–GAG phosphate, while the second scaffold composed of PLGA/PGA. Both scaffolds were implanted on the defects made either in the medial femoral condyle or the lateral trochlear sulcus. *In vivo* evaluations revealed that the collagen-GAC scaffold became stiffer and

provided radical mechanical reinforcement after 12 weeks in comparison with the other scaffold. After 26 weeks, defects treated with collagen-GAC had a significantly higher content of hyaline cartilage in comparison with defects treated with PLGA/PGA scaffolds, 75% - 50% respectively. In addition, the Stellar's histological score in the lateral trochlear sulcus was significantly higher when treated with the collagen-GAC scaffold than PLGA/PGA scaffolds (Figure 1.26) [228].

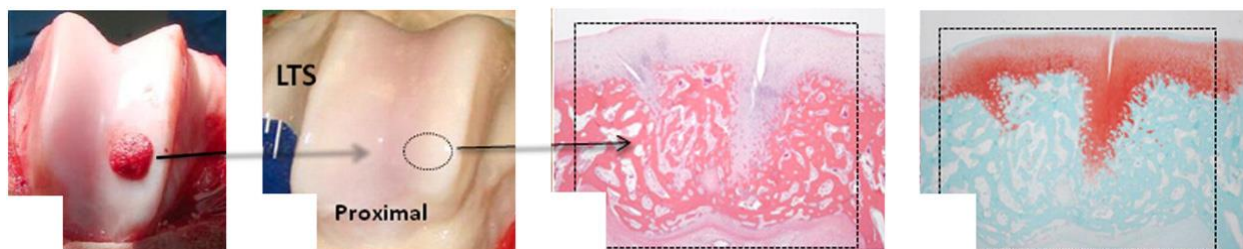


Figure 1.26 *In vivo* repair. Photographs of an osteochondral defect site in the lateral trochlear sulcus (A) immediately after and (B) 26 weeks after implantation of a collagen-GAG scaffold along with the (C) H&E and (D) Safranin-O with fast green histological stains of the explants [228].

Another bi-phasic but stratified scaffold for osteochondral regeneration was devolved by Chen et al. [229]. The upper layer of the scaffold for cartilage regeneration was made from collagen sponge, while the lower layer for bone regeneration was made from PLGA 75:25 and naturally derived collagen. To fabricate the porous PLGA-collagen base layer, a particulate-leaching technique was used. Briefly the scaffold was immersed in a type I collagen solution following by the addition of collagen acidic solution to one side of the scaffold until solidified. The collagen/PLGA-collagen scaffold was pre-seeded with BMSCs and cultured for 1 week *in vitro* as an *ex vivo* step prior to an *In vivo* implantation in femoral condyle beagle model. Four months after implantation, it was found that cartilage and a bone-like tissues were formed in the respective layers. Additional *In vivo* data revealed that the implant well integrated with the surrounding host tissues suggesting that collagen/PLGA-collagen bi-phasic scaffold is useful for osteochondral tissue engineering.

Growth factors have been also used along with scaffolds as a strategy for osteochondral tissue engineering to enhance chondrocytes proliferation and to cue cells to form the specific tissues found in the native OC. Huang et al. devolved a poly(L -lactic acid)/ amorphous calcium phosphate (ACP/PLLA) hybrid scaffold incorporated with basic Fibroblasts Growth Factor (bFGF) for osteochondral regeneration [230]. The scaffold was implanted in a femoral condyle osteochondral defect in a rabbit model for 4 and 12 weeks. Untreated defects and PLLA scaffolds incorporated with bFGF were used as controls. *In vivo* assessments revealed that the PLLA-bFGF treated defects presented better defect regeneration when compared to the untreated group in all time points. Although PLLA-bFGF group showed a good defect regeneration, only low amount of collagen type II was observed with a completely negative expression to aggrecan. On the other hand, ACP/PLLA treated defect was completely filled with well-established cartilage tissue and cartilaginous ECM after 12 weeks. In addition, an extensive collagen type II production was observed and high levels of aggrecan gene expression were detected.

Growth factors have been also incorporated in a gradient fashion to establish a scaffold for osteochondral interface regeneration. Mohan et al. devolved a growth factor gradient scaffold that consisted of TGF-B1 and BMP-2 in combination with PLGA microspheres for osteochondral repair [231]. TGF-B1 was used to establish chondrogenesis at the upper portion of the scaffold, while BMP-2 was used to establish osteogenesis at the lower portion of the scaffold. Combining both factors in a gradient fashion in a single scaffold was based on the hypothesis that the combination of both factors can facilitated the formation of the zonal cartilage, subchondral bone as well as the interface in between. However, the scaffold was composed of a chondrogenic layer of TGF-B1-loaded PLGA microspheres, the osteogenic layer was composed of BMP-2 or BMP-

2/HA-loaded PLGA microspheres with a gradient transition between both factors in the middle. Blank PLGA scaffold or blank gradient PLGA and PLGA/HA scaffolds were used as controls. Scaffold were implanted in a medial condyle osteochondral defect in a rabbit model for 6 and 12 weeks. It was observed that after 6 and 12 weeks, a great extent of cartilage and subchondral bone similar to that found in the native tissue were achieved in the growth factors loaded groups comparing to the controls based on the gross morphology, MRI and histological data. In addition, TGF-B/BMP-2/HA-loaded PLGA microspheres group showed well edge integration with the host bone comparing to all the other groups. These data suggest that incorporating both BMP-2 and HA can facilitate better bone ingrowth and integration to the host bone. In addition, the results suggest that TGF-B1 may also enhance cartilage regeneration and the combination between both factors may facilitate the interface regeneration.

Integrating cell based approaches along with growth factors has been also considered in the creation of an osteochondral repair scaffold. Various cell types have been used to aid in the regeneration of osteochondral defect such as progenitor cells and tissue specific cells such as chondrocytes for cartilage regeneration and osteoblasts for bone regeneration [232]. Due to the very small number of chondrocytes found in the cartilage, as well as the difficulties associated with maintaining their phenotype in culture, they may not be transitional [233]. In fact, the thorough digestion required to the cartilage matrix by collagenase in order to isolate chondrocytes may be harmful to the cells. Furthermore, chondrocytes lose their proliferation capabilities as well as their capability to produce collagen type II and I as soon as the fourth passage is reached by 29,000 folds when compared to the freshly isolated chondrocytes [234]. Due to the aforementioned limitations associated with chondrocytes isolation, maintenance and usage, many

researches shifted to the use of progenitor cells such as stem cells due to their source availability in various body parts, rapid proliferation, and their potential to undergo chondrogenic and osteogenic differentiation, which marks them as ultimately useful for osteochondral tissue engineering [235].

Cell aggregation at the osteochondral defect has been shown to be crucial for extra cellular matrix synthesis and proteins production to support OC tissue regeneration [109]. In a study by et al, a novel cell-based approach that mostly focused on supporting the aggregation of bone marrow mesenchymal stem cells (rBMSC) for osteochondral regeneration has been devolved [109]. In this study, Different densities of isolated rat rBMSC aggregates were encapsulated in fibrin hydrogel and injected in a rat osteochondral defect model. Four experimental groups have been involved for the *In vivo* study as follows, fibrin gel encapsulated with high density of rBMSC aggregates, low of rBMSC aggregates, sham and fibrin hydrogel alone filling the defect. 8 weeks post implantation, various post-vivo evolutions have been conducted in order to evaluate the tissue regeneration including; gross morphology observations, H&E, Safranin O for GAGs, collagen I, II, and aggrecan immunostaining. Gross morphology analysis showed that fibrin gel encapsulated with high density of rBMSC aggregates demonstrated a complete repaired to the defect, with much smoother texture surrounding the defect area and color similar to the native cartilage in comparison with the other groups including the sham. Immunohistochemistry showed an extensive GAC and collagen type II production with a moderate staining of Safranin O in the high-density aggregates group comparing to the low density and fibrin alone. In addition, Collagen type I was evident in all groups and stained deeper in the defect filled with high density aggregates. These recent findings demonstrate the potential of employing cell-based approaches, more specifically, high

cellular aggregates densities in facilitating osteochondral tissue regeneration. In this study, fibrin gel encapsulated with high densities of cell aggregates facilitated deep bone formation and full thickness cartilage formation, which suggest that it can be used as a candidate for osteochondral tissue regeneration.

In summary, both stratified and gradient scaffolds in conjunction with growth alone or in combination with cells have been suggested to be great candidate for cartilage-interface-bone regeneration. Results from the literature highlighted the limitations towards osteochondral regeneration as well as demonstrated all the possible strategists that can be applied in order to facilitate OC regeneration. Further studies are indeed required in order to prove the capabilities of stratified and gradient scaffold for osteochondral regeneration to accelerate clinical translation.

1.2.4. Cell-Cell Interaction to Form Interfaces in Ligament/Tendon-to-Bone Junctions.

It is well established that tendon-to-bone healing following an ACL reconstruction does not result in adequate graft integration at the bone tunnel; rather it results in the formation of a fibrovascular or fibrocartilaginous tissue that lacks all biological and mechanical functions of the native fibrocartilage tissue [71]. The formation of a nonmineralized fibrovascular within the bone tunnel results in a weak link at the graft-to-bone fixation site. However, developing a fibrocartilage zone at the insertion side (outside the bone tunnel) will physiologically be more relevant to promote biological fixation.

The formation of fibrocartilage zone upon attaching tendon directly to bone in some cases led to the hypothesis that the interactions between cells derived from tendon (e.g., fibroblasts) and bone (e.g., osteoblasts) play a crucial role in the regeneration of the fibrocartilage interface at the

insertion site [98]. The previously discussed study adopted by Fujioka et al. [71] revealed that cellular organization at the native insertion site was observed over time after an Achilles tendon has been sutured to the original attachment site. This study demonstrated the feasibility to fibroblasts-to-osteoblasts interactions at the insertion site which may result in the formation of fibrocartilage matrix similar to that found at the native tissue junction. Based on these findings, it was hypothesized that fibroblasts-to-osteoblasts interaction interpose interface regeneration through two mechanisms: (1) osteoblasts, fibroblasts, or both undergo transdifferentiation or phenotypic changes, and (2) progenitor stem cells or MSCs recruit to the graft-bone interface, where they differentiate into fibrochondrocytes and form the fibrocartilage interface [98].

To further examine the aforementioned hypothesis and observations, one of the studies made an attempt to mimic the *In vivo* interactions between fibroblasts and osteoblasts during ACL recantations by creating a co-culture system in vitro. In this system, a hydrogel divider was added in the middle of the culture well that separated the well into two equal chambers. Fibroblasts were seeded in one chamber, and osteoblasts were seeded in the other chamber (Figure 1.27) [99]. When both cells reached confluency, the divider hydrogel was removed allowing the cells to migrate and interact at the interface region, which resulted in the formation fibrocartilage-like rejoin. These findings demonstrate the potential of fibrocartilage interface regeneration as a result of the interactions between fibroblasts and osteoblasts at the insertion site.

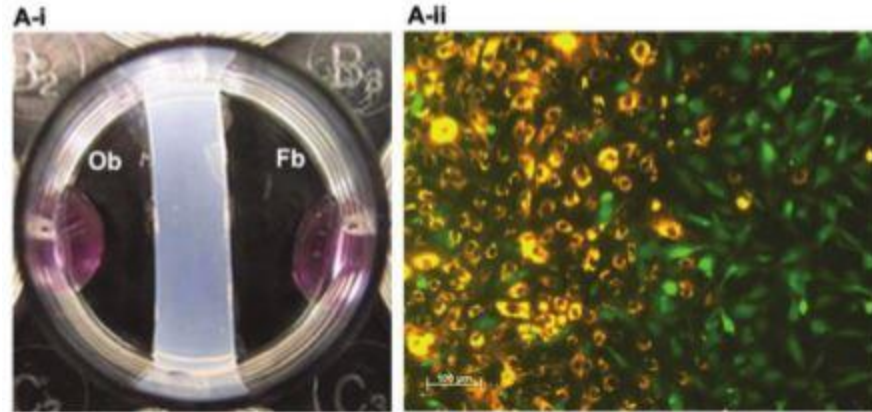


Figure 1.27 (Ai) In vitro co-culture model to evaluate the interactions of interface-relevant cells of fibroblasts and osteoblast permit heterotypic and homotypic cell-cell interactions [99]. (Aii) Co-culture models to evaluate interaction of interface-relevant cells. (A-i) In vitro coculture model of fibroblasts (Fb) and osteoblasts (Ob) permit heterotypic and homotypic cell-cell interactions. (A-ii) Fibroblast (CFDA-SE, green) and osteoblast (CM-DiI, orange-red) distribution at day 7, bar = 100 μ m [99].

1.2.5. Cell-Cell Interaction to Form Interfaces in Muscle-Tendon Junction.

Although the exact mechanism of MTJ development is not well understood, very limited number of studies revealed that the interaction between tenocytes and myotubes is an essential process that leads to the formation of specialized muscle-tendon interface (MTJ) [93]. In fact, the development of MTJ is influenced by some factors that are essential to establish a functional muscle-tendon interface including; interactions within muscle and tendon cells, interactions between the future forming muscle and tendon tissues in addition to some functional and structural interactions between tenocytes and myotubes at the site of future MTJ [93]. These interactions take place gradually until a complete and functional MTJ is formed. First, cells within tendon interact forming a rich collagen matrix. Muscle cells interaction results in the formation of well devolved muscle tissue that consists of myofibers. Myofibers then, apply a lateral force to the tendon by the muscle contraction, and in response to this contractile force applied to the tendon, tenocytes and the tendon's ECM components such as collagen fibers align themselves in the direction of the applied

force. This allows for a direct contact between tendon and muscle through long cytoplasmic processes. This direct contact enables the tapered ends of the muscle myofibers to embed into the ECM of the tendon, forming a well-developed MTJ through the creation of a network of overlapping muscles and tendon tissues with a greater surface area for adhesion (Figure 1.28) [70, 93].

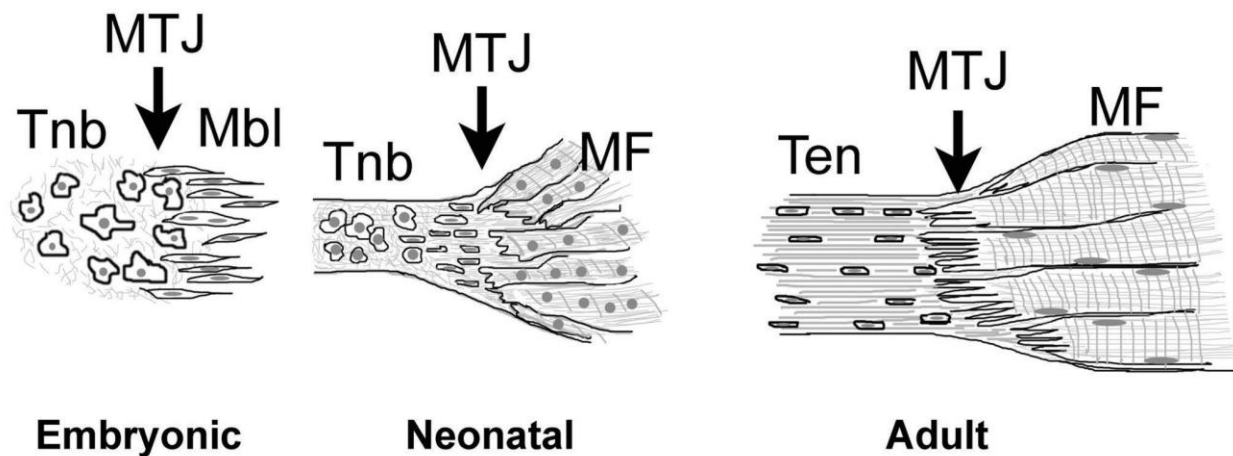


Figure.1.28. Schematic picture of the MTJ structural development from early embryonic and neonatal to adult stages. MTJ: myotendinous junctions; Tnb: tenoblasts; Mbl: myoblasts; Ten: tenocytes; MF: muscle fibers [93].

In an attempt to address the mechanism of the MTJ's development, Larkin et al. developed an in vitro model of three-dimensional (3-D) skeletal muscle-tendon constructs based on the hypothesis that engineered in vitro 3-D skeletal muscle-tendon constructs would develop MTJs resemble those found during fetal development *In vivo* [92]. To validate the hypothesis, MTJs structures *In vivo* has been compared to those developed in 3-D skeletal muscle constructs co-cultured with engineered self-organized tendon constructs (SOT), or segments of adult (ART) or fetal rat tail (FRT) by means of electron microscopy [92]. In vitro evaluations revealed that some of the myofibers of the engineered 3-D skeletal muscle-FRT and -SOT constructs only displayed emerging finger-like sarcolemmal projections surrounded by collagen fibers, which structurally

resemble fetal MTJs *In vivo*. In addition, a complete muscle-interface-tendon junction was developed on the muscle-FRT constructs. These findings suggest that the muscle-FRT constructs model could be used for studies of developmental mechanisms involved in the establishment of interfaces among all four muscular-skeletal tissues: muscle, tendon and cartilage/bone.

1.2.6. Cell-Cell Interaction to Form Interfaces in Cartilage-Bone Junction.

Cell-cell interactions is important for the formation of a tissue interface. The interactions between many cells types have been examined to evaluate their contributions in the formation of cartilage-bone interface in the osteochondral tissue by co-culturing cells relevant to tissue types like fibroblasts, osteoblasts and chondrocytes, or stem cells such as mesenchymal stem cells (MSCs) in a biomimetic 3D microenvironment [392 ,393].

Jiang et al. studied whether relevant tissues cells such as chondrocytes and osteoblasts can contribute and interact to form the interface found at the cartilage-bone junction [394]. In this study, a stratified agarose hydrogel and composite microspheres of polylactide-co-glycolide (PLGA) and 45S5 bioactive glass (BG) scaffold mimicking the three distinct yet continuous regions of cartilage, calcified cartilage and bone has been developed. The scaffold was developed in order to evaluate the potential of osteochondral interface formation by coculturing chondrocytes at the agarose hydrogel phase, and osteoblast at the PLGA-BG phase. In vitro analysis showed extensive chondrogenesis and improved graft mechanical property over time. In addition, it was shown that PLGA-BG phase promoted chondrocyte mineralization, which in turns aided the formation of the interface region and bone. These results demonstrate the potential of co-culturing relevant tissue cells such as chondrocytes and osteoblasts in the formation of osteochondral interface.

In a similar approach, Chen et al. created a stem cell-derived osteochondral interface using an interface-specific microenvironment in 3D configuration via multilayered co-culturing [395]. In this study, MSCs were encapsulated in collagen microspheres, which guided their differentiation into chondrogenic and osteogenic functional units that enabled the formation of the mediated interface. The pre-differentiated functional microspheres layers were combined to form a tri-layered scaffold with the chondrogenic microspheres on top, osteogenic microspheres at the bottom, intermediating with an undifferentiated layer of MSCs encapsulated in collagen microspheres. Culturing the tri-layered construct in a chondrogenic medium generated a continuous calcified interface with hypertrophic chondrocytes and extensive production of collagen type X. In addition, intermediating the undifferentiated MSC with the two differentiated layers in the coculture system resulted in enhanced integration of the three distinct phases enabling the formation of an osteochondral -like interface. These data suggest the potential of coculture differentiated and undifferentiated MSCs in an appropriate 3D microenvironment for the regeneration of osteochondral interface.

Findings from these two studies suggest that both, tissue-relevant cells as well as stem cells have the potential to interact when co-cultured in biomimetic 3D microenvironments and form an interface-like tissue. Further studies are indeed required in order to study the interactions of these cells in more complex heterogenic environment for prolonged times to examine their potential to sustain the formation of the interface-like tissue.

1.3.Coaxial and Uniaxial Electrospinning

There are four major tissues in the human body: connective, epithelial, nervous, and muscles [341]. Regardless the tissue type and function, the extracellular matrix (ECM) of these tissues is composed of an intricate network of interconnected macromolecules such as proteins and polysaccharides [342]. During the tissue development, these macromolecules are secreted and adequately organized by cells, once secreted and organized, they can then be seen as non-woven network of bundle structured fibers known as the (ECM). The ECM as whole functions as scaffolding for tissues within the body, providing the appropriate three-dimensional framework for proper cell attachment, proliferation and multitude of signaling pathways (Figure 1.29) [343-345].

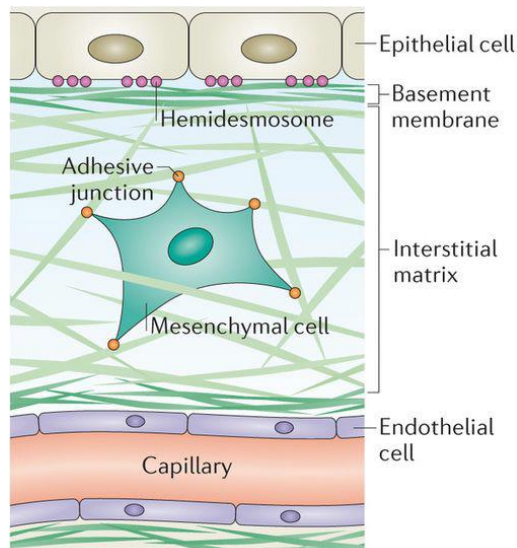


Figure 1.29: Extracellular (interstitial) matrix. [346].

Macromolecules are found in different densities and organization depending on the function each tissue is intended to do. For example, connective tissues such as bone, ligament and skin have denser and more highly organized ECM structure than other tissues such as brain and adipose due to the increased demand for mechanical support, structure and protection [342-345, 347-358].

However, like any other tissue, these tissues are prone to injuries or trauma that can lead to tissue damage or degeneration. In some cases, damaged tissues can restore their function and structural integrity after injuries by following the normal body's self-repair mechanics, however, if self-repair mechanisms are overstrained, in the case of a complete ECM damage such as full thickness wounds, or third-degree burns, the need for tissue repair is indeed required in order to restore the structure and the function of these damaged tissues. Due to the fact that the microenvironment of the healing site is complex and involves a large number of molecules, which require a cascade of events for wound closure to occur, a well tissue engineered scaffold with an accurate structural, and physiochemical representation of the natural ECM will be required in order to restore the functional and structural integrity of the damaged tissues [359].

Scaffold is an essential component in tissue engineering because it physically supports cells and provides conditions for cell attachment, proliferation, migration, and differentiation, in addition to its ability to act as a reservoir for growth factor and other biomolecules are known to encourage the healing process. If the general and tissue-specific scaffold requirement are not met, tissue restoration and regeneration will not be accomplished [360]. Ideally, a scaffold should provide cells with a variety of physical, chemical, and biological cues that are naturally inherited by the native ECM to facilitate cell growth and function [361]. *In vivo*, cells are found entrapped within an ECM, in which they are provided with all the necessary physical and chemical cues that guide their development, arrangement and regenerative abilities by molecular interactions between specific cell membrane receptors and signaling cues from surrounding ECM material [361]. To duplicate the *in vivo* environment, the scaffold should exhibit controllable physical, chemical and mechanical properties, cell adhesion properties and growth factor release kinetics [362]. An ideal tissue engineering scaffold should be biocompatible that maintains cell viability *in vitro* and do

not elicit any immune response upon implantation *in vivo*. Also, the scaffold should be biodegradable with a degradation rate compatible to the rate of the neo-tissue formation to fully be replaced with newly formed tissue. The scaffold should also be highly porous to facilitate cell migration, proliferation, nutrition diffusion and waste removal, and should also exhibit biomimetic mechanical and architectural properties resembling those found at the native tissue [363]. Besides, the scaffold should serve as a reservoir for local, sustained, and controlled growth factors delivery to regulate cellular activities in order to help induce neovascularity and promote tissue regeneration.

Several technologies have been employed in the past few years aiming to produce scaffolds with location-specific topographies for functional and integrative tissue regeneration. Amongst all, nanotechnology is one of the very promising technologies that have shown many advances in the field of tissue engineering and regenerative medicine. Nanotechnology encompasses materials and structures on the nanometer scale, i.e., in the range from several micrometers down to few nanometers [364]. Compared to conventional macro-sized and bulk materials, nanostructures exhibit many unique advantages that include an extraordinarily high surface area per volume ratio, tunable optical emission as well as super paramagnetic behavior, which can be successfully exploited for a variety of health care applications such as biosensors and drug delivery [364]. Several nano-sized materials or structures such as nanotubes, nanocrystals, nanowires, nanocomposites, nanorods, nanospheres, and nanofibers have been employed for various high technology applications [364]. Nanofibers, for instance, have received a great deal of interest and are being explored for a wide variety of applications. In tissue engineering, nanofibers are being used as drug agent delivery, wound dressing materials, and as porous three-dimensional scaffolds

for engineering various tissues such as skin, blood vessels, nerve, tendon, bone, and cartilage [364]. The intrinsic properties of nanofibers such as high surface to mass ratio, low density, high pore volume, variable pore size and exceptional mechanical properties and more importantly the structural resemblance to the native ECM, have encouraged scientists to develop several fabrication methods for the synthesis of nanofibers. Some of these methods are phase separation, self-assembly and electrospinning. Of these, electrospinning is the most frequently chosen technique for the production of nanofibers because it is a simple, cost-effective, versatile process and is the only technique that can produce at a large scale continuous nanofiber for industrial applications [365]. Very limited number of studies have reported the production of nanofibers using self-assembly and phase separation [365].

1.3.1. The Electrospinning Technique

Electrospinning is a relatively old technique that was first patented in the early 1900 by Cooley. as an apparatus to prepare threads for the textile production [366]. The first apparatus setup consisted on grounded rotors that operated at a voltage of 10kv to collect fibers as strands for making fabric [367, 368]. Although this is a relatively old technique, it has been only used in the medical field over the past 10 years, in particular for the fabrication of tissue engineering scaffolds for growth factors delivery, cell based approaches or combined to stimulate the regeneration or regrowth [369-373]. Electrospinning is currently one of the most extensively used technique for tissue engineering scaffold fabrication due to the resemblance to the native ECM exhibited by electrospun scaffolds, and its ability to process a wide range of different natural and synthetic materials with different fibers orientations and diameters that can go to the sub-microns or nanometer scale depending on the applications needs. In addition, electrospun scaffolds possess biomimicry fibrous structure with high pore volume ranging between 60-90%, which is important

for cell infiltration and motility [252]. The general component for the normal electrospinning setup consist of a syringe to hold the polymer solution, two electrodes (positive and negative), a collector, and a high DC voltage supply (Figure 1.30) [374].

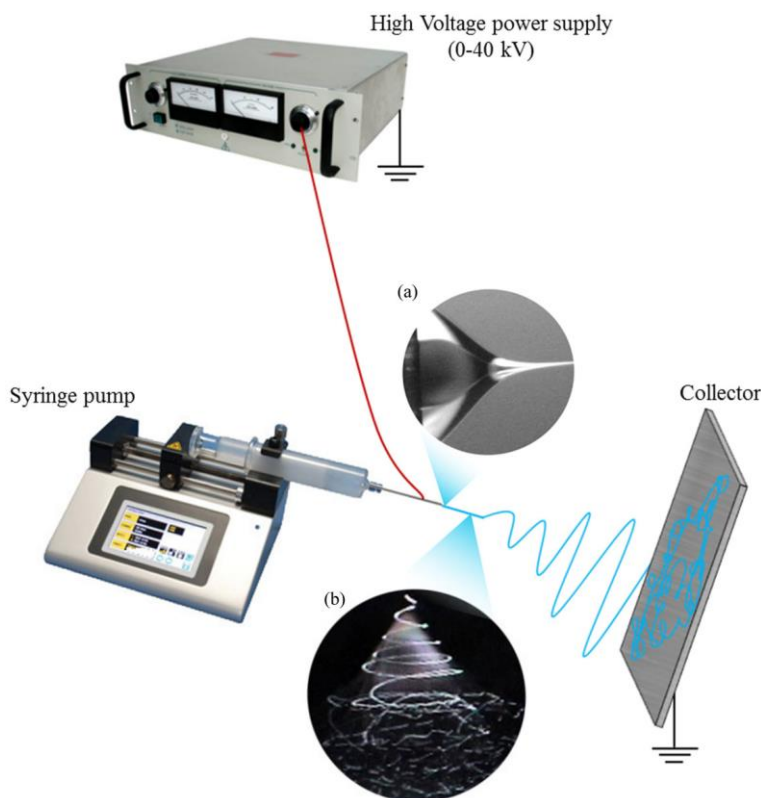


Figure 1.30: Schematic representation of electrospinning basic set up. a) Image of Taylor cone forming at the spinneret during the electrospinning process. [390]. b) Image of polymeric filament forming from Taylor cone and moving toward the collector. [391]

Briefly, polymer granules or powder are dissolved in the appropriate solvent until a viscous, homogeneous and completely dissolved polymer solution is obtained. A complete dissolution of the polymer is very important for a successful bead-free production of electrospun fibers. The polymer solution is then loaded into a syringe, and placed in an apparatus pump for electrospinning. During electrospinning, an electrical field of high voltage is applied at the syringe needle tip that creates large enough forces at the surface of the polymer solution to overcome the surface tension, resulting in the ejection of an electrically charged jet that solidifies into an

electrically charged fibers. The needle tip is normally placed some distance away from the collection unit to allow branching and drawing of the fibers to occur. [253, 254]. During electrospinning, if the droplet that appears at the tip of the needle was shaped into a Taylor cone geometry, this indicates that the electrospinning parameter and the setup as whole is producing quality of nanofiber. This is considered as the ideal case in electrospinning. On the other hand, if the droplet was shaped into a forked cone, this is an indication that there is an edge effect in the electrical field applied to the polymer solution. This is usually due to the high voltage magnitude applied during electrospinning and it can be overcome by reducing the voltage applied [375-377]. Taylor cone geometry can be seen in (Figure 1.30).

1.3.2. General Electrospinning Parameters

Polymer concentration, polymer solution viscosity, polymer molecular weight, chosen solvent, surface tension, vapor pressure, flow rate, applied voltage, distance between the needle tip to the collecting unit are all non-independent important electrospinning parameters that mainly affect the fiber diameter, mechanical properties and the overall morphology of the electrospun fibrous scaffold [378-380]. The polymer concentration and molecular weight can directly affect the overall viscosity of the polymer solution. Chain entanglements also have a direct effect on both the polymer solution concentration and the molecular weight, in which the fiber-producing jet can be prevented from breaking, allowing for a longer and continuous fiber deposition. However, if the chain entanglements are increased, the polymer solution viscosity increases as a result, leading to increase in the surface tension that creates a forked cone shaped droplet during electrospinning. This however, can be manipulated by reducing the voltage applied to maintain the Taylor shaped droplet during the process [379]. If the polymer solution concentration was high, this will result in

a smaller deposition area and instability in fiber deposition that can be seen as breaking in the fiber producing jet [382]. In addition, the polymer solution concentration and viscosity can directly affect the overall surface morphology of the deposited fibers, by either creating a smooth nanofiber surface or nanofibers beads-containing [383]. The choice of the solvent is another important electrospinning parameter that can hugely affect the overall quality of the fibers. Solvents are used to dissolve polymer and prepare them for electrospinning, however, a wide range of organic and non-organic solvents can be utilized to dissolve polymers with various conductivities that can be tuned to a specific polymer and the application need in order to achieve the best desirable fiber morphology [382, 384, 835]. Interactions between the polymer molecules and solvent, the resultant polymer solution viscosity as well as the fiber morphology are all dependent on the solvent choice [384, 386]. The utilization of the un-appropriate solvent can sometimes lead to undesirable effects such as the creation of large number of pores at the surface of the fibers, which can negatively affect the overall quality of the fibrous scaffold (Figure 1.31). The presence of these pores however, can lead to burst release effects in case of drug deliver and can also accelerate the drug release and/or the device degradation. The pores are caused because of the uncomplete evaporation of the solvent upon deposition, creating void spaces in the resultant fibers due to the long contact of the remaining unevaporated solvent with the fiber surface [387, 388]. One last important consideration is that during electrospinning, most fibers tend to get collected at the grounded target, however, due to the fact that the surface of these fibers is highly charged, they have also the possibility of getting deposited on almost every surface in the vicinity [389]. To overcome this issue, the area of the grounded target should be specific to the desired fibrous mat area. This will allow for a complete collection of the elctrospun fibers without losing any. All the aforementioned are important electrospinning parameters that need to be considered during the

process in order to achieve a controlled system that increases the accuracy of the resultant fibers geometry.

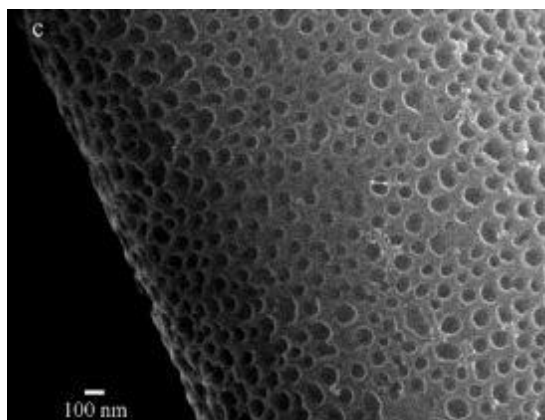


Figure 1.31: Porous electrospun fibers. 28 wt% polystyrene in tetrahydrofuran (15kV) [387].

1.3.3. Electrospinning Strategies for Drug Delivery

One of the most interesting features of the nanofibers is the ability to couple them with regenerative agents such as growth factors or biomolecules that are known to encourage the healing processes. The high ratio of surface to volume of produced nanofibers can increase drug loading and cell attachment attributes [297]. Different electrospinning strategies such as “uniaxial” and “coaxial” electrospinning have been employed in order to achieve steady release rates of the encapsulated agents over a period of time [297]. In both strategies, the choice of the biomaterial represents a key component in the development of sustained and controlled release electrospun nanofibers [297]. a wide variety of different non-biodegradable and biodegradable synthetic and naturally derived biomaterials have been used for the synthesis of electrospun nanofibers [297]. Amongst all, the most relevant biomaterials used for sustained and controlled released are biodegradable polyesters such as PLA, PGA, PLGA, and PCL [398]. Common but rarely used non-biodegradable synthetic biomaterials for sustained growth factor and biomolecules release include polyurethane (PU), polycarbonate, and nylon-6 [399]. Naturally derived biomaterials such as collagen, silk,

gelatin, alginate and chitosan have also been investigated for sustained growth factors and biomolecules delivery from nanofibers [400]. Natural biomaterials are generally used to bypass the biocompatibility limitations associated with synthetic biomaterials. Although natural biomaterials possess enhanced biocompatibility properties, they are un-electrospunable, unless they are blended with another synthetic biomaterial, which limit their use by their one as drug delivery vehicles [401]. Regardless the type of the material, one important factor that largely effect the release profile of the encapsulated agents from nanofibers is the method of encapsulation.

1.3.3.1.Uniaxial Electrospinning for Drug Delivery

Uniaxial electrospun nanofibers demonstrate a relatively simple, and scalable strategy to achieve rapid and sustained release of the encapsulated bioactive agents. The uniaxial electrospinning setup is relatively similar to the previously discussed setup (Figure 1.30), where a syringe to hold the polymer solution is required, in addition to two electrodes (positive and negative), a collector, and a high DC voltage. The same exact methodology as previously described is applied during the uniaxial electrospinning technique, and the addition of the bioactive agent during the polymer solution preparation before electrospinning would be the only difference. When applying the uniaxial electrospinning methods, drug encapsulation is achieved through a single step, because the drug is dissolved or dispersed in the polymeric solution [398]. Drug encapsulation efficiency, drug dispersion into the fibers as well as the release rate are all characteristics factors determined by the interactions between the polymer solution and the drug, which is further affected by the physiochemical properties of the polymer [398]. However, to obtain a uniform drug release kinetics from uniaxially produced nanofibers, bioactive agents have to completely be homogenized with the polymer solution prior to electrospinning. This, can be achieved through the appropriate

selection of the polymer to protein. For example, hydrophobic polymers such as PLA, PGA, and PLGA can easily be homogenized with hydrophobic proteins such as BMP-2 or PDGF-BB [402]. On the other hand, hydrophilic drugs are not miscible with hydrophobic polymers but are easily homogenized with hydrophilic polymers such as gelatin, PEG, and PVA [402]. In cases where the protein and the polymer of interest are immiscible, they can be forced to be homogenized by emulsifying using ultra-sonication method [403]. This however, can improve the suspension of the bioactive agent in the organic solvent [403]. Therefore, homogenization between the polymer and the proteins as well as the formulation properties are all important parameters that can potentially affect the drug release kinetics.

Although uniaxial electrospinning is thought to be relatively simple and easy to perform, bioactive agents may lose their bioactivity due to conformational changes in the organic solution environment [402]. In another word, the process of emulsifying the protein, which involves physical stirring, homogenization or ultra-sonication can potentially damage the proteins' bioactivity [402]. Several methods have been developed in order to improve the stability of proteins as well as to protect them from the harsh environment they undergo prior to electrospinning. One strategy is to use salt complexation instead of ultra-sonication in order to improve the proteins' solubility in organic solvents [404]. This method resulted in retention of almost 90% of Lysozyme oleate bioactivity after it has been incorporated by Li et al. into uniaxially electrospun scaffold [404]. Another strategy is to minimize the hydrophobic interaction of the bioactive agent and the organic solvent during electrospinning by using hydrophilic additives [405]. In one study, it has been reported that the addition of hydrophilic polymers such as PEG and gelatin in aqueous protein solution can be beneficial for improving the protein solubility. In

addition, it has been reported that the addition of hydroxyapatite (HAp) in PLGA solution could preserve the bioactivities of the loaded BMP-2, as the protein could potentially attach to the hydrophilic particles, escaping from the harsh electrospinning process [406].

It is very well known from the literature that uniaxially electrospun scaffold incorporated bioactive agent exhibit high initial burst release followed by sustained release close to linear mode depending on the polymer choice [407-409]. Regardless the polymer type, the burst release usually takes place within the first 12 – 24 h [410]. The high initial burst release is possibly attributed to the localization of certain fractions of the protein molecules near the surface of the fibers [410]. After the first high burst release phase, the protein release kinetics are mainly driven by the degradation rate of the polymer as well as protein diffusion [410]. For example, proteins loaded into the slowly degraded PCL will exhibit a steady and prolonged release profile when compared to the release of proteins loaded into the relatively fast degraded PLGA, where a sustained release mode is displayed first, followed by increased release rate upon the degradation of the polymer [411].

In order to examine the release kinetics and the effectiveness of the uniaxial electrospun nanofibers encapsulated bioactive agents, Nie et al. developed a three-dimensional uniaxially electrospun PLGA/HA composite nanofiber scaffold for protein delivery and bone regeneration [412]. In this study, BMP-2 was physically blended with the polymer solution prior to electrospinning and in vitro release profile of the encapsulated protein was reported. Although data revealed that the protein release lasted for up to 2 weeks, a very high initial burst release was

observed at the first few hours. This high burst release can cause undesirable side effect and interfere with the surrounding tissues when the device is implanted *in vivo*.

It was expected that fibers with larger diameter would overcome drawbacks associated with the initial burst release observed in the uniaxially electrospun nanofibers and would also create a longer path length for drug to diffuse. This hypothesis however, has been examined by Chen et al. In this study, PLA uniaxial electrospun nanofiber scaffolds have been fabricated with two different fibers diameters, ~ 1550 nm and ~ 200 nm [413]. Chlortetracycline, an anti-inflammatory drug agent, was uniaxially encapsulated in both fibrous scaffold and the release behavior of the drugs from both scaffolds has been investigated in vitro. In vitro drug release results showed that both scaffold could not avoid the initial burst release as both showed very high initial burst release of the drug. Further investigations showed that the larger-diameter fibers could sustained the release for a longer time when compared to the smaller-diameter fibers, which released all the encapsulated protein in a shorter time. Findings from this study show that the initial high burst release issue of the uniaxial electrospun nanofiber could not be resolved through the manipulation of the nanofiber diameter, but suggest that uniaxial encapsulation of the drug in larger-diameter fibers can be beneficial for a long-term release.

Drawback associated with delivering growth factors from uniaxially produced nanofibers such as the initial high burst release as well as the fast release of the encapsulated bioactive agent encouraged scientists to try another approach aiming to bypass this issue. In an attempt to overcome the fast release of growth factors from uniaxial electrospun nanofiber, Okuda et al. developed a poly-L-lactide-co-ε-caprolactone (PLCL) uniaxial electrospun nanofiber mat using

sequential electrospinning to generate a multilayered scaffold [414]. The scaffold design consisted of three different layers, in which the drug is incorporated in the middle layer and being sandwiched by the other two layers to delay the release of the bioactive agent from the middle layer. This design however resulted in minimal burst release followed by a sustained close to linear release of the agent. Although this approach seems to address the limitations of the burst and fast release associated with the uniaxially produced nanofibers, multilayered fibrous scaffold could prove to be problematic in tissue engineering applications [414]. Cells seeded on multilayered scaffold were shown to accelerate the degradation rate of the scaffold due to the cell infiltration through the multiple layers, resulting in a complete release of the encapsulated drug at the middle layer.

Drawbacks associated with the uniaxial electrospinning technique such as the high initial burst release, fast release of the encapsulated bioactive agent as well as the harsh environment that the bioactive agent has to undergo during the encapsulation process mark the need for finding more functional and integrative alternatives that bypass the issue of the burst and fast release as well as protect the bioactive agents from harsh loading environment.

1.3.3.2.Coaxial Electrospinning for Drug Delivery

Coaxial electrospinning, also referred to as co-electrospinning, was first patented in the early 2000 by Sun et al. to overcome the burst release limitations associated the conventional uniaxial electrospinning methods [415,416]. Incorporation of growth factors coaxially in the core shell of the polymeric nanofiber has been shown to exhibit precise control over the location of the drug within the core-shell of the nanofibers [417]. The main advantage of coaxial electrospinning over

the uniaxial is that it generates core and sheath fibers by physical separation between the core and the sheath through the utilization of two electrospinning tips and two solutions (Figure 1.32) [418]. The core generally contains the growth factor solution and the sheath contains the polymeric solution. This nanofiber structure will allow for more of a spatial control over growth factors delivery and will hugely minimize any possibility of burst release when compared to the conventional uniaxial nanofiber [418]. In addition, this process is used to load a wide variety of agents into nanofibers that could potentially lose their bioactivity and functionality unless they are in fluid or non-denaturing environment [418]. The setup for coaxial electrospinning is relatively similar to the uniaxial electrospinning, except for the nozzle configuration [360]. The coaxial nozzle consists of two separate inner and outer concentric nozzles, in which the outer nozzle is normally fed by the polymer solution, while the inner nozzle is fed by bioactive agent's solution [360]. Each nozzle is controlled by a separate syringe pump to allow for controlling the flow rate of every nozzle [360].

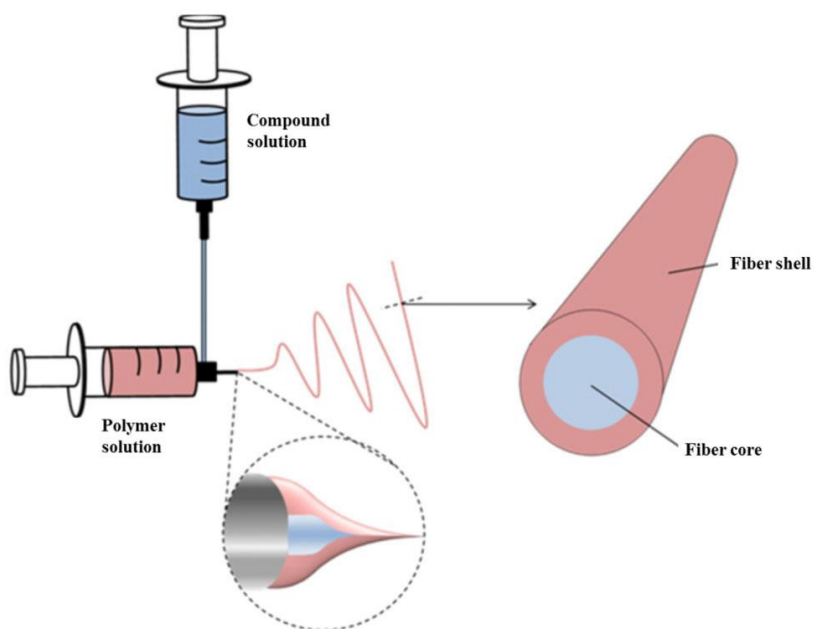


Figure 1.32. Schematic representation of coaxial electrospinning setup. [419]

Although this technique has been developed more than 15 years ago [420], tissue engineers have recently started to consider the application of coaxial electrospinning to deliver growth factors and/or biomolecules 10 years ago. When compared to the uniaxial electrospinning, this technique has gained [421]. Coaxial electrospinning has received tremendous interest by researchers because the produced core-shell fibers that have a great potential in preserving the protein during the electrospinning process, resulting in retention to its bioactivity [360]. It has been reported that another factor attribute to the preservation of the loaded protein bioactivity in the core-shell of the coaxial nanofibers is that during the coaxial electrospinning process, only the outer fiber surface gets exposed to the electric charge, whereas the protein at the inner core is not charged at all [422]. This however plays a significant role in the preservation of the bioactivity of the loaded in the core-shell of the coaxial nanofibers when compared to the uniaxial nanofibers. This has been further investigated by Ji et al. where the activities of the loaded ALP protein have been compared both in the uniaxially and coaxially electrospun fibers [423]. Low ALP activities were observed in the uniaxial nanofibers in comparison to the coaxial nanofibers, suggesting that high voltage and contact with the organic solvents are harmful to the loaded bioactive agent.

An important parameter that can largely affect the integrity of the final core-shell architecture is the miscibility between the two solutions, the polymer solution and the bioactive agent's solution used in the core-shell. Another considerable variable is the flow rate of both solutions, the polymer and the core, which can be tuned in order to set the thickness of the shell and the diameter of the core. Increasing the flow rate of the polymer solution and decreasing the flow rate of the core solution normally results in a thicker shell and a narrower core, this however, would result in very sustained and prolonged release over time with minimal to no initial burst release [424]. In a study

by Wang et al. dimethyloxallylglycine (DMOG) was coaxially loaded into the hydrophobic PLA [424]. Two scaffolds with different fiber diameter have been produced, where one scaffold had fiber diameters of \sim (120 nm) and the other scaffold had fiber diameter of \sim (230nm). In vitro release data revealed that both groups had a similar minimal initial burst release. However further investigations revealed that the thin shell scaffolds showed almost 70% cumulative drug release within 11 days, whereas the thick shell showed the same cumulative release after 30 days in culture. These observations strongly indicated that the sustained release depends on the polymer shell thickness.

The distribution of the bioactive agent within the core structure as well as the final morphology of the overall fiber can highly affect the release behavior of the drug from the core [425]. However, to obtain a uniform drug distribution within the core structure as well as a regular core-shell fiber morphology, a compatible solvent with known evaporation rate has to be used. For example, if core solvent evaporates faster than the shell solvent, a hollow fiber is obtained. This hollow fiber structure can cause insufficient interfacial compatibility between the core and the shell, resulting in delamination at the interface. Also, if the shell solvent evaporates faster than the core solvent, the core solvent will be entrapped within the core-shell of the fiber, causing some portions of the shell polymer to be dissolved and thus, producing a porous structure of a fiber that can result in higher rates of burst release [425]. Therefore, choosing the appropriate solvent for the core and the shell polymer is of importance to achieve desirable release outcome.

1.3.3.3.Coaxial and Uniaxial Electrospinning for Drug Delivery

A wealth number of studies has compared the release profile of the coaxially electrospun nanofiber scaffolds to the uniaxially electrospun nanofiber scaffolds. In a study by Sahoo et al.

bFGF was coaxially and uniaxially incorporated in PLGA electrospun nanofiber scaffold [426]. The encapsulation efficacy of the bFGF in both groups was shown to be similar. In vitro release data showed that the growth factor from the uniaxial nanofibers showed higher burst release when compared to the coaxial. In addition, while the uniaxial nanofibers released all of the encapsulated protein within 7 days, the coaxial nanofibers could sustain the release for up to 14 days. Both scaffolds were further seeded with mesenchymal stem cells and the effect of the different growth factor incorporation methods on the proliferation and differentiation of MSCs has been investigated. At predetermined time points, cells showed a rapid increase in cell proliferation, collagen production as well as gene expression in the uniaxial electrospun nanofiber group when compared to the coaxial. This however, is attributed to the effect of the burst and fast release of the growth factor, which stimulated the rapid proliferation and differentiation of the cultured cells when compared to the coaxial group, which showed sustained release of the loaded protein over time. Findings from this study demonstrate the effect of the different growth factor incorporation methods on the cell behavior such as cell proliferation and differentiation. Although the initial high burst release, followed by fast release of the growth factor from the uniaxial nanofibers resulted in a significant increase in cell proliferation and differentiation in vitro when compared to the coaxial nanofibers, this is undesirable in an in vivo setting, where the high initial burst release can cause interference and damage to the other surrounding tissues, thus, resulting in increased in complications rather than eliminating an existed one.

To examine the effect of the coaxial electrospun nanofibers in vivo, Wei et al. developed a very unique, elegant and novel coaxial electrospun polycaprolactone (PCL)/polyvinyl alcohol (PVA) core-sheath nanofiber (NF) blended with both hydroxyapatite nanorods (HA) and type I collagen

(Col) (PCL^{Col}/PVA^{HA}) for the treatment of osseointegration [427]. Doxycycline (Doxy) and dexamethasone (Dex) were successfully incorporated into the PCL^{Col}/PVA^{HA} NFs for controlled release. In vitro evaluation revealed that the PCL^{Col}/PVA^{HA} NFs are biocompatible and enhanced the adhesion and proliferation of murine pre-osteoblasts MC3T3 cells. In addition, the release of Doxy and Dex from coaxial PCL^{Col}/PVA^{HA} NFs showed more controlled release when compared to the uniaxial NFs. Furthermore, using an *ex vivo* porcine bone implantation model they found that the PCL^{Col}/PVA^{HA} NFs bind firmly on the titanium rod surface and the NFs coating remained intact on the surface of titanium rods after pullout. No disruption or delamination was observed after the pullout test. To examine the scaffold's capability to enhance osseointegration *in vivo*, the scaffold was directly deposited on a titanium (Ti) implant surface during electrospinning. the implant was further implanted an infected tibia rat model. *In vivo* evaluations revealed that the coating the implant with PCL^{Col}/PVA^{HA} NFs enhanced bone osseointegration at the implant site at 2,4 and 8 weeks when compared to the implant coated with the uniaxial scaffold or un-coated. These findings indicate that coaxial PCL/PVA NF coating doped with Doxy and/or other drugs have great potential in enhancing implant osseointegration and preventing infection.

1.3.4. Techniques and Potential Applications for Coaxial Electrospinning:

More complex drug delivery systems can be created through the utilization of coaxial electrospinning for more integrative tissue regeneration [428]. For example, the inner core of the electrospun fiber could be composed the slowly biodegradable polymer PCL, loaded with an osteogenic protein such as BMP-2, whereas the outer shell could be composed of a blend of PLGA-gelatin-VEGF. BMP-2 has been shown to promote the differentiation of osteoblasts and induce bone formation [429], while VEGF has been shown to promote vascularization [430]. By theory,

VEGF loaded at the outer shell of the nanofiber would be released into the tissue enticement before BMP-2 encapsulated at the inner core of the fiber upon implantation in vivo. Thus, the scaffold is design to promote the delivery of the loaded protein in two stages, the first for promoting vascularization throughout the implant, while the precise and the steady release of the loaded BMP-2 at the core-shell of the nanofiber should promote the differentiation of the local precursor cells as well as induce the formation of bone over time. PCL has been chosen to be at the core shell of the nanofiber and loaded with BMP-2 due to its slow degradation, which will result in releasing BMP-2 in a steady fashion over a prolonged period of time [431]. The fast release of VEGF was shown to enhance the regeneration process in dual delivery systems with BMP-2, thus it was chosen to be blended at the outer shell for this reason [432]. In addition, blending gelatin along with PLGA would enhance the surface properties of the device, which in turns can increase the biocompatibility of the scaffold and enhance cell adhesion, proliferation, therapy tissue regeneration [433]. The thickness of the outer shell and the diameter of the core shell have to be adjust so that an optimal delivery ratio of both growth factors is archived. Such an approach would be beneficial in wide verity of tissue engineering applications where multiple release of growth factors is required in a sequential manner.

1.4. Research Objectives and Specific Aims

The objective of this work is to develop an integrated graft system composed of three different continuous phases, each engineered to support the culture of a particular cell type, (1) dermal fibroblasts, (2) ligament fibroblasts and (3) osteoblasts. Specifically, the *in vitro* capability of the integrated graft system to sustain the biological properties of the three different cell types such as cell viability, proliferation and phenotype in the heterogenic cellular environment will be investigated. The major research goals are organized into four specific aims:

Specific Aim I: Fabricate and characterize the three different phases within the integrated graft to determine the morphological and physical properties for use *in vitro*, specially related to the morphological integrity.

Specific Aim II: Evaluate the capability of the three different phases within the integrated graft system to serve as suitable drug carriers for sustained and controlled release over growth factors.

Specific Aim III: Isolate and phenotypic characterize the three different cell types: dermal fibroblasts, ligament fibroblasts and osteoblasts; in addition to *in vitro* evaluating the capability of the three different phases within the integrated graft system to support their viability and proliferation over time.

Specific Aim IV: Evaluate the *in vitro* capability of the integrated graft system to sustain the biological properties of the three different cell types such as cell viability, proliferation and phenotype in the heterogenic cellular environment.

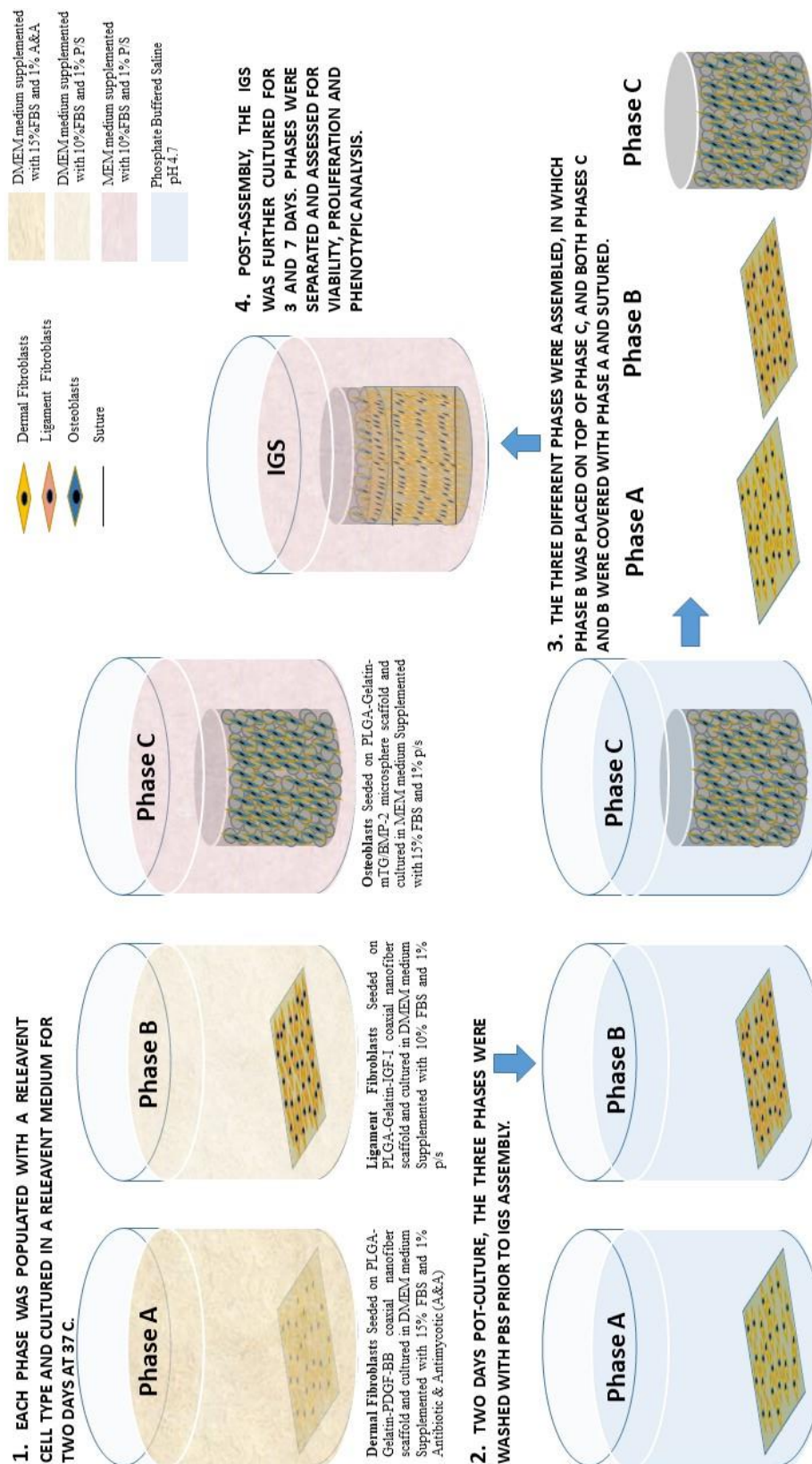


Figure 1.33. A schematic showing the three steps involved in establishing the integrated graft system.

1.5.References:

1. Murphy MB, Monvivais K, Caplan AI. Mesenchymal stem cells: Environmentally responsive therapeutics for regenerative medicine. *Experimental and Molecular Medicine*. 2013
2. <https://www.woundcarecenters.org/article/wound-basics/different-types-of-wounds>
3. <http://www.woundsource.com/blog/difference-between-acute-and-chronic-wounds>
4. Laurencin CT, Nair LS. Regenerative engineering: approaches to limb regeneration and other grand challenges. *Regenerative Engineering and Translational Medicine*. 2015; 1:13.
5. Patrick P Spicer, James D Kretlow, Simon Young, John A Jansen, F Kurtis Kasper & Antonios G Mikos. Evaluation of bone regeneration using the rat critical size calvarial defect *Nature Protocols* 7, 1918–1929 (2012) doi:10.1038/nprot.2012.113
6. The Quest toward limb regeneration: a regenerative engineering approach Cato T. Laurencin Lakshmi S. Nair *Regenerative Biomaterials*, Volume 3, Issue 2, 1 June 2016, Pages 123–125
7. Talmo CT, Aghazadeh M, Bono JV. Perioperative complications following total joint replacement. *Clin Geriatr Med*. 2012; 28:471–487. [PubMed: 22840309]
8. [8] Iyer, Subramania. “Vascularised Composite Allotransplants: Transplant of Upper Extremities and Face.” *Indian Journal of Plastic Surgery: Official Publication of the Association of Plastic Surgeons of India* 48.2 (2015): 111–118. *PMC*. Web. 3 Nov. 2017.
9. Khademhosseini A, Vacanti JP, Langer R. Progress in tissue engineering. *Sci Am*. 2009; 300:64– 71.
10. Chiarello E, Cadossi M, Tedesco G, Capra P, Calamelli C, Shehu A, Giannini S.

Aging Clin Exp Res. 2013 Oct;25 Suppl 1:S101-3. doi: 10.1007/s40520-013-0088-8. Epub 2013 Sep 18

11. Ikada, Yoshito. “Challenges in Tissue Engineering.” *Journal of the Royal Society Interface* 3.10 (2006): 589–601. *PMC*. Web. 17 Sept. 2017.
12. Repair of human articular cartilage after implantation of autologous chondrocytes. *Richardson JB, Caterson B, Evans EH, Ashton BA, Roberts S J Bone Joint Surg Br. 1999 Nov; 81(6):1064-8.*
13. Clinical experience using cultured epithelial autografts leads to an alternative methodology for transferring skin cells from the laboratory to the patient. *Hernon CA, Dawson RA, Freedlander E, Short R, Haddow DB, Brotherston M, MacNeil S Regen Med. 2006 Nov; 1(6):809-21.*
14. Campana, V. et al. “Bone Substitutes in Orthopaedic Surgery: From Basic Science to Clinical Practice.” *Journal of Materials Science. Materials in Medicine* 25.10 (2014): 2445–2461. *PMC*. Web. 20 Sept. 2017.
15. Reichert WM, Ratner BD, Anderson J, Coury A, Hoffman AS, Laurencin CT, Tirrell D. 2010 panel on the Biomaterials Grand Challenges. *J Biomed Mater Res A. 2011; 96:275.*
16. Laurencin CT, Kahn Y, Regenerative Engineering,
17. Musculoskeletal Tissue Regeneration: the Role of the Stem Cells
18. MIKOS, ANTONIOS G. et al. “Engineering Complex Tissues.” *Tissue engineering* 12.12 (2006): 3307. *PMC*. Web. 15 Sept. 2017.
19. 1. A. Atala, Engineering organs. *Curr. Opin. Biotechnol.* 20, 575–592 (2009).
20. H. H. Lu, S. D. Subramony, M. K. Boushell, X. Zhang, Tissue engineering strategies for the regeneration of orthopedic interfaces. *Ann. Biomed. Eng.* 38, 2142–2154 (2010).

21. P. J. Yang, J. S. Temenoff, Engineering orthopedic tissue interfaces. *Tissue Eng. Part B* Rev. 15, 127–141 (2009).
22. Bioreactors in tissue engineering
23. Langer R Vacanti JP Tissue engineering. *Science*. 1993; 260:920926
24. Skalak, R. Tissue Engineering: Proceedin of a Workshop; Granlibakken, Lake Tahoe, California. February 2629, 1988; New York, NY: Liss 1988 _
25. Qu, Dovina et al. “Engineering Complex Orthopaedic Tissues via Strategic Biomimicry.” *Annals of biomedical engineering* 43.3 (2015): 697–717. *PMC*. Web. 15 Sept. 2017.
26. Rao RT, Browe DP, Lowe CJ, Freeman JW. An overview of recent patents on musculoskeletal interface tissue engineering. *Connect Tissue Res*. 2016;57(1):53-67. doi: 10.3109/03008207.2015.1089866. Epub 2015 Nov 17.
27. Kim, Ha Sung, Jong Keun Seon, and Ah Reum Jo. “Current Trends in Anterior Cruciate Ligament Reconstruction.” *Knee Surgery & Related Research* 25.4 (2013): 165–173. *PMC*. Web. 20 Sept. 2017.
28. Galatz LM, Ball CM, Teefey SA, Middleton WD, Yamaguchi K. The outcome and repair integrity of completely arthroscopically repaired large and massive rotator cuff tears. *J Bone Joint Surg Am*. 2004; 86-A:219–224. [PubMed: 14960664]
29. Jeffrey P. Spalazzi, Stephen B. Doty, Kristen L. Moffat, William N. Levine, and Helen H. Lu. *Tissue Engineering*. December 2006, 12(12): 3497-3508.
30. Nawata, K., T. Minamizaki, Y. Yamashita, and R. Teshima. Development of the attachment zones in the rat anterior cruciate ligament: changes in the distributions of proliferating cells and fibrillar collagens during postnatal growth. *J. Orthop. Res*. 20:1339–1344, 2002.

31. Liu, S. H., V. Panossian, R. al Shaikh, et al. Morphology and matrix composition during early tendon to bone healing. *Clin. Orthop. Relat. Res.* 339:253–260, 1997.
32. Rodeo, S. A., S. P. Arnoczky, P. A. Torzilli, et al. Tendonhealing in a bone tunnel. A biomechanical and histological study in the dog. *J. Bone Joint Surg. Am.* 75:1795–1803, 1993.
33. Benjamin, M., E. J. Evans, and L. Copp. The histology of tendon attachments to bone in man. *J. Anat.* 149:89–100, 1986.
34. Woo, S. L., J. Maynard, and D. L. Butler. Ligament, tendon, and joint capsule insertions to bone. In: *Injury and Repair of the Musculoskeletal Soft Tissues*, edited by S. L. Woo, J. A. Bulkwater. Savannah, Georgia: American Academy of Orthopaedic Surgeons, 1988
35. [35] Tissue engineering strategies for the regeneration of orthopedic interfaces.
Lu HH, Subramony SD, Boushell MK, Zhang X. *Ann Biomed Eng.* 2010 Jun;38(6):2142-54. doi: 10.1007/s10439-010-0046-y. Epub 2010 Apr 27. Review.
36. An overview of recent patents on musculoskeletal interface tissue engineering
37. Benjamin, M., Evans, E.J., and Copp, L. The histology of tendon attachments to bone in man. *J. Anat.* 149, 89, 1986.
38. Woo, S.L., and Buckwalter, J.A. AAOS/NIH/ORS workshop. Injury and repair of the musculoskeletal soft tissues. Savannah, Georgia, June 18-20, 1987. *J. Orthop. Res.* 6, 907, 1988.
39. Tien, Y. C., T. T. Chih, J. H. Lin, et al. Augmentation of tendon-bone healing by the use of calcium-phosphate cement. *J. Bone Joint Surg. Br.* 86:1072–1076, 2004.

40. Huangfu, X., and J. Zhao. Tendon-bone healing enhancement using injectable tricalcium phosphate in a dog anterior cruciate ligament reconstruction model. *Arthroscopy* 23:455–462, 2007.
41. Mutsuzaki, H., M. Sakane, H. Nakajima, et al. Calciumphosphate-hybridized tendon directly promotes regeneration of tendon-bone insertion. *J. Biomed. Mater. Res. A* 70:319–327, 2004.
42. Rodeo, S. A., K. Suzuki, X. H. Deng, et al. Use of recombinant human bone morphogenetic protein-2 to enhance tendon healing in a bone tunnel. *Am. J. Sports Med.* 27:476–488, 1999.
43. Cooper, J. A., H. H. Lu, F. K. Ko, et al. Fiber-based tissueengineered scaffold for ligament replacement: design considerations and in vitro evaluation. *Biomaterials* 26:1523– 1532, 2005.
44. Lu, H. H., J. A. Cooper, Jr., S. Manuel, et al. Anterior cruciate ligament regeneration using braided biodegradable scaffolds: in vitro optimization studies. *Biomaterials* 26(23):4805–4816, 2005.
45. Cooper, Jr., J. A., J. S. Sahota, W. J. Gorum, et al. Biomimetic tissue-engineered anterior cruciate ligament replacement. *Proc. Natl Acad. Sci. USA* 104:3049–3054, 2007.
46. Biomaterials 23:4131–4141, 2002. Altman, G. H., R. L. Horan, P. Weitzel, et al. The use of long-term bioresorbable scaffolds for anterior cruciate ligament repair. *J. Am. Acad. Orthop. Surg.* 16:177–187, 2008.
47. Kimura Y, Hokugo A, Takamoto T, Tabata Y, Kurosawa H. Regeneration of anterior cruciate ligament by biodegradable scaffold combined with local controlled release of basic fibroblast growth factor and collagen wrapping. *Tissue Eng Pt C Meth.* 2008; 14:47–57.

48. [48] Paxton JZ, Donnelly K, Keatch RP, Baar K. Engineering the bone-ligament interface using polyethylene glycol diacrylate incorporated with hydroxyapatite. *Tissue Eng Pt A*. 2009; 15:1201–1209.
49. [49] Ma J, Goble K, Smietana M, Kostrominova T, Larkin L, Arruda EM. Morphological and functional characteristics of three-dimensional engineered bone-ligament-bone constructs following implantation. *J Biomech Eng*. 2009; 131:101017.
50. [50] Ma J, Smietana MJ, Kostrominova TY, Wojtys EM, Larkin LM, Arruda EM. Three-dimensional engineered bone-ligament-bone constructs for anterior cruciate ligament replacement. *Tissue Eng Pt A*. 2012; 18:103–116.
51. Cooper RR, Misol S. Tendon and ligament insertion. A light and electron microscopic study. *J Bone Joint Surg Am*. 1970; 52:1–20. [PubMed: 4189231]
52. Matyas JR, Anton MG, Shrive NG, Frank CB. Stress governs tissue phenotype at the femoral insertion of the rabbit MCL. *J Biomech*. 1995; 28:147–157. [PubMed: 7896857]
53. Spalazzi JP, Gallina J, Fung-Kee-Fung SD, Konofagou EE, Lu HH. Elastographic imaging of strain distribution in the anterior cruciate ligament and at the ligament-bone insertions. *J Orthop Res*. 2006; 24:2001–2010. [PubMed: 16900541]
54. Benjamin M, Toumi H, Ralphs JR, Bydder G, Best TM, Milz S. Where tendons and ligaments meet bone: attachment sites (‘entheses’) in relation to exercise and/or mechanical load. *J Anat*. 2006; 208:471–490. [PubMed: 16637873]
55. Hems T, Tillmann B. Tendon entheses of the human masticatory muscles. *Anat Embryol*. 2000; 202:201–208. [PubMed: 10994993]
56. Spalazzi, J. P., E. Dagher, S. B. Doty, X. E. Guo, S. A. Rodeo, and H. H. Lu. In vivo evaluation of multi-phased scaffold designed for orthopaedic interface tissue engineering

- and soft tissue-to-bone integration. *J. Biomed. Mater. Res. A* 86A(1):1–12, 2008.
57. Spalazzi, J. P., S. B. Doty, K. L. Moffat, et al. Development of controlled matrix heterogeneity on a triphasic scaffold for orthopedic interface tissue engineering. *Tissue Eng.* 12:3497–3508, 2006
58. Spalazzi, J. P., K. L. Moffat, and H. H. Lu. Design of a novel stratified scaffold for ACL-to-bone interface tissue engineering. In: *8th International Symposium on Ligaments and Tendons*, 2008
59. Subramony SD, Qu D, Ma R, et al. In vitro optimization and in vivo evaluation of a multiphased nanofiber-based synthetic ACL scaffold. *Transactions of the 60th Orthopaedic Research Society*. 2014
60. Samavedi S, Vaidya P, Gaddam P, Whittington AR, Goldstein AS. Electrospun meshes possessing region-wise differences in fiber orientation, diameter, chemistry and mechanical properties for engineering bone-ligament-bone tissues. *Biotechnol Bioeng.* 2014
61. Samavedi S, Guelcher SA, Goldstein AS, Whittington AR. Response of bone marrow stromal cells to graded co-electrospun scaffolds and its implications for engineering the ligament-bone interface. *Biomaterials*. 2012; 33:7727–7735. [PubMed: 22835644]
62. Samavedi S, Olsen Horton C, Guelcher SA, Goldstein AS, Whittington AR. Fabrication of a model continuously graded co-electrospun mesh for regeneration of the ligament–bone interface. *Acta Biomater.* 2011; 7:4131–4138. [PubMed: 21791254]
63. Samavedi S, Vaidya P, Gaddam P, Whittington AR, Goldstein AS. Electrospun meshes possessing region-wise differences in fiber orientation, diameter, chemistry and mechanical properties for engineering bone-ligament-bone tissues. *Biotechnol Bioeng.*

2014

64. Oh SH, Park IK, Kim JM, Lee JH. In vitro and in vivo characteristics of PCL scaffolds with pore size gradient fabricated by a centrifugation method. *Biomaterials* 2007;28(9):1664–71
65. Chang CH, Chen CH, Su CY, Liu HT, Yu CM. Rotator cuff repair with periosteum for enhancing tendon-bone healing: a biomechanical and histological study in rabbits. *Knee Surg Sports Traumatol Arthrosc.* 2009; 17:1447–1453
66. Moffat KL, Cassilly RT, Subramony SD, et al. *In vivo* evaluation of a bi-phasic nanofiber-based scaffold for integrative rotator cuff repair. *Transactions of the 56th Orthopaedic Research Society.* 2010
67. Engler AJ, Sen S, Sweeney HL, Discher DE. Matrix elasticity directs stem cell lineage specification. *Cell* 2006;126(4):677–89.
68. Platt MA. Tendon repair and healing. *Clin Podiatr Med Surg* 2005; 22:553–60
69. Benjamin M, Ralphs J. Tendons and ligaments-an overview. *Histol Histopathol* 1997;12:1135–44
70. Regeneration techniques for bone-to-tendon and muscle-to-tendon interfaces reconstruction
71. Fujioka, H., R. Thakur, G. J. Wang, et al. Comparison of surgically attached and non-attached repair of the rat Achilles tendon-bone interface. Cellular organization and type X collagen expression. *Connect. Tissue Res.* 37:205– 218, 1998.
72. Inoue, N., K. Ikeda, H. T. Aro, et al. Biologic tendon fixation to metallic implant augmented with autogenous cancellous bone graft and bone marrow in a canine model. *J. Orthop. Res.* 20:957–966, 2002.

73. Chang CH, Chen CH, Su CY, Liu HT, Yu CM. Rotator cuff repair with periosteum for enhancing tendon-bone healing: a biomechanical and histological study in rabbits. *Knee Surg Sports Traumatol Arthrosc.* 2009; 17:1447–1453. [PubMed: 19440695]
74. Sundar S, Pendegrass CJ, Blunn GW. Tendon bone healing can be enhanced by demineralized bone matrix: a functional and histological study. *J Biomed Mater Res B.* 2009; 88:115–122.
75. Moffat KL, Cassilly RT, Subramony SD, et al. *In vivo* evaluation of a bi-phasic nanofiber-based scaffold for integrative rotator cuff repair. *Transactions of the 56th Orthopaedic Research Society.* 2010
76. Zhang X, Caldwell JM, Easley J, et al. *In vivo* evaluation of a biomimetic biphasic scaffold in sheep. *Transactions of the 60th Orthopaedic Research Society.* 2014
77. Ma, Z., M. Kotaki, R. Inai, and S. Ramakrishna. Potential of nanofiber matrix as tissue-engineering scaffolds. *Tissue Eng.* 11:101–109, 2005.
78. Pham, Q. P., U. Sharma, and A. G. Mikos. Electrospinning of polymeric nanofibers for tissue engineering applications: a review. *Tissue Eng.* 12:1197–1211, 2006.
79. Moffat, K. L., A. S. Kwei, J. P. Spalazzi, et al. Novel nanofiber-based scaffold for rotator cuff repair and augmentation. *Tissue Eng. Part A* 15:115–126, 2009.
80. Li XR, Xie JW, Lipner J, Yuan XY, Thomopoulos S, Xia YN. Nanofiber scaffolds with gradations in mineral content for mimicking the tendon-to-bone insertion site. *Nano Lett.* 2009; 9:2763–2768. [PubMed: 19537737]
81. Liu W, Yeh YC, Lipner J, Xie J, Sung HW, Thomopoulos S, Xia Y. Enhancing the stiffness of electrospun nanofiber scaffolds with a controlled surface coating and mineralization. *Langmuir.* 2011; 27:9088–9093. [PubMed: 21710996]

82. Liu W, Lipner J, Xie J, Manning CN, Thomopoulos S, Xia Y. Nanofiber scaffolds with gradients in mineral content for spatial control of osteogenesis. *ACS Appl Mater Interfaces*. 2014; 6:2842–2849. [PubMed: 24433042]
83. [83] Shi J, Wang L, Zhang F, Li H, Lei L, Liu L, Chen Y. Incorporating protein gradient into electrospun nanofibers as scaffolds for tissue engineering. *ACS Appl Mater Interfaces*. 2010; 2:1025–1030. [PubMed: 20423122]
84. Altman, G.H.; Diaz, F.; Jakuba, C.; Calabro, T.; Horan, R.L.; Chen, J.; Lu, H.; Richmond, J.; Kaplan, D.L. Silk-based biomaterials. *Biomaterials* 2003, 24, 401–416.
85. [85]Reichert, W. “., Ratner, B. D., Anderson, J., Coury, A., Hoffman, A. S., Laurencin, C. T. and Tirrell, D. (2011), 2010 Panel on the Biomaterials Grand Challenges. *J. Biomed. Mater. Res.*, 96A: 275–287. doi:10.1002/jbm.a.32969
86. Laurencin CT, Ambrosio AA, Borden MD., et al. Annual review of biomedical engineering. In: Yarmush MI, editor. (ed). *Annual Reviews*. Palo Alto, 1999, 19–46
87. Liu W, Lipner J, Xie J, Manning CN, Thomopoulos S, Xia Y. Nanofiber scaffolds with gradients in mineral content for spatial control of osteogenesis. *ACS Appl Mater Interfaces*. 2014; 6:2842–2849
88. Yang, P. J., and J. S. Temenoff. Engineering orthopedic tissue interfaces. *Tissue Eng. Part B Rev*. 15:127–141,2009.
89. Kim J-H, Oh SH, Min HK, Lee JH. 2017. Dual growth factor-immobilized asymmetrically porous membrane for bone-to-tendon interface regeneration on rat patellar tendon avulsion model. *J Biomed Mater Res Part A* 2015:00A:000–000.
90. Lu HH, Thomopoulos S. Functional attachment of soft tissues to bone: development, healing, and tissue engineering. *Annu Rev Biomed Eng* 2013;15(1):201–26.

91. Yang, P. J., and J. S. Temenoff. Engineering orthopedic tissue interfaces. *Tissue Eng. Part B Rev.* 15:127–141,2009.
92. Larkin LM, Calve S, Kostrominova TY, Arruda EM. Structure and functional evaluation of tendon-skeletal muscle constructs engineered in vitro. *Tissue Eng.* 2006; 12:3149–3158. [PubMed: 17518629]
93. Kostrominova TY, Calve S, Arruda EM, Larkin LM. Ultrastructure of myotendinous junctions in tendon-skeletal muscle constructs engineered in vitro. *Histol Histopathol.* 2009; 24:541–550.
94. Syam Nukavarapu, Joseph Freeman, Cato Laurencin *Regenerative Engineering of Musculoskeletal Tissues and Interfaces,*
95. Ladd MR, Lee SJ, Stitzel JD, Atala A, Yoo JJ. Co-electrospun dual scaffolding system with potential for muscle tendon junction tissue engineering. *Biomaterials.* 2011; 32:1549–1559. [PubMed: 21093046]
96. Kyung H-S, Kim S-Y, Oh C-W, et al. Tendon-to bone tunnel healing in a rabbit model: the effect of periosteum augmentation at the tendon-to-bone interface. *Knee Surg Sports Traumatol Arthrosc* 2003; 11:9–15.
97. Trotter JA, Eberhard S, Samora A. Structural connections of the muscle-tendon junction. *Cell Motility* 1983; 3:431–8.
98. Rodeo SA, Arnoczky SP, Torzilli PA, Hidaka C, Warren RF. Tendon-healing in a bone tunnel: a biomechanical and histological study in the dog. *J Bone Joint Surg Am* 1993; 75:1795.
99. Wang IE, Shan JM, Chen FH, Lu HH. Effects of osteoblast and fibroblast interactions on cell growth and differentiation. *Biochem Biophys Res Commun.* 2006 Submitted

100. Kostrominova TY, Calve S, Arruda EM, Larkin LM. Ultrastructure of myotendinous junctions in tendon-skeletal muscle constructs engineered in vitro. *Histol Histopathol.* 2009; 24:541–550.
101. Moutos, F. T.; Freed, L. E.; Guilak, F. A biomimetic three- dimensional woven composite scaffold for functional tissue engineering of cartilage. *Nat. Mater.* 2007, 6, 162–167.
102. Moutos, F. T.; Freed, L. E.; Guilak, F. A biomimetic three- dimensional woven composite scaffold for functional tissue engineering of cartilage. *Nat. Mater.* 2007, 6, 162–167.
103. Current Concepts and Challenges in Osteochondral Tissue Engineering and Regenerative Medicine Current Concepts and Challenges in Osteochondral Tissue Engineering and Regenerative Medicine^[1]_{SEP}
104. Eyre DR, Wu JJ. Collagen structure and cartilage matrix integrity. *J Rheumatol Suppl* 1995;43.
105. Aigner T, Reichenberger E, Bertling W, Kirsch T, Stoss H, Vondermark K. Type-X collagen expression in osteoarthritic and rheumatoid articular cartilage. *Virchows Arch B Cell Pathol Incl Mol Pathol* 1993;63
106. Flannery CR, Hughes CE, Schumacher BL, Tudor D, Aydelotte MB, Kuettner KE, et al. Articular cartilage super ficial zone protein (SZP) is homologous to megakaryocyte stimulating factor precursor and is a multifunctional proteoglycan with potential growth-promoting, cytoprotective, and lubricating properties in cartilage metabolism. *Biochem Biophys Res Commun* 1999;254.

107. Hunziker EB, Michel M, Studer D. Ultrastructure of adult human articular cartilage matrix after cryotechnical processing. *Microsc Res Tech* 1997;37.
108. Muir H, Bullough P, Maroudas A. The distribution of collagen in human articular cartilage with some of its physiological implications. *J Bone Joint Surg Br* 1970;52.
109. Sridharan, B., Laflin, A. D., Holtz, M. A., Pacicca, D. M., Wischmeier, N. K. and Detamore, M. S. (2017), In vivo evaluation of stem cell aggregates on osteochondral regeneration. *J. Orthop. Res.*, 35: 1606–1616. doi:10.1002/jor.23467 Biometric paper
110. Langer, R., *Acc Chem Res* (2000) 33, 94.
111. Atala, A., *Rejuvenation Res* (2004) 7, 15.
112. Bonassar, L. J., and Vacanti, C. A., *J Cell Biochem Suppl* (1998) 30-31, 29.
113. The Quest toward limb regeneration: a regenerative engineering approach Cato T. Laurencin Lakshmi S. Nair *Regenerative Biomaterials*, Volume 3, Issue 2, 1 June 2016, Pages 123–125
114. Martin, I., et al., *Trends Biotechnol* (2004) 22, 80.
115. Guven S, Chen P, Inci F, Tasoglu S, Erkmen B, et al. (2015) Multiscale assembly for tissue engineering and regenerative medicine. *Trends in Biotechnology* 33: 269-279.
116. biomaterials and scaffold for tissue engineering (biomematic)
117. Ma, PX. Tissue Engineering. In: Kroschwitz, JI., editor. *Encyclopedia of Polymer Science and Technology*. Third. 12. John Wiley & Sons, Inc.; Hoboken, NJ: 2005. p. 261-291.
118. Brown, B.N., et al. *Biomaterials* (2009) 30 (8), 1482.
119. Lyons, F., et al., *Biomaterials* (2010) 31(35), 9232.
120. J. Marler , J. Upton , R. Langer , J. P. Vacanti , *Adv Drug Delivery Rev.* 1998 , 33

, 165 .

121. Engler AJ, Sen S, Sweeney HL, Discher DE. Matrix elasticity directs stem cell lineage specification. *Cell*. 2006; 126:677–689. doi: 10.1016/j.cell.2006.06.044.
122. Jianming Li, Sean Connell and Riya Shi, *Biomimetic Architectures for Tissue Engineering* Purdue University USA
123. Taek Gyoung Kim, Heungsoo Shin, and Dong Woo Lim, *Biomimetic Scaffolds for Tissue Engineering*
124. Pearle AD, Warren RF, Rodeo SA. Basic science of articular cartilage and osteoarthritis. *Clin Sports Med* 2005;24
125. Venn M, Maroudas A. Chemical composition and swelling of normal and osteoarthritic femoral-head cartilage.1. Chemical composition. *Ann Rheum Dis* 1977;36.
126. P. Friedl , *Curr. Opin. Cell Biol.* 2004 , 16 , 14 .
127. R. G. Flemming , C. J. Murphy , G. A. Abrams , S. L. Goodman , P. F. Nealey , *Biomaterials* 1999 , 20 , 573 .
128. D. H. Kim , H. Lee , Y. K. Lee , J. M. Nam , A. Levchenko , *Adv. Mater.* 2010 , 22 , 4551 .
129. L. J. Chen and M. Wang, “Production and evaluation of biodegradable composites based on PHB-PHV copolymer,” *Biomaterials*, vol. 23, no. 13, pp. 2631–2639, 2002.
130. Peter x Ma *Biomimetic Materials for Tissue Engineering*
131. Z. Yin , X. Chen , J. L. Chen , W. L. Shen , T. M. H. Nguyen , L. Gao , H. W. Ouyang , *Biomaterials* 2010 , 31 , 2163 .
132. E. Rosines , H. J. Schmidt , S. K. Nigam , *Biomaterials* 2007 , 28 , 4806.

133. Ma, P. X., and Choi, J. W., *Tissue Eng.* (2001) 7, 23
134. Zhao, F., *et al.*, *Biomaterials* (2002) 23, 3227
135. Sherwood, J. K., *et al.*, *Biomaterials* (2002) 23, 4739
136. Liu, X. H., and Ma, P. X., *Ann. Biomed. Eng.* (2004) 32, 477
137. Vacanti, J. P., and Robert, R. S., US Patent 5,770,193, (1998)
138. Ginty, P. J., *et al.*, *Proc. Natl. Acad. Sci. USA* (2006) 103, 7426
139. Owen SC, Shoichet MS. J. Design of three-dimension biomimetic scaffolds. *Biomed. Mater. Res. A*. 2010; 94A:1321–1331.
140. M. Borden, S. F. El-Amin, M. Attawia, and C. T. Laurencin, “Structural and human cellular assessment of a novel microsphere- based tissue engineered scaffold for bone repair,” *Biomaterials*, vol. 24, no. 4, pp. 597–609, 2003.
141. M. Borden, M. Attawia, Y. Khan, and C. T. Laurencin, “Tissue engineered microsphere-based matrices for bone repair: design and evaluation,” *Biomaterials*, vol. 23, no. 2, pp. 551–559, 2002.
142. T. Jiang, W. I. Abdel-Fattah, and C. T. Laurencin, “In vitro evaluation of chitosan/poly(lactic acid-glycolic acid) sintered microsphere scaffolds for bone tissue engineering,” *Biomaterials*, vol. 27, no. 28, pp. 4894–4903, 2006.
143. Boschetti F¹, Tomei AA, Turri S, Swartz MA, Levi M. Design, fabrication, and characterization of a composite scaffold for bone tissue engineering. *Int J Artif Organs*. 2008 Aug;31(8):697-707.
144. T. Jiang, Y. Khan, L. S. Nair, W. I. Abdel-Fattah, and C. T. Laurencin, “Functionalization of chitosan/poly(lactic acid-glycolic acid) sintered microsphere

- scaffolds via surface heparinization for bone tissue engineering,” *Journal of Biomedical Materials Research A*, vol. 93, no. 3, pp. 1193–1208, 2010.
145. Pramanik S, Agarwal AK, Rai KN (2005) Development of high strength hydroxyapatite for hard tissue replacement. *Trends in Biomaterials & Artificial Organs* 19: 46–51.
 146. Rupani A, Hidalgo-Bastida LA, Rutten F, Dent A, Turner I, et al. (2012) Osteoblast activity on carbonated hydroxyapatite. *Journal of Biomedical Materials Research Part A* 100A: 1089–1096.
 147. Byung-Soo Kim, PLGA/Hydroxyapatite composite Biomaterial by Gas Bubble Formation
 148. Y. Takahashi, M. Yamamoto, Y. Tabeta Enhanced osteoinduction by controlled release of bone morphogenetic protein-2 from biodegradable sponge composed of gelatin and beta-tricalcium phosphate *Biomaterials*, 26 (2005), pp. 4856-4865
 149. H. Kaneko, T. Arakawa, H. Mano, T. Kaneda, A. Ogasawara, M. Nakagawa, *et al.* Direct stimulation of osteoclastic bone resorption by bone morphogenetic protein (BMP)-2 and expression of BMP receptors in mature osteoclasts *Bone*, 27 (2000), pp. 479-486
 150. E.M. Langenfeld, Y. Kong, J. Langenfeld Bone morphogenetic protein 2 stimulation of tumor growth involves the activation of Smad-1/5 *Oncogene*, 25 (2006), pp. 685-692
 151. F. Liu, N. Bloch, K.R. Bhushan, A.M. De Grand, E. Tanaka, S. Solazzo, *et al.* Humoral BMP-2 is sufficient for inducing breast cancer microcalcification *Mol Imaging*, 7 (2008), pp. 175-186

152. H. Petite, V. Viateau, W. Bensaid, A. Meunier, C. de Pollak, M. Bourguignon, *et al.* Tissue-engineered bone regeneration Nat Biotechnol, 18 (2000), pp. 959-963
153. H. Kim, H.W. Kim, H. Suh Sustained release of ascorbate-2-phosphate and dexamethasone from porous PLGA scaffolds for bone tissue engineering using mesenchymal stem cells Biomaterials, 24 (2003), pp. 4671-4679
154. H. Oshina, S. Sotome, T. Yoshii, I. Torigoe, Y. Sugata, H. Maehara, *et al.* Effects of continuous dexamethasone treatment on differentiation capabilities of bone marrow-derived mesenchymal cells Bone, 41 (2007), pp. 575-583
155. H. Kaji, T. Sugimoto, M. Kanatani, K. Nishiyama, K. Chihara Dexamethasone stimulates osteoclast-like cell formation by directly acting on hemopoietic blast cells and enhances osteoclast-like cell formation stimulated by parathyroid hormone and prostaglandin E2 J Bone Miner Res, 12 (1997), pp. 734-741
156. N. Jaiswal, S.E. Haynesworth, A.I. Caplan, S.P. Bruder Osteogenic differentiation of purified, culture-expanded human mesenchymal stem cells in vitro J Cell Biochem, 64 (1997), pp. 295-312
157. A. Martins, A.R.C. Duarte, S. Faria, A.P. Marques, R.L. Reis, N.M. Neves Osteogenic induction of hBMSCs by electrospun scaffolds with dexamethasone release functionality Biomaterials, 31 (2010), pp. 5875-5885
158. Bilezikian, J. P., Raisz, L. G. & Martin, T. J. *Principles of bone biology* (Elsevier, Amsterdam; London, 2008).
159. <https://www.google.com/patents/WO2006074550A1?cl=en>

160. Chowdhury P, Matyas JR, Frank CB. The "epiligament" of the rabbit medial collateral ligament: a quantitative morphological study. *Connect Tissue Res* 1991; 27:33-50.
161. Amiel D, Chu CR, Lee J. Effect of loading on metabolism and repair of tendons and ligaments. In: Funk FJ, Hunter LY (eds) *Repetitive Motion Disorders of the Upper Extremity*. Am Acad Orthop Surg, Rosemont; 1995:217-230.
162. Frank CB. Ligament structure, physiology and function. *Musculoskelet Neuronal Interact*. 2004 Jun;4(2):199-201.
163. Seibel, M. J., Robins, S. P. & Bilezikian, J. P. *Dynamics of bone and cartilage metabolism*
164. Roshan James and Cato T. Laurencin, "Musculoskeletal Regenerative Engineering: Biomaterials, Structures, and Small Molecules," *Advances in Biomaterials*, vol. 2014, Article ID 123070, 12 pages, 2014. doi:10.1155/2014/123070
165. Groeneveld EH, van den Bergh JP, Holzmann P, Bruggenkate CM, Tuinzing DB, Burger EH. Mineralization processes in demineralized bone matrix grafts in human maxillary sinus floor elevations. *J Biomed Mater Res*. 1999; 48:393–402. [PubMed: 10421679]
166. Wilmink, J., A. Wilson, and A. Goodship, Functional significance of the morphology and micromechanics of collagen fibres in relation to partial rupture of the superficial digital flexor tendon in racehorses. *Research in Veterinary Science*, 1992. 53: p. 354–359.
167. Berenson, M., et al., Proteoglycans of human rotator cuff tendons. *Journal of Orthopaedic Research*, 1996. 14(4): p. 518-525.

168. Vogel, K. and T. Koob, Structural specialization in tendons under compression. *International Review of Cytology*, 1989. 115: p. 267-293.
169. Koob, T. and K. Vogel, Site-related variations in glycosaminoglycan content and swelling properties of bovine flexor tendon. *Journal of Orthopaedic Research*, 1987. 5(3): p. 414-424.
170. Lawler, J., The structural and functional properties of thrombospondin. *Blood*, 1986. 67(5): p. 1197-1209.
171. Sharma, P. and N. Maffulli, Biology of tendon injury: healing, modeling and remodeling. *Journal of musculoskeletal & neuronal interactions*, 2006. 6(2): p. 181-190.
172. Eleftheriou, F., et al., Binding of tenascin-X to decorin. *FEBS Letters*, 2001. 495(1-2): p. 44-47.
173. Danylchuk KD, Finlay JB, Krcek JP. Microstructural organization of human and bovine cruciate ligaments. *Clin Orthop* 1978;131:294 –298.
174. Akeson WH, Woo SLY, Amiel D, Frank CB. The chemical basis of tissue repair: Ligament biology. In: Hunter LY, Funk FJ, editors. *Rehabilitation of the Injured Knee*. St. Louis, MO: CV Mosby; 2004. p 92.
175. Noyes FR, Grood ES. The strength of the anterior cruciate ligament in humans and Rhesus monkeys. *J Bone Joint Surg Am* 1976; 58:1074 –1082.
176. Woo SL, Hollis JM, Adams DJ. Tensile properties of the human femur-anterior cruciate ligament-tibia complex. The effects of specimen age and orientation. *Am J Sports Med* 1991; 19:217–234.
177. Hutmacher DW. Scaffolds in tissue engineering bone and cartilage. *Biomaterials* 2000; 21:2529 –2543.

178. Ge Z, Yang F, Goh JC, Ramakrishna S, Lee EH. Biomaterials and scaffolds for ligament tissue engineering. *J Biomed Mater Res A*. 2006 Jun 1;77(3):639-52
179. Amiel D, Billings E, Aksson WH. Ligament structure, chemistry, and physiology. In: Daniel D, Akeson W, O'Connor J, editors. *Knee Ligaments: Structure, Function, Injury, and Repair*. New York: Raven; 1990. p 77–91.
180. Koob TJ, Hernandez DJ. Material properties of polymerized NDGA-collagen composite fibers: Development of biologically based tendon constructs. *Biomaterials* 2002; 23:203–212.
181. Lee CH, Singla A, Lee Y. Biomedical applications of collagen. *Int J Pharm* 2001;221(1/2):1–22.
182. Kuo, Catherine K, Joseph E Marturano, and Rocky S Tuan. “Novel Strategies in Tendon and Ligament Tissue Engineering: Advanced Biomaterials and Regeneration Motifs.” *Sports Medicine, Arthroscopy, Rehabilitation, Therapy & Technology: SMARTT 2* (2010): 20. *PMC*. Web. 12 Oct. 2017.
183. Jiang P, Liu H, Wang C, Wu L, Huang J, Guo C. Tensile behavior and morphology of differently degummed silkworm (*Bombyx mori*) cocoon silk fibres. *Mat Lett*. 2006;60:919–925. doi: 10.1016/j.matlet.2005.10.056
184. Mechanical comparison of 10 suture materials before and after in vivo incubation. *Greenwald D, Shumway S, Albear P, Gottlieb L J Surg Res*. 1994 Apr; 56(4):372-7.
185. Physico-chemical properties of silk fibroin membrane as a biomaterial. *Minoura N, Tsukada M, Nagura M Biomaterials*. 1990 Aug; 11(6):430-4.

186. Freed LE, Vunjak-Novakovic G, Biron RJ, Eagles DB, Lesnoy DC, Barlow SK, Langer R. Biodegradable polymer scaffolds for tissue engineering. *Biotechnology (NY)* 1994; 12:689 – 693.
187. Ligament tissue engineering using synthetic biodegradable fiber scaffolds. *Lin VS, Lee MC, O'Neal S, McKean J, Sung KL Tissue Eng.* 1999 Oct; 5(5):443-52
188. Rezwan, K., et al., Biodegradable and bioactive porous polymer/inorganic compositescaffolds for bone tissue engineering. *Biomaterials*, 2006. 27(18): p. 3413-3431.
189. Migliaresi C, Fambri L, Cohn D. A study on the in vitro degradation of poly(lactic acid). *J Biomater Sci Polym Ed* 1994;5:591– 606.
190. Gentile, Piergiorgio et al. “An Overview of Poly(lactic-co-Glycolic) Acid (PLGA)-Based Biomaterials for Bone Tissue Engineering.” *International Journal of Molecular Sciences* 15.3 (2014): 3640–3659. *PMC*. Web. 15 Sept. 2017
191. Engineer, C.; Parikh, J.; Raval, A. Review on hydrolytic degradation behavior of biodegradable polymers from controlled drug delivery system. *Trends Biomater. Artif. Organs* 2011, 25, 79–85.
192. Chiquet-Ehrismann R, Tucker RP. Connective tissues: signalling by tenascins. *Int J Biochem Cell Biol.* 2004;36:1085–1089. doi: 10.1016/j.biocel.2004.01.007.
193. Bagnaninchi, P., et al., Tissue engineering for tendon repair. *Br J Sports Med*, 2006: p. bjsm.2006.030643.
194. Takasugi, H., et al., Three-dimensional architecture of blood vessels of tendonsdemonstrated by corrosion casts. *Hand*, 1978. 10(1): p. 9-15.
195. Caglar Yilgor,¹ Pinar Yilgor Huri,² and Gazi Huri³, Tissue Engineering Strategies in Ligament Regeneration

196. Rezwan, K., et al., Biodegradable and bioactive porous polymer/inorganic composite scaffolds for bone tissue engineering. *Biomaterials*, 2006. 27(18): p. 3413-3431.
197. Salgado, A., O. Coutinho, and R. Reis, Bone Tissue Engineering: State of the Art and Future Trends. *Macromolecular Bioscience*, 2004. 4(8): p. 743-765.
198. Gunatillake, P. and R. Adhikari, Biodegradable synthetic polymers for tissue engineering. *European Cells and Materials*, 2003. 5: p. 1-16.
199. Vert, M., et al., Bioresorbability and biocompatibility of aliphatic polyesters. *Journal of Materials Science: Materials in Medicine*, 1992. 3(6): p. 432-446.
200. Yang, S., et al., The Design of Scaffolds for Use in Tissue Engineering. Part I. Traditional Factors. *Tissue Engineering*, 2001. 7(6): p. 679-689.
201. Cooper JA, Lu HH, Ko FK, Freeman JW, Laurencin CT. Fiberbased tissue-engineered scaffold for ligament replacement: Design considerations and in vitro evaluation. *Biomaterials* 2005;26:1523–1532.
202. M. Deie, T. Marui, C. R. Allen et al., “The effects of age on rabbit MCL fibroblast matrix synthesis in response to TGF- β 1 or EGF,” *Mechanisms of Ageing and Development*, vol. 97, no. 2, pp. 121–130, 1997.
203. K. A. Hildebrand, S. L. Y. Woo, D. W. Smith et al., “The effects of platelet-derived growth factor-BB on healing of the rabbit medial collateral ligament. An in vivo study,” *American Journal of Sports Medicine*, vol. 26, no. 4, pp. 549–554, 1998.
204. P. G. Murphy, B. J. Loitz, C. B. Frank, and D. A. Hart, “Influence of exogenous growth factors on the synthesis and secretion of collagen types I and III by explants of normal and healing rabbit ligaments,” *Biochemistry and Cell Biology*, vol. 72, no. 9-10, pp. 403–409, 1994.

205. T. Marui, C. Niyibizi, H. I. Georgescu et al., "Effect of growth factors on matrix synthesis by ligament fibroblasts," *Journal of Orthopaedic Research*, vol. 15, no. 1, pp. 18–23, 1997.
206. S. C. Scherping, C. C. Schmidt, H. I. Georgescu, C. K. Kwok, C. H. Evans, and S. L. Y. Woo, "Effect of growth factors on the proliferation of ligament fibroblasts from skeletally mature rabbits," *Connective Tissue Research*, vol. 36, no. 1, pp. 1–8, 1997.
207. M. L. Batten, J. C. Hansen, and L. E. Dahners, "Influence of dosage and timing of application of platelet-derived growth factor on early healing of the rat medial collateral ligament," *Journal of Orthopaedic Research*, vol. 14, no. 5, pp. 736–741, 1996.
208. [208] C. C. Schmidt, H. I. Georgescu, C. K. Kwok et al., "Effect of growth factors on the proliferation of fibroblasts from the medial collateral and anterior cruciate ligaments," *Journal of Orthopaedic Research*, vol. 13, no. 2, pp. 184–190, 1995.
209. A. K. Letson and L. E. Dahners, "The effect of combinations of growth factors on ligament healing," *Clinical Orthopaedics and Related Research*, no. 308, pp. 207–212, 1994.
210. J. Lee, M. H. Green, and D. Amiel, "Synergistic effect of growth factors on cell outgrowth from explants of rabbit anterior cruciate and medial collateral ligaments," *Journal of Orthopaedic Research*, vol. 13, no. 3, pp. 435–441, 1995.
211. Carmeliet P, Conway EM. Growing better blood vessels. *Nat Biotechnol* 2001;19:1019–1020.
212. P. G. Murphy, B. J. Loitz, C. B. Frank, and D. A. Hart, "Influence of exogenous growth factors on the synthesis and secretion of collagen types I and III by explants of

- normal and healing rabbit ligaments,” *Biochemistry and Cell Biology*, vol. 72, no. 9-10, pp. 403–409, 1994.
213. T.Marui, C. Niyibizi, H. I. Georgescu et al., “Effect of growth factors on matrix synthesis by ligament fibroblasts,” *Journal of Orthopaedic Research*, vol. 15, no. 1, pp. 18–23, 1997.
 214. Yahia L. Ligaments and ligamentoplasties. Berlin, Heidelberg: Springer; 1997
 215. J.A.Cooper Jr., J. S. Sahota,W. J. GorumII, J.Carter, S. B. Doty, and C. T. Laurencin, “Biomimetic tissue-engineered anterior cruciate ligament replacement,” *Proceedings of the National Academy of Sciences of the United States of America*, vol. 104, no. 9, pp. 3049–3054, 2007.
 216. Freeman JW¹, Woods MD, Cromer DA, Wright LD, Laurencin CT. Tissue engineering of the anterior cruciate ligament: the viscoelastic behavior and cell viability of a novel braid-twist scaffold. *J Biomater Sci Polym Ed*. 2009;20(12):1709-28. doi: 10.1163/156856208X386282.
 217. Laurencin CT, Aronson Mark T, Nair Lakshmi Sreedharan, inventor; Soft Tissue Regeneration, Inc, assignee. Mechanically competent scaffold for ligament and tendon regeneration patent US8486143 B2, 2014.
 218. Thayer PS, Verbridge SS, Dahlgren LA, Kakar S, Guelcher SA, Goldstein AS. 2016. Fiber/collagen composites for ligament tissue engineering: influence of elastic moduli of sparse aligned fibers on mesenchymal stem cells. *J Biomed Mater Res Part A* 2016;104A:1894–1901.
 219. Pauly Hannah M., Sathy Binulal N., Olvera Dinorath, McCarthy Helen O., Kelly Daniel J., Popat Ketul C., Dunne Nicholas J., and Haut Donahue Tammy Lynn. Tissue

220. Willems, N. M., Langenbach, G. E., Everts, V. & Zentner, A. The microstructural and
221. Gobbi A, Kon E, Berruto M, Filardo G, Delcogliano M, Boldrini L, et al. Patellofemoral full-thickness chondral defects treated with second-generation autologous chondrocyte implantation. *Am J Sports Med* 2009;37
222. [22] add anything related
223. Gobbi A, Kon E, Berruto M, Filardo G, Delcogliano M, Boldrini L, et al. Patellofemoral full-thickness chondral defects treated with second-generation autologous chondrocyte implantation. *Am J Sports Med* 2009;37
224. McNickle AG, Provencher MT, Cole BJ. Overview of existing cartilage repair technology. *Sports Med Arthrosc* 2008;16
225. Chu CR, Coutts RD, Yoshioka M, Harwood FL, Monosov AZ, Amiel D. Articular-cartilage repair using allogeneic perichondrocyte-seeded biodegradable porous polylactic acid (Pla) — a tissue-engineering study. *J Biomed Mater Res* 1995;29
226. Malda J, Woodfield TBF, van der Vloodt F, Wilson C, Martens DE, Tramper J, et al. The effect of PEGT/PBT scaffold architecture on the composition of tissue engineered cartilage. *Biomaterials* 2005;26
227. Coburn JM, Gibson M, Monagle S, Patterson Z, Elisseeff JH. Bioinspired nanofibers support chondrogenesis for articular cartilage repair. *Proc Natl Acad Sci U S A* 2012;109.
228. Getgood AMJ, Kew SJ, Brooks R, Aberman H, Simon T, Lynn AK, et al.

- Evaluation of early-stage osteochondral defect repair using a biphasic scaffold based on a collagen-glycosaminoglycan biopolymer in a caprine model. *Knee* 2012;19
229. Chen GP, Sato T, Tanaka J, Tateishi T. Preparation of a biphasic scaffold for osteochondral tissue engineering. *Mater Sci Eng C Biomim Supramol Syst* 2006;26
230. Huang X¹, Yang D, Yan W, Shi Z, Feng J, Gao Y, Weng W, Yan S. Osteochondral repair using the combination of fibroblast growth factor and amorphous calcium phosphate/poly(L-lactic acid) hybrid materials. *Biomaterials*. 2007 Jul;28(20):3091-100. Epub 2007 Mar 18.
231. Mohan N, Dormer NH, Caldwell KL, Key VH, Berkland CJ, Detamore MS. Continuous gradients of material composition and growth factors for effective regeneration of the osteochondral interface. *Tissue Eng Part A* 2011;17
232. Jiang J, Tang A, Ateshian GA, Guo XE, Hung CT, Lu HH. Bioactive stratified polymer ceramic-hydrogel scaffold for integrative osteochondral repair. *Ann Biomed Eng* 2010;38
233. Csaki C, Schneider PRA, Shakibaei M. Mesenchymal stem cells as a potential pool for cartilage tissue engineering. *Ann Anat* 2008;190
234. Frohlich M, Malicev E, Gorenek M, Knezevic M, Velikonja NK. Evaluation of rabbit auricular chondrocyte isolation and growth parameters in cell culture. *Cell Biol Int* 2007;31
235. In 't Anker PS, Noort WA, Scherjon SA, Kleijburg-van der Keur C, Kruisselbrink AB, van Bezooijen RL, et al. Mesenchymal stem cells in human second-trimester bone marrow, liver, lung, and spleen exhibit a similar immunophenotype but a heterogeneous multilineage differentiation potential. *Haematologica* 2003;88.

236. Bullough, R., et al., Disability and Rehabilitation, in press.
237. Sharma, P. and N. Maffulli, Biology of tendon injury: healing, modeling and remodeling. *Journal of musculoskeletal & neuronal interactions*, 2006. 6(2): p. 181-190.
238. Giovannini, S., et al., Multilineage differentiation potential of equine blood-derived fibroblast-like cells. *Differentiation*, 2007. epub.
239. Wang, J.H.C., Mechanobiology of tendon. *Journal of Biomechanics*, 2006. 39(9): p.1563-1582.
240. Steadman, J., R. Forster, and J. Silferskiold, Rehabilitation of the knee. *Clinical Sports Medicine*, 1989. 8: p. 605-627.
241. Zeichen, J., M. van Griensven, and U. Bosch, The Proliferative Response of Isolated Human Tendon Fibroblasts to Cyclic Biaxial Mechanical Strain. *Am J Sports Med*, 2000.28(6): p. 888-892.
242. C. T. Laurencin, M. A. Attawia, H. E. Elgendy, and K. M. Herbert, "Tissue engineered bone-regeneration using degradable polymers: the formation of mineralized matrices," *Bone*, vol. 19, no. 1, 1996.
243. R. A. Jain, C. T. Rhodes, A. M. Railkar, A. W. Malick, and N. H. Shah, "Controlled delivery of drugs from a novel injectable in situ formed biodegradable PLGA microsphere system," *Journal of Microencapsulation*, vol. 17, no. 3, pp. 343–362, 2000
244. J. H. Brauker, V. E. Carr-Brendel, L. A. Martinson, J. Crudele, W. D. Johnston, and R. C. Johnson, "Neovascularization of synthetic membranes directed by membrane micro architecture," *Journal of Biomedical Materials Research*, vol. 29, pp. 1517–1524, 1995.

245. J. H. Brauker, V. E. Carr-Brendel, L. A. Martinson, J. Crudele, W. D. Johnston, and R. C. Johnson, "Neovascularization of synthetic membranes directed by membrane micro architecture," *Journal of Biomedical Materials Research*, vol. 29, pp. 1517–1524, 1995.
246. J. J. Klawitter and S. F. Hulbert, "Application of porous ceramics for the attachment of load-bearing internal orthopedic applications," *Journal of Biomedical Materials Research A Symposium*, vol. 2, pp. 161–168, 1971.
247. S. Yang, K. F. Leong, Z. Du, and C. K. Chua, "The design of scaffolds for use in tissue engineering—part I: traditional factors," *Tissue Engineering*, vol. 7, no. 6, pp. 679–689, 2001.
248. K. Whang, K. E. Healy, D. R. Elenz et al., "Engineering bone regeneration with bioabsorbable scaffolds with novel microarchitecture," *Tissue Engineering*, vol. 5, no. 1, pp. 35–51, 1999.
249. I. V. Yannas, E. Lee, D. P. Orgill, E. M. Skrabut, and G. F. Murphy, "Synthesis and characterization of a model extracellular matrix that induces partial regeneration of adult mammalian skin," *Proceedings of the National Academy of Sciences of the United States of America*, vol. 86, no. 3, pp. 933–937, 1989.
250. Sosnowski, S., P. Wozniak, and M. Lewandowska-Szumiel, Polyester scaffolds with bimodal pore size distribution of tissue engineering. *Macromolecular Bioscience*, 2006. 6(6): 425–434.
251. R. Langer and J. P. Vacanti, "Tissue engineering," *Science*, vol. 260, no. 5110, pp. 920–926, 1993
252. Reneker DH, Chun I. Nanometer diameter fibers of polymer, produced by

- electrospinning. *Nanotechnology* 1996;7:216–223
253. Pham, Q.P., U. Sharma, and A.G. Mikos, Electrospinning of polymeric nanofibers for tissue engineering applications: A review. *Tissue Engineering*, 2006. 12(5): 1197–1211.
 254. Reneker, D.H. and I. Chun, Nanometre diameter fibres of polymer, produced by electrospinning. *Nanotechnology*, 1996. 7: 216–223.
 255. Okamoto, M. and B. John, Synthetic biopolymer nanocomposites for tissue engineering scaffolds. *Progress in Polymer Science*, 2013. 38: 1487–1503.
 256. Huinan Liu and Thomas J. Webster Bioinspired nanocomposite for orthopedic applications
 257. Clark RA, Ghosh K, Tonnesen MG. Tissue engineering for cutaneous wounds. *J Invest Dermatol* 2007; 127: 1018–29.
 258. Lara Yildirim, Nguyen T.K. Thanh, and Alexander M. Seifalian ,Skin regeneration scaffolds: a multimodal bottom-up approach
 259. David J. Wong and Howard Y. Chang, skin tissue engineering
 260. Huang, S.; Fu, X. Naturally derived materials-based cell and drug delivery systems in skin regeneration. *J. Control. Release Off. J. Control. Release Soc.* 2010, 142, 149–159.
 261. Lu, L.; Peter, S.J.; Lyman, M.D.; Lai, H.L.; Leite, S.M.; Tamada, J.A.; Uyama, S.; Vacanti, J.P.; Langer, R.; Mikos, A.G. In vitro and in vivo degradation of porous poly(DL-lactic-co-glycolic acid) foams. *Biomaterials* 2000, 21, 1837–1845.
 262. Oh, S.H.; Kang, S.G.; Kim, E.S.; Cho, S.H.; Lee, J.H. Fabrication and characterization of hydrophilic poly(lactic-co-glycolic acid)/poly(vinyl alcohol) blend cell scaffolds by melt-molding particulate-leaching method. *Biomaterials* 2003, 24, 4011–

4021.

263. Rowlands, A.S.; Lim, S.A.; Martin, D.; Cooper-White, J.J. Polyurethane/poly(lactic-co-glycolic) acid composite scaffolds fabricated by thermally induced phase separation. *Biomaterials* 2007, 28, 2109–2121.
264. Pailler-Mattei C, Beca S, Zahouani H. In vivo measurements of the elastic mechanical properties of human skin by indentation tests. *Med Engin Phys* 2008; 30: 599-606.
265. De Filippo RE, Atala A. Stretch and growth: the molecular and physiologic influences of tissue expansion. *Plast Reconstr Surg* 2002; 109: 2450-62.
266. Sanders JE, Goldstein BS, Leotta DF. Skin response to mechanical stress: adaptation rather than breakdown – a review of the literature. *J Rehab Res Develop* 1995; 32: 214-26.
267. Silver FH, Seehra GP, Freeman JW, Devore D. Viscoelastic properties of young and old human dermis: a proposed molecular mechanism for elastic energy storage in collagen and elastin. *J Appl Polymer Sci* 2002; 86: 1978-85.
268. Silver FH, Siperko LM, Seehra GP. Mechanobiology of force transduction in dermal tissue. *Skin Res Technol* 2003; 9: 3-23.
269. Wong VW, Akaishi S, Longaker MT, Gurtner GC. Pushing back: wound mechanotransduction in repair and regeneration. *J Invest Dermatol* 2011; 131: 2186-96.
270. Simpson CL, Patel DM, Green KJ. Deconstructing the skin. Cytoarchitectural determinants of epidermal morphogenesis. *Nat Rev Mol Cell Biol* 2011; 12: 565-80.
271. Takei T, Mills I, Arai K, Sumpio BE. Molecular basis for tissue expansion: clinical implications for the surgeon. *Plast Reconstr Surg* 1998; 102: 247-58.

272. Buganza Tepole A, Gosain AK, Kuhl E. Stretching skin – the physiological limit and beyond. *Int J Nonlin Mech* 2012; 47: 938-49.
273. Buganza Tepole A, Ploch CJ, Wong, J, et al. Growing skin: a computational model for skin expansion in reconstructive surgery. *J Mech Phys Solids* 2011; 59: 2177-90.
274. Pailler-Mattei C, Beca S, Zahouani H. In vivo measurements of the elastic mechanical properties of human skin by indentation tests. *Med Engin Phys* 2008; 30: 599-606.
275. [275] Wu JZ, Dong RG, Smutz WP, Schopper AW. Modeling of time dependent force response of fingertip to dynamic loading. *J Biomech* 2003; 36: 383-92.
276. [276] Kathyr F, Imberdis C, Vescovo P, et al. Model of the viscoelastic behaviour of skin in vivo and study of anisotropy. *Skin Res Technol* 2004; 10: 93-103.
277. Pailler-Mattei C, Beca S, Zahouani H. In vivo measurements of the elastic mechanical properties of human skin by indentation tests. *Med Engin Phys* 2008; 30: 599-606.
278. Boyer G, Laquieze L, Le Bot A, et al. Dynamic indentation on human skin in vivo: ageing effects. *Skin Res Technol* 2009; 15: 55-67.
279. Mariola Pawlaczyk¹, Monika Lelonkiewicz¹, Michał Wieczorowski. Age-dependent biomechanical properties of the skin
280. Vogel HG. Age dependence of mechanical and biochemical properties of human skin. Part I. Stress-strain experiments, skin thickness and biochemical analysis. *Bioeng Skin* 1987; 3: 67-91.
281. Vogel HG. Age dependence of mechanical and biochemical properties of human skin. Part II. Hysteresis, relaxation, creep and repeated strain experiments. *Bioeng Skin*

1987; 3: 41-176.

282. Alberts B, Johnson A, Lewis J, Raff M & Roberts K. Molecular Biology of The Cell; Garland Science: New York, NY, USA. 2002 .
283. Norhayati MM, Mazlyzam AL, Asmah R, Fuzina H, Aminuddin BS, Ruszymah BH & Fauziah O. Collagen fibers an important entity in skin tissues remodeling. Med J Malaysia. 2004;59:184-85.
284. Norouzi, M.; Boroujeni, S.M.; Omidvarkordshouli, N.; Soleimani, M. Advances in skin regeneration: Application of electrospun scaffolds. Adv. Healthc. Mater. 2015, 4, 1114–1133.
285. Holmgren, S.K.; Bretscher, L.E.; Taylor, K.M.; Raines, R.T. A hyperstable collagen mimic. Chem. Biol. 1999, 6, 63–70.
286. Rho, K.S.; Jeong, L.; Lee, G.; Seo, B.M.; Park, Y.J.; Hong, S.D.; Roh, S.; Cho, J.J.; Park, W.H.; Min, B.M. Electrospinning of collagen nanofibers: Effects on the behavior of normal human keratinocytes and early-stage wound healing. Biomaterials 2006, 27, 1452–1461.
287. Sedlarik, K.M.; Schoots, C.; Fidler, V.; Oosterbaan, J.A.; Kloppe, J.P. [comparative animal experiment studies of the effect of exogenous collagen on healing of a deep skin wound]. Unfallchirurgie 1991, 17, 1–13.
288. Sedlarik, K.M.; Schoots, C.; Oosterbaan, J.A.; Kloppe, J.P. [healing of a deep skin wound using a collagen sponge as dressing in the animal experiment]. Aktuelle Traumatol. 1992, 22, 219–228.
289. Patino, M.G.; Neiders, M.E.; Andreana, S.; Noble, B.; Cohen, R.E. Collagen as an implantable material in medicine and dentistry. J. Oral Implantol. 2002, 28, 220–225.

290. Shen, X.; Nagai, N.; Murata, M.; Nishimura, D.; Sugi, M.; Munekata, M. Development of salmon milt DNA/salmon collagen composite for wound dressing. *J. Mater. Sci. Mater. Med.* 2008, 19, 3473–3479.
291. Mitra, T.; Sailakshmi, G.; Gnanamani, A.; Raja, S.T.; Thiruselvi, T.; Gowri, V.M.; Selvaraj, N.V.; Ramesh, G.; Mandal, A.B. Preparation and characterization of a thermostable and biodegradable biopolymers using natural cross-linker. *Int. J. Biol. Macromol.* 2011, 48, 276–285.
292. Sailakshmi, G.; Mitra, T.; Gnanamani, A.; Kumara Raja, S.T.; Thiruselvi, T.; Selvaraj, N.V.; Ramesh, G.; Mandal, A.B. Bonding interactions and stability assessment of biopolymer material prepared using type III collagen of avian intestine and anionic polysaccharides. *J. Mater. Sci. Mater. Med.* 2011, 22, 1419–1429.
293. Ghica, M.V.; Albu, M.G.; Leca, M.; Popa, L.; Moisescu, S.T. Design and optimization of some collagen-minocycline based hydrogels potentially applicable for the treatment of cutaneous wound infections. *Die Pharm.* 2011, 66, 853–861.
294. Kempf, M.; Miyamura, Y.; Liu, P.Y.; Chen, A.C.; Nakamura, H.; Shimizu, H.; Tabata, Y.; Kimble, R.M.; McMillan, J.R. A denatured collagen microfiber scaffold seeded with human fibroblasts and keratinocytes for skin grafting. *Biomaterials* 2011, 32, 4782–4792.
295. Lee, J.; Tae, G.; Kim, Y.H.; Park, I.S.; Kim, S.H. The effect of gelatin incorporation into electrospun poly(L-lactide-co-epsilon-caprolactone) fibers on mechanical properties and cytocompatibility. *Biomaterials* 2008, 29, 1872–1879. [CrossRef] [PubMed]
296. Mota, A.; Sahebghadam Lotfi, A.; Barzin, J.; Hatam, M.; Adibi, B.; Khalaj, Z.; Massumi, M. Human bone marrow mesenchymal stem cell behaviors on PCL/gelatin

- nanofibrous scaffolds modified with a collagen IV-derived RGD containing peptide. *Cell J.* 2014, 16, 1–10.
297. Choi, Y.S.; Lee, S.B.; Hong, S.R.; Lee, Y.M.; Song, K.W.; Park, M.H. Studies on gelatin-based sponges. Part III: A comparative study of cross-linked gelatin/alginate, gelatin/hyaluronate and chitosan/hyaluronate sponges and their application as a wound dressing in full-thickness skin defect of rat. *J. Mater. Sci. Mater. Med.* 2001, 12, 67–73.
 298. Ulubayram, K.; Nur Cakar, A.; Korkusuz, P.; Ertan, C.; Hasirci, N. Egf containing gelatin-based wound dressings. *Biomaterials* 2001, 22, 1345–1356.
 299. Min, B.M.; Lee, G.; Kim, S.H.; Nam, Y.S.; Lee, T.S.; Park, W.H. Electrospinning of silk fibroin nanofibers and its effect on the adhesion and spreading of normal human keratinocytes and fibroblasts in vitro. *Biomaterials* 2004, 25, 1289–1297.
 300. Mottaghitab, F.; Farokhi, M.; Zaminy, A.; Kokabi, M.; Soleimani, M.; Mirahmadi, F.; Shokrgozar, M.A.; Sadeghizadeh, M. A biosynthetic nerve guide conduit based on silk/swnt/fibronectin nanocomposite for peripheral nerve regeneration. *PLoS ONE* 2013, 8, e74417.
 301. Min, B.M.; Jeong, L.; Nam, Y.S.; Kim, J.M.; Kim, J.Y.; Park, W.H. Formation of silk fibroin matrices with different texture and its cellular response to normal human keratinocytes. *Int. J. Biol. Macromol.* 2004, 34, 281–288.
 302. Comparison of an occlusive and a semi-occlusive dressing and the effect of the wound exudate upon keratinocyte proliferation. *Madden MR, Nolan E, Finkelstein JL, Yurt RW, Smeland J, Goodwin CW, Hefton J, Staiano-Coico L J Trauma.* 1989 Jul; 29(7):924-30; discussion 930-1.

303. Panilaitis B, Altman GH, Chen JS, Jin HJ, Karageorgiou V, Kaplan DL. *Biomaterials*. 2003;24:3079.
304. Meinel L, Hofmann S, Karageorgiou V, Kirker-Head C, McCool J, Gronowicz G, Zichner L, Langer R, Vunjak-Novakovic G, Kaplan DL. *Biomaterials*. 2005;26:147
305. Shao ZZ, Vollrath F. *Nature*. 2002;418:741.
306. Motta A, Fambri L, Migliaresi C. *Macromol Chem Physic*. 2002;203:1658.
307. Jin HJ, Park J, Karageorgiou V, Kim UJ, Valluzzi R, Kaplan DL. *Adv Funct Mater*. 2005;15:1241.
308. Hu X, Shmelev K, Sun L, Gil ES, Park SH, Cebe P, Kaplan DL. *Biomacromolecules*. 2011;12:1686.
309. Wang Y, Rudym DD, Walsh A, Abrahamsen L, Kim HJ, Kim HS, Kirker-Head C, Kaplan DL. *Biomaterials*. 2008;29:3415
310. Martino MM, Tortelli F, Mochizuki M, Traub S, Ben-David D, Kuhn GA, Müller R, Livne E, Eming SA & Hubbell JA. Engineering the growth factor microenvironment with fibronectin domains to promote wound and bone tissue healing. *Sci Transl Med*. 2011;3(100): 100.
311. Roy DC, Mooney NA, Raeman CH, Dalecki D & Hocking D. Fibronectin Matrix Mimetics Promote Full Thickness Wound Repair in Diabetic Mice. *Tissue Eng Part A*. 2013; 19(21-22): 2517-26.
312. Bush KA, & Pins GD. Carbodiimide conjugation of fibronectin on collagen basal lamina analogs enhances cellular binding domains and epithelialization. *Tissue Eng Part A*. 2010;16(3):829-38.
313. Rosso F, Marino G, Giordano A, Barbarisi M, Parmegiani D & Barbarisi A. Smart

- materials as scaffolds for tissue engineering. *J. Cell. Physiol.* 2005;203: 465-70.
314. Future Prospects for Scaffolding Methods and Biomaterials in Skin Tissue Engineering: A Review, Atul A. Chaudhari, Komal Vig, Dieudonné Radé Baganizi, Rajnish Sahu, Saurabh Dixit, Vida Dennis, Shree Ram Singh and Shreekumar R. Pillai
 315. Dinarvand, P.; Hashemi, S.M.; Seyedjafari, E.; Shabani, I.; Mohammadi-Sangcheshmeh, A.; Farhadian, S.; Soleimani, M. Function of poly (lactic-co-glycolic acid) nanofiber in reduction of adhesion bands. *J. Surg. Res.* 2012, 172, e1–e9.
 316. Chen, H.; Peng, Y.; Wu, S.; Tan, L.P. Electrospun 3D Fibrous Scaffolds for Chronic Wound Repair. *Materials* 2016, 9, 272.
 317. Evaluation of PLA membranes for wound healing
http://shodhganga.inflibnet.ac.in/bitstream/10603/13274/11/11_chapter%206.pdf
 318. Pinzón-García AD, Cassini-Vieira P, Ribeiro CC, de Matos Jensen CE, Barcelos LS, Cortes ME, Sinisterra RD . Efficient cutaneous wound healing using bixin-loaded PCL nanofibers in diabetic mice. *J Biomed Mater Res B Appl Biomater.* 2017 Oct;105(7):1938-1949. doi: 10.1002/jbm.b.33724.
 319. Aghdam, R. M., Najarian, S., Shakhesi, S., Khanlari, S., Shaabani, K. and Sharifi, S. (2012), Investigating the effect of PGA on physical and mechanical properties of electrospun PCL/PGA blend nanofibers. *J. Appl. Polym. Sci.*, 124: 123–131. doi:10.1002/app.35071
 320. Rahman-Neishaboor, E., et al., Composite Hydrogel Formulations of Stratafin to Control MMP-1 Expression in Dermal Fibroblasts. *Pharmaceutical Research*, 2009. 26(8): p. 2002-2014.

321. Leung , R. Hartwell , H. Yang , E. Rahmani-Neishaboor 2 , Y. L , F. Ko1, A. Ghahary2 .POLYMER-BASED COMPOSITE NANOFIBRES FOR WOUND HEALING APPLICATIONS V.
322. Mogosanu, G.D.; Grumezescu, A.M. Natural and synthetic polymers for wounds and burns dressing. *Int. J. Pharm.* 2014, 463, 127–136.
323. Alaribe, F.N.; Manoto, S.L.; Motaung, S. Scaffolds from biomaterials: Advantages and limitations in boneand tissue engineering. *Biol. Sect. Cell Mol. Biol.* 2016, 71, 353–366.
324. Debels, H.; Hamdi, M.; Abberton, K.; Morrison, W. Dermal matrices and bioengineered skin substitutes: A critical review of current options. *Plast. Reconstr. Surg. Glob. Open* 2015, 3, e284.
325. Nyame, T.T.; Chiang, H.A.; Leavitt, T.; Ozambela, M.; Orgill, D.P. Tissue-engineered skin substitutes. *Plast. Reconstr. Surg.* 2015, 136, 1379–1388.
326. Norouzi, M.; Boroujeni, S.M.; Omidvarkordshouli, N.; Soleimani, M. Advances in skin regeneration: Application of electrospun scaffolds. *Adv. Healthc. Mater.* 2015, 4, 1114–1133.
327. Ma, Z.; Kotaki, M.; Inai, R.; Ramakrishna, S. Potential of nanofiber matrix as tissue-engineering scaffolds. *Tissue Eng.* 2005, 11, 101–109.
328. Bhattarai, S.R.; Bhattarai, N.; Yi, H.K.; Hwang, P.H.; Cha, D.I.; Kim, H.Y. Novel biodegradable electrospun membrane: Scaffold for tissue engineering. *Biomaterials* 2004, 25, 2595–2602.
329. Venugopal J, Zhang YZ, Ramakrishna S. In vitro culture of human dermal fibroblasts on electrospun polycaprolactone collagen nanofibrous membrane. *Artif Organs*

- 2006; 30: 438–44.
330. Dieckmann C, Renner R, Milkova L, Simon JC. Regenerative medicine in dermatology: biomaterials, tissue engineering, stem cells, gene transfer and beyond. *Exp Dermatol* 2010; 19: 697– 706.
 331. Prabhakaran MP, Venugopal J, Laleh GM, Dan K, Guorui J, Ramakrishna S. Stem cells and nanostructures for advanced tissue regeneration. *Adv Polym Sci* 2012; 246: 21– 62.
 332. Wu Y, Chen L, Scott PG, Tredget EE. Mesenchymal stem cells enhance wound healing through differentiation and angiogenesis. *Stem Cells* 2007; 25: 2648–59.
 333. Lara Yildirim¹, Nguyen T.K. Thanh^{2,3}, and Alexander M. Seifalian^{1,4} Skin regeneration scaffolds: a multimodal bottom-up approach
 334. Yang Y, Xia T, Zhi W, et al. Promotion of skin regeneration in diabetic rats by electrospun core-sheath fibers loaded with basic fibroblast growth factor. *Biomaterials*. 2011; 32:4243–4254.
 335. Yang F, Murugan R, Wang S, et al. Electrospinning of nano/micro scale poly (L-lactic acid) aligned fibers and their potential in tissue engineering. *Biomaterials*. 2005; 26:2603–2610.
 336. Ji Suk Choi, Seung Ho Choi, Hyuk Sang Yoo. Coaxial electrospun nanofibers for treatment of diabetic ulcers with binary release of multiple growth factors
 337. Creation of hair follicles in tissue-engineered skin grafts
<https://www.google.com/patents/US20120276154>
 338. Maiké Keck, Daniela Haluza, David B. Lumenta, Sonja Burjak, Bettina Eisenbock, Lars-Peter Kamolz, Manfred Frey. Construction of a multi-layer skin substitute:

Simultaneous cultivation of keratinocytes and preadipocytes on a dermal template Author
links open overlay panel

- 339. Paunescu V, Deak E, Herman D, Siska IR, Seifried E. In vitro differentiation of human mesenchymal stem cells to epithelial lineage. *J Cell Mol Med* 2007; 11: 502–8.
- 340. Ma K, Liao S, He L, Lu J, Ramakrishna S, Chan CK. Effects of nanofiber/stem cell composite on wound healing in acute full-
- 341. Light, D.B.; Cooley, D.A. *Cells, Tissues, and Skin*; Chelsea House Publishers: Philadelphia, PA, USA, 2004.
- 342. B. Alberts, A. Johnson, J. Lewis, M. Raff, K. Roberts, P. Walter, *Cell junctions, cell adhesion, and the extracellular matrix*, (2002).
- 343. R.F. Diegelmann, M.C. Evans, Wound healing: an overview of acute, fibrotic and delayed healing, *Front Biosci* 9(1) (2004) 283- 289.
- 344. F. Rosso, A. Giordano, M. Barbarisi, A. Barbarisi, From cell–ECM interactions to tissue engineering, *Journal of cellular physiology* 199(2) (2004) 174-180.
- 345. B. Alberts, A. Johnson, J. Lewis, M. Raff, K. Roberts, P. Walter, *The extracellular matrix of animals*, (2002).
- 346. F.M. Watt, W.T.S. Huck, Role of the extracellular matrix in regulating stem cell fate, *Nat Rev Mol Cell Biol* 14(8) (2013) 467-473.
- 347. F.M. Watt, H. Fujiwara, Cell-extracellular matrix interactions in normal and diseased skin, *Cold Spring Harb Perspect Biol* 3(4) (2011).
- 348. E. Boland, P. Espy, G. Bowlin, *Tissue Engineering Scaffolds*, *Encyclopedia of Biomaterials and Biomedical Engineering*, Second Edition (Online Version), CRC Press 2008, pp. 2828-2837.

349. X. Wen, D. Shi, N. Zhang, Applications of nanotechnology in tissue engineering, Handbook of nanostructured biomaterials and their applications in nanobiotechnology 2 (2005) 393-414.
350. S. Partridge, H. Davis, The chemistry of connective tissues. 3. Composition of the soluble proteins derived from elastin, Biochemical Journal 61(1) (1955) 21.
351. W.F. Daamen, J. Veerkamp, J. Van Hest, T. Van Kuppevelt, Elastin as a biomaterial for tissue engineering, Biomaterials 28(30) (2007) 4378-4398.
352. G.H. Altman, R.L. Horan, H.H. Lu, J. Moreau, I. Martin, J.C. Richmond, D.L. Kaplan, Silk matrix for tissue engineered anterior cruciate ligaments, Biomaterials 23(20) (2002) 4131-4141.
353. H. Liu, H. Fan, Y. Wang, S.L. Toh, J.C. Goh, The interaction between a combined knitted silk scaffold and microporous silk sponge with human mesenchymal stem cells for ligament tissue engineering, Biomaterials 29(6) (2008) 662-674.
354. Y.K. Seo, G.M. Choi, S.Y. Kwon, H.S. Lee, Y.S. Park, K.Y. Song, Y.J. Kim, J.K. Park, The biocompatibility of silk scaffold for tissue engineered ligaments, Key Engineering Materials, Trans Tech Publ, 2007, pp. 73-76.
355. S. Toh, T. Teh, S. Vallaya, J. Goh, Novel silk scaffolds for ligament tissue engineering applications, Key Engineering Materials, Trans Tech Publ, 2006, pp. 727-730.
356. H. Yoshimoto, Y. Shin, H. Terai, J. Vacanti, A biodegradable nanofiber scaffold by electrospinning and its potential for bone tissue engineering, Biomaterials 24(12) (2003) 2077-2082.

357. K. Fujihara, M. Kotaki, S. Ramakrishna, Guided bone regeneration membrane made of polycaprolactone/calcium carbonate composite nano-fibers, *Biomaterials* 26(19) (2005) 4139-4147.
358. S.A. Sell, P.S. Wolfe, K. Garg, J.M. McCool, I.A. Rodriguez, G.L. Bowlin, The Use of Natural Polymers in Tissue Engineering: A Focus on Electrospun Extracellular Matrix Analogues, *Polymers* 2(4) (2010) 522.
359. S. Enoch, D. J. Leaper, *Surgery* 2005, 23, 37
360. Abrigo M, McArthur SL, Kingshott P. Electrospun nanofibers as dressings for chronic wound care: advances, challenges, and future prospects. *Macromol Biosci.* 2014 Jun;14(6):772-92. doi: 10.1002/mabi.201300561. Epub 2014 Mar 28.
361. Taek Gyoung Kim , Heungsoo Shin , * and Dong Woo Lim, Biomimetic Scaffolds for Tissue Engineering
362. Guven S, Chen P, Inci F, Tasoglu S, Erkmen B, et al. (2015) Multiscale assembly for tissue engineering and regenerative medicine. *Trends in Biotechnology* 33: 269-279.
363. biomaterials and scaffold for tissue engineering (biomimetic)
364. Kumbar SG, James R, Nukavarapu SP, Laurencin CT. Electrospun nanofiber scaffolds: engineering soft tissues. *Biomed Mater.* 2008 Sep;3(3):034002. doi: 10.1088/1748-6041/3/3/034002. Epub 2008 Aug 8.
365. Vasita, R.; Katti, D.S. Nanofibers and their applications in tissue engineering. *Int. J. Nanomed.* 2006, 1, 15–30.
366. F. Anton, Process and apparatus for preparing artificial threads, Google Patents, 1934.

367. S. Sell, C. Barnes, M. Smith, M. McClure, P. Madurantakam, J. Grant, M. McManus, G. Bowlin, Extracellular matrix regenerated: tissue engineering via electrospun biomimetic nanofibers, *Polymer International* 56(11) (2007) 1349-1360.
368. W. Liu, S. Thomopoulos, Y. Xia, Electrospun nanofibers for regenerative medicine, *Advanced healthcare materials* 1(1) (2012) 10-25.
369. E.D. Boland, T.A. Telemeco, D.G. Simpson, G.E. Wnek, G.L. Bowlin, Utilizing acid pretreatment and electrospinning to improve biocompatibility of poly (glycolic acid) for tissue engineering, *Journal of Biomedical Materials Research Part B: Applied Biomaterials* 71(1) (2004) 144-152.
370. L. Kolacna, J. Bakesova, F. Varga, E. Kostakova, L. Plánka, A. Necas, D. Lukas, E. Amler, V. Pelouch, Biochemical and biophysical aspects of collagen nanostructure in the extracellular matrix, *Physiological Research* 56 (2007) S51.
371. M. Schindler, I. Ahmed, J. Kamal, A. Nur-E-Kamal, T.H. Grafe, H.Y. Chung, S. Meiners, A synthetic nanofibrillar matrix promotes in vivo-like organization and morphogenesis for cells in culture, *Biomaterials* 26(28) (2005) 5624-5631.
372. T. Telemeco, C. Ayres, G. Bowlin, G. Wnek, E. Boland, N. Cohen, C. Baumgarten, J. Mathews, D. Simpson, Regulation of cellular infiltration into tissue engineering scaffolds composed of submicron diameter fibrils produced by electrospinning, *Acta biomaterialia* 1(4) (2005) 377-385.
373. J. Zeltinger, J.K. Sherwood, D.A. Graham, R. Müller, L.G. Griffith, Effect of pore size and void fraction on cellular adhesion, proliferation, and matrix deposition, *Tissue engineering* 7(5)(2001) 557-572.

374. Reneker, D.H.; Chun, I. Nanometre diameter fibres of polymer, produced by electrospinning. *Nanotechnology* 1996, 7, doi:10.1088/0957-4484/7/3/009.
375. D.H. Reneker, I. Chun, Nanometre diameter fibres of polymer, produced by electrospinning, *Nanotechnology* 7(3) (1996) 216.
376. G.H. Kim, Electrospinning process using field-controllable electrodes, *Journal of Polymer Science Part B: Polymer Physics* 44(10) (2006) 1426-1433.
377. J.M. Deitzel, J. Kleinmeyer, D. Harris, N.C. Beck Tan, The effect of processing variables on the morphology of electrospun nanofibers and textiles, *Polymer* 42(1) (2001) 261-272.
378. S. Ramakrishna, *An Introduction to Electrospinning and Nanofibers*, World Scientific 2005.
379. C.J. Buchko, L.C. Chen, Y. Shen, D.C. Martin, Processing and microstructural characterization of porous biocompatible protein polymer thin films, *Polymer* 40(26) (1999) 7397-7407.
380. L. Larrondo, R. St John Manley, Electrostatic fiber spinning from polymer melts. I. Experimental observations on fiber formation and properties, *Journal of Polymer Science: Polymer Physics Edition* 19(6) (1981) 909-920.
381. Z. Li, C. Wang, *One-dimensional nanostructures: electrospinning technique and unique nanofibers*, Springer 2013.
382. C. Mit-uppatham, M. Nithitanakul, P. Supaphol, Ultrafine electrospun polyamide-6 fibers: effect of solution conditions on morphology and average fiber diameter, *Macromolecular Chemistry and Physics* 205(17) (2004) 2327-2338.

383. V. Morozov, T. Morozova, N. Kallenbach, Atomic force microscopy of structures produced by electrospraying polymer solutions, *International Journal of Mass Spectrometry* 178(3) (1998) 143-159.
384. T. Jarusuwannapoom, W. Hongrojjanawiwat, S. Jitjaicham, L. Wannatong, M. Nithitanakul, C. Pattamaprom, P. Koombhongse, R. Rangkupan, P. Supaphol, Effect of solvents on electrospinnability of polystyrene solutions and morphological appearance of resulting electrospun polystyrene fibers, *European Polymer Journal* 41(3) (2005) 409-421.
385. M.M. Demir, I. Yilgor, E. Yilgor, B. Erman, Electrospinning of polyurethane fibers, *Polymer* 43(11) (2002) 3303-3309.
386. H. Fong, I. Chun, D. Reneker, Beaded nanofibers formed during electrospinning, *Polymer* 40(16) (1999) 4585-4592.
387. S. Megelski, J.S. Stephens, D.B. Chase, J.F. Rabolt, Micro-and nanostructured surface morphology on electrospun polymer fibers, *Macromolecules* 35(22) (2002) 8456-8466.
388. M.M. Demir, I. Yilgor, E. Yilgor, B. Erman, Electrospinning of polyurethane fibers, *Polymer* 43(11) (2002) 3303-3309.
389. S. Ramakrishna, *An Introduction to Electrospinning and Nanofibers*, World Scientific 2005.
390. I. G. Loscertales, A. Barrero, I. Guerrero, R. Cortijo, M. Marquez, A. M. G~n~an-Calvo, *Science* 2002, 295, 1695.
391. D. H. Reneker, A. L. Yarin, *Polymer* 2008, 49, 2387.

392. Jiang J, Nicoll SB, Lu HH. Co-culture of osteoblasts and chondrocytes modulates cellular differentiation in vitro. *Biochem Biophys Res Commun*. 2005 Dec 16;338(2):762-70. Epub 2005 Oct 17.
393. Wang, I.-N. E., Shan, J., Choi, R., Oh, S., Kepler, C. K., Chen, F. H. and Lu, H. H. (2007), Role of osteoblast–fibroblast interactions in the formation of the ligament-to-bone interface. *J. Orthop. Res.*, 25: 1609–1620. doi:10.1002/jor.20475
394. Jiang J, Tang A, Ateshian GA, Guo XE, Hung CT, Lu HH. Bioactive stratified polymer ceramic-hydrogel scaffold for integrative osteochondral repair. *Ann Biomed Eng*. 2010 Jun;38(6):2183-96. doi: 10.1007/s10439-010-0038-y. Epub 2010 Apr 22.
395. Cheng HW, Luk KD, Cheung KM, Chan BP. In vitro generation of an osteochondral interface from mesenchymal stem cell-collagen microspheres. *Biomaterials*. 2011 Feb;32(6):1526-35. doi: 10.1016/j.biomaterials.2010.10.021. Epub 2010 Nov
396. <http://strengthtrainingforyou.blogspot.com/2015/07/acl-reconstruction-and-rehab.html>
397. Shih-Feng Chou, Daniel Carson, Kim A. Woodrow. Current strategies for sustaining drug release from electrospun nanofibers
398. McDonald PF, Lyons JG, Geever LM, Higginbotham CL. In vitro degradation and drug release from polymer blends based on poly(DL-lactide), poly(L-lactideglycolide) and poly(e-caprolactone). *J. Mater. Sci*. 2010; 45:1284–1292.
399. [399] Verreck G, Chun I, Rosenblatt J, Peeters J, Dijck AV, Mensch J, Noppe M, Brewster ME. Incorporation of drugs in an amorphous state into electrospun nanofibers composed of a water-insoluble, nonbiodegradable polymer. *J. Control. Release*. 2003;

92:349–360.

400. Piskin E, Bolgen N, Egri S, Isoglu IP. Electrospun matrices made of poly(alpha-hydroxy acids) for medical use. *Nanomedicine*. 2007; 2:441–457.
401. R. Khajavi, M. Abbasipour, *Sci. Iran*. 2012, 19, 2029.398
402. Ji, Wei et al. “Bioactive Electrospun Scaffolds Delivering Growth Factors and Genes for Tissue Engineering Applications.” *Pharmaceutical Research* 28.6 (2011): 1259–1272. *PMC*. Web. 3 Nov. 2017.
403. Release pattern and structural integrity of lysozyme encapsulated in core-sheath structured poly(DL-lactide) ultrafine fibers prepared by emulsion electrospinning. *Yang Y, Li X, Qi M, Zhou S, Weng J Eur J Pharm Biopharm*. 2008 May; 69(1):106-16
404. Encapsulation and controlled release of lysozyme from electrospun poly(epsilon-caprolactone)/poly(ethylene glycol) non-woven membranes by formation of lysozyme-oleate complexes. *Li Y, Jiang H, Zhu K J Mater Sci Mater Med*. 2008 Feb; 19(2):827-32
405. Polymer-protein interactions. Comparison of experiment and excluded volume theory. *Knoll D, Hermans J J Biol Chem*. 1983 May 10; 258(9):5710-5.
406. Three-dimensional fibrous PLGA/HAp composite scaffold for BMP-2 delivery. *Nie H, Soh BW, Fu YC, Wang CH Biotechnol Bioeng*. 2008 Jan 1; 99(1):223-34.
407. Development of a nanostructured DNA delivery scaffold via electrospinning of PLGA and PLA-PEG block copolymers. *Luu YK, Kim K, Hsiao BS, Chu B, Hadjiargyrou MJ Control Release*. 2003 Apr 29; 89(2):341-53
408. Poly(vinyl alcohol) nanofibers by electrospinning as a protein delivery system and the retardation of enzyme release by additional polymer coatings. *Zeng J, Aigner A,*

Czubayko F, Kissel T, Wendorff JH, Greiner A *Biomacromolecules*. 2005 May-Jun; 6(3):1484-8.

409. Encapsulation and controlled release of lysozyme from electrospun poly(epsilon-caprolactone)/poly(ethylene glycol) non-woven membranes by formation of lysozyme-oleate complexes. Li Y, Jiang H, Zhu K J *Mater Sci Mater Med*. 2008 Feb; 19(2):827-32.
410. Coaxial electrospinning of (fluorescein isothiocyanate-conjugated bovine serum albumin)-encapsulated poly(epsilon-caprolactone) nanofibers for sustained release. Zhang YZ, Wang X, Feng Y, Li J, Lim CT, Ramakrishna S *Biomacromolecules*. 2006 Apr; 7(4):1049-57.
411. Weng, Lin, and Jingwei Xie. "Smart Electrospun Nanofibers for Controlled Drug Release: Recent Advances and New Perspectives." *Current pharmaceutical design* 21.15 (2015): 1944–1959. Print.
412. Nie H, Soh BW, Fu YC, Wang CH. Three-dimensional fibrous PLGA/HAp composite scaffold for BMP-2 delivery. *Biotechnol Bioeng*. 2008 Jan 1; 99(1):223-34
413. Chen SC, Huang XB, Cai XM, Lu J, Yuan J, Shen J. The influence of fiber diameter of electrospun poly(lactic acid) on drug delivery. *Fibers Polym*. 2012; 9:1120–1125.
414. Okuda T, Tominaga K, Kidoaki S. Time-programmed dual release formulation by multilayered drug-loaded nanofiber meshes. *J Control Release*. 2010; 143:258–264.
415. Sun ZC, Zussman E, Yarin AL, Wendorff JH, Greiner A. Compound core-shell polymer nanofibers by co-electrospinning. *Adv Mater*. 2003; 15(22):1929–1932. doi: 10.1002/adma.200305136.

416. Su Y, Su Q, Liu W, Lim M, Venugopal JR, Mo X, Ramakrishna S, Al-Deyab SS, El-Newehy M. Controlled release of bone morphogenetic protein 2 and dexamethasone loaded in core-shell PLLACL-collagen fibers f
417. Yang Y, Xia T, Zhi W, et al. Promotion of skin regeneration in diabetic rats by electrospun core-sheath fibers loaded with basic fibroblast growth factor. *Biomaterials*. 2011; 32:4243–4254.
418. Yang F, Murugan R, Wang S, et al. Electrospinning of nano/micro scale poly (L-lactic acid) aligned fibers and their potential in tissue engineering. *Biomaterials*. 2005;26:2603–2610.
419. N. G. Rim, C. S. Shin, H. Shin, *Biomed. Mater.* 2013, 8, 1.
420. Doshi J, Reneker DH. Electrospinning process and applications of electrospun fibers. *J Electrostat.* 1995; 35:151–160. doi: 10.1016/0304-3886(95)00041-8
421. Poly (vinyl alcohol) nanofibers by electrospinning as a protein delivery system and the retardation of enzyme release by additional polymer coatings. *Zeng J, Aigner A, Czubayko F, Kissel T, Wendorff JH, Greiner A Biomacromolecules. 2005 May-Jun; 6(3):1484-8.*
422. Electrospinning of polymeric nanofibers for tissue engineering applications: a review. *Pham QP, Sharma U, Mikos AG Tissue Eng. 2006 May; 12(5):1197-211.*
423. Fibrous scaffolds loaded with protein prepared by blend or coaxial electrospinning. *Ji W, Yang F, van den Beucken JJ, Bian Z, Fan M, Chen Z, Jansen JA Acta Biomater. 2010 Nov; 6(11):4199-207*
424. Chen, S.C., Huang, X.B., Cai, X.M. et al. *Fibers Polym* (2012) 13: 1120. <https://doi.org/10.1007/s12221-012-1120-x>

425. Dayal P, Kyu T. Porous fiber formation in polymer–solvent system undergoing solvent evaporation. *J. Appl. Phys.* 2006; 100:043512
426. Sahoo, S., Ang, L. T., Goh, J. C.-H. and Toh, S.-L. (2010), Growth factor delivery through electrospun nanofibers in scaffolds for tissue engineering applications. *J. Biomed. Mater. Res.*, 93A: 1539–1550. doi:10.1002/jbm.a.32645
427. Song W¹, Seta J, Chen L, Bergum C, Zhou Z, Kanneganti P, Kast RE, Auner GW, Shen M, Markel DC, Ren W, Yu X. Doxycycline-loaded coaxial nanofiber coating of titanium implants enhances osseointegration and inhibits *Staphylococcus aureus* infection. *Biomed Mater.* 2017 Jul 5;12(4):045008. doi: 10.1088/1748-605X/aa6a26
428. Su Y, Su Q, Liu W, et al. Dual-drug encapsulation and release from core-shell nanofibers. *J Biomater Sci Polym Ed.* 2012; 23:861 871.
429. Liu T, Gao Y, Sakamoto K, Minamizato T, Furukawa K, Tsukazaki T, Shibata Y, Bessho K, Komori T, Yamaguchi A. BMP-2 promotes differentiation of osteoblasts and chondroblasts in Runx2-deficient cell lines. *J Cell Physiol.* 2007 Jun;211(3):728-35.
430. Hoeben A, Landuyt B, Highley MS, Wildiers H, Van Oosterom AT, De Bruijn EA. Vascular endothelial growth factor and angiogenesis. *Pharmacol Rev.* 2004 Dec;56(4):549-80.
431. Kim, Bo-Ram et al. “*In Vitro* and *In Vivo* Studies of BMP-2-Loaded PCL–Gelatin–BCP Electrospun Scaffolds.” *Tissue Engineering. Part A* 20.23-24 (2014): 3279–3289. *PMC*. Web. 3 Nov. 2017.
432. Young S, Patel ZS, Kretlow JD, Murphy MB, Mountziaris PM, Baggett LS, Ueda H, Tabata Y, Jansen JA, Wong M, Mikos AG. Dose effect of dual delivery of vascular

endothelial growth factor and bone morphogenetic protein-2 on bone regeneration in a rat critical-size defect model. *Tissue Eng Part A*. 2009 Sep;15(9):2347-62. doi: 10.1089/ten.tea.2008.0510.

433. Banerjee, Indranil, Debasish Mishra, and Tapas K. Maiti. "PLGA Microspheres Incorporated Gelatin Scaffold: Microspheres Modulate Scaffold Properties." *International Journal of Biomaterials* 2009 (2009): 143659. *PMC*. Web. 3 Nov. 2017.

CHAPTER 2

SYNTHESIS, CHARACTERIZATION AND IN VITRO DEGRADATION OF THE DIFFERENT PHASES WITHIN THE INTEGRATED GRAFT SYSTEM

2.1.Introduction

An ideal tissue engineering scaffold should possess a number of essential properties. The scaffold should be biocompatible that maintains cell viability *in vitro* and do not elicit any immune response upon implantation *in vivo*. In addition, the scaffold should be highly porous to facilitate cell migration, proliferation, nutrition diffusion and waste removal. The scaffold should also exhibit biomimetic architectural properties resembling those found at the native tissue, and more importantly, the scaffold should be biodegradable with a degradation rate compatible to the rate of the neo-tissue formation to be fully replaced with newly formed tissue. Moreover, the degradation by-products should not be toxic and should be mediated by the body's biological system. However, the desired scaffold's parameters can be tailored based on the material choice [1, 35]

A number of biodegradable natural and synthetic biomaterials including polymers have been developed for tissue engineering applications [1]. Amongst all the biodegradable polymers, PLGA or poly lactic-*co*-glycolic acid is considered as one of the most extensively studied and used biomaterials as a drug carrier and a scaffold material for tissue engineering applications. PLGA has received a tremendous amount of interest due to its biocompatibility, tunable biodegradability and mechanical properties as well as controlled and sustained release of growth factors; and most importantly it is an FDA approved polymer for certain applications [2, 3]. One considerable drawback about PLGA is that it lacks all the ligands required for cell attachments and proliferation, which can result in poor cell adaption to the matrix and thus, poor tissue formation [33]. Gelatin

is a remarkable natural biomaterial that also has been widely investigated as a promising implantable biomaterial for a number of tissue engineering applications. [34] The most intriguing properties that attract research interests are its cell/tissue compatibility, biodegradability, and functionality. In addition, gelatin inherits all the necessary arginine-glycineaspartic acid (RGD) sequences that allow for enhanced cell adhesion, and it is less immunogenic. A great deal of studies has focused on the development of composites biomaterials that combined gelatin and other materials, mainly syntactic polymers for achieving tissue engineering scaffolds that exhibit the biocompatibility of the natural polymers, and the tuned biodegradability and mechanical properties of the synthetic polymers for functional and integrative tissue regeneration. PLGA/gelatin composite was shown to support cellular attachment, proliferation, as well as to support the regeneration of a variety of tissues *In vivo* such as bone, skin, and ligament. The unique properties of PLGA/gelatin made it one of the favorable composite biomaterial for most researchers [4, 5, 25, 26].

PLGA is a linear copolymer that can be synthesized at different ratios between its constituent monomers, lactic (LA) and glycolic acid (GA) (Figure 2.1).

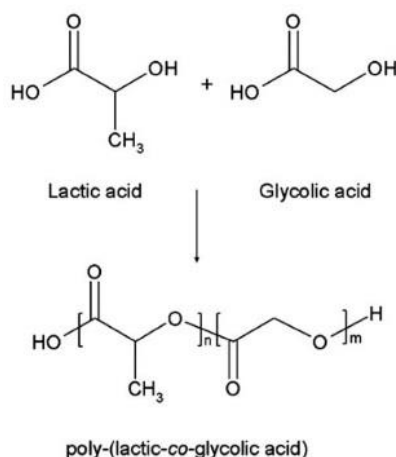


Figure 2.1 Chemical structure of poly(lactic-co-glycolic acid) and its monomers [6].

Depending on the ratio of lactide to glycolide used for the polymerization, different forms, degradation and mechanical properties of PLGA can be obtained, where the higher the lactic content to glycolic generally exhibits prolonged degradation rates, and higher mechanical integrity. These are usually identified in regard to the monomers' ratio used (*i.e.*, PLGA 85:15 identifies a copolymer consisted of 85% lactic acid and 15% glycolic acid) [6].

PLGA undergoes degradation by hydrolysis of its ester linkages, through bulk or surface erosion, in aqueous environments. Briefly, the degradation process can be described in four main steps: (i) **hydration**: water penetrates into the amorphous region, which disturbs the van der Waals forces and hydrogen bonds, resulting in a decrease in the glass transition temperature (T_g); (ii) **initial degradation**: cleavage of covalent bonds, with a decrease in the molecular weight; (iii) **constant degradation**: carboxylic end groups auto-catalyze the degradation process, resulting in loss in mass and integrity by massive cleavage of the backbone covalent bonds; (iv) **solubilization**: the fragments are further cleaved to molecules that are soluble in the aqueous environment [7]. As described previously [6], there are certain parameters that influence the degradation behavior of PLGA such as, (i) **molecular weight**: where PLGA with high MW (60 – 200 kDa) exhibits longer degradation rates; (ii) **the ratio between lactide acid to glycolide acid**: PLGA with higher content of LA are less hydrophilic and thus, absorb less water resulting in slow degradation rates, as a consequence of the presence of methyl side groups in poly-lactide acid making it more hydrophobic than poly-glycolide acid. (iii) **Stereochemistry**: during the fabrication process of PLGA a mixture of D and L lactic acid monomers are most commonly used, as the rate of water penetration is higher in amorphous D, L regions, leading to accelerated PLGA degradation; and (iv) **end-group functionalization**: polymers that are end-capped with esters generally demonstrate longer degradation half-lives [8, 9, 6]. One more important aspect that is strongly related to the

parameters influencing PLGA degradation is the shape of the device, depending on the water accessibility within it. In addition, the acidic surrounding medium can also play a role in accelerating the degradation process in PLGA due to the autocatalysis [6].

Another considerable property about PLGA is that it can be easily processed into a wide variety of different structures depending on the application needs through well-developed fabrication techniques. Some of the most extensively used fabrication techniques to process PLGA are (1) double emulsion solvent evaporation for the production of PLGA microspheres, and (2) uniaxial electrospinning technique for the production of uniaxial PLGA nanofibers, and (3) coaxial electrospinning technique for the production of PLGA coaxial electropun nanofibers.

2.1.1. Microsphere Fabrication Technique

The fabrication of microsphere scaffolds was first established in 1998 by Laurencin et al. Microspheres are fabricated using the single emulsion technique, briefly, a solution of organic PLGA in Dichloromethane (DCM) is generally added to an aqueous polyvinyl alcohol (PVA) surfactant (Figure 2.2). The mixture is let to stir under a certain speed inside of a chemical hood to allow the solvent to evaporate. The end product of this process is a pellet of solidified microspheres, which are collected, rinsed, freeze or air dried and sieved to the desired diameter size range.

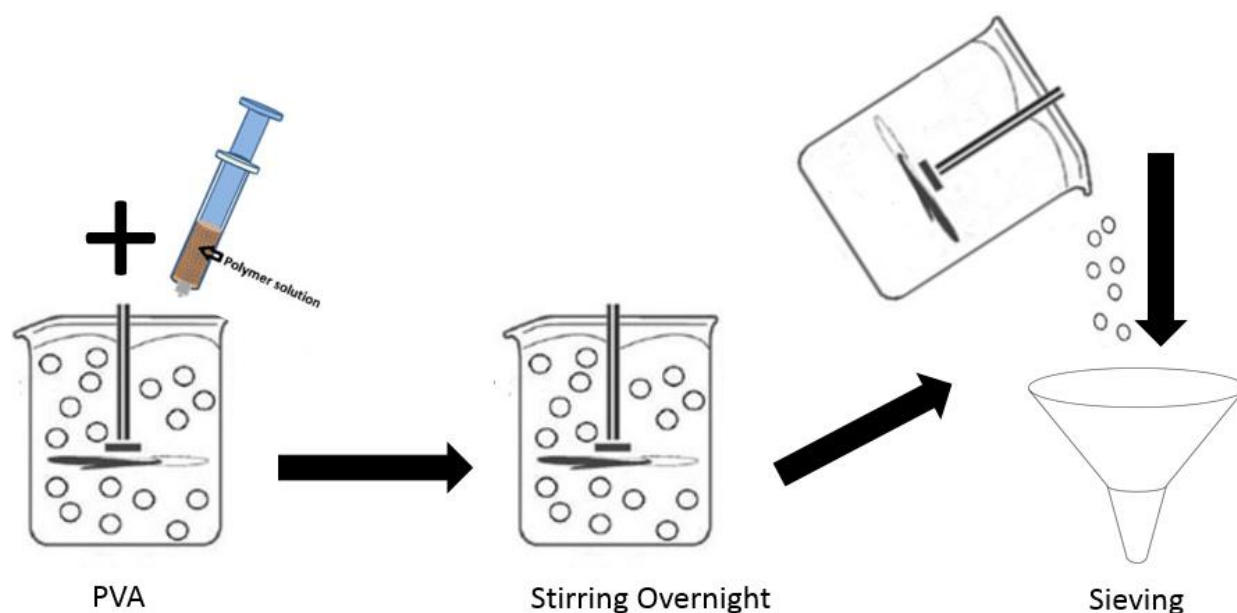


Figure 2.2 Fabrication process of PLGA Microsphere through the single water/oil emulsion technique.

To construct scaffolds, microspheres with the desired particle size distribution are poured into a mold, generally stainless-steel mold, then heated above the glass transition temperature of PLGA ($T_g \sim 58^\circ\text{C}$) until they are thermally fused into the desired three-dimensional shape and morphology [10,11]. The advantages of using PLGA to develop 3D sintered microsphere scaffolds with a porous interconnected structure for bone tissue engineering has been demonstrated. These scaffolds were shown to possess mechanical properties controllable pore size and pore volume that are relatively close to the native tissue ECM, which makes them ultimately ideal for bone regeneration [12, 13].

2.1.2. Uniaxial Electrospinning Technique:

Electrospinning is an easy and low-cost approach to fabricate fibrous matrices. Briefly, the polymer is dissolved in an organic solvent, generally Hexafluoro-2-propanol (HFIP) to make the

polymer solution. Polymer solution is then loaded in a capillary tube and confined by its surface tension, and the ejection of polymer solution is accomplished when it is exposed to an electric field such that the electrostatic repulsion overcomes the surface tension. During the process of electrospinning, the solvent evaporates when the solution-jet travels in air, leaving behind polymeric fibers which gets deposited on the collector [14–15]. Thus, continuous fibers are collected to form a non-woven fabric that mimics the fibrous network of native ECM, with fiber sizes similar to ECM fibrils [16, 17].

2.1.3. Coaxial Electrospinning Technique:

Coaxial electrospinning was mainly developed to overcome the burst release limitations associated the conventional methods of blending the growth factor directly with the polymer solution and uniaxially electrospin them [10]. This can be done by incorporating the growth factors coaxially in the core-shell of the polymeric nanofiber during electrospinning [11]. The main advantage of coaxial electrospinning over the uniaxial is that it generates core and sheath fibers by physical separation between the core and the sheath through the utilization of two electrospinning tips and two solutions (Figure 2.3) [12]. The core generally contains the growth factor solution and the sheath contains the polymeric solution. This nanofiber structure will allow for more of a spatial control over growth factors delivery and will hugely minimize any possibility of burst release when compared to the conventional uniaxial nanofiber [12]. Advantages of the coaxial electrospinning made it an area of a significant interest for many researches for more effective drug delivery and thus, tissue regeneration.

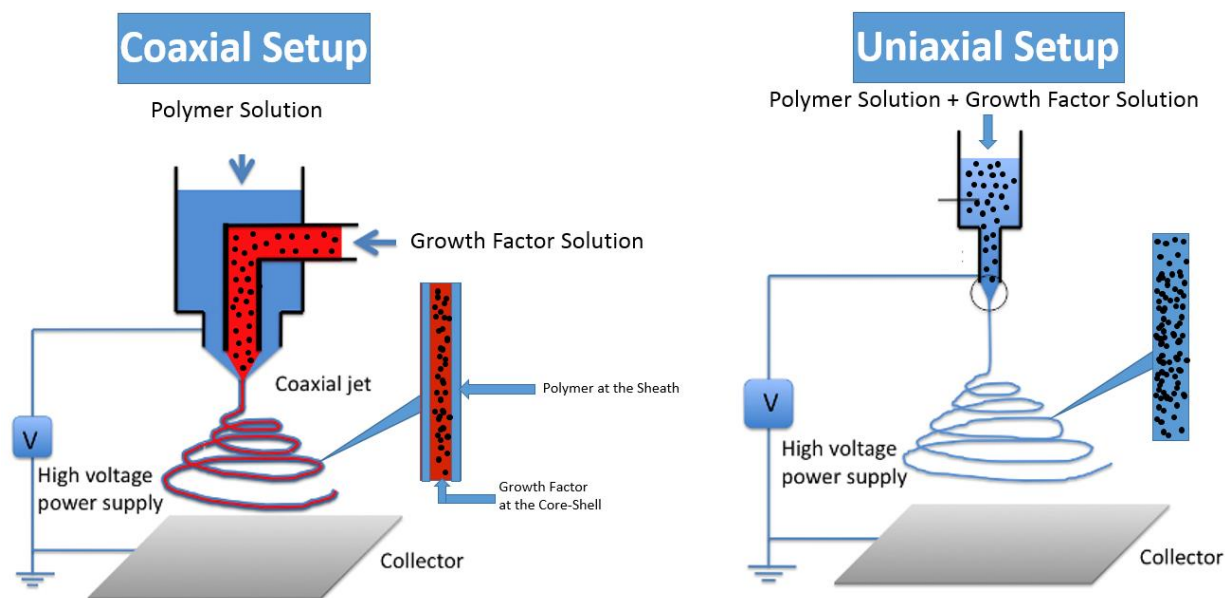


Figure 2.3 Schematic of coaxial electrospinning setup, and the conventional uniaxial electrospinning setup.

These artificial extracellular matrices were shown to possess mechanical properties, controllable pore size and nanofibers diameter that are relatively close to the native tissues, which render them ultimately ideal for tissue engineering applications. Thus, maintaining the mechanical, physical and morphological integrity of the scaffold for the appropriate timeframe is a key element for successful tissue regeneration [18 - 21].

In this aim, PLGA was mainly used as a scaffold biomaterial to fabricate the three different phases within integrated graft system and gelatin was introduced to serve as a drug carrier as well as to enhance the biocompatibility of the overall scaffold. Scaffold fabrication was either through electrospinning for the production of coaxial and uniaxial PLGA nanofibers, or through single emulsion technique for the production of PLGA microspheres. Post-fabrication, the three different phases were morphologically evaluated using SEM to examine the exterior surface and the overall morphology as well as to assist in the particle size analysis. TEM analysis have also been conduct in order to verify the core-shell in the coaxial nanofibers. In addition, *in vitro* degradation characteristics of both PLGA coaxial and uniaxial electrospun nanofibers and microsphere scaffolds were examined to evaluate the morphological and physical integrity, specifically weight loss, swelling rate, water uptake and pH changes over time. These characteristics were essential to observe in order to evaluate the capability of the three different phases to maintain their morphological integrity over time. This helped us examining their suitability for further analysis throughout the study.

2.2. Materials and Methods:

85:15 Poly(lactide-co-glycolide) (PLGA) (MW ~ 94,000 kDa) was purchased from (Absorbable Polymers, Birmingham, AL, USA), Hexafluoro-2-propanol (HFIP) was purchased from (Acros Organics, USA), Gelatin Type A from Pork (Porcine skin) was purchased from (MP Biomedical, OH, USA), Microbial Transglutaminase (mTG) was Purchased from (Ajinomoto, Japan), Dulbecco's Phosphate-Buffered Saline (PBS) of pH 7.4 wash purchased from Gibco (Grand Island, NY), Dichloromethane (DCM) was purchased from (Fisher Scientific, USA).

2.2.1. Fabrication of PLGA-Gelatin Coaxial Electrospun Nanofibers Scaffolds

PLGA (85:15) granules were dissolved in HFIP at 16 % wt and stirred overnight at room temperature to prepare the (shell solution) of nanofibers. To prepare the core solution, gelatin powder type A was dissolved in HFIP at 4% wt and stirred overnight at room temperature. An electrospinning pump (NE 300 SYRINGE pumps, USA) was used in order to fabricate the coaxial PLGA-Gelatin nanofibers. The setting to prepare the coaxial scaffolds consisted of two coaxial syringe pumps with different flow rates. In this study, the PLGA solution was used to form the outer shell and the gelatin solution was used to form the inner core. These two solutions were loaded into two separate 10 ml syringes and connected to the coaxial needles, a 16 G (ID = 1.6 mm) outer needle and a 22 G (ID = 0.7 mm) inner needle, respectively, and then concentrically placed. The electrospinning parameters were as follows: (applied voltage: 10 kV; 1.5 mL/h for the sheath flow rate and 0.75 mL/h for the core flow rate). The tip of the needle was placed 10 cm away from the collector. The electrospinning process lasted for 1.5 h. Coaxial electrospun nanofibers were peeled from the collector and stored under vacuumed desiccator until use.

2.2.2. Fabrication of PLGA Uniaxial Electrospun Nanofibers Scaffolds

PLGA (85:18) granules were dissolved at 16% wt in HFIP with stirring to form clear, homogeneous, and viscous solution. PLGA solution was loaded into 10 ml plastic syringe and electrospun at flow rate of 0.75 mL/h through a 20-gauge blunt needle with the electrospinning pump (NE 300 SYRINGE pumps, USA) at an applied voltage of 10 kv. The tip of the needle was placed 10 cm away from the collector. The electrospinning process lasted for 3.5 h. Uniaxial electrospun nanofibers were peeled from the collector and stored under vacuumed desiccator until use.

2.2.3. Fabrication of PLGA Microspheres

Single emulsion solvent evaporation technique was used to fabricate PLGA microspheres. PLGA granules were dissolved at 12.5% wt in Dichloromethane (DCM) in glass vials. Vials were vortexed for 1 h at a speed of 550 RPM until clear, homogeneous, and viscous solution was obtained. Next, PLGA solution was added via a thin stream into 1% PVA solution in a 1000 ml beaker and it was let to stir at (300 RPM) overnight to allow the solvent to evaporate. After that, microspheres were collected, filtered, air dried and then they were stored in -20 °C for 24 h to freeze any residual water particle inside of the microspheres. Next, microspheres were freeze dried for 48 h and were then sieved to obtain the desired particle size range 300-600 µm.

2.2.4. Fabrication of Gelatin-mTG Hydrogel

Gelatin gel formation was initiated by mTG addition. For hydrogel preparation, 3% wt gelatin powder type A was dissolved in preheated phosphate-buffered saline (PBS) at 50 °C and it was let to stir on a stirrer plate for 15 minutes at 500 RPM to completely dissolve the powder. The mTG

solution was prepared by dissolving 10% wt mTG in preheated PBS at 50 °C, then it was let to stir on a stirrer plate for 15 minutes at 500 RPM. As soon as both gelatin and mTG completely dissolved in PBS, the temperature of the stirrer plate was adjusted to 37 °C and they were let to stir for another 15 minutes to allow for the temperature drop. Next, to initiate the crosslinking reaction between gelatin and mTG for the hydrogel preparation, mTG solution was mixed with the 3% wt gelatin solution at a ratio of 1:11.5 under stirrer speed of 500 RPM at 37 °C. The mixture was let to stir for 5 minutes until a semi-viscus solution is fabricated and ready to be injected.

2.2.5. Fabrication of PLGA-Gelatin-mTG Microsphere Scaffolds

To fabricate the three-dimensional scaffolds and incorporate it with gelatin-mTG hydrogel, PLGA microspheres were poured into a 10 mm x 10 mm stainless steel mold and heated for 90°C for 90 minutes. These parameters allowed the microspheres to fuse together forming the 3D scaffolds. After 90 minutes, the stainless-steel mold was removed from the oven and allowed to cool to room temperature for 2 hours. Next, scaffolds were removed and the semi-viscus gelatin-mTG hydrogel was injected inside of the microsphere scaffold using an insulin syringe until all pores were filled and it was allowed to gel at 37 °C.

2.2.6. Scanning Electron Microscopy (SEM)

Both electrospun nanofibers scaffolds, and microsphere scaffolds were morphologically evaluated under scanning electron microscopy after fabrication, and over the 8 weeks period of time during the degradation study to evaluate the morphological changes over time. Samples were assessed using FEI Nova NanoSEM 450 (FEI Ltd., Tokyo, Japan) at a working distance of 5 mm and an acceleration voltage of 18 kV. Scaffolds were mounted on 15 mm stubs and were gold sputter

coated using (Polaron E5100) for 3 minutes to eliminate surface charging. Finally, the coated samples were loaded into the SEM and high magnification images of each experimental group were taken and analyzed.

2.2.7. Particle Size Distribution and Pore Size Analysis

Three different images from every samples were obtained and analyzed for particle size distribution and pore using Image J software. Briefly, 200 particles were selected from every image of the three images of the single sample. Data from the three different images of the single sample were used to determine the size and average size distribution as well as the pore size for every scaffold type. The same analysis was carried out on both electrospun nanofibers scaffolds.

2.2.8. Transmission Electron Microscopy (TEM)

TEM analysis were conducted on both the Coaxial and the uniaxial electrospun nanofibers to confirm the coaxial structure. Observations were prepared by directly depositing the spun fibers onto copper grids of 300 mesh. The samples for TEM images were analyzed using (FEI Tecnai 12 G2 Spirit BioTWIN) transmission electron microscope and all images were recorded in GATAN ESW 500 camera.

2.2.9. Degradation of PLGA Coaxial, Uniaxial Electrospun Nanofibers Scaffolds and Sintered Microsphere Scaffolds

An 8 weeks' degradation study was conducted on the coaxial and the uniaxial elctrospun nanofibers, as well as PLGA-Gelatin-mTG and PLGA-Gelatin-mTG Free microsphere scaffolds. However, both uniaxial electrospun nanofibers and PLGA-Gelatin-mTG Free served as controls. Briefly, the initial weights of all samples were recorded. Next, uniaxial and the coaxial elctrospun

nanofibers groups were cut into (1 cm X 1 cm) squares and placed individually in the wells of 24-well plates with the addition of 2 ml of PBS per well. PLGA-Gelatin-mTG and PLGA-Gelatin-mTG Free microsphere scaffolds were also placed individually in the wells of 24-well plates and 2 ml of PBS was added per well with an N=3 per time point for every group. PBS was completely collected for pH measurements and replaced with fresh PBS every three days from all groups throughout the 8 weeks. Three samples from every groups were harvested every week to assess for weight loss, swelling rate and water uptake analysis. For weight loss analysis, the harvested samples were air dried, and then stored at – 20 for 24 h. Samples were then freeze dried for 48 h to insure complete removal of water. The lyophilized scaffolds were weighed and the change of scaffold mass was recorded as a percentage of mass loss using the following formula:

$$\text{Weight Loss Rate} = \frac{W_i - W_d}{W_i} \times 100$$

Where W_i is the initial weight, and W_d is the dry weight.

For swelling rate and water uptake analysis, samples were harvested, and the wet weight was recorded directly. Next, samples were air dried, and then stored at – 20 °C for 24 h. Next samples were freeze dried for 48 h to insure complete removal of water. The Swelling rate and water uptake analysis were conducted using the following formula:

$$\text{Swelling Rate} = \frac{W_w - W_d}{W_d} \times 100$$

Where W_w is the wet weight, and W_d is the dry weight.

Weight loss, swelling rates, water uptake and pH measurements were plotted against time in weeks.

2.2.10. Statistical Analysis

Data are presented as mean \pm standard deviation (SD). All statistical analyses were performed using the Statistical Software Prism GraphPad (Version 5) using two-way Analysis of Variance (ANOVA) with a Tukey test for Post Hoc parameter comparisons. Statistical significance was set at $p < 0.05$.

2.3. Results

2.3.1. PLGA-Gelatin Coaxial and PLGA Uniaxial Electrospun Nanofibers Scaffolds

2.3.1.1. Scanning Electron Microscopy (SEM)

Both PLGA-Gelatin coaxial nanofibers and PLGA uniaxial nanofibers have been successfully fabricated. Electrospinning PLGA-Gelatin resulted in a 9 cm X 9 cm fibrous mat with a thickness of $\sim 350 - 400 \mu\text{m}$, whereas electrospinning PLGA alone resulted in ununiformed deposition of nanofibers on the collector with less mat thickness when electrospun for the same duration of $\sim 80 \mu\text{m}$ (Figure 2.4). Size distribution analysis on Image J revealed that the nanofiber size distribution in both the coaxial and the uniaxial electrospun mats range between 400 nm - 1100 μm with an average size diameter of $800 \pm 155 \text{ nm}$ in the coaxial case and $752 \pm 175 \text{ nm}$ in the uniaxial case (Figure 2.5, Figure 2.6). PLGA coaxial and uniaxial electrospun nanofiber scaffolds had pore sizes of $50 \pm 41 \mu\text{m}$ and $53 \pm 32 \mu\text{m}$ respectively. SEM images demonstrate the smooth surface of the nanofibers in both groups. In addition, both coaxial and uniaxial seem to mimic the native tissue ECM morphologically with high porosity throughout. The 8 weeks morphology analysis showed

a slight change in morphology compared to the initial morphology in both groups (Figure 2.7, Figure 2.8). However, after 5 weeks of incubation at 37 °C the coaxial group started swelling significantly and showed change in morphology when compared to the uniaxial group. The change in morphology was noticed due to the small pores created at the surface of the nanofibers.

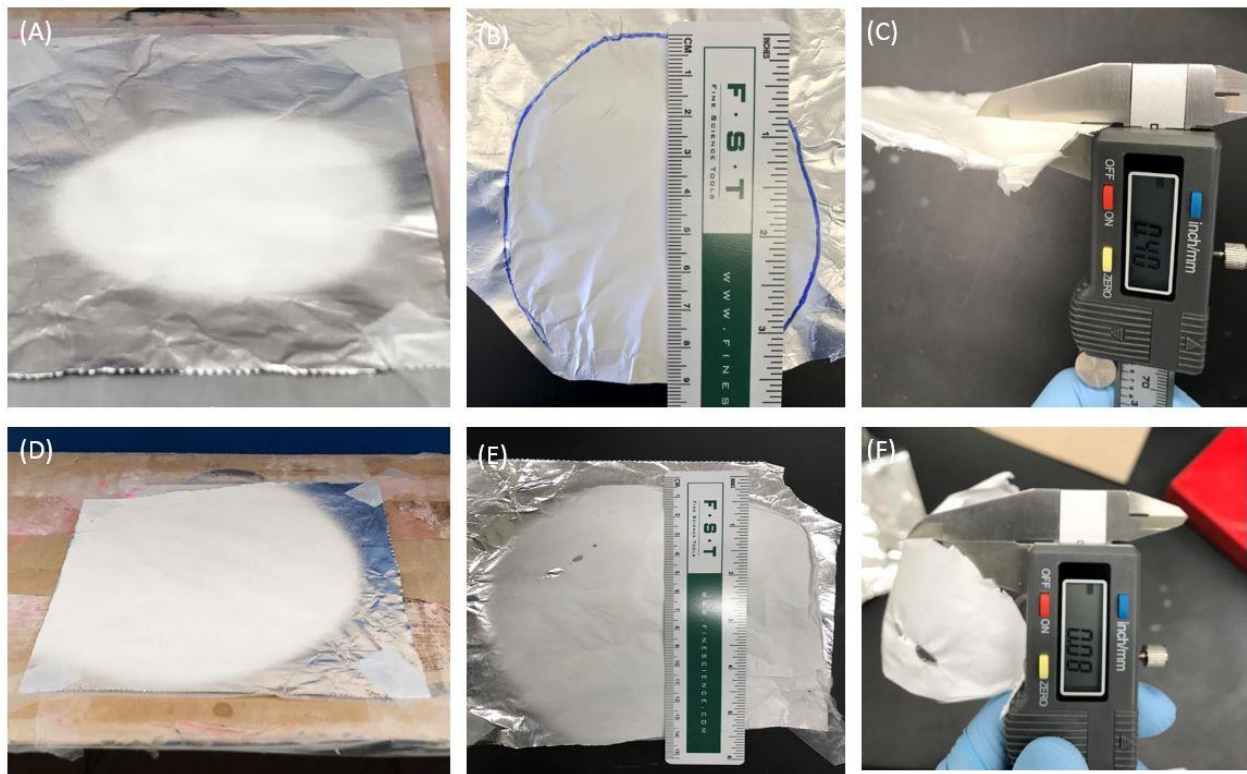


Figure 2.4 PLGA-Gelatin coaxial electrospun nanofiber mat (A) a uniform deposition during electrospinning (B) the resultant 9 x 9 cm coaxial electrospun mat, and (C) coaxial electrospun mat thickness (400 μm); and PLGA uniaxial electrospun nanofiber mat (D), uninform deposition of nanofibers during electrospinning that can be noticed from the bigger mat area when compared to the coaxial group (E), the resultant un-uniformly deposited mat, and (F) uniaxial electrospun mat thickness of ~ 80 μm when electrospun for 1.5h, which is the same duration used for electrospinning PLGA-Gelatin that results in a mat with a thickness of ~ 400 μm.

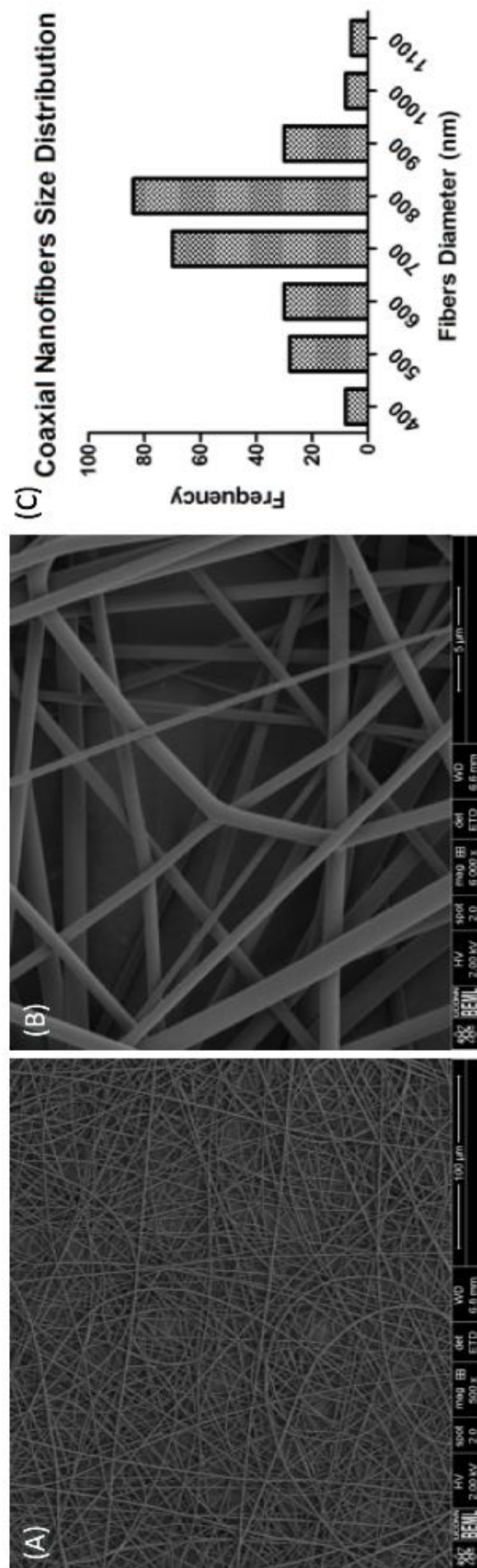


Figure 2.5 SEM images of PLGA-Gelatin Coaxial electrospun nanofibers showing (A) overall morphology of the electrospun (Scale bar 100 μm), (B) morphology of nanofibers showing the smooth fibers surface (Scale bar 5 μm), and (C) PLGA-Gelatin Coaxial electrospun nanofibers size distribution (400 nm – 1100 nm).

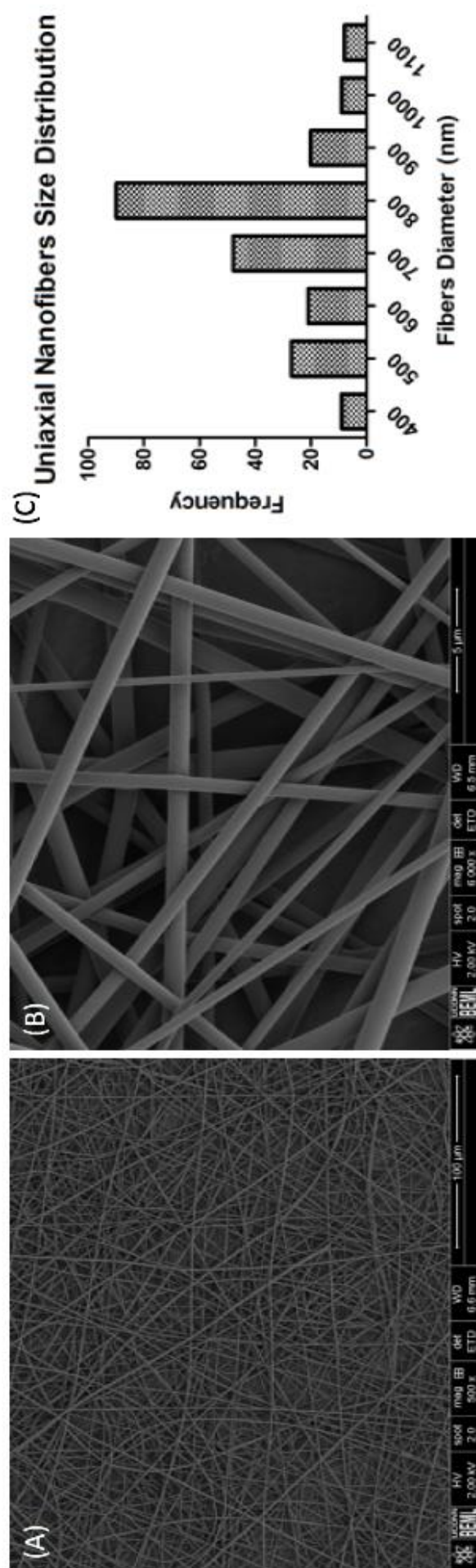
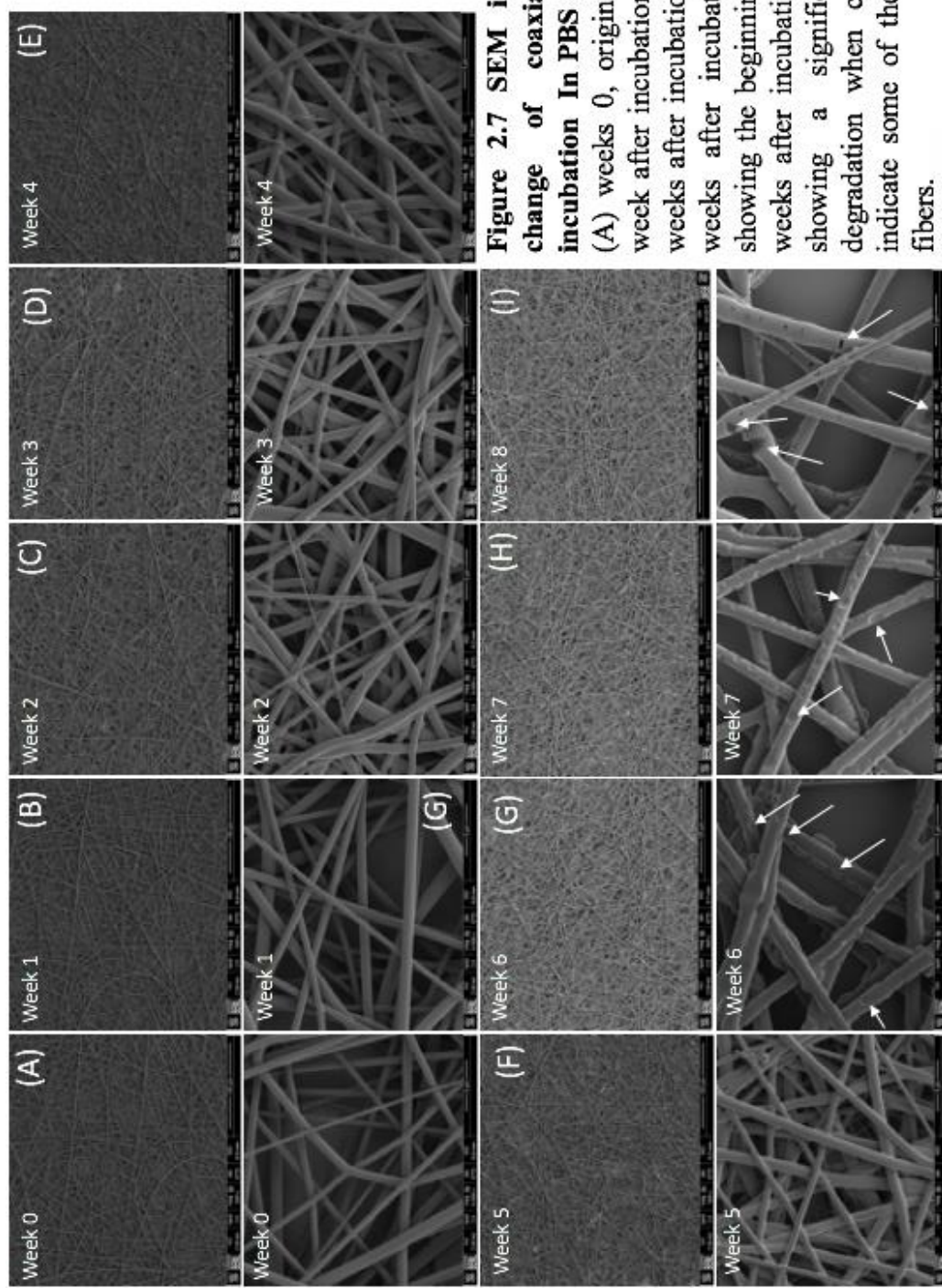
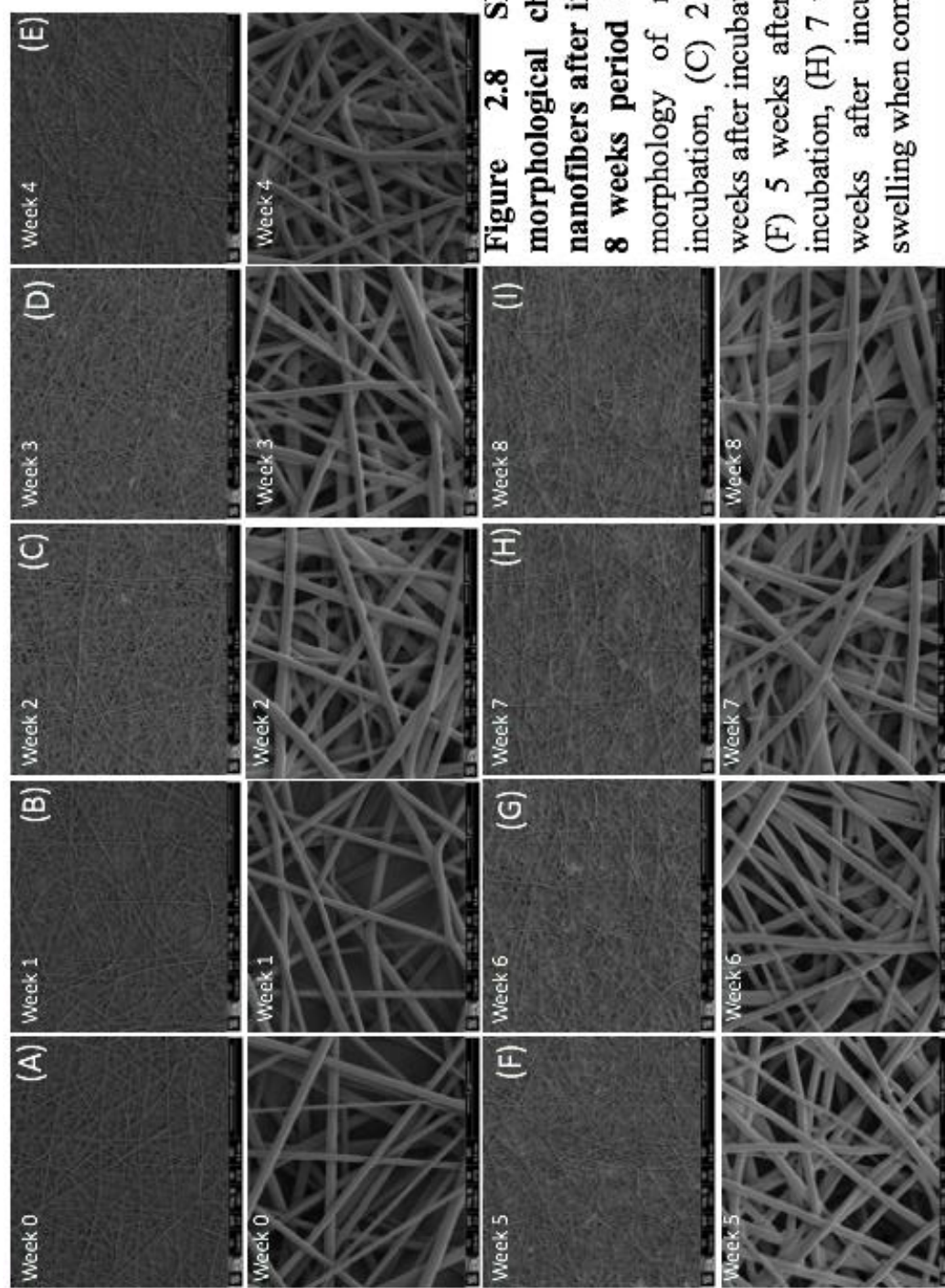


Figure 2.6 SEM images of PLGA Uniaxial electrospun nanofibers showing (A) overall morphology of the electrospun (Scale bar 100 μm), (B) morphology of nanofibers showing the smooth fibers surface (Scale bar 5 μm), and (C) PLGA Uniaxial electrospun nanofibers size distribution (100 nm – 1100 nm).





2.3.1.2. Transmission Electron Microscopy (TEM)

The interior structure of the composite fibers was investigated by TEM to confirm the presence of the coaxial structure (Figure 2.9). As expected, the core-shell nanofibers had a clear core-sheath structure with a core-sheath of ~ 781 nm, a fiber diameter of 1000 nm and a sheath thickness of 219 nm, while the uniaxial electrospun nanofiber, which served as control; did not have similar interior morphology.

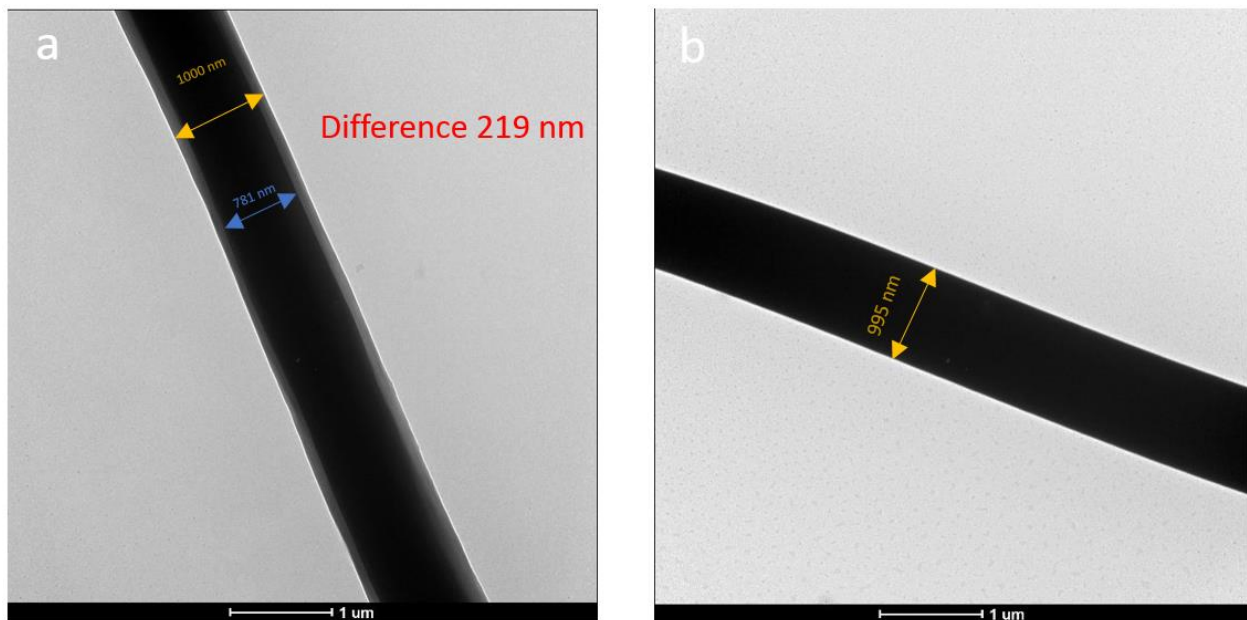


Figure 2.9. TEM images. (a) PLGA-Gelatin Coaxial nanofiber with a core-sheath of ~ 781 nm, a fiber diameter of 1000 nm and a sheath thickness of 219 nm, and (b) Uniaxial nanofiber.

2.3.2. PLGA-Gelatin-mTG and PLGA-Gelatin-mTG Free Sintered Microspheres

Scaffolds

2.3.2.1. Scanning Electron Microscopy (SEM)

PLGA Microspheres were successfully fabricated and sintered forming a highly porous and interconnected 3D scaffold with pore size of $175 \pm 87 \mu\text{m}$ and average microsphere size diameter of $(460 \pm 95 \mu\text{m})$. Sintered PLGA microsphere scaffolds incorporated with Gelatin-mTG and sintered PLGA Gelatin-mTG Free scaffolds, which served as controls were visualized under SEM for particle size and morphological analysis. SEM images showed the smooth surface and high porosity throughout the 3D structure in both groups (Figure 2.10, Figure 2.11). Particle size analysis revealed that the micro-particle size distribution was within the target diameter range of 300 - 600 μm . The incorporated gelatin in the PLGA-Gelatin-mTG group was also observed filling the porosity within the microsphere structure, which indicates the complete penetration of the hydrogel within the scaffold. Over the 8 weeks, microspheres in both groups did not show a significant change in surface morphology (Figure 2.12, Figure 2.13). Only a slight increase in surface erosion was gradually observed from the SEM images over time in both groups. However, scaffolds in both groups started to loss structural integrity and brake down over the 8 weeks, which was evidenced by the appearance of cracks between the adjacent microspheres. Cracks between the adjacent microspheres started to appear starting from the 3rd week in the PLGA-Gelatin-mTG free group, and from the 5th week in the PLGA-Gelatin-mTG group.

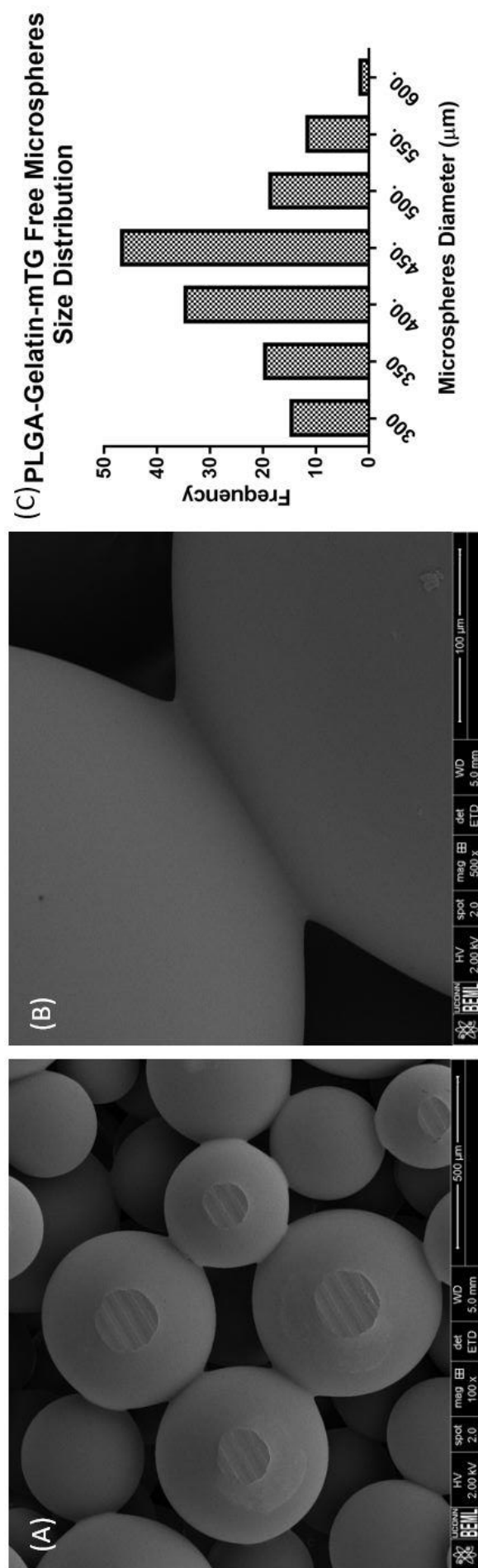


Figure 2.10 SEM images of PLGA-Gelatin- mTG Free sintered microspheres showing (A) overall morphology of the sintered microspheres (Scale bar 500 μm), (B) high magnification image of the interconnectivity between microspheres (Scale bar 100 μm), and (C) PLGA-mTG Free sintered microspheres (300 μm– 600 μm).

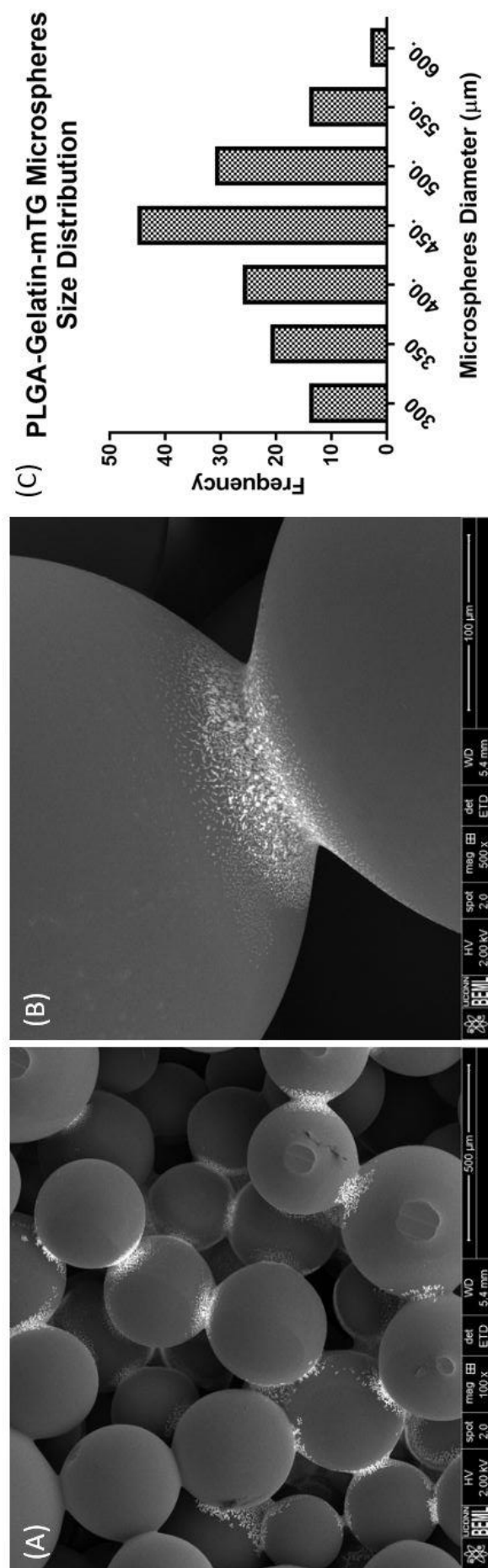


Figure 2.11 SEM images of PLGA-Gelatin- mTG sintered microspheres showing (A) overall morphology of the sintered microspheres (Scale bar 500 μm), (B) high magnification image of the interconnectivity between microspheres (Scale bar 100 μm), and (C) PLGA-mTG sintered microspheres (300 μm – 600 μm).

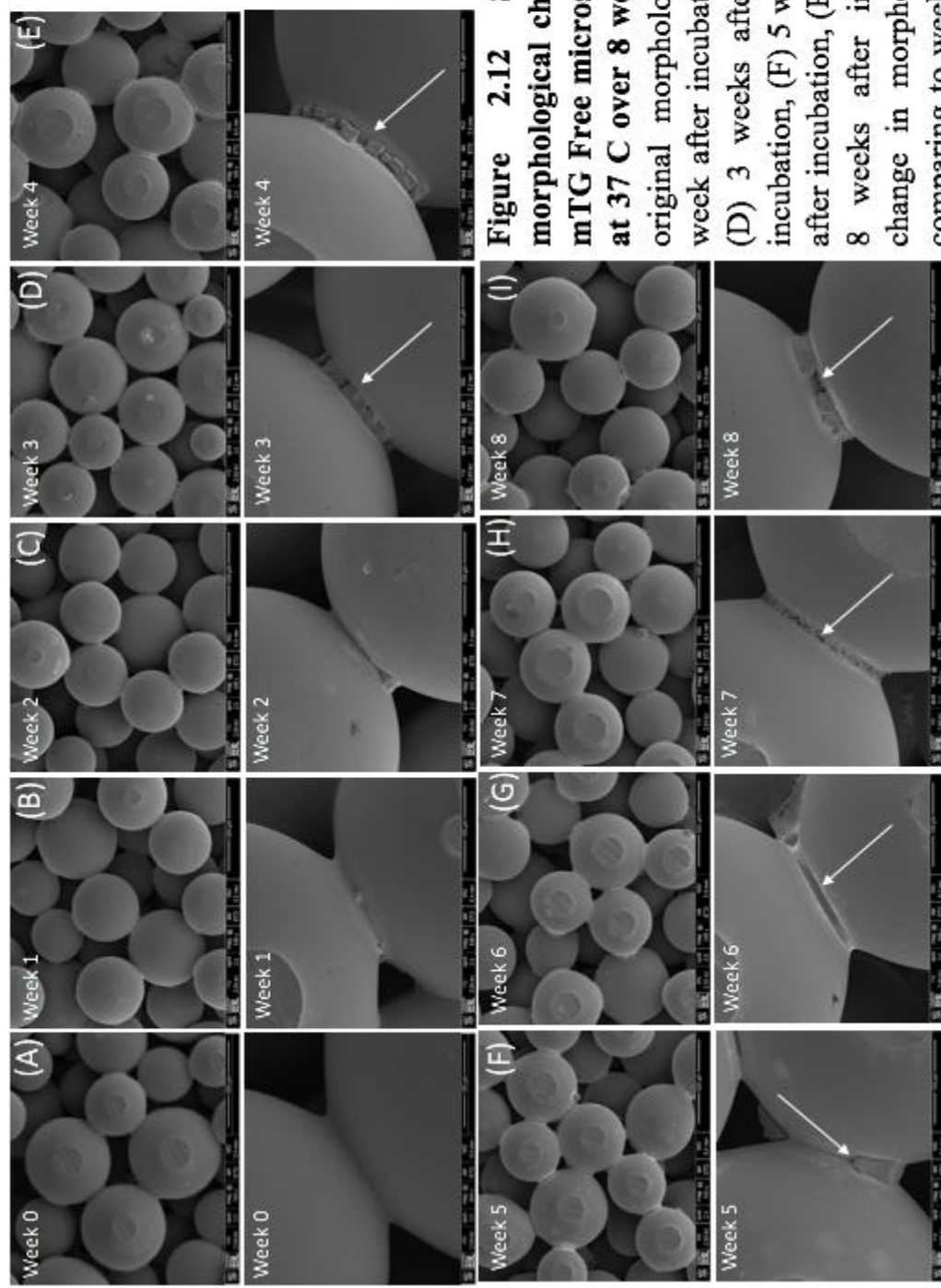


Figure 2.12 SEM images showing the morphological change of sintered PLGA-Gelatin-mTG Free microspheres after incubation in PBS at 37°C over 8 weeks period of time. (A) weeks 0, original morphology of sintered microspheres, (B) 1 week after incubation, (C) 2 weeks after incubation, (D) 3 weeks after incubation, (E) 4 weeks after incubation, (F) 5 weeks after incubation, (G) 6 weeks after incubation, (H) 7 weeks after incubation, and (I) 8 weeks after incubation showing a significant change in morphology at the interconnected pore comparing to week 0. White arrows indicates cracks between the adjacent microspheres.

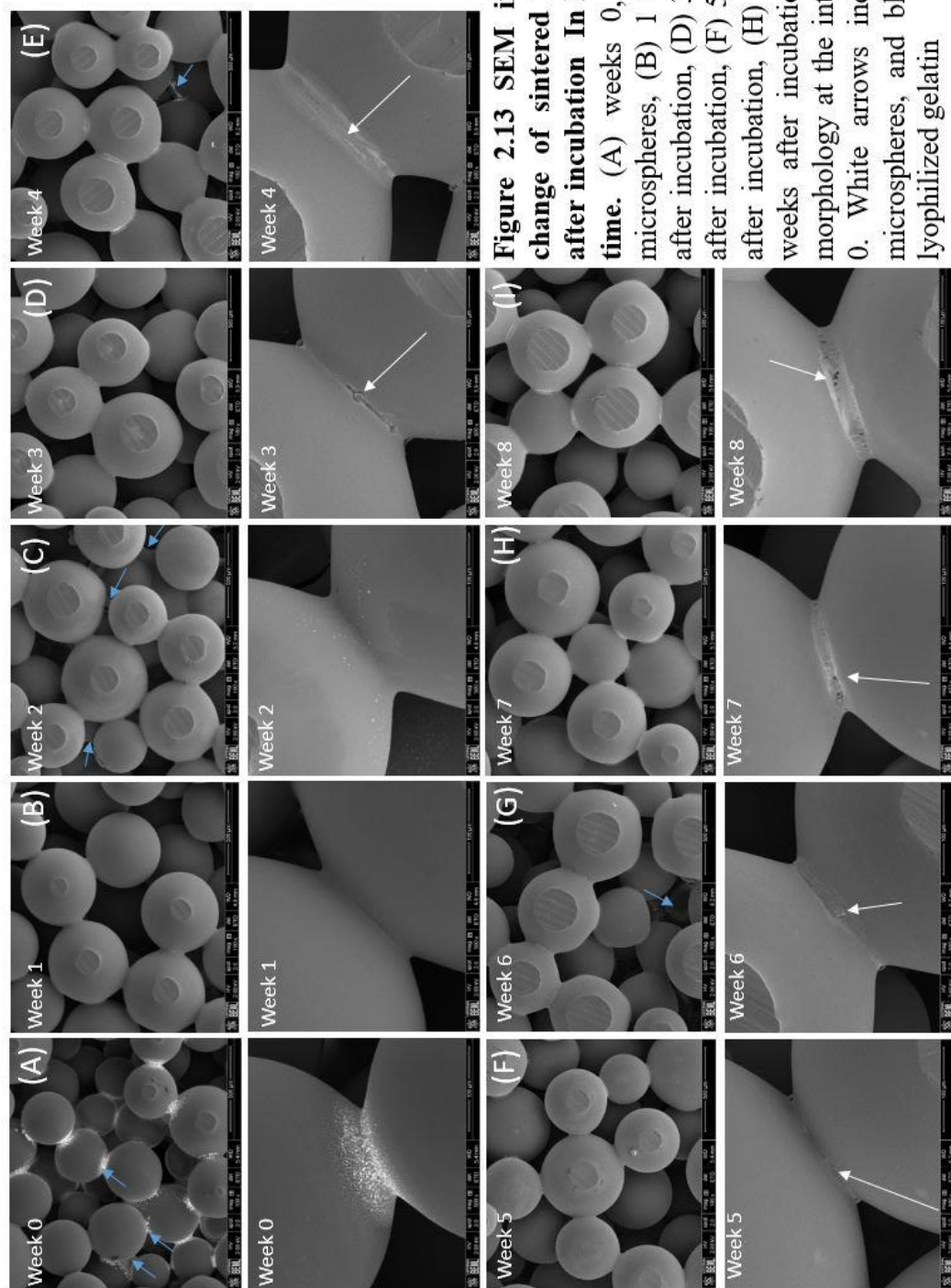


Figure 2.13 SEM images showing the morphological change of sintered PLGA-Gelatin-mTG microspheres after incubation In PBS at 37 C over 8 weeks period of time. (A) weeks 0, original morphology of sintered microspheres, (B) 1 week after incubation, (C) 2 weeks after incubation, (D) 3 weeks after incubation, (E) 4 weeks after incubation, (F) 5 weeks after incubation, (G) 6 weeks after incubation, (H) 7 weeks after incubation, and (I) 8 weeks after incubation showing a significant change in morphology at the interconnected pore comparing to week 0. White arrows indicate cracks between the adjacent microspheres, and blue arrows indicate presence of the lyophilized gelatin

2.3.3. PLGA Coaxial-Gelatin and PLGA Uniaxial Electrospun Nanofibers Scaffolds

Degradation Behavior

A comprehensive degradation study on PLGA-Coaxial and Uniaxial (control) nanofibers was carried out. Weight loss, swelling rates and pH change of all scaffolds were evaluated over 8 weeks period of time including the controls after incubation in PBS at 37°C.

2.3.3.1. Weight loss: PLGA-Gelatin Coaxial nanofibers showed significant increase in weight loss over time comparing to PLGA Uniaxial Nanofibers (Figure 2.14). Initially, PLGA-Gelatin Coaxial group expressed higher weight loss comparing to the other group at weeks 1, 2, 3 and 4; but no significant difference was noted. The Coaxial group started significantly losing weight at week four to the end of the experiment. This indicates that most of the PLGA covering the outer shell of the coaxial structure have severely degraded over time (Figure 2.8). This curve indicates that the structure is stable for the first 4 weeks, and then it starts to lose its stability when it rapidly starts degrading starting at week 5.

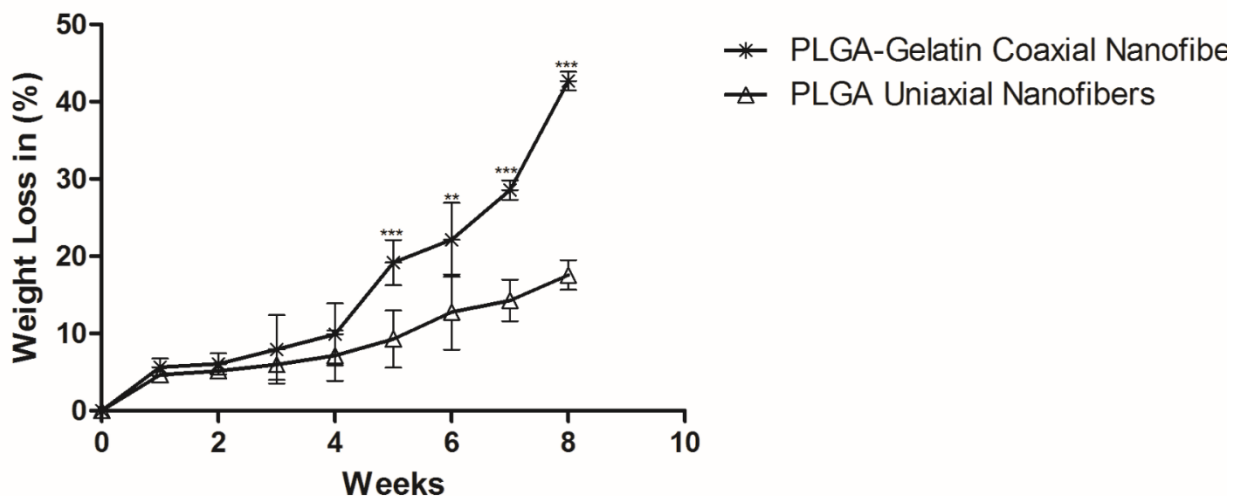


Figure 2.14 Weight loss of PLGA-Gelatin coaxial nanofibers and PLGA uniaxial nanofibers curve over 8 weeks after incubation in PBS at 37 °C.

2.3.3.2.Swelling: PLGA-Gelatin coaxial nanofibers showed significant increase in swelling rate over time comparing to PLGA Uniaxial Nanofibers (Figure 2.15). Even though, PLGA-Gelatin Coaxial group expressed higher weight loss comparing to the other group at weeks 1, 2, 3 and 4; no significant difference was noted. Due to the sever degradation taking place to the outer shell structure at week 5, water started to rapidly diffuse to the core structure causing a significant increase in swelling rate over time in the PLGA-Gelatin coaxial group comparing to the other group. These findings indicate that the structure is stable over the 8 weeks with more stability from week 1 – 4.

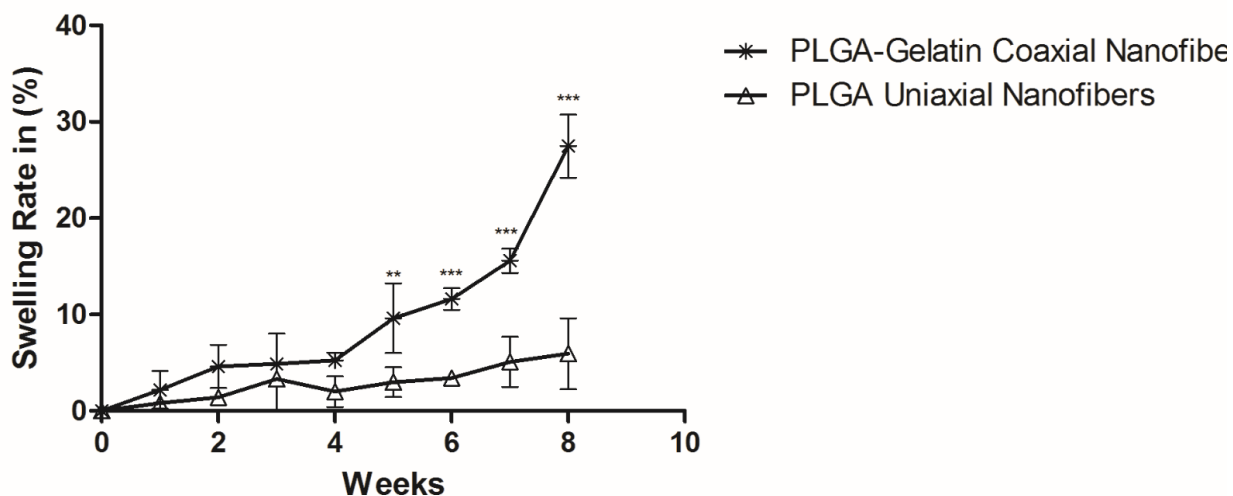


Figure 2.15 Swelling Rate of PLGA-Gelatin coaxial nanofibers and PLGA uniaxial nanofibers curve over 8 weeks after incubation in PBS at 37 °C.

2.3.3.3.pH change: The pH curve clearly indicates the difference in the medium acidity between the groups over time (Figure 2.16). PLGA-Gelatin coaxial Nanofiber showed a severe drop in pH over time comparing to the other group. The drop in the pH indicates how the coaxial structure accelerates the degradation rate of the nanofibers, by allowing water to rapidly diffuse to the core structure causing the inner portion of PLGA shell to degrade too. Even though the pH drop in the PLGA-Gelatin coaxial group was severe compared to the other group, it was still within the neutral range ~ 6.9.

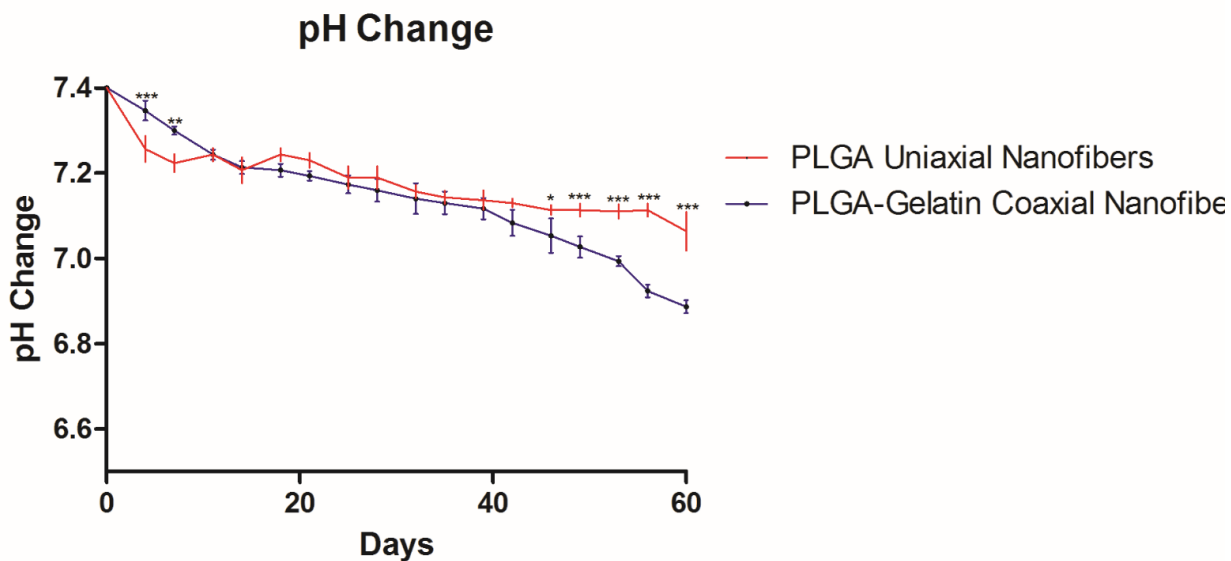


Figure 2.16 pH change of PLGA-Gelatin coaxial nanofibers and PLGA uniaxial nanofibers curve over 8 weeks after incubation in PBS at 37 °C.

2.3.4. PLGA-Gelatin-mTG and PLGA-Gelatin-mTG Free Sintered Microsphere Scaffolds

Degradation Behaviors

A comprehensive degradation study on PLGA-Gelatin-mTG and PLGA-Gelatin-mTG Free (control) scaffolds was carried out. Weight loss, water uptake rates and pH change of all scaffolds were evaluated over 8 weeks period of time including the controls after incubation in PBS at 37C.

2.3.4.1. Weight loss: PLGA-Gelatin-mTG Free scaffolds showed higher weight loss over after 8 weeks compared to PLGA-Gelatin-mTG scaffolds (Figure 2.17). Both scaffolds expressed almost similar weight loss rates in the first 6 weeks. PLGA-Gelatin-mTG Free started to rapidly loss weight after week 7 compared to the other group. Weight loss was significantly higher in PLGA-Gelatin-mTG Free compared to PLGA-Gelatin-mTG after 8 weeks of incubation at 37 C which indicates that water diffusion is restricted from penetration towards the core of the scaffold in the PLGA-Gelatin-mTG group due to the incorporation of the Gelatin-mTG hydrogel within the scaffold.

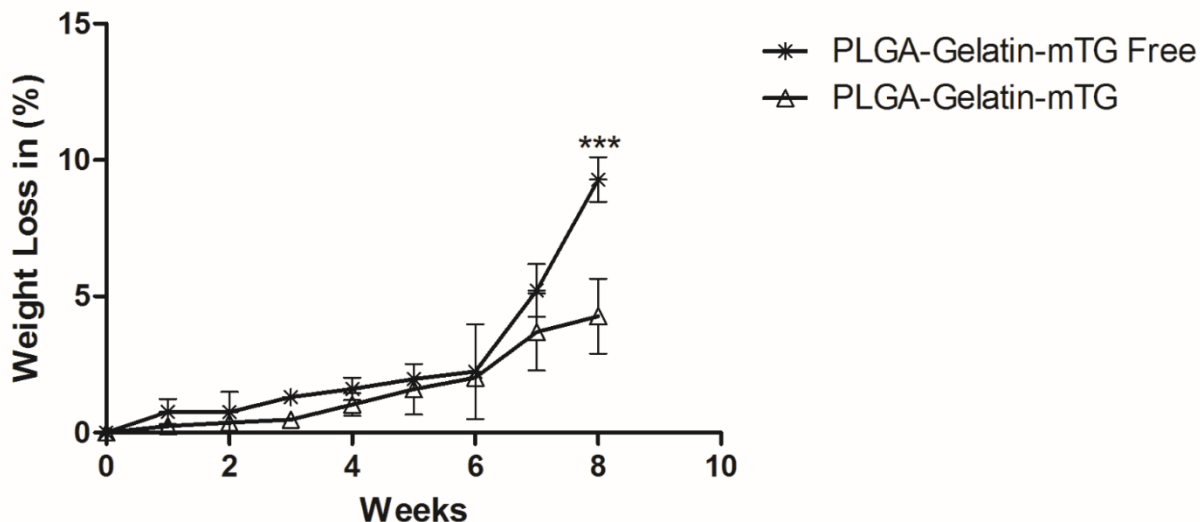


Figure 2.17 Weight loss of PLGA-Gelatin-mTG microsphere scaffold and PLGA-Gelatin-mTG Free microsphere scaffold curve over 8 weeks after incubation in PBS at 37 °C.

2.3.4.2. Water uptake: Water uptake in PLGA-Gelatin-mTG scaffolds was higher compared to the other group starting from the second week of the experiment (Figure 2.18). In the first four weeks, water uptake was almost similar between the groups and no significant differences was noticed. After week 4, water uptake started to rapidly increase in the PLGA-mTG group comparing to the other group. At week 8, both groups had similar water uptake rates, which indicate the complete degradation of gelatin within the PLGA microsphere scaffold; which in turns decreased the water uptake rate in the PLGA-Gelatin-mTG group and brought both group to the same level of water uptake.

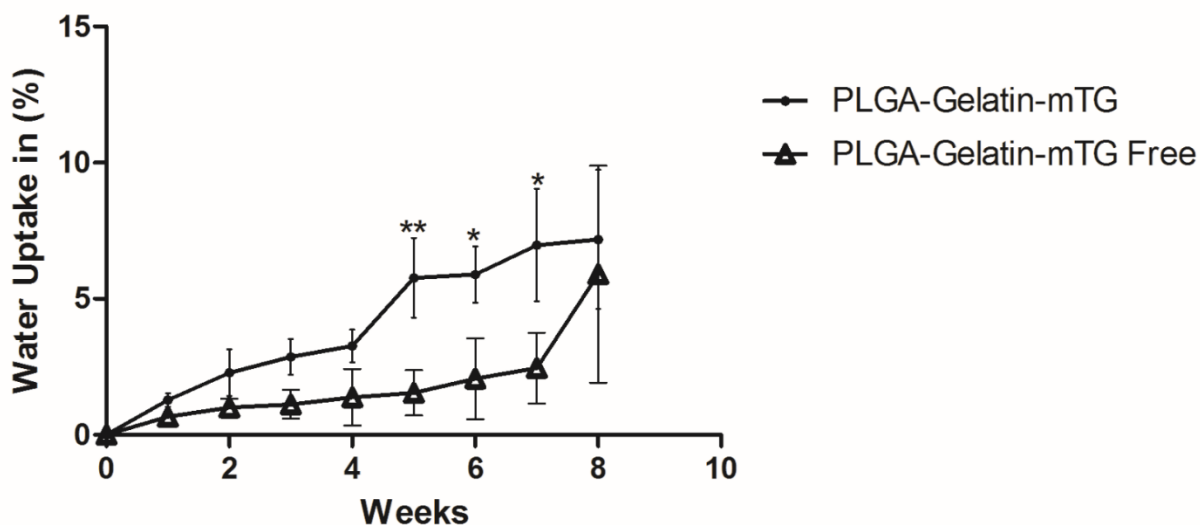


Figure 2.18 Water uptake of PLGA-Gelatin-mTG microsphere scaffold and PLGA-Gelatin-mTG Free microsphere scaffold curve over 8 weeks after incubation in PBS at 37 °C.

2.3.4.3.pH change: pH change behaviors was significantly different between the groups over the 8 weeks (Figure 2.19). PLGA-Gelatin-mTG group had a lower pH drop over time comparing to the other group. This indicates that the embedded hydrogel within the substrate is restricting water diffusion to the core of the scaffold, which in turn causes the pH to slowly drop down due to the minimal degradation of the scaffold taking place at the core of the scaffold, which in turns resulted in minimal acidic degradation byproducts releasing to the surrounding medium. Even though large amount of water was restricted from penetrating to the core of the scaffold, water still could penetrate easily through the pores within the hydrogel based on the water uptake analysis; which would not negatively affect cells performance.

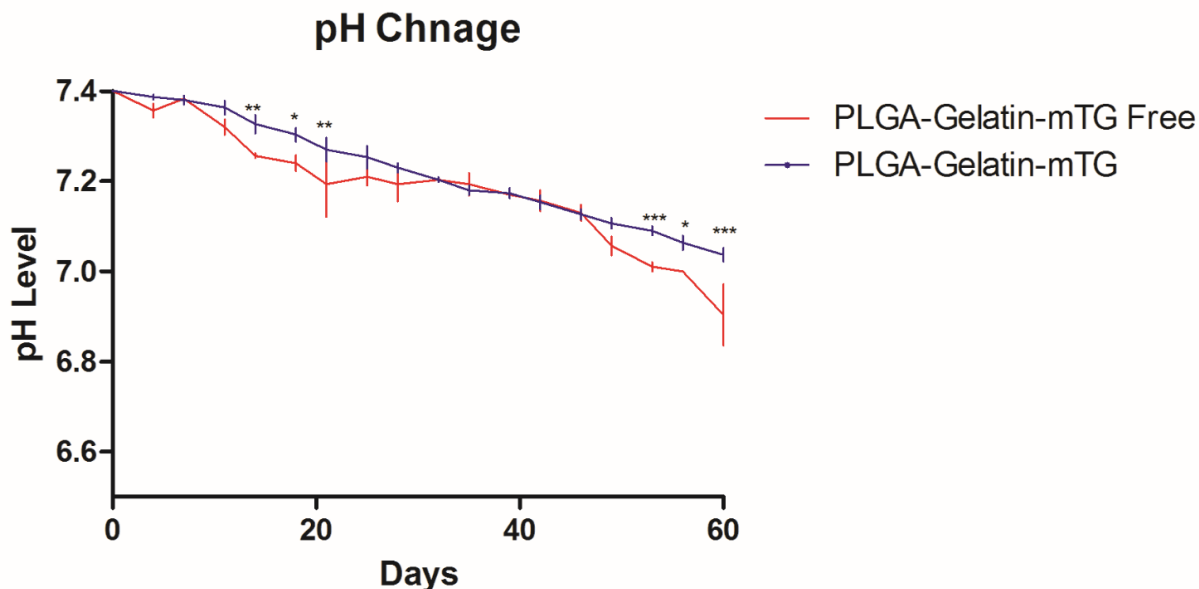


Figure 2.19 pH change of PLGA-Gelatin-mTG microsphere scaffold and PLGA-Gelatin-mTG Free microsphere scaffold curve over 8 weeks after incubation in PBS at 37 °C.

2.4. Discussion:

Poly(lactide-co-glycolide) (PLGA) is one of the most extensively investigated biodegradable synthetic polymer for a wide variety of tissue engineering applications such as bone, and soft tissue engineering [1]. PLGA exhibits a wide variety of unique properties that made it the favorable material for most researchers which include, excellent biocompatibility, tunable biodegradability, mechanical properties, spatial delivery over growth factors and most importantly it is an FDA approved polymer [1, 33].

PLGA undergoes degradation via non-enzymatic hydrolysis [35]. Its degradation by-products, lactic acid and glycolic acid are natural metabolites and non-toxic. In addition, they can easily be eliminated out of the body in the form of carbon dioxide and water through the normal body metabolism process. One limitation associated with PLGA is that it lacks all the ligands required for cell attachments and proliferation, which can result in poor cell adaption to the matrix and thus, poor tissue formation [35]. Gelatin is a remarkable natural biomaterial that also has been widely investigated as a promising implantable biomaterial for a number of tissue engineering applications. [34] The most intriguing properties that attract research interests are its cell/tissue compatibility, biodegradability, and functionality. In addition, gelatin inherits all the necessary arginine-glycine-aspartic acid (RGD) sequences that allow for enhanced cell adhesion, and it is less immunogenic. The only limitation associated with gelatin is that it possesses very poor mechanical properties that limit its use for load-bearing applications. The native ECM resembles some properties that are found in synthetic materials only or natural materials only, therefore, composite scaffolds are the best solution to address the disadvantages of both natural and synthetic scaffolds, as it helps in the mutual enhancement of the scaffold properties and thereby allowing controlled

degradation and mechanical properties as well as improving the biocompatibility, and providing cells with all the necessary physical and chemical cues that are naturally inherited by the natural ECM, to achieve the best possible biomimicry of the native ECM [36].

Scaffolds represent important components for tissue engineering. They act as temporary templates for tissue regeneration and construction. However, the degradation properties, as well as the morphological integrity of the scaffold, is of importance for effective tissue regeneration [35].

In this study, the three different phases were successfully fabricated and characterized. The fabrication techniques in the synthesis of the three different phases varied, due to the fact that every tissue type has its own specific ECM morphology, which had to be mimicked during the fabrication process of these scaffolds. Phase A&B were fabricated from PLGA-gelatin coaxial electrospun nanofibers to support fibroblast culture for soft tissue regeneration, and Phase C was fabricated from gelatin embedded PLGA microspheres to support osteoblasts culture for bone regeneration. The different phases were evaluated using SEM to determine the exterior surface morphology as well as to assist in the particle size analysis. In addition, degradation behaviors of the three phases were also evaluated over 8 weeks period of time, which included weight loss, swelling rate, water uptake, and pH change analysis.

SEM images of the electrospun mats showed a highly porous fibrous structure in both groups the coaxial and the uniaxial, which mimics the native tissue ECM morphology. Nanofiber size distribution and average diameter have been found to be within the appropriate range for ligament and skin tissue regeneration with nanofiber size diameter ranging between 400 nm – 1100 μ m with

an average size diameter of 800 ± 155 nm in the coaxial case and 752 ± 175 nm in the uniaxial case [29]. The 8 weeks morphology analysis showed a slight change in morphology with noticed fiber swelling over time. After 5 weeks of incubation at 37 °C, the coaxial fibers started to significantly swell and morphologically change when compared to the uniaxial group based on SEM and the swelling analysis. Pores were created at the surface of the coaxial nanofibers starting from the 5th week, increase the permeability of water and thus, causing rapid swelling to the nanofibers.

TEM analysis were conducted on both the coaxial nanofibers and the uniaxial nanofibers, which confirmed the coaxial structure in our nanofibers system. The difference between the core-sheath to the sheath of the nanofiber was calculated to be ~ 219 nm, which suggest promising results for a sustained and a controlled release of growth factors from the coaxial nanofibers.

Our results showed that over 8 weeks, PLGA-Gelatin coaxial nanofibers showed significant weight loss and swelling rates (45%, 29%) when compared to the other group (18%, 9%), respectively, after incubation in PBS at 37 °C. The results also revealed that PLGA-Gelatin Coaxial nanofibers are stable for the first 4 – 5 weeks, which is considered to be enough time for healthy fibroblasts to produce good amount of ECM in which they can attach after the severe degradation of PLGA nanofibers [29]. Although our results showed a significant difference in pH drop over the 8 weeks period of time in the coaxial group comparing to the Uniaxial group, the pH was still within the neutral range (pH 6.9). PLGA nanofibers are known for their *in vitro* and *in vivo* stability and morphological integrity for prolonged period of time, however, due to the fact that the coaxial nanofibers possess a hollow structure at the core of their fibers, they are prone to swell more rapidly when compared to the uniaxial nanofiber. The coaxial nanofibers display a smaller sheath

thickness when compared to the uniaxial, this however, by its turn causes water to diffuse to the core of the fiber more rapidly than the uniaxial, filling the core and causing a rapid swelling to the fiber. The significant weight loss of the coaxial nanofibers when compared to the uniaxial nanofibers is attributed to the polymer volume within the fiber. In the coaxial nanofibers, PLGA occupies only ~ 21% of the total volume of the fiber, whereas the other 79% is occupied by the gelatin located at the core-shell of the fiber. On the other hand, PLGA occupies 100% of the total volume of the fibers in the uniaxial nanofibers. However, due to the less PLGA content in the coaxial nanofibers, they exhibited a significant weight loss over time when compared to the uniaxial.

Gelatin hydrogel incorporated within the microsphere scaffold was cross-linked with microbial transglutaminase or mTG. Both gelatin and mTG are biocompatible and have no diverse effects upon degradation [30]. Gelatin was incorporated within the microsphere matrix to serve as a drug carrier for growth factor delivery. We chose gelatin because it has been demonstrated in several reports that gelatin exhibits sustained and controlled local delivery with minimal burst release of incorporated growth factors [32]. In addition, gelatin-mTG hydrogels have been shown to be good candidate for cell-based approaches [31].

The degradation behavior of PLGA-Gelatin-mTG microsphere scaffold and PLGA-Gelatin-mTG Free scaffold was also evaluated over 8 weeks period of time after incubation in PBS at 37 °C. The incorporated gelatin hydrogel in the PLGA-Gelatin-mTG group restricted water from freely penetrating throughout the structure resulting in a minimal weight loss over time comparing to the PLGA-Gelatin-mTG Free group. In the gelatin group, degradation only occurred to the outer

surface of the scaffold due to the presence of the gelatin in the other areas within the scaffold, whereas in the other group, degradation took place throughout the entire structure equally (Figure 2.12, Figure 2.13).

Water uptake in the PLGA-Gelatin-mTG group was higher compared to the PLGA-Gelatin-mTG Free in the first four weeks with no significant difference. At week 5 through week 7, water uptake started to significantly increase in the gelatin group comparing to the PLGA-Gelatin-mTG Free group. This indicates that small amount of water is penetrating through the gelatin hydrogel during the incubation time. Although water was restricted from freely penetrating through the matrix, it was able to penetrate through the hydrogel its self in small amounts, which can be good for cells that migrate inside the hydrogel in culture. Since only the outer surface of the microsphere scaffold in the PLGA-Gelatin-mTG is degrading over time, the surrounding medium should contain less degradation by-products when compared to the other group. This has been further proven in the pH change analysis where the pH in the PLGA-Gelatin-mTG Free group significantly dropped over the 8 weeks when compared to the gelatin group. Although the change in pH was significant in the PLGA-Gelatin-mTG free group, it was still within the neutral range.

Over the 8 weeks, microspheres in both groups did not show a significant change in surface morphology, only a slight increase in surface erosion was gradually observed from the SEM images over time in both groups. However, scaffolds in both groups started to lose structural integrity and break down over the 8 weeks, which was evidenced due to the appearance of cracks between the adjacent microspheres, with fewer cracks in the gelatin incorporated group. This is how sintered PLGA microsphere scaffolds normally lose their mechanical and structural integrity

over time when cultured at 37 C, cracks between the adjacent microsphere take place until all microspheres are unfused, in addition to the surface erosion taking place at the surface of the microspheres, simultaneously.

2.5 Conclusion

The different phases within the IGS have been successfully fabricated with a morphology resembling those found at the native tissue and with the appropriate particle size. We were able to verify the core-shell structure using TEM analysis. Degradation studies revealed that the water uptake in PLGA-Gelatin-mTG was increasing over time, implying that water is penetrating through the hydrogel, which indicates the suitability of the substrate for further cell-based studies. Our results indicated that PLGA coaxial nanofibers are stable for up to 5 weeks, which is considered to be enough time for fibroblasts to produce a sufficient amount of ECM in which they can attach to upon the sever degradation of the substrate. Also, pH analysis showed that pH was still within the neutral range after 8 weeks in all groups. These findings demonstrate the potential of utilizing these scaffolds for further drug release and cell-based studies to investigate their capability of supporting spatial release over growth factors, as well as enhancing cellular performance such as cell attachment and proliferation.

2.6 References

1. Makadia, Hirenkumar K., and Steven J. Siegel. "Poly Lactic-*co*-Glycolic Acid (PLGA) as Biodegradable Controlled Drug Delivery Carrier." *Polymers* 3.3 (2011): 1377–1397. *PMC*. Web. 15 Sept. 2017.
2. Yang S., Leong K.F., Du Z., Chua C.K. The design of scaffolds for use in tissue engineering. Part I. Traditional factors. *Tissue Eng.* 2001;7:679–689
3. Jiang T., Abdel-Fattah W.I., Laurencin C.T. In vitro evaluation of chitosan/poly(lactic acid-glycolic acid) sintered microsphere scaffolds for bone tissue engineering. *Biomaterials*. 2006;27:4894–4903.
4. White L.J., Kirby G.T.S., Cox H.C., Qodratnama R., Qutachi O., Rose F.R.A.J. Accelerating protein release from microparticles for regenerative medicine applications. *Mater Sci Eng C Mater Biol Appl.* 2013;33:2578–2583.
5. Kirby G.T.S., White L.J., Rahman C.V., Cox H.C., Qutachi O., Rose F.R.A.J. PLGA-based microparticles for the sustained release of BMP-2. *Polymers*. 2011;3:571–586.
6. Gentile, Piergiorgio et al. "An Overview of Poly(lactic-*co*-Glycolic) Acid (PLGA)-Based Biomaterials for Bone Tissue Engineering." *International Journal of Molecular Sciences* 15.3 (2014): 3640–3659. *PMC*. Web. 15 Sept. 2017
7. Engineer, C.; Parikh, J.; Raval, A. Review on hydrolytic degradation behavior of biodegradable polymers from controlled drug delivery system. *Trends Biomater. Artif. Organs* 2011, 25, 79–85.
8. Wu, X.S.; Wang, N. Synthesis, characterization, biodegradation, and drug delivery application of biodegradable lactic/glycolic acid polymers. Part II: Biodegradation. *J. Biomater. Sci. Polym. Ed.* 2001, 12, 21–34.

9. Lu, L.C.; Peter, S.J.; Lyman, M.D.; Lai, H.L.; Leite, S.M.; Tamada, J.A.; Vacanti, J.P.; Langer, R.; Mikos, A.G. In vitro degradation of porous poly(L-lactic acid) foams. *Biomaterials* 2000, 21, 1595–1605.
10. Jabbarzadeh, E., Deng, M., Lv, Q., Jiang, T., *et al.* VEGF-incorporated biomimetic poly(lactide-co-glycolide) sintered microsphere scaffolds for bone tissue engineering. *Journal of Biomedical Materials Research Part B: Applied Biomaterials* **100**, 2187-2196 (2012).
11. Laurencin, C. T., Ko, F. K., Attawia, M. A. & Borden, M. D. Studies on the development of a tissue engineered matrix for bone regeneration. *Cells and Materials* **8**, 175-181 (1998).
12. Borden M, Attawia M, Khan Y, Laurencin CT. Tissue engineered microsphere-based matrices for bone repair: Design and evaluation. *Biomaterials* 2002; **23**: 551–559.
13. Borden M, Attawia M, Laurencin CT. The sintered microsphere matrix for bone tissue engineering: In vitro osteoconductivity studies. *J Biomed Mater Res* 2002; **61**: 421–429.
14. Electrospinning of nanofibers: Reinventing the wheel? *Adv. Mater.* **2004**, 16, 1151–1170.
15. Zhang, Y.Z.; Lim, C.T.; Ramakrishna, S.; Huang, Z.M. Recent development of polymer nanofibers for biomedical and biotechnological applications. *J. Mater. Sci. Mater. Med.* **2005**, 16, 933–946.
16. Barnes, C.P.; Sell, S.A.; Boland, E.D.; Simpson, D.G.; Bowlin, G.L. Nanofiber technology: Designing the next generation of tissue engineering scaffolds. *Adv. Drug Deliv. Rev.* **2007**, 59, 1413–1433.
17. Smith, L.A.; Ma, P.X. Nano-fibrous scaffolds for tissue engineering. *Colloids Surf. B Biointerfaces* **2004**, 39, 125–131.

18. Kim, C.H.; Khil, M.S.; Kim, H.Y.; Lee, H.U.; Jahng, K.Y. An improved hydrophilicity via electrospinning for enhanced cell attachment and proliferation. *J. Biomed. Mater. Res. Part B Appl. Biomater.* **2006**, 78B, 283–290.
19. Patel, S.; Kurpinski, K.; Quigley, R.; Gao, H.F.; Hsiao, B.S.; Poo, M.M.; Li, S. Bioactive nanofibers: Synergistic effects of nanotopography and chemical signaling on cell guidance. *Nano Lett.* **2007**, 7, 2122–2128.
20. Culturing of skin fibroblasts in a thin PLGA–collagen hybrid mesh. *Biomaterials*. 2005 May;26(15):2559-66.
21. Chiquet-Ehrismann R, Tucker RP. Connective tissues: signalling by tenascins. *Int J Biochem Cell Biol.* 2004;36:1085–1089. doi: 10.1016/j.biocel.2004.01.007.
22. Liu, X., Lim, J. Y., Donahue, H. J., Dhurjati, R., *et al.* Influence of substratum surfacechemistry/energy and topography on the human fetal osteoblastic cell line hFOB 1.19: Phenotypic and genotypic responses observed in vitro. *Biomaterials* **28**, 4535-4550 (2007).
23. Lee, W. -K., Lee, S. -M. & Kim, H. -M. Effect of surface morphology of calcium phosphate on osteoblast-like HOS cell responses. *Journal of Industrial and Engineering Chemistry* **15**, 677- 682 (2009).
24. Huang ZM, Zhang YZ, Kotaki M, Ramakrishna S. A review on polymer nanofibers by electrospinning and their applications in nanocomposites. *Compos Sci Technol* 2003;63:2223–53

25. Jing Z, Xu XY, Chen XS, Liang QZ, Bian XC, Yang LX, Jing XB. Biodegradable electrospun fibers for drug delivery. *J Control Release* 2003;92:227–31.
26. Su Y, Su Q, Liu W, Lim M, Venugopal JR, Mo X, Ramakrishna S, Al-Deyab SS, El-Newehy M. Controlled release of bone morphogenetic protein 2 and dexamethasone loaded in core-shell PLLACL-collagen fibers f
27. Nagiah, Naveen et al. “Highly Compliant Vascular Grafts with Gelatin-Sheathed Coaxially Structured Nanofibers.” *Langmuir : the ACS journal of surfaces and colloids* 31.47 (2015): 12993–13002. *PMC*. Web. 17 Sept. 2017.
28. Stevens KR, Einerson NJ, Burmania JA, Kao WJ. In vivo biocompatibility of gelatin-based hydrogels and interpenetrating networks. *J Biomater Sci Polym Ed.* 2002;13(12):1353-66.
29. Tracy, Lauren E., Raquel A. Minasian, and E.J. Caterson. “Extracellular Matrix and Dermal Fibroblast Function in the Healing Wound.” *Advances in Wound Care* 5.3 (2016): 119–136. *PMC*. Web. 17 Sept. 2017.
30. Changhai Ru, Feilong Wang, Ming Pang, Lining Sun, Ruihua Chen, and Yu Sun. Suspended, Shrinkage-Free, Electrospun PLGA Nanofibrous Scaffold for Skin Tissue Engineering, *ACS Appl. Mater. Interfaces*, 2015, 7 (20), pp 10872–10877
31. Yang, Gang et al. “Enzymatically Crosslinked Gelatin Hydrogel Promotes the Proliferation of Adipose Tissue-Derived Stromal Cells.” Ed. María Ángeles Esteban. *PeerJ* 4 (2016): e2497. *PMC*. Web. 17 Sept. 2017.
32. Patel, Zarana S. et al. “Biodegradable Gelatin Microparticles as Delivery Systems for the Controlled Release of Bone Morphogenetic Protein-2.” *Acta biomaterialia* 4.5 (2008): 1126–1138. *PMC*. Web. 17 Sept. 2017.
33. Makadia, Hirenkumar K., and Steven J. Siegel. “Poly Lactic-co-Glycolic Acid (PLGA) as

- Biodegradable Controlled Drug Delivery Carrier.” *Polymers* 3.3 (2011): 1377–1397. *PMC*. Web. 29 Oct. 2017.
34. Echave MC, Saenz del Burgo L, Pedraz JL, Orive G. Gelatin as Biomaterial for Tissue Engineering. *Curr Pharm Des.* 2017;23(24):3567-3584.
35. Chan, B. P., and K. W. Leong. “Scaffolding in Tissue Engineering: General Approaches and Tissue-Specific Considerations.” *European Spine Journal* 17.Suppl 4 (2008): 467–479. *PMC*. Web. 29 Oct. 2017.
36. Rashi Nigam and Babita Mahanta. An Overview of Various Biomimetic Scaffolds: Challenges and Applications in Tissue Engineering. *Biomedical Engineering Department, VIT University, Vellore, India*

CHAPTER 3

IN VITRO EVALUATION OF PDGF-BB AND IGF-I RELEASE FROM COAXIAL-GELATIN, UNIAXIAL NANOFIBER SCAFFOLDS, AND BMP-2 FROM PLGA-GELATIN-MTG INCROPORATED MICROPSERE SCAFFOLD

3.1.Introduction

Growth factors are soluble-secreted signaling polypeptides capable of instructing specific cellular responses in a biological environment [1]. The specific cellular response triggered by growth factor signaling can result in a very wide range of cell actions, including cell survival, and control over migration, differentiation or proliferation of a specific subset of cells. Several growth factors have extensively been used for tissue engineering applications such as BMP-2, for bone tissue regeneration [5], PDGF-BB and IGF-I for mostly skin, and ligament tissue regeneration applications respectively [6, 7]. These Growth factors are endogenously secreted in the body by cells themselves, but in very minimal amounts that cannot aid in tissue regeneration in the case of large trauma. This led to the importance of finding optimal methods to exogenously deliver these molecules for tissue engineering applications. For therapeutic and regenerative effects, tissue should be exposed to these exogenous growth factors with adequate doses for relatively long timeframe, which can range from days to weeks. The use of high dosage, however, can results in limited efficiency due to the short half-life most growth factors and undesirable side-effects, such as neovascularization, or non-targeted tissue or growth of tumors in the context of delivery of antigenic growth factors [2, 3]. The need of finding effective methods in delivering exogenous factors has established much enthusiasm and numerous clinical trials, but the results of many of these trials have been largely disappointing. Interestingly, the trials that have shown benefit all contain a common denominator, the presence of a material carrier, suggesting strongly that spatial and temporal control over the location and bioactivity of factors after introduction into the body is

crucial to achieve tangible therapeutic and regenerative effect [4].

Polymeric materials have been extensively used to allow controlled, sustained, and local delivery of growth factors, providing the necessary spatial and temporal gradients to regulate the extent and pattern of tissue formation [4]. In addition, they can also allow to control the kinetics and dose of protein release while also protecting the protein from degradation until released [4].

Growth factors can be incorporated into these polymeric delivery devices in a variety of different ways in which the release rate can be tuned and controlled. A variety of processing techniques have been developed to bypass issues of burst release such as incorporation of growth factors coaxially in the core-shell of the fiber during electrospinning, or incorporating of factors in hydrogels [4].

Electrospinning has been widely used as a drug delivery method for tissue engineering applications [8, 9]. However, to overcome the burst release limitations associated with the conventional uniaxial electrospinning methods, the introduction of the coaxial structure has come along the way, which has been shown to overcome the problem of burst release [10]. Incorporation of growth factors coaxially in the core shell of the polymeric nanofiber has been shown to exhibit precise control over the location of the drug within the core-shell of the nanofibers [11] the main advantage of coaxial electrospinning over the uniaxial is that it generates core and sheath fibers by physical separation between the core and the sheath through the utilization of two electrospinning tips and two solutions (Figure 3.1) [12]. The core generally contains the growth factor solution and the sheath contains the polymeric solution. This nanofiber structure will allow for more of a spatial control over growth factor delivery and will hugely minimize any possibility of burst release when

compared to the conventional uniaxial nanofiber [12]. In addition, this process is used to load a wide variety of agents into nanofibers that could potentially lose their bioactivity and functionality unless they are in fluid or non-denaturing environment [12]. Advantages of the coaxial electrospinning made it one area of a significant interest for many researches for more effective drug delivery and thus, tissue regeneration.

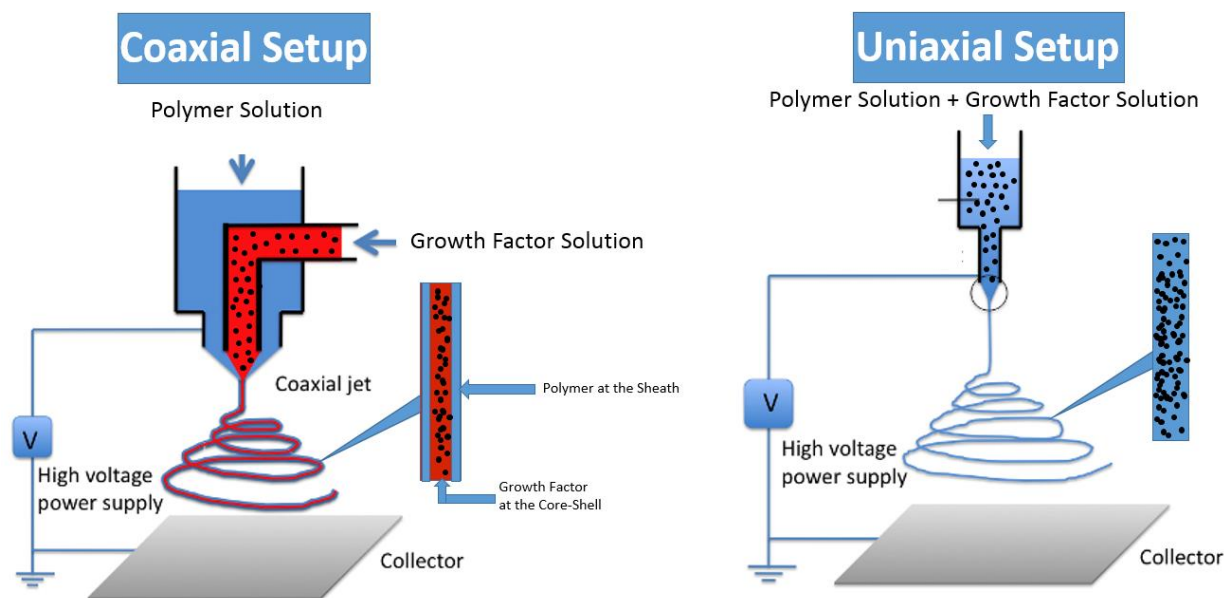


Figure 3.1 Schematic of coaxial electrospinning setup, and the conventional uniaxial electrospinning setup.

Hydrogels have been also widely used as prolonged, sustained, and controlled release systems for growth factors and other molecules [13]. Some of the most extensively used hydrogels include alginate, chitosan, collagen and gelatin hydrogels [14]. Gelatin for instance, is well-known for its prolonged growth factor delivery, characterized by a small initial burst release and showing no tissue damaging residual material upon degradation [15]. Many ways can be employed in order to crosslink gelatin such as physical, chemical or enzymatic crosslinking. However, physically crosslinking gelatin generally results in mechanically weak construct due to the low degree of crosslinking, which only occurs at the surface of the material and does not crosslink the gelatin all

the way through. The chemical crosslinking of gelatin can result in cytotoxic side-effects or/and immunological responses from the host upon implantation *in vivo* due to the toxicity of most of the utilized chemicals. Compared to the previous two methods, enzymatically crosslinked gelatin is considered the gold standard among all the crosslinking methods for crosslinking gelatin because it results in strong mechanical properties due to the excellent crosslinking extent throughout the hydrogel, and most enzymes are biocompatible and do not elicit any immunological responses with the host after implantation. Despite the advantages associated with the enzymatic crosslinking of gelatin, most enzymes are very expensive [32]. Recently, studies have reported the use of an enzyme named “Microbial Transglutaminase” or (mTG) for enzymatically crosslinking gelatin [32]. Distinct from all the other enzymes, this enzyme is very cheap and it is widely available. This enzyme has been proven to be biocompatible and noncytotoxic in crosslinking gelatin and collagen-based scaffolds [33, 34]. Gelatin crosslinking can be initiated by mixing various amounts of mTG with gelatin under certain conditions. The addition of mTG to gelatin catalyzes the formation of an amide bond between the carboxylic acid groups of glutamic acid and the ϵ -amino group of lysine, causing a complete crosslink to gelatin throughout [35]. Gelatin-mTG hydrogel has been used as a drug delivery system and it was shown to cause retention to the incorporated growth factor due to the covalent binding of the factor to gelatin initiated by mTG. Retention of the growth factor, however, does not eliminate its bioactivities as shown in previous reports [33].

The *in vitro* release profile of the covalently bound growth factors from enzymatically crosslinked gelatin hydrogels undergoes two phases. In the first phase, a very minimal burst release of about 7-8% of the total loaded growth factor can be observed [15, 16]. The second phase, which shows

the sustained and the controlled release of the remaining loaded factor is suggested to be based on enzymatic degradation of the crosslinked gelatin through either exogenous degradative enzymes such as collagenase type I or endogenous secreted enzymes such as cell-associated enzymatic activity, therapy releasing the bound growth factor [13]. This implies that if the degrading enzymes are not presented as part of the releasing medium, rapid release of the loaded growth factor will be hard to be accomplished, resulting in very minimal release of the loaded growth factor over time [16].

In this aim, PDGF-BB and IGF-I were coaxially incorporated in the core-shell of PLGA nanofibers and in vitro release studies were carried out over 30 days to examine the release profiles of these two factors from the core-shell of PLGA nanofibers. In addition, BMP-2 was incorporated in an enzymatically cross-linked gelatin hydrogel for a sustained and controlled release. The gelatin hydrogel was used as a releasing carrier that was further injected within PLGA microsphere scaffold to examine the release of BMP-2 from the incorporated PLGA microsphere scaffold with gelatin-mTG/BMP-2. These evaluations are indeed essential to conduct in order to test the aforementioned devices' abilities in supporting spatial release over the incorporated growth factors.

3.2. Materials and Methods:

85:15 Poly(lactide-co-glycolide) (PLGA) (MW ~ 94,000 kDa) was purchased from (Absorbable Polymers, Birmingham, AL, USA), Hexafluoro-2-propanol (HFIP) was purchased from (Acros Organics, USA), Gelatin Type A from Pork (Porcine skin) was purchased from (MP Biomedical, OH, USA), Microbial Transglutaminase (mTG) was Purchased from (Ajinomoto, Japan), Dichloromethane (DCM) was purchased from (Fisher Scientific, USA), PDGF-BB, IGF-I and BMP-2 growth factors were purchased from (Fisher Scientific, USA), all ELISA kits were also purchased from (Fisher Scientific, USA), collagenase type I powder was purchased from (ThermoFisher Scientific, IL, USA), Alkaline Phosphatase Substrate Kit was purchased from (BIO-RAD, CA, USA), Pierce BCA Protein Assay kit was purchased from (Thermo Scientific, IL, USA), Dulbecco's Phosphate-Buffered Saline (PBS) of pH 7.4, MEM Alpha (1X) Minimum Essential Medium, Trypsin-EDTA (0.25%) phenol red, Penicillin-Streptomycin (10,000 U/mL), and Fetal Bovine Serum (FBS) were purchased from Gibco (Grand Island, NY).

3.2.1. Fabrication of PLGA-Gelatin-PDGF and IGF-1 Coaxial Nanofiber Scaffolds

PLGA (85:15) granules were dissolved in HFIP at 16 % wt and stirred overnight at room temperature to prepare the (shell solution) of nanofibers. To prepare the core solution, gelatin powder type A was dissolved in HFIP at 4% wt and stirred overnight at room temperature. At the day of electrospinning, both growth factors were reconstituted at a concentration of 1 mg/ml, and 81 µl of the reconstitution of either PDGF-BB and IGF-I were added to 1.5 ml of gelatin solutions and stirred for 15 minutes to allow the growth factor to homogenize with the gelatin solution. An electrospinning pump (NE 300 SYRINGE pumps, USA) was used in order to fabricate the coaxial PLGA-Gelatin nanofibers. The setting to prepare the coaxial scaffolds consisted of two coaxial

syringe pumps with different flow rates. In this study, the PLGA solution was used to form the outer shell and the gelatin-growth factors solution was used to form the inner core. These two solutions were loaded into two separate 10 ml syringes and connected to the coaxial needles, a 16 G (ID = 1.6 mm) outer needle and a 22 G (ID = 0.7 mm) inner needle, respectively, and then concentrically placed. The electrospinning parameters were as follows: (applied voltage: 10 kV; 1.5 mL/h for the sheath flow rate and 0.75 mL/h for the core flow rate). The tip of the needle was placed 10 cm away from the collector. The electrospinning process lasted for 1.5 h. Coaxial electrospun nanofibers were peeled from the collector and stored under vacuumed desiccator for 24 hours to insure complete evaporation of solvent.

3.2.2. Transmission Electron Microscopy (TEM)

TEM analysis were conducted on both the coaxial and the uniaxial electrospun nanofibers incorporated with PDGF-BB and IGF-I to evaluate the core structure efficiency. Observations were prepared by directly depositing the spun fibers onto copper grids of 300 mesh. The samples for TEM images were analyzed using (FEI Tecnai 12 G2 Spirit BioTWIN) transmission electron microscopy and all images were recorded in GATAN ESW 500 camera.

3.2.3. Fabrication of PLGA-PDGF-BB and IGF-I Uniaxial Nanofiber Scaffolds

PLGA (85:18) granules were dissolved at 16% wt in HFIP with stirring to form clear, homogeneous, and viscous solution. From the same patch used for the coaxial nanofibers fabrication, reconstitution of both PDGF-BB and IGF-I were directly added to 3.5 ml of PLGA solution and stirred for 30 minutes to allow the growth factor to homogenize with the polymer solution. PLGA-growth factors solution was loaded into 10 ml plastic syringe and electrospun at

flow rate of 0.75 mL/h through a 20-gauge blunt needle with the electrospinning pump NANON-01A (MECC, Fukuoka, Japan) at an applied voltage of 10 kv. The tip of the needle was placed 10 cm away from the collector. The electrospinning process lasted for 1.5 h. Uniaxial electrospun nanofibers were peeled from the collector and stored under vacuumed desiccator for 24 hours to insure complete evaporation of solvent.

3.2.4. Fabrication of PLGA Microspheres

Single emulsion solvent evaporation technique was used to fabricate PLGA microspheres. PLGA granules were dissolved at 12.5% wt in Dichloromethane (DCM) in glassy vials. Vials were vortexed for 1 h at a speed of 550 RPM until clear, homogeneous, and viscous solution was obtained. Next, PLGA solution was added via a thin stream into 1% PVA solution in a 1000 ml beaker and it was let to stir at (300 RPM) overnight to allow the solvent to evaporate. After that, microspheres were collected, filtered, air dried and then they were stored in -20 for 24 h to freeze any residual water particle inside of the microspheres. Next, microspheres were freeze dried for 48 h and were then sieved to obtain the desired particle size range 300 – 600 μm .

3.2.5. Incorporation of BMP-2 in Gelatin-mTG Hydrogel

Gelatin gel formation was initiated by mTG addition. For hydrogel preparation, 3% wt gelatin powder type A was dissolved in preheated phosphate-buffered saline (PBS) at 50 °C and it was let to stir on a stirrer plate for 15 minutes at 500 RPM to completely dissolve the powder. The mTG solution was prepared by dissolving 10% wt mTG in preheated PBS at 50 °C, then it was let to stir on a stirrer plate for 15 minutes at 500 RPM. As soon as both gelatin and mTG completely dissolved in PBS, the temperature of the stirrer plate was adjusted to 37 °C and they were let to

stir for another 15 minutes to allow for the temperature drop. Next, to initiate the cross-linking reaction between gelatin and mTG for the hydrogel preparation, mTG solution was mixed with the 3% wt gelatin solution at a ratio of 1:11.5 under stirrer speed of 500 RPM at 37 °C. The mixture was let to stir for 5 minutes until a semi-viscous solution is fabricated and ready to be injected. BMP-2 incorporation was done by adding 1 µg of BMP-2 in 100 µl of gelatin-mTG solution and mix them gently.

3.2.6. Fabrications of PLGA Microspheres Scaffold Incorporated Gelatin/BMP-2-mTG

To fabricate the three-dimensional scaffolds and use it to incorporate gelatin-mTG/BMP-2 hydrogel within it, PLGA microspheres were poured into a (10 mm x 10 mm) stainless steel mold and heated for 90°C for 90 minutes. These parameters allowed the microspheres to fuse together forming the 3D scaffolds. After 90 minutes, the stainless-steel mold was removed from the oven and allowed to cool to room temperature for 2 hours. Next, scaffolds were removed and the semi-viscous gelatin-mTG/BMP-2 hydrogel was injected inside of the microsphere scaffold using an insulin syringe until all porosity were filled and it was allowed to gel at 37 °C for 1 hours.

3.2.7. In vitro PDGF-BB and IGF-I Release from Coaxial and Uniaxial PLGA Electrospun Nanofiber Scaffolds

The resultant coaxial electrospun nanofibers scaffolds (N=5) were cut into (1 cm X 1 cm) squares, and the uniaxial electrospun nanofibers scaffolds (N=5) were cut into (1.5 cm X 1.5 cm) squares were loaded into 5 ml glassy vials after. The glassy vials were filled with 2 ml of PBS with pH 7.4 and were then placed on an orbital shaker at 37 °C. At predetermined time points (0, 1, 4, 6, 8 h and then every day for 2 weeks, and then every week for 2 weeks), 125 µl from each sample were

collected and replaced with 125 μ l fresh PBS. Collected samples were stored at -20°C for later analysis. The release profiles of PDGF-BB and IGF-I were analyzed using ELISA-kit following the manufacturer's instructions. Cumulative release over a period of 30 days was performed on all samples. The protein content in the nanofibers for the two electrospinning methods (coaxial and uniaxial) was determined by base-surfactant method [24]. Briefly, Scaffolds of each group (N = 5) were subjected to hydrolysis in 0.1N NaOH, 5M Urea, 0.08% SDS in 50 mM Tris extraction medium at 37°C for 3 h. After neutralization with 0.1N HCL and centrifugation, the protein concentration in the supernatant was measured using ELISA kits.

3.2.8. In vitro BMP-2 Release from PLGA-Gelatin-mTG Scaffolds

PLGA-Gelatin-mTG Microsphere scaffolds were loaded into 5 ml glassy vials and filled with 5 ml of PBS with pH 7.4 and they were then placed on an orbital shaker at 37°C . At predetermined time points (0, 1 4, 6, 8 h and then every day for 2 weeks), 250 μ l from every sample were collected and replaced with 250 μ l fresh PBS. Collected samples were stored at -20°C for later analysis. The release profiles of BMP-2 was analyzed using ELISA following the manufacturer's instructions.

3.2.9. Extraction of BMP-2 from Gelatin-mTG Hydrogel

The same scaffolds from the release experiment were harvested and used for the extraction step to examine the amount of BMP-2 left, and to ensure that the protein is remained and it wasn't digested or lost during the preparation or the injection step. In order to extract the protein, the gelatin hydrogel had to be digested first. First, every scaffold was placed in a new 5 ml vial and was filled with 5 ml of 0.1% collagenase type I solution in PBS. Vials were placed in an orbital shaker and were left to agitate for overnight at 37°C at a maximum speed to insure a complete digestion of

the gelatin hydrogel within the microsphere scaffold. The next day, the solution content from every vial was collected and assayed using ELISA-kit for BMP-2 content after neutralization with 0.1N HCL and centrifugation. Results were plotted as a function of remaining BMP-2 content and were compared to the control, which underwent the same digestion procedure. The control in this case was PLGA microsphere scaffold incorporated with gelatin-mTG hydrogel without BMP-2.

3.2.10. Alkaline Phosphate Activity Assay

To examine the bioactivities of the retained BMP-2, MC3T3 cells were seeded on PLGA-Gelatin-mTG incorporated microsphere scaffolds and ALP activities were measured on days 7 and 14. Briefly, PLGA-Gelatin-mTG scaffolds were placed in triplicates/ group in low-binding 24-well plates, and MC3T3 cells were seeded on every scaffold at a density of 5×10^4 cells/scaffold. Three experimental groups were included in the study, PLGA-Gelatin- mTG/BMP-2 (100 ng/scaffold), PLGA-Gelatin-mTG with BMP-2 physically adsorbed on the surface (100 ng/ scaffold) (positive control), and PLGA-Gelatin-mTG without BMP-2 (negative control). 1 mL of α MEM culture medium supplemented with 10% Fetal bovine serum (FBS), and 1% Penicillin Streptomycin (p/s) was added to every well and medium was change every 3 days during the experiment length. At the predetermined time points, culture medium was removed, scaffolds were washed twice with PBS, and then 500 μ l of 0.25 trypsin solution was added to every well to detach the cells from every scaffold. The detached cells were then collected, and centrifuged at 1500 RPM for 5 minutes to get a pellet. Pellet was washed with PBS and the centrifugation step was repeated twice to insure the complete removal of any trypsin or medium residual. Cells were then lysed in 0.1 % Triton X-100 through a freeze-thaw cycle. Cells were then centrifuged and the cell layer

supernatant was collected for every sample to be assayed for total protein (BCA) and ALP content. ALP results were then normalized to BCA data for more accurate results.

3.2.11. Statistical Analysis

Data are presented as mean \pm standard deviation (SD). All statistical analyses were performed using the Statistical Software Prism GraphPad (Version 5) using two-way Analysis of Variance (ANOVA) with a Tukey test for Post Hoc parameter comparisons. Statistical significance was set at $p < 0.05$.

3.3.Results:

3.3.1. PDGF-BB and IGF-I Release from Coaxial and Uniaxial Electrospun Nanofiber Scaffolds

Coaxial and uniaxial nanofibers for each growth factors had almost similar average protein content of 1000 ± 201 ng for coaxial PLGA-Gelatin-PDGF and 994 ± 189 for uniaxial PLGA-PDGF, where the coaxial PLGA-Gelatin-IGF-I had an average protein content of 989 ± 190 ng and 991 ± 181 for the uniaxial PLGA-IGF-I. Both PDGF-BB and IGF-I demonstrated a sustained and a controlled release kinetics over the 30 days period of time from the coaxial nanofibers in comparison with the uniaxial nanofibers (Figure 3.2). A notable high burst release of both growth factors from the uniaxial nanofibers was detected in comparison with the coaxial, which showed a very minimal burst release at the beginning and continued on releasing both growth factors in a sustained and controlled fashion. Compared to the uniaxial nanofibers of both growth factors, which released all the encapsulated PDGF-BB and IGF-I in ~ 14 days, the coaxial nanofibers could sustain the release till 21 days. Overall, PDGF-BB showed a slower release in both cases the coaxial and the uniaxial in comparison with the release of IGF-I from both the coaxial and the

uniaxial.

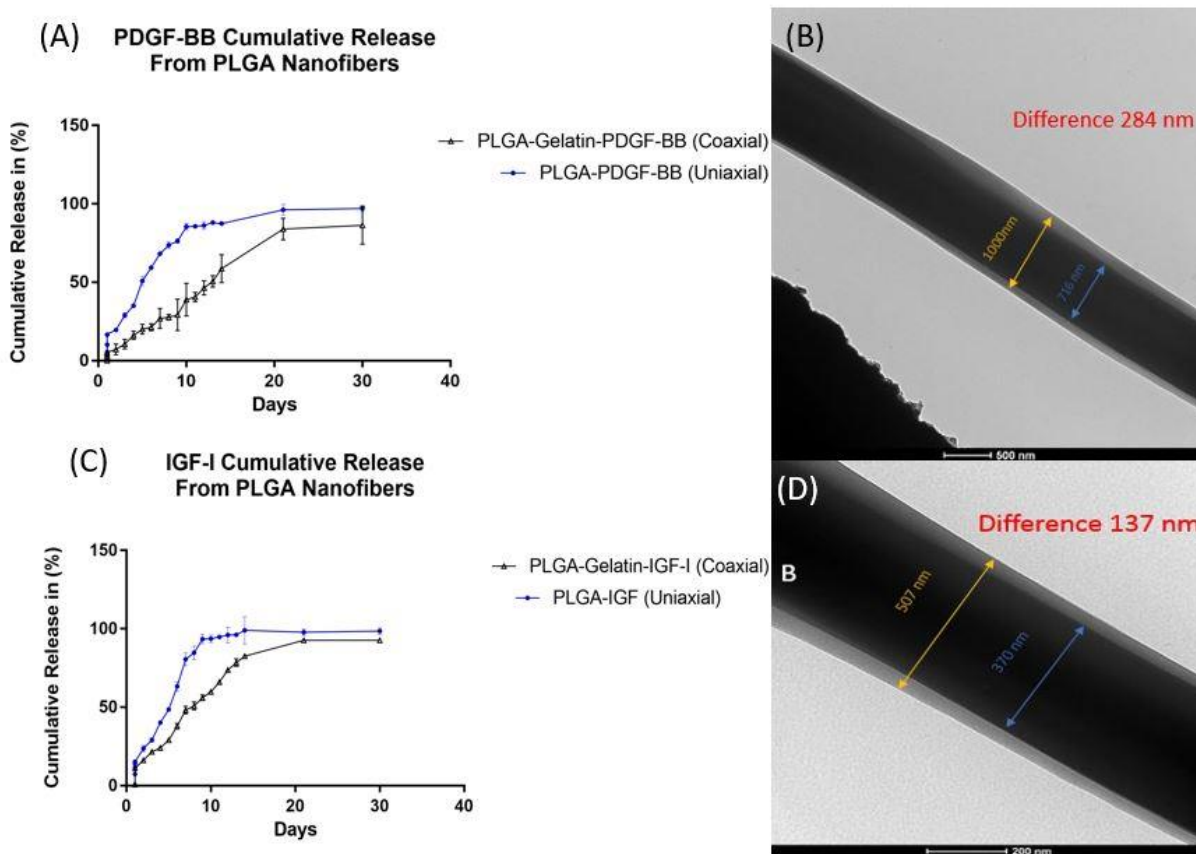


Figure 3.2 PDGF-BB and IGF-I release profiles from coaxial and uniaxial PLGA electrospun nanofibers. (A) PDGF-BB release profile from coaxial nanofibers and uniaxial nanofibers, (B) TEM image showing PDGF-BB in the core sheath of PLGA nanofiber with a sheath thickness of 284 nm, (C) IGF-I release profile from coaxial nanofibers and uniaxial nanofibers and (D) TEM image showing IGF-I in the core sheath of PLGA nanofiber with a sheath thickness of 137 nm.

3.3.2. BMP-2 Release from Gelatin-mTG Incorporated Microsphere Scaffolds

The potential of the injectable Gelatin-mTG gel to serve as a protein delivery vehicle was evaluated in vitro by following the release of BMP-2 from the gels as a function of time. After the collection of all the samples during the 14 days release study, they were used to conduct ELISA assay in order to determine the amount of protein released at every collected time point. No significant release was detected during the 14 days indicating that BMP-2 was retained within the hydrogel.

In order to validate this, we digested cross-linked gelatin within the microsphere scaffolds using 0.1% collagenase solution in order to release the protein to the medium, and the supernatant was collected and used to assay the protein content. We found that in all the 5 samples the protein was retained inside of the hydrogel and has not been released during the 14 days release study (Figure 3.3). The average retained protein from the 5 samples was calculated to be 967.5 ± 205 ng.

3.3.3. Alkaline Phosphate Activity of MC3T3 Seeded on PLGA-Gelatin-mTG/ BMP-2

Microsphere Scaffolds

In order to evaluate the osteoinductivity of the retained protein and its ability to stimulate cellular behaviors when retained has been evaluated by conducting an ALP experiment for 14 days. At day 7, the physically adsorped-BMP-2 group had a higher ALP content when compared to the retained BMP-2 group, and significantly high when compared to the negative control group (Figure 3.3). At day 14, ALP content was the highest in the retained BMP-2 group when compared to the added-BMP-2 group, and significantly higher when compared to the negative control. These data demonstrate that the retention of BMP-2 did not negatively affect the osteoinductivity and thus, resulted in enhancing ALP activities in MC3T3 cells over time.

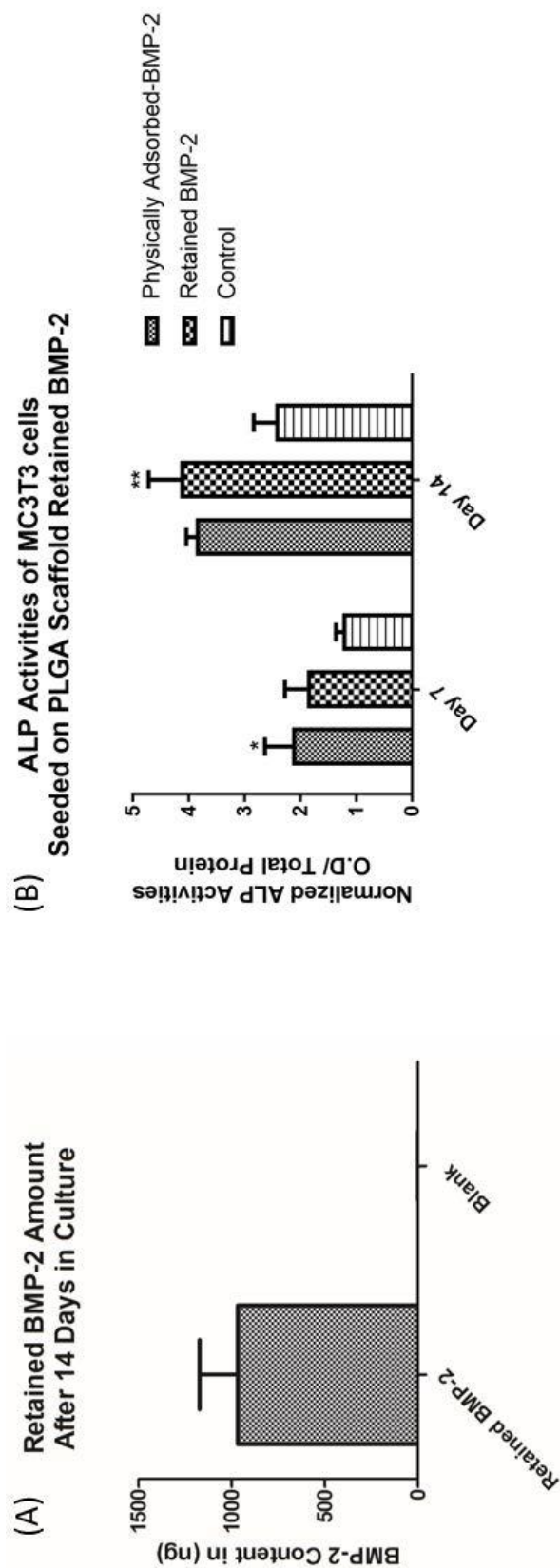


Figure 3.3. (A) The average of the retained BMP-2 in the enzymatically cross-linked geatin-mTG hydrogel, and (B) ALP activates Of MC3T3 cell lines seeded on PLGA-Gelatin-mTG scaffold in the three different experimental groups shown in the figure.

3.4.Discussion:

Growth factors can be incorporated into these polymeric delivery devices in a variety of different ways in which the release rate can be tuned and controlled. A variety of processing techniques have been developed to bypass issues of burst release such as incorporation of growth factors coaxially at the core-shell of the nanofiber during electrospinning, or incorporating of factors in hydrogels.

The beauty of the electrospinning technique is that it offers a possibility of incorporating protein growth factors within polymer nanofibers, which could then serve as a source of continued and controlled release of the growth factor [18, 19, 20, 21, 22]. Coaxial electrospinning is a modified version of the conventional uniaxial technique, which allows for more of a prolonged, sustained and controlled release rates of the incorporated protein [23]. During coaxial electrospinning, the growth factor solution, which intended to be at the core-shell of the nanofiber, is physically separated from the polymer solution, which acts as the sheath for the core. They are then electrospun simultaneously with varying electrospinning parameters through two overlapping needles and then collected. This results in a very organized structure of a nanofiber that consist of a growth factor incorporated at the core-shell, and a polymeric sheath that covers the core. Depending on the degradation rate of the polymeric sheath, the release rate can be tuned [4].

Such a method, not only offers the possibility of exhibiting a controlled and sustained release, but also protects the protein from the organic solvent used to dissolve the outer polymeric coat, and also enables electrospinning of a protein solution that is otherwise not “electro-spinnable” [18, 21].

Another considerable method of growth factor delivery is through incorporating the protein within hydrogels, such as gelatin. Enzymatically crosslinked gelatin hydrogels possess great characteristics in providing a sustained and controlled release of growth factors [25]. As discussed previously, growth factors incorporated within enzymatically crosslinked gelatin hydrogels undergo two release profile phases, as the first exhibits a very minimal burst release, while the second phase exhibits a prolonged and sustained release of incorporated growth factor over time [13, 15, 16]. Therefore, these observations suggest that gelatin is a great candidate for drug delivery-based approaches.

In this aim, PDGF-BB and IGF-I were either coaxially incorporated in the core shell of PLGA nanofibers or directly blended with the polymer solution and *in vitro* release studies were conducted over 30 days to examine the release profiles of these two factors from the core-shell of PLGA nanofibers and from PLGA nanofibers. In addition, BMP-2 was incorporated in an enzymatically cross-linked gelatin hydrogel for a sustained and controlled release. The gelatin hydrogel was used as a drug carrier that was then injected within PLGA microsphere scaffold to examine the release of BMP-2 from the incorporated PLGA microsphere scaffold gelatin-BMP-2.

The protein content has been evaluated in both coaxial and uniaxial nanofibers of both growth factors. This was done by cutting the resultant coaxial electrospun scaffolds into 1 cm X 1 cm and the uniaxial electrospun scaffolds into 1.5 X 1.5 cm with an N= 5 each, and measuring the protein content in all samples using ELISA kits. However, it was found that coaxial and uniaxial nanofibers for each growth factors had almost similar average protein content of 1000 ± 201 ng for coaxial PLGA-Gelatin-PDGF and 994 ± 189 for uniaxial PLGA-PDGF, where the coaxial

PLGA-Gelatin-IGF-I had an average protein content of 989 ± 190 ng and 991 ± 181 for the uniaxial PLGA-IGF-I. Based on these data, we were able to determine the protein content as a function of scaffold dimension for every growth factor in every case. Where all coaxial electrospun nanofiber scaffold had a protein content of $\sim 1 \mu\text{g} / 1\text{cm} \times 1\text{cm}$, and all uniaxial electrospun nanofiber scaffolds had protein content of $\sim 1 \mu\text{g} / 1.5 \text{ cm} \times 1.5 \text{ cm}$ for both factors.

The release data revealed that both PDGF-BB and IGF-I demonstrated a sustained and a controlled release kinetics over the 30 days period of time from the coaxial nanofibers in comparison with the uniaxial nanofibers as shown in the previous (figure 3.2). This demonstrate the spatial control offered by the coaxial nanofibers over the uniaxial. A high notable burst release of both growth factors from the uniaxial nanofibers was detected in comparison with the coaxial, which showed a very minimal burst release at the beginning and continued on releasing both growth factors in a sustained and controlled fashion. The initial burst release from the uniaxial nanofibers was due to the facts that some of the growth factors was present at the surface of the nanofibers, which caused the burst release as soon as the scaffold was submerged in the releasing medium. Distinct from the uniaxial, growth factors in the coaxial nanofibers are all contained at core-shell of the nanofiber, which minimized the chance of a burst release as shown in a previous work [26].

Compared to the uniaxial nanofibers of both growth factors, which released all the encapsulated PDGF-BB and IGF-I in ~ 14 days, the coaxial nanofibers could sustain the release till 21 days. Overall, PDGF-BB showed a slower release in both cases (the coaxial and the uniaxial) in comparison to the release of IGF-I from both the coaxial and the uniaxial. This may be due to the fact that the difference in thickness between the core-shell and the sheath in the coaxial-PDGF-BB

nanofiber was larger than in the coaxial-IGF-I, which in turns delayed the release of PDGF-BB when compared to IGF-I (Figure 3.4). Another reason may be attributed to the molecular mass of each protein, where the mass of PDGF-BB is 12.3 kDa and IGF-I is 7.6 kDa. It is well-known based on the literature that the release kinetics from any device is dependent on the protein molecular mass, in which the smaller the protein molecular mass the faster it releases, and the larger the protein molecular mass, the slower and more sustained it releases. This implies that if small and large molecular mass proteins were incorporated in the same exact device, the release profiles will vary due to the variation in the protein molecular mass [17].

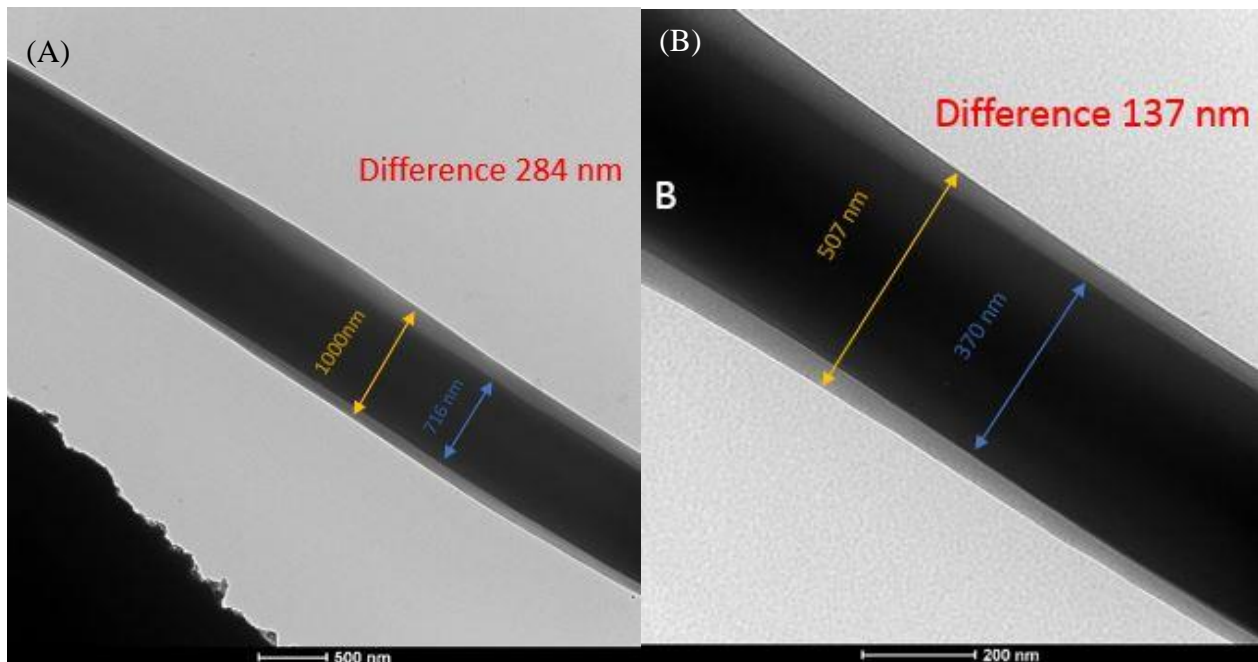


Figure 3.4 TEM images of PLGA coaxial electrospun nanofibers with growth factors incorporated at the core-shell of the nanofiber (A) TEM image showing PDGF-BB in the core sheath of PLGA nanofiber with a sheath thickness of 284 nm, (B) TEM image showing IGF-I in the core sheath of PLGA nanofiber with a sheath thickness of 137 nm.

The potential of the injectable gelatin-mTG gel to serve as a protein delivery vehicle was evaluated *in vitro* by following the release of BMP-2 from the gels embedded in PLGA microsphere scaffolds

as a function of time. After the collection of all the samples during the 14 days release study, they were used to conduct ELISA assay in order to determine the amount of protein released at every collected time point. No significant release was detected during the 14 days suggesting that BMP-2 was retained within the hydrogel. In order to validate this, we digested the cross-linked gelatin embedded within the microsphere scaffolds using 0.1% collagenase solution in order to enable the release of the bound protein to the medium, and the supernatant was collected and used to assay the protein content. We found that in all the five samples the protein was retained inside of the hydrogel and has not been released during the 14 days release study (Figure 3.3). The average retained protein from the five samples was calculated to be 967.5 ± 205 ng. This implies that the low protein release from the enzymatically crosslinked gelatin hydrogel was attributed to the covalent bonding initiated between BMP-2 and gelatin as a result of the enzymatic crosslinking with mTG, which resulted in a complete retention to the protein [33]. In fact, a previous study has shown that the release of BMP-2 from the enzymatically crosslinked gelatin hydrogel is very hard to be accomplished *in vitro* with the absence of a degradative enzyme. In this study, they revealed that the incubation of gelatin-mTG hydrogels in collagenase containing medium could accelerate the degradation of hydrogel when compared to incubation in normal medium, thereby enabling the bound protein to be released [33]. In our current study, gelatin-mTG was incubated in normal PBS that did not contain any degradative enzymes. This, however, explains the reason for the complete retention of BMP-2 in gelatin-mTG in our case.

Because collagenase was found to be selective toward digesting both gelatin crosslinked with mTG and non-crosslinked gelatin and had no effect on BMP-2, it was chosen as a digestion agent in the current study to free the immobilized BMP-2. Although the binding sites where gelatin attaches

onto BMP-2 still need to be elucidated, they do not seem to be covalently binding to the active sites of BMP-2. When gelatin-mTG/BMP-2 is exposed to collagenase, these covalent bonds between gelatin and non-active sites of BMP-2 get digested by the added collagenase, however, if the bonds occurred at the BMP-2 active site, the residual gelatin fragment after digestion would have blocked the BMP-2 active site permanently [33].

To further examine the osteoinductivity of the retained protein and its ability to stimulate cellular behaviors when retained, ALP experiment has been conducted for 14 days. At day 7, the physically adsorbed-BMP-2 group had a higher ALP content when compared to the retained BMP-2 group, and significantly high when compared to the negative control group. This is because cells in the physically adsorbed BMP-2 were in a direct contact with the protein, which was bound to their BMP receptors upon seeding, stimulating them to achieve higher ALP levels in the first 7 days when compared to the cells in the retain BMP-2 group, which had to invade inside of the microsphere scaffold to come in a direct contact with gelatin-mTG/BMP-2 and start secreting cell-associated enzymes in order to degrade the crosslinked gelatin to free the bound BMP-2. At day 14, ALP content was the highest in the retained BMP-2 group when compared to the physically adsorbed-BMP-2 group, and significantly higher when compared to the negative control. This is due to the fact that in the retained BMP-2 groups, the protein was releasing in a sustained and controlled manner upon the enzymatic degradation of the crosslinked gelatin by the cell-associated enzymes activity, whereas in the physically adsorbed BMP-2, the entire protein was removed during the medium change at day 7, which caused the ALP activities to drop over time. These data demonstrate that the retention of BMP-2 did not negatively affect the osteoinductivity of the retained factor and thus, resulted in enhancing ALP activities in MC3T3 cells over time.

Previous reports have shown positive correlation between the retention of BMP-2 within the matrix upon implantation and the osteoinductive activity, owing to its significantly short *in vivo* half-life [30, 31]. On the other hand, several other studies have shown that direct injection of BMP-2 does not result in bone formation in the absence of a suitable carrier [27]. Clinical delivery of BMP-2, thus involves adsorption on a collagen sponge, which shows a burst release due to weak matrix–protein interactions [28, 29]. The burst release along with the supraphysiological doses used however, leads to side effects such as inflammation and ectopic bone formation. These findings demonstrate the potential of retaining BMP-2 within the gelatin matrix in maintaining the levels of osteoinductive activities of BMP-2 *in vitro* and *in vivo*.

3.5. Conclusion:

In conclusion, incorporation of growth factor coaxially at the core-shell of coaxial PLGA nanofibers resulted in a prolonged, sustained and controlled release of both growth factors PDGF-BB and IGF-I. Although both factors were incorporated within the same carrier, PDGF-BB expressed a slower release profile when compared to IGF-I. This might have been due to the thickness variations between the core-shell and the sheath in both growth factor carriers, or due to the fact that PDGF-BB has a larger molecular mass of 12.3 kDa when compared to IGF-I, which has a molecular mass of 7.6 kDa. Incorporation of BMP-2 within gelatin resulted in the retention of the protein. The retained proteins' bioactivities and osteoinductivities were examined through the ALP study conducted, resulting in an increase of ALP induction of the seeded MC3T3 cells over time for 14 days. This suggests that retention of the protein doesn't affect its bioactivities nor osteoinductivities. Our data suggest that both the coaxial nanofibers and gelatin-mTG are two promising drug carriers for effective tissue regeneration.

3.6 References:

1. Cross M., Dexter T. M. 1991. Growth factors in development, transformation, and tumorigenesis. *Cell* 64, 271–280. doi: 10.1016/0092-8674(91)90638-F
2. S. E. Epstein, S. Fuchs, Y. F. Zhou, R. Baffour, R. Kornowski, *Cardiovasc. Res.* 2001, 49, 532.
3. M. J. Post, R. Laham, F. W. Sellke, M. Simons, *Cardiovasc. Res.* 2001, 49, 522
4. Tayalia P, Mooney DJ. Controlled growth factor delivery for tissue engineering, *Adv Mater.* 2009 Sep 4; 21(32-33):3269-85. doi: 10.1002/adma.200900241.
5. Zhang BJ, Han ZW, Duan K, Mu YD, Weng J. *J Biomed Mater Res A.* 2017 Sep 7. doi: 10.1002/jbm.a.36210. [Epub ahead of print]
6. Nocini PF, Menchini Fabris GB, Gelpi F, Lotti J, Favero V, Zanotti G, Jurlaro A, Roszkopf I, Lotti T, Barone A, Castegnaro G, De Santis D. *J Biol Regul Homeost Agents.* 2017 Apr-Jun;31(2 Suppl. 2):1-13
7. Reckenbeil J, Kraus D, Stark H, Rath-Deschner B, Jäger A, Wenghoefer M, Winter J, Götz W. *Arch Oral Biol.* 2017 Jan;73:142-150. doi: 10.1016/j.archoralbio.2016.10.010. Epub 2016 Oct 15. PMID:27769028
8. Huang ZM, Zhang YZ, Kotaki M, Ramakrishna S. A review on polymer nanofibers by electrospinning and their applications in nanocomposites. *Compos Sci Technol* 2003; 63:2223–53
9. Jing Z, Xu XY, Chen XS, Liang QZ, Bian XC, Yang LX, Jing XB. Biodegradable electrospun fibers for drug delivery. *J Control Release* 2003; 92:227–31.
10. Su Y, Su Q, Liu W, Lim M, Venugopal JR, Mo X, Ramakrishna S, Al-Deyab SS, El-Newehy M. Controlled release of bone morphogenetic protein 2 and dexamethasone loaded

in core-shell PLLACL-collagen fibers f

11. Yang Y, Xia T, Zhi W, et al. Promotion of skin regeneration in diabetic rats by electrospun core-sheath fibers loaded with basic fibroblast growth factor. *Biomaterials*. 2011; 32:4243–4254.
12. Yang F, Murugan R, Wang S, et al. Electrospinning of nano/micro scale poly (L-lactic acid) aligned fibers and their potential in tissue engineering. *Biomaterials*. 2005; 26:2603–2610.
13. Michelle T. Poldervaart, Huanan Wang, Johan van der Stok, Harrie Weinans, Sander C. G. Leeuwenburgh, F. Cumhur Öner Sustained Release of BMP-2 in Bioprinted Alginate for Osteogenicity in Mice and Rats
14. Zhu, Junmin, and Roger E Marchant. “Design Properties of Hydrogel Tissue-Engineering Scaffolds.” *Expert review of medical devices* 8.5 (2011): 607–626. *PMC*. Web. 1 Oct. 2017.
15. Ikada Y, Tabata Y (1998) Protein release from gelatin matrices. *Adv Drug Deliv Rev* 31: 287–301.
16. Ikada Y, Tabata Y (1998) Protein release from gelatin matrices. *Adv Drug Deliv Rev* 31: 287–301.
17. Sandor M, Ensore D, Weston P, Mathiowitz E. Effect of protein molecular weight on release from micron-sized PLGA microspheres.
18. Chew SY, Wen J, Yim EK, Leong KW. Sustained release of proteins from electrospun biodegradable fibers. *Biomacromolecules* 2005; 6:2017–2024.
19. Casper CL, Yamaguchi N, Kiick KL, Rabolt JF. Functionalizing electrospun fibers with biologically relevant macromolecules. *Biomacromolecules* 2005; 6:1998–2007.

20. Liao IC, Chew SY, Leong KW. Aligned core-shell nanofibers delivering bioactive proteins. *Nanomedicine* 2006; 1:465–471
21. Li C, Vepari C, Jin HJ, Kim HJ, Kaplan DL. Electrospun silk-BMP-2 scaffolds for bone tissue engineering. *Biomaterials* 2006; 27:3115–3124.
22. Zhang YZ, Wang X, Feng Y, Li J, Lim CT, Ramakrishna S. Coaxial electrospinning of (fluorescein isothiocyanate-conjugated bovine serum albumin)-encapsulated poly(epsilon-cap-lactone) nanofibers for sustained release. *Biomacromolecules* 2006; 7:1049–1057.
23. Iang H, Hu Y, Li Y, Zhao P, Zhu K, Chen W. A facile technique to prepare biodegradable coaxial electrospun nanofibers for controlled release of bioactive agents. *J Controlled Release* 2005; 108:237–243.
24. Gupta RK, Chang A-C, Griffin P, Rivera R, Guo Y-Y, Siber GR. Determination of protein loading in biodegradable polymer microspheres containing tetanus toxoid. *Vaccine* 1997; **15**: 672–678.
25. Patel, Zarana S. et al. “Biodegradable Gelatin Microparticles as Delivery Systems for the Controlled Release of Bone Morphogenetic Protein-2.” *Acta biomaterialia* 4.5 (2008): 1126–1138. *PMC*. Web. 15 Oct. 2017.
26. Sambit Sahoo, Lay Teng Ang, James Cho-Hong Goh, Siew-Lok Toh Growth factor delivery through electrospun nanofibers in scaffolds for tissue engineering applications. ISSN: 1552-4965, 1552-4965, 1549-3296; DOI: 10.1002/jbm.a.32645. *Journal of biomedical materials research.* , 2010, Vol.93(4), p.1539-1550
27. H. P. Hsu, J. M. Zanella, S. M. Peckham and M. Spector, *J Orthop Res*, 2006, 24, 1660-1669
28. M. Geiger, R. H. Li and W. Friess, *Adv. Drug Deliv. Rev.*, 2003, 55, 1613-1629

29. W. Friess, H. Uludag, S. Fokkett, R. Biron and C. Sargeant, *Int. J. Pharm.*, 1999, 185, 51-60
30. M. Geiger, R. H. Li and W. Friess, *Advanced drug delivery reviews*, 2003, 55, 1613-1629
31. A. R. Poynton and J. M. Lane, *Spine*, 2002, 27, S40-48.
32. James B. Rose, Settimio Pacelli, Alicia J. El Haj, Harminder S. Dua, Andrew Hopkinson, Lisa J. White, Felicity R. A. J. Rose. Gelatin-Based Materials in Ocular Tissue Engineering. *Materials*, 2014, 7, 3106-3135; doi:10.3390/ma7043106
33. Kuwahara K, Fang JY, Yang Z, Han B. Enzymatic crosslinking and degradation of gelatin as a switch for bone morphogenetic protein-2 activity. *Tissue Eng Part A*. 2011 Dec; 17(23-24):2955-64. doi: 10.1089/ten.tea.2011.0290. Epub 2011 Sep 1
34. Kuwahara, K., Yang, Z., Slack, G.C., Nimni, M.E., and Han, B. Cell delivery using an injectable and adhesive transglutaminase-gelatin gel. *Tissue Eng Part C Methods* 16, 609, 2010.
35. Yung, C.W.; Wu, L.Q.; Tullman, J.A.; Payne, G.F.; Bentley, W.E.; Barbari, T.A. Transglutaminase crosslinked gelatin as a tissue engineering scaffold. *J. Biomed. Mater. Res. Part a* 2007, 83, 1039–1046.

CHAPTER 4

PRIMARY CELL ISOLATION, AND IN VITRO BIOCOMPATIBILITY AND CHARACTERIZATION OF THE THREE DIFFERENT CELLS CULTURED WITH THE RELEVANT PHASES

4.1.Introduction

The goal of regenerative engineering is to design a system capable of facilitating the regeneration of lost or damaged tissues. This may be accomplished by combining various species from the three primary components of tissue engineering: cells, growth factors and scaffolds.

4.1.1. Cells

Cells are the building blocks of the of tissues in the living organism, it is believed that cells present in the grafted tissue play a crucial role in effective and promising tissue healing and regeneration. Currently, most tissue engineering approaches involve isolating and expanding cells in vitro [1]. However, Cell source is an important parameter to consider when applying tissue engineering strategies to restore lost tissue and function [1].

Primary cells for instance, also referred to as mature cells, are differentiated cells that are committed to performing given cell type-specific functions. These cells are generally obtained via primary cultures originating from small pieces of donor tissue. For example, a small skin biopsy may be performed in order to isolate keratinocytes and dermal fibroblasts, the two main cell types in skin, or bone biopsy in order to isolate osteoblasts, the main cell type responsible for the synthesis of collagen type I in bone. Once isolated, these cells may be cultured and expanded

in vitro to yield the desired number of cells required for creation of tissue-engineered skin or bone [2].

One advantage of using mature cells in tissue engineering strategies is that it enables tissue-organ regeneration using the patient's own cells, thus eliminating concerns of immunogenicity. Additionally, many works have concentrated on characterizing many mature cell types and their responses to various biological factors, thus facilitating the tissue engineer's ability to predict and control cell behavior and tissue formation. However, in situations where a tissue sample of proliferative cells can be obtained using minimally invasive means, the use of primary cells as a component of the tissue engineering platform represents a viable strategy. Hence, skin, ligament and bone are examples of tissues that contain readily accessible mature cells that can grow outside the body and remain capable of generating their corresponding tissue type [3].

4.1.1.1.Primary Dermal Fibroblasts

Dermal fibroblasts are resident mesenchymal cells that are found between the epidermis and the hypodermis layer of the skin. Dermal fibroblasts are primarily responsible for synthesizing collagen, glycosaminoglycan and some other protein molecules including laminin and fibronectin [3,4]. These synthesized components by dermal fibroblasts support the structural and mechanical integrity of the skin. In addition, dermal fibroblasts are responsible for creating long fibrous bands of connective tissue which anchor the skin to the fascia of the body during skin. Therefore, without dermal fibroblasts, the largest and heaviest organ would not tightly adhere to body's frame. Dermal fibroblasts have been shown to play a vital role in supporting cutaneous wound healing and skin repair [3]. More importantly, autologous dermal fibroblasts are believed to promote skin

regeneration and rejuvenation, making them an ideal cell source for wound healing applications [5]. The wound healing process undergoes four major phases: homeostasis, inflammation, proliferation and remodeling [6]. During the third proliferative phase of the wound healing process, dermal fibroblasts begin to proliferate and migrate into the wound bed to produce extracellular matrix (ECM) proteins, which makes them critical during this phase. Extracellular matrix protein serves as a scaffold for inflammatory cell migration and granulation tissue generation. The generated granulation tissue act as a temporary substrate upon which re-epithelization by keratinocytes takes place to start regenerating the epidermal layer. In addition to the vital role of dermal fibroblasts in synthesizing the extracellular matrix through the production of ECM proteins and supporting re-epithelization, they further differentiate into myofibroblasts that generate wound contracture. Later, myofibroblasts-derived dermal fibroblasts undergo apoptosis resulting in a decreased cellular density while the remaining dermal fibroblasts begin to produce collagen type I. The unique plasticity of dermal fibroblasts as it transitions from producing ECM to promoting wound contracture to the synthesis of Type I collagen makes it an attractive candidate for cellular based therapies in wound healing [5, 6].

Dermal fibroblasts can be obtained through simple biopsy procedures where the skin is thoroughly cleaned and a small injection of a local anesthetic to numb the skin is made. A sample of skin is then taken by a biopsy from the numb area of the skin. The sample is then transferred under sterile conditions to for dermal fibroblasts isolations. Once isolated, these cells may be cultured and expanded in vitro to yield the desired number of cells required for creation of tissue-engineered skin [7]

4.1.1.2.Primary Ligament fibroblasts

Ligament fibroblasts are the main cell type of ligament, and are found entrapped with the collagen matrix of the ligament tissue. Ligament fibroblasts are primarily responsible for synthesizing collagen types I and III along with some other extracellular matrix proteins such as proteoglycans, elastin, fibronectin and laminin [8, 9]. Proteoglycans and elastin provide the ligament with the mechanical and structural support, whereas fibronectin and laminin serve as adhesive proteins [9]. These fibroblasts are also responsible for maintaining, repairing, and remodeling of the ligament [9]. Several studies have demonstrated the ability of ligament fibroblasts to enhance ACL regeneration marking them as the most suitable cells for the further study and development of tissue-engineered ligament [10]. In addition, pre-seeded grafts with mature ligament fibroblasts and implanted in a rabbit ACL model were shown to result in extensive collagen type I and III production as well as α -smooth muscle actin [11]. These findings demonstrate the potential of primary ligament fibroblasts to serve as a candidate for ligament tissue engineering.

Ligament fibroblasts can be obtained through biopsy procedures, where the knee joint is extended, and the area around the knee is deeply cleaned. A needle can be then inserted until it reached the ACL, and the biopsy can be taken. The sample is then transferred under sterile conditions to for ligament fibroblasts isolations. Once isolated, these cells may be cultured and expanded in vitro to yield the desired number of cells required for creation of tissue-engineered ligament [12]

4.1.1.3.Primary Osteoblasts

Osteoblasts are single nucleated cells and one of the three cell types found in human bone. They are specialized terminally differentiated products of mesenchymal stem cells that are responsible

for synthesis the bone's dense crosslinked collagen matrix including osteocalcin, osteopontin, osteonectin, osteoprotegerin (OPG), bone morphogenetic proteins (BMPs), and glycoproteins which compose the organic matrix of bone [13].

In organized and well-connected groups, osteoblasts participate in matrix mineralization through the production and deposition of hydroxyapatite and calcium phosphate, which provide strength to the bone. When an osteoblast is entrapped into the collagen matrix, it becomes an osteocyte, the most abundant cell type in bone. Bone is a dynamic tissue that is constantly being remodeled by osteoblasts, which produce and secrete matrix proteins and transport mineral into the matrix, and osteoclasts, which break down the tissues. Bone remodeling is a continuous process that lasts during the human's life maintaining the hemostasis of bone [13, 14]. Osteoblasts play a vital role in bone formation, growth and repair, as they are solely responsible for formation of the bony matrix [15]. Several studies have demonstrated the ability of osteoblasts to adapt with several substrates during osteogenesis, owing their vital role in bone tissue engineering [16, 17, 18].

Bone osteoblasts can be easily obtained from individuals through a bone biopsy procedure, where an incision through the skin is made to expose the area of the bone, followed by a needle insertion and extraction of the bone. The bone is then taken under sterile condition, where it undergoes digestion step to isolate the cells. Once isolated, these cells may be cultured and expanded in vitro to yield the desired number of cells required for creation of tissue-engineered bone [19].

4.1.1.4.Primary Cells Characterization

Primary cells are generally isolated from heterogeneous cellular environment, thus, characterizing their phenotype is important to ensure the homogeneity of the isolated cellular population. The phenotype of primary cells can be characterized either by their morphology, or based on the expression of specific cellular markers such as proteins or gene expressions. Morphological characterization is the simplest and the most direct way to characterize primary cells, and it is done by observing the cell size, shape and structure. For example, fibroblasts can easily be identified by their elongated flattened, oblong or triangular cytoplasm structure [20], and osteoblasts can be identified by their round, flattened structure [21]. On the other hand, cells can also be identified through the detection of specific markers such as proteins or genes that are only expressed by these cells via a specific combination of antibodies and the target antigen. These bound antibodies can then be detected using several different methods. For example, Immunocytochemistry (ICC) is one common method that is extensively being used in order to evaluate whether or not cells in a particular sample express the protein or gene in question. Briefly, an antibody is a secreted gene or protein that is found at the surface of the cell or intracellularly and it acts as a receptor for antigens. An antigen is a molecule that is produced to match a specific antibody intracellularly or at the surface of the cell after it comes into contact with it. Once the antigen is specifically bound to the antibody of interest, it can then be labeled with a secondary antibody for the detection of the expression of certain genes or proteins in the sample. In case the antigen was not specific to the antibody of interest (protein, gene), the secondary antibody will not find an antigen to bind into, and therapy no response will be initiated. However, in cases where the antigen is bound to the antibody of interest, the secondary antibody will find antigens to bind into resulting in the initiation of a tailored response that can be seen as colors or a fluorescent tag. The samples can then be

visualized using a fluorescence microscope to confirm the expression of the protein or the gene of interest [22].

4.1.1.5. Morphological Characterization and Specific Markers of Primary Dermal Fibroblasts

4.1.1.5.1. Morphological Characterization

Freshly isolated dermal fibroblasts can morphologically be identified by their well-known elongated flattened form, oblong or triangular. Dermal fibroblasts exhibit thicker central parts of the body and two narrow peripheral processes with smooth lateral edges. They may be 50 to 100 μm long, up to 30 μm at its broadest, and only about 3 μm at its thickest [20].

4.1.1.5.2. Dermal Fibroblasts Specific Marker

The lack of suitable dermal fibroblasts marker led to the poor understanding of the mechanisms that control the growth and activation of fibroblasts in vivo [29]. Recently, the effort of biologist led to the discovery of several markers that are believed to be specific for dermal fibroblasts and are used to confirm their phenotype [29]. Two of the most commonly measured dermal fibroblastic markers are Vimentin and TE-7.

4.1.1.5.2.1. Vimentin

Vimentin is an intracellular protein mainly located in the cytosol and it has been shown to be involved in wound healing in that it coordinates fibroblast proliferation and keratinocyte differentiation during healing process [24]. Vimentin is one of the most commonly used marker to identify dermal fibroblasts, and it can also be expressed in cells of mesenchymal origin including

mayofibroblasts [23]. Recent data showed that it plays a vital role in numerous cellular processes, with functions in cell adhesion, migration and invasion, signaling, differentiation, cytoskeletal rearrangements, and regulation of cell morphology and plasticity [24]. In relation to tissue repair, vimentin has been also shown to be involved in mesenchymal repair cells during to regulate the collective movement of the lens epithelium in response to an injury [25]. In wound healing, vimentin has been shown to show high level of expression following injures to directly be involved in regulating the cellular processes and interactions that are required for proper regeneration and healing, confirming its vita role to serve as an integrator of the processes that occur during wound healing [24]. The lack of vimentin can lead to a severe deficiency in fibroblast growth, and thus, minimizing their vital regenerative capacity [24]. These data suggest that vimentin can be used as a great candidate to identify dermal fibroblasts.

4.1.1.5.2.2.TE-7

TE-7 is a surface protein mainly located on the cell membrane of dermal fibroblasts [63]. Similarly, to vimentin, TE-7 is another fibroblast-specific connective tissue protein marker that can be used to identify dermal fibroblasts and distinguish them from other cell types such as human peripheral blood monocyte-derived fibrocytes, endothelial cells, chondrocytes, macrophages [26]. TE-7 antibody has been shown to serve as useful tool for the assessment of thymic epithelial culture contamination with dermal fibroblasts, and the identification of cells of mesodermal origin in the fetus, indicating its specificity to dermal fibroblasts [30]. Although TE-7 has been shown to be specific for dermal fibroblasts, it still can be expressed in other fibroblastic cells such as lung and muscle fibroblasts in varying densities, with the highest expression in dermal fibroblasts [27, 29] Minimal information is available regarding the protein.

4.1.1.6. Morphological Characterization and Specific Markers of Primary Ligament

Fibroblasts

4.1.1.6.1. Morphological Characterization

Similarly, to dermal fibroblasts, ligament fibroblasts also display either elongated, oblong or triangular cytoplasmic structure after they are freshly isolated. They also show a thicker central part and two narrow peripheral processes with smooth lateral edges. Ligament fibroblasts are known to make contact with their neighboring cells upon confluency. These contacts are adhesions that distort the known elongated structure of the freshly isolated fibroblasts. Upon the complete contact with the neighboring cells, they make a meshwork-like structure. This structure is one of the unique ways to recognize fibroblasts. Cells at the boarder of the meshwork display a concave-like structure that helps other neighboring cells to get in contact and thereby be part of the meshwork. It is believed that when fibroblasts display this smooth, slightly concave bordered meshwork structure, this is an indication that they are under considerable tension between their adhesions to neighboring cell. The tensions are very probably developed by an actin-myosin system [20, 28].

4.1.1.6.2. Ligament Fibroblasts Specific Markers

Ligament fibroblasts produce certain specific proteins that can be used as markers to confirm their phenotype. Two of the most commonly measured ligament fibroblastic markers used for ligament fibroblast identifications are markers are Scleraxis and Tenomodulin.

4.1.1.6.2.1 Scleraxis

The scleraxis protein is a member of the basic helix-loop-helix (bHLH) superfamily of transcription factors, and it is the earliest marker known for ligament and tendon [31]. Currently two genes (SCXA) and (SCXB) have been identified to code for identical scleraxis proteins [31]. It is believed that Scleraxis is expressed at the early stages of ligament and tendon formation, and at the early stages of the formation of some muscle/tendon attachments [32]. Previous studies revealed that scleraxis is a highly specific marker for all connective tissues mediating the attachments of muscle to bone, and bone to bone, indicating their specificity to tendons and ligament [32]. Scleraxis has shown to upregulate other genes that are strongly expressed in ligament and tendon tissues, such as collagen I, collagen XIV, tenomodulin (Tnmd), and fibroblast growth factor (FGF) [33, 34]. Both fibroblasts growth factor (FGF) and transforming growth factor beta 1 have been shown to play a vital role in the induction scleraxis during the development stages of ligaments and tendons [35]. Overexpression of Scleraxis was shown to induce ligamentous-lineage differentiation of MSCs and improves ligament formation [36]. Further, it was shown that cells expressing Scleraxis are necessary for the establishment of junctions between hyaline cartilage and tendons/ligaments [37]. These results suggest that SCX can be used as a suitable marker to identify ligament fibroblasts.

4.1.1.6.2.2 Tenomodulin

Tenomodulin, also referred to as (tendin), (myodulin), (Tnmd) and (TeM) is a type II transmembrane glycoprotein containing a C-terminal anti-angiogenic domain and is predominantly expressed in dense connective tissues including tendons and ligaments [38, 39]. Tenomodulin is localized on the X chromosome and accounts for an approximately 1.4 kb

transcript and a predicted protein consisting of 317 amino acids [40]. Although the exact function and mechanism of TNMD is still unclear, it was shown to play a vital role in ligament and tendons maturation [41, 42]. The lack of TNMD was shown to increase the deficiency of tenocytes proliferation in newborn mice and disrupted adult collagen fibril structure [43]. The proliferation, migration and tube formation of vascular endothelial cells were shown to be inhibited by the soluble form of TNMD containing the C-terminal ChM-I like domain, in addition to blocking the growth of malignant melanoma by inhibiting angiogenesis [44]. Therefore, marking it as a suitable phenotypic marker for later events during ligaments and tendons development.

4.1.1.7. Morphological Characterization and Specific Markers of Primary Osteoblasts

4.1.1.7.1. Morphological Characterization

Freshly isolated bone osteoblasts are known to display a flattened and slightly slender structure. During the first few days post isolation, these cells normally are sparse and display relatively short cytoplasmic processes of 2-5 μm in length. Once reached confluency, osteoblasts no longer maintain their slender shape and they become smaller and create a meshwork [21].

4.1.1.7.2. Osteoblasts Specific Markers

Certain molecular components are produced by osteoblasts that can be employed as specific marker to confirm their phenotype. However, every marker is known to contribute in the bone homeostasis and also known to have a specific location related to its function [45]. Two of the most commonly measured osteoblastic markers are Alkaline Phosphate (ALP), and osteocalcin (OCN).

4.1.1.7.2.1. Alkaline Phosphate (ALP)

Alkaline Phosphate (ALP) is an enzyme that causes the phosphate ester to be hydrolyzed from different types of molecules such as nucleotides and proteins. ALP was named according to its enhanced activities at high pH levels [45]. Although it can be found within all tissues of the human body, it highly concentrates in number of tissues such as bone, liver, placenta, and kidney [45]. ALP is known to be found in three different isoenzymes forms which are, tissue non-specific, intestinal, and placental. The tissue nonspecific isoenzyme is found in bone tissue, in an isoform that can be differentiated from its two other isoforms (found in the liver and kidney) according to their different carbohydrate moieties on the same polypeptide backbone [45, 46]. ALP has been shown to participate in the bone mineralization process [47]. In bone, ALP is a glycoprotein that is found on the cell membrane of osteoblasts, and is known to be one of the most commonly measured phenotypic osteoblast marker [48]. In stem cells, ALP expressions are known to be at their lowest comparing to already matured fully differentiated cells osteoblasts [48, 49]. These finding indicate that ALP is a great candidate that can be used as an osteoblastic marker to identify their phenotype.

4.1.1.7.2.2. Osteocalcin (OCN)

Osteocalcin (OCN) is the most abundant non-collagenous protein in bone tissue. OCN is a calcium-binding protein that is extensively produced by fully differentiation osteoblast, and its function is dependent on vitamin K [50]. Although the exact mechanism of how OCN functions is not clear, it is known for its vital role in the bone mineralization process, as it supports the binding of calcium phosphate CaP to the bone matrix. Only in the presence of ionic calcium, OCN can contain gamma- carboxy-glutamic acid (Gla), which allows it to undergo a specific conformational

change that permits the protein to bind to the bone mineral [50]. Since OCN largely supports the bone mineralization process, it is primarily synthesized at the early stages of the matrix mineralization or may be synthesized during the matrix mineralization stages of osteoblastic development [45]. Therefore, during these mineralization development stages, osteoblasts intend to produce large amounts of OCN that some of it that can also be emitted into the blood. It is for this reason that serum levels of OCN are considered to be indicative of new bone formation. These findings suggest that OCN can be used as an indicative marker for matured primary osteoblasts.

4.1.2. Scaffolds

4.1.2.1. General Scaffold Requirements

Beside the vital role of cells in tissue engineering, scaffold is another essential component that act as the framework for tissue regeneration. Scaffolds essentially act as a template for tissue formation and usually seeded with healthy isolated cells or/and incorporated with growth factors, depending on the application needs [51]. Ideally, a scaffold should provide cells with a variety of physical, chemical, and biological cues that are naturally inherited by the native ECM to facilitate cell growth and function [52]. In vivo, cells are found entrapped within an ECM, in which they are provided with all the necessary physical and chemical cues that guide their development, arrangement and regenerative abilities by molecular interactions between specific cell membrane receptors and signaling cues from surrounding ECM material [52]. To duplicate the in vivo environment, the scaffold should exhibit controllable physical, chemical and mechanical properties, cell adhesion properties and growth factor release kinetics [53]. Generally, an ideal tissue engineering scaffold should be biocompatible that maintains cell viability in vitro and do not elicit any immune response upon implantation in vivo. In addition, the scaffold should be

biodegradable with a degradation rate compatible to the rate of the neotissue formation to fully be replaced with newly formed tissue. The scaffold should also be highly porous to facilitate cell migration, proliferation, nutrition diffusion and waste removal, and should also exhibit biomimetic mechanical and architectural properties resembling those found at the native tissue [54]. In addition, the scaffold should serve as a reservoir for local, sustained, and controlled growth factors delivery to regulate cellular activities in order to help induce neovascularity and promote tissue regeneration.

4.1.2.2. Scaffold Materials

Providing a proper niche for cell adhesion, migration, and proliferation is generally based on the material choice. Biomaterials used for tissue engineering scaffold are mainly classified into two categories, naturally derived and synthetic biomaterials. Natural biomaterials can be further classified into proteins (silk, collagen, gelatin, fibrinogen, elastin, keratin, actin, and myosin), polysaccharides (cellulose, amylose, dextran, chitin, and glycosaminoglycan), or polynucleotides (DNA, RNA). Natural biomaterials are known for their excellent biocompatibility, bioactive properties, and good interactions with cells, owing to enhanced cellular performance in biological systems [55]. Despite all of their advantages, natural biomaterials possess poor physical and mechanical properties, which limit their use for load-bearing applications. Synthetic biomaterials on the other hand, are further characterized into degradable and non-degradable synthetic polymers. Biodegradable synthetic polymers are preferred over the non-degradable polymers due to their degradability nature, which in turn facilitates a faster neo-tissue ingrowth and better tissue infiltration, in addition to minimizing the chance for a secondary surgery after implantation [55]. A wide range of synthesized biodegradable polymers such as, poly(lactic acid) (PLA), poly(glycolic

acid) (PGA), poly(lactic-co-glycolic acid) (PLGA), poly-L-lactic acid (PLLA), and polycaprolactone PCL, have been used for many musculoskeletal tissues and skin tissue engineering due to their intrinsic tailored properties [55]. Although synthetic polymers have the advantages of tailoring their properties such as, porosity, degradation rate, physical and mechanical characteristics for specific applications and needs, they possess poor biocompatibility and lack all the ligands required for cell attachments and proliferation, which can result in poor cell adaption to the matrix and thus, poor tissue formation. Limitations associated with both natural and synthetic biomaterials limit their use on their own in many tissue engineering applications where both mechanical and biocompatibility are highly required. The native ECM resembles some properties that are found in synthetic materials only or natural materials only, therefore, composite scaffolds are the best solution to address the disadvantages of both natural and synthetic scaffolds, as it helps in the mutual enhancement of the scaffold properties and thereby allowing controlled degradation and mechanical properties as well as improving the biocompatibility, and providing cells with all the necessary physical and chemical cues that are naturally inherited by the natural ECM, to achieve the best possible biomimicry of the native ECM [56].

One great example of a composite biomaterials that is suggested to be used in skin, ligament and bone tissue engineering is PLGA/Gelatin. PLGA is known for its tailored mechanical and degradation properties in addition to the easy processability into a wide variety of different structures; and gelatin is known to inherit all the necessary arginine-glycine-aspartic acid (RGD) sequences that allows for enhanced cell adhesion, and it is less immunogenic [57, 58]. However, this elegant combination between PLGA/gelatin, in which PLGA provides the mechanical and structural support to the scaffold, whereas gelatin influences cell adhesion and proliferation is

expected to positively influence tissue regeneration. Norouzi et al. developed a PLGA/gelatin coaxial electrospun nanofiber scaffold for skin regeneration. In this study, gelatin was coaxially electrospun with PLGA where the core-shell was consisted of gelatin to increase biocompatibility and cellular adhesion and the fiber sheath was consisted of PLGA for mechanical reinforcement. The scaffold was pre-seeded with human dermal fibroblasts and the scaffold's biocompatibility along with the gene expression of collagen type I and III have been evaluated [81]. *In vitro* results showed a significant increase in cell number over time along with extensive production of collagen type I and III when compared to the control, indicating the potential of PLGA/gelatin composite to serve as a scaffold material for wound healing applications and suggesting that it can serve a composite biomaterial for other tissue engineering application such as ligament TE. Additionally, PLGA/gelatin as a biomaterial has been shown to enhance osteoblasts adhesion and proliferation *in vitro* and bone regeneration *in vivo* [82]. Findings from these studies demonstrate the potential of PLGA/gelatin to serve as a composite biomaterial for various tissue engineering applications.

4.1.3. Growth Factors Delivery

Growth factors are endogenously secreted in the body by cells themselves, but in very minimal amounts that cannot aid in tissue regeneration in the case of large trauma, which necessitates the sustained and controlled delivery of exogenous growth factors to aid in the regeneration process. As discussed in section 3.1., several methods can be employed in order to achieve a sustained and controllable release over growth factors for more effective tissue regeneration outcomes. It was demonstrated that incorporation of growth factors in the core-shell of the fiber during electrospinning will result in the production of a scaffold that can serve as a great candidate for sustained and controlled with minimal burst release. In addition, gelatin hydrogel was

demonstrated to be a good drug delivery vehicle for growth factors. Thus, providing the most suitable growth factor delivery profiles is crucial for functional tissue regeneration. Growth factors are soluble-secreted signaling polypeptides capable of instructing specific cellular responses in a biological environment [59]. Cell producing Growth factors has the ability to elicit an effect from either itself, or another targeted cell. According to their function, growth factors can be autocrine, paracrine or endocrine [64]. Autocrine growth factors signal back to the cell from which they are secreted, paracrine growth factors signal to neighboring cells, and endocrine growth factors are secreted into the blood stream in order to travel to distant target cells [64]. Cells reside in metabolically active tissues are more likely to continually respond to dynamic combinations of factors that provide them with information about their surrounding environment.

According to their effect, growth factors can further be classified into cytokines or chemokines. Cytokines are growth factors that stimulate proliferation or differentiation of the target cell, while chemokines are growth factors that induce cellular migration [64]. Cells receive information from growth factors through specific bindings of the growth factors to their corresponding cell receptors, which are found integrated in the cell's plasma membrane. Once the growth factor is bound to its specific associated receptor, an intercellular response is stimulated [64]. The specific cellular response triggered by growth factor signaling can result in a very wide range of cell actions, including cell survival, and control over migration, differentiation or proliferation of a specific subset of cells. Several growth factors have been extensively used for tissue engineering applications such as BMP-2, for bone tissue regeneration [60], PDGF-BB and IGF-I for mostly skin, and ligament tissue regeneration applications respectively [61, 62].

4.1.3.1. Platelet-Derived Growth Factor-BB (PDGF-BB)

PDGF is a dimeric glycoprotein from a superfamily that include various forms of PDGF such as PDGF-BB, AA, and AB, depending on the composition of the two molecular chains of the dimer. It was originally isolated from platelets, but it is now known to be secreted by many cell types [65]. PDGF is involved throughout all stages of normal wound healing and is known to stimulate the chemotaxis of a variety of cell types including fibroblasts. It mainly stimulates the proliferation of fibroblasts and other originating mesenchymal cell and is involved in macrophage activation during wound healing [66]. In addition to its ability to promote tissue remodeling by stimulating fibroblasts to produce both collagenase and collagen, PDGF-BB is responsible for the differentiation of fibroblasts into their contractile phenotype, therapy resulting in accelerated wound healing [67]. PDGF-BB was shown to decrease the wound volume dramatically after skin injuries in humans [68]. Additionally, it was shown that wounds treated with PDGF-BB had higher level of fibroblasts differentiation in vitro and neovascularization in vivo comparing to controls in humans [69]. these findings suggest that PDGF-BB correlate in extensive collagen production and reduced wound volume during wound healing, owing its vital role for wound healing application and skin regeneration.

4.1.3.2. Insulin-Like Growth Factor-I (IGF-I)

IGF-I, also called somatomedin C, is a human protein encoded with IGF1 gene [70]. IGF-I is also a hormone that plays an important role in childhood growth and continues to have anabolic effects in adults, making it ideal for the treatment of growth failure [70]. IGF-I is produced throughout the human's life, with a highest rate of production during the pubertal growth spurt, and starts to lower in production as the person ages [71]. IGF-I is primary produced by the liver as an endocrine hormone as well as in target tissues in a paracrine/autocrine fashion [72]. In ligament

tissue engineering, IGF-I was shown to increase the metabolic activities and proliferation of ligament fibroblasts both in vitro and vivo in a rabbit MCL model, which resulted in enhanced healing of the ruptured ligament [73]. In addition, IGF-I is believed to attribute to an anti-inflammatory effect in vivo, therapy decreasing the recovery time after tendon and ligament injuries [74]. It was also reported that ligament treated with IGF-I in combination with PDGF had increased rupture force, stiffness, and breaking energy in vivo [75]. Additionally, IGF-I was shown to enhance the proliferation and osteogenic differentiation of human ligament fibroblasts, resulting in enhanced ligament-bone osteointegration [76]. These promising findings demonstrate the role of IGF-I in enhancing ligament healing and regeneration.

4.1.3.3 Bone Morphogenetic Protein 2 (BMP-2)

Bone Morphogenetic Proteins are part of the transforming growth factor- β (TGF- β) gene superfamily. Several reports have highlighted the important role of BMPs in the development of bone and cartilage [77]. Bone Morphogenetic proteins are known to regulate in the formation of new cartilage and bone by binding to extracellular receptors that, like all TGF- β proteins, are serine/threonine receptor kinases. This binding however, stimulates intracellular kinases to initiate a cascade of events that ultimately leads to mRNA-directed production of proteins such as osteocalcin and alkaline phosphatase, which are necessary for bone remodeling and mineralization [77]. Although many types of BMPs have been extensively studied for their osteoinductive capabilities, BMP-2, 4 and 7 are the most commonly used and studied members of the growth factor family due to the fact that their receptors have been well identified [78]. BMP-2 for instance, is known to promote the differentiation of cells into the osteoblast lineage and upregulate the calcification of bone defects, which can result in increased bone formation [79]. Additionally, it

was shown that BMP-2 can enhance the proliferation of mature osteoblasts and promote their production of collagen and other extracellular matrix proteins, which results in enhanced bone formation [80].

In this aim, we sought to isolate and characterize three different primary cells, dermal fibroblasts, ligament fibroblasts as well as osteoblasts. Post characterizations, the three different cell types will be further used to investigate the capability of the three different phases with the integrated graft system to support their viability and proliferation at different time points. In addition, the effect of the different growth factors incorporation methods (coaxial Vs uniaxial, or gelatin incorporation Vs. surface absorption) and releasing profiles (minimal burst release Vs. rapid burst release) on the cell proliferation will be investigated.

4.2. Materials and Methods:

85:15 Poly(lactide-co-glycolide) (PLAGA) (MW ~ 94,000 kDa) was purchased from (Absorbable Polymers, Birmingham, AL, USA), Hexafluoro-2-propanol (HFIP) was purchased from (Acros Organics, USA), Gelatin Type A from Pork (Porcine skin) was purchased from (MP Biomedical, OH, USA), Microbial Transglutaminase (mTG) was Purchased from (Ajinomoto, Japan), Dichloromethane (DCM) was purchased from (Fisher Scientific, USA), PDGF-BB, IGF-I and BMP-2 growth factors were purchased from (Fisher Scientific, USA), Dulbecco's Phosphate-Buffered Saline (PBS) of pH 7.4, MEM Alpha (1X) Minimum Essential Medium, DMEM/F-12 (1:1) (Dulbecco's Modified Eagle Medium/Nutrient Mixture F-12), Antibiotic-Antimycotic (100X), Trypsin-EDTA (0.25%) phenol red, Fetal Bovine Serum, Qualified, Penicillin-Streptomycin (10,000 U/mL), and Hank's balanced salt solution (HBSS) were purchased from Gibco (Grand Island, NY), collagenase type I powder was purchased from (ThermoFisher Scientific, IL, USA), Liberase Blendzyme 3 was purchased from Sigma-Aldrich (Milwaukee, WI), primary antibodies, IgG monoclonal unconjugated Anti-Alkaline Phosphatase (ab108337), IgG3 monoclonal unconjugated Anti-Osteocalcin antibody (ab13420), IgG monoclonal unconjugated Anti-SCXA antibody (ab58655), IgG monoclonal unconjugated Anti-tenomodulin antibody (ab203676), IgG monoclonal unconjugated Anti-TE-7 antibody (ab197896), IgG monoclonal unconjugated Anti-Vimentin antibody (ab92547), and the compatible secondary antibodies, IgG polyclonal Goat Anti-Rabbit IgG H&L (Alexa Fluor® 488) (ab150077), and IgG polyclonal Goat Anti-Mouse IgG H&L (Alexa Fluor® 488)(ab150113) were purchased from (Abcam, MA, USA), DAPI (4',6-Diamidino-2-Phenylindole, Dihydrochloride), and anti-fade mounting medium, LIVE/DEAD™ Viability/Cytotoxicity Kit were purchased from (Invitrogen, USA), and CellTiter

96® AQueous One Solution Cell Proliferation Assay (MTS) was purchased from (Promega Inc, USA).

4.2.1 Fabrication of PLGA-Gelatin Coaxial Nanofiber Scaffolds

As described previously, PLGA (85:15) granules were dissolved in HFIP at 16 % wt and stirred overnight at room temperature to prepare the (shell solution) of nanofibers. To prepare the core solution, gelatin powder type A was dissolved in HFIP at 4% wt and stirred overnight at room temperature. At the day of electrospinning, both growth factors were reconstituted at a concentration of 1 mg/ml, and 81 µl of the reconstitution of either PDGF-BB and IGF-I were added to 1.5 ml of gelatin solutions and stirred for 15 minutes to allow the growth factor to homogenize with the gelatin solution. In the case of coaxial nanofibers with no growth factors, gelatin solution was used alone in the core-shell. An electrospinning pump (NE 300 SYRINGE pumps, USA) was used alone in the core-shell. An electrospinning pump (NE 300 SYRINGE pumps, USA) was used in order to fabricate the coaxial PLGA-Gelatin nanofibers. The setting to prepare the coaxial scaffolds consisted of two coaxial syringe pumps with different flow rates. In this study, the PLGA solution was used to form the outer shell and the gelatin-growth factors or free of growth factors solutions were used to form the inner core. PLGA solution or either gelatin-growth factors or free of growth factors solution were loaded into two separate 10 ml syringes and connected to the coaxial needles, a 16 G (ID = 1.6 mm) outer needle and a 22 G (ID = 0.7 mm) inner needle, respectively, and then concentrically placed. The electrospinning parameters were as follows: (applied voltage: 10 kV; 1.5 mL/h for the sheath flow rate and 0.75 mL/h for the core flow rate). The tip of the needle was placed 10 cm away from the collector. The electrospinning process lasted for 1.5 h. Coaxial electrospun nanofibers were peeled from the collector and stored under vacuumed desiccator for 24 hours to insure complete evaporation of solvent.

4.2.2 Fabrication of PLGA Uniaxial Nanofiber Scaffolds

PLGA (85:18) granules were dissolved at 16% wt in HFIP with stirring to form clear, homogeneous, and viscous solution. From the same batch used for the coaxial nanofibers fabrication, 81 μ l reconstitution of both PDGF-BB and IGF-I were directly added to 3.5 ml of PLGA solution and stirred for 30 minutes to allow the growth factor to homogenize with the polymer solution. In the case of uniaxial nanofibers with no growth factors, PLGA solution was electrospun alone. PLGA-growth factors or PLGA solutions were loaded into 10 ml plastic syringe and electrospun at flow rate of 0.75 mL/h through a 20-gauge blunt needle with the electrospinning pump (NE 300 SYRINGE pumps, USA) at an applied voltage of 10 kv. The tip of the needle was placed 10 cm away from the collector. The electrospinning process lasted for 3.5 h. Uniaxial electrospun nanofibers were peeled from the collector and stored under vacuumed desiccator for 24 hours to insure complete evaporation of solvent.

4.2.3 Fabrication of PLGA Microspheres

As previously described, single emulsion solvent evaporation technique was used to fabricate PLGA microspheres. PLGA granules were dissolved at 12.5% wt in Dichloromethane (DCM) in glassy vials. Vials were vortexed for 1 h at a speed of 550 RPM until clear, homogeneous, and viscous solution was obtained. Next, PLGA solution was added via a thin stream into 1% PVA solution in a 1000 ml beaker and it was let to stir at (300 RPM) overnight to allow the solvent to evaporate. After that, microspheres were collected, filtered, air dried and then they were stored in -20 for 24 h to freeze any residual water particle inside of the microspheres. Next, microspheres were freeze dried for 48 h and were then sieved to obtain the desired particle size range 300 – 600 μ m.

4.2.4 Incorporation of BMP-2 in Gelatin-mTG Hydrogel

Gelatin gel formation was initiated by mTG addition. For hydrogel preparation, 3% wt gelatin powder type A was dissolved in preheated phosphate-buffered saline (PBS) at 50 °C and it was let to stir on a stirrer plate for 15 minutes at 500 RPM to completely dissolve the powder. The mTG solution was prepared by dissolving 10% wt mTG in preheated PBS at 50 °C, then it was let to stir on a stirrer plate for 15 minutes at 500 RPM. As soon as both gelatin and mTG completely dissolved in PBS, the temperature of the stirrer plate was adjusted to 37 °C and they were let to stir for another 15 minutes to allow for the temperature drop. Next, to initiate the cross-linking reaction between gelatin and mTG for the hydrogel preparation, mTG solution was mixed with the 3% wt gelatin solution at a ratio of 1:11.5 under stirrer speed of 500 RPM at 37 °C. The mixture was let to stir for 5 minutes until a semi-viscus solution is fabricated and ready to be injected. BMP-2 incorporation was done by adding 1 µg of BMP-2 in 100 µl of gelatin-mTG solution and mix them gently.

4.2.5 Fabrications of PLGA Microspheres Scaffold Incorporated Gelatin-mTG/BMP-2

To fabricate the three-dimensional scaffolds and use it to either incorporate gelatin-mTG/BMP-2 or gelatin-mTG hydrogels within it, PLGA microspheres were poured into a 10 mm x 10 mm stainless steel mold and heated for 90 °C for 90 minutes. These parameters allowed the microspheres to fuse together forming the 3D scaffolds. After 90 minutes, the stainless-steel mold was removed from the oven and allowed to cool to room temperature for 2 hours. Next, scaffolds were removed and the semi-viscus gelatin-mTG/BMP-2 hydrogel was injected inside of the microsphere scaffold using an insulin syringe until all porosity were filled and it was allowed to gel at 37 °C for 1 hours. In the case of the physical adsorption, 1 µg of BMP-2 was physically

poured on PLGA-Gelatin-mTG microsphere scaffolds and was let to dry out for 1 h to ensure attachment of the protein.

4.2.6 Primary Cells Isolations

6-8 weeks old (150 – 200 g) Lewis rats were obtained from (Charles River Laboratories, CT, USA) and used for all primary cell isolations. All the animal experiments were approved by the Institutional Animal Care and Use Committee (IACUC) at the University of Connecticut Health Center, CT, Farmington, USA.

4.2.6.1 Primary Dermal Fibroblasts Isolation and in Culture Maintenance

Animals were euthanized with CO₂ for 10 minutes until they are ready to be handled. Next, cervical dislocation technique was performed after euthanizing the animals with CO₂ to confirm the death of the animals. Animals were lightly sprayed with 70% ethanol, and more extensively around the incision site to prevent any chance of having contamination. Skin from underarm was selected to be dissected because skin in that particular site is usually thinner, contains less fat, and the fur is less dense. The fur around the site of incision was completely shaved with a sharp scalpel. Approximately 1 cm² of skin fragment was collected by pinching the skin with a tissue forceps, and carefully cutting with scissor with paying attention not to cut the fat layer with the skin. Dissected tissue fragment was then placed in in 50 mL tubes containing sterile PBS with 1% Antibiotic-Antimycotic. Under the hood, the tissue fragment was transferred into a 10-cm tissue culture dish and it was cut into small pieces (~ 1 mm) using a scalpel. Using the same scalpels, the small skin fragments were transferred into a sterile 30 mL beaker with a sterile stir bar containing

30 mL DMEM/F12 medium with 0.14 Wunsch units/ mL Liberase Blendzyme 3, and 1% Antibiotic-Antimycotic. The beaker was covered with sterile alumni foil and incubated at 37 °C stirring slowly for 120 minutes. Next, the solution with the tissue fragments were transferred into a sterile 50 mL tube, and 20 mL of DMEM/F-12 medium supplemented with 15% FBS, and 1% Antibiotic-Antimycotic was added to the solution to stop the Liberase digestion. The tube was then placed for centrifugation and was centrifuged at 524 g for 5 minutes. Next, the supernatant was removed and the pellet was re-suspended with 40 ml of warm of DMEM/F-12 medium supplemented with 15% FBS, and 1% Antibiotic-Antimycotic and it was centrifuged again for 5 minutes. This process was repeated 2 times to insure the complete removal of the trace Liberase. At the last centrifugation cycle, the supernatant was removed, and the pellet was resuspended with 10 mL of DMEM/F-12 medium supplemented with 15% FBS, and 1% Antibiotic-Antimycotic and transferred into 10 cm tissue culture dish and placed in a tissue incubator at 37°C, 5%CO₂, 3%O₂. The tissue culture plate was let for 7 days at the incubator without changing the medium to allow all cells to exit the tissue fragments and to adhere on the TCP. At day 7, the medium was changed and it was let for another 7 days to allow the cells to completely exit the tissue fragments and adhere on the TCP. After 14 days, cells were trypsinized with 0.25 EDTA trypsin, harvested, and plated on new T-75 flasks at a density of 5×10^5 cells/flask with EMEM supplemented with 15% FBS, 1X Penicillin/Streptomycin, non-essential amino acids, and sodium pyruvate. EMEM media will support growth of fibroblasts only and other cell types will die or stop proliferating. Cells were never frozen and were used at the second passage for further experiments.

4.2.6.2 Primary Ligament Fibroblasts Isolation and in Culture Maintenance

All animals were euthanized following the same procedure as mentioned previously for ligament

dissections and isolation. The area around the knee was extensively sprayed with 70 % ethanol and scrubbed with betadine scrub solution to kill all bacteria around the incision site, then it was draped. A straight midline longitudinal incision was made using a blade, extending from the distal fourth of the femur to the tibial tuberosity. The skin and the subcutaneous fascia were retracted to expose the patellar tendon, which was then excised by a parapatellar incision that runs the length of the tendon from the tibial to the sartorius muscle. The tendon was then bisected, and the fat pad and the patella were dissected from the tendon. A deeper incision into the joint capsule was made to expose the femoral condyles and the tibial plateau. The ACL and MCL (anterior cruciate ligament and medial collateral ligament) were transected from the bone insertion sites at either ends to insure a dissection of a full ACL and MCL. The dissected ligaments were placed in sterile 50 mL tube containing PBS with 1% Penicillin/Streptomycin. Under a sterile tissue culture hood, the ligament fragments were transferred into a 10 cm tissue culture dishes with 2 ml of PBS to keep the tissue hydrated. Ligaments were diced into very small pieces of approximately 1 mm using a sharp scalpel. Using the same scalpels, the small ligament fragments were transferred into a sterile 30 mL beaker with a sterile stir bar containing 30 mL of filtered collagenase type I solution in DMEM/F-12 medium with 1% Penicillin/Streptomycin. The beaker was covered with sterile alumni foil and incubated at 37 C stirring slowly for 4 hours. Next, the solution was poured through 70 um nylon mesh to hold any undigested tissue fragments. 20 mL of fresh and warm DMEM/F-12 supplemented with 10% FBS and 1% P/S was added to the solution to stop the collagenase digestion, then it was centrifuged at 500g for 10 in a sterile 50 mL tube. Post centrifugation, the supernatant was removed, and the pellet was resuspended with 1 mL of fresh warm DMEM/F-12 medium supplemented with 10% FBS and 1% P/S. cells were plated in 25 cm flask and 4-5 mL medium was further added. Flask was placed in a tissue incubator at 37°C, 5%CO₂, 3%O₂. Medium

was changed every 2 days, and 7 days post plating, when the flask reached ~ 90% confluence, cells were trypsinized with 0.25 EDTA trypsin solution and harvested then plated into a new T-150 flask at a density of 6×10^5 cells/flask for further expansion. Cells were never frozen and were used at the second passage for further experiments.

4.2.6.3 Primary Bone Osteoblasts Isolation and in Culture Maintenance

All animals were euthanized following the same procedure as mentioned previously for long bone dissections and isolation. The area around the femur was extensively sprayed with 70 % ethanol and scrubbed with betadine scrub solution to kill all bacteria around the incision site. A straight midline longitudinal incision was made using a blade, extending from the distal end of the knee joint to the hip joint. The skin and the subcutaneous fascia were retracted to expose the long femur bone. Muscles covering the femur were removed with a sharp scalpel to clearly expose the bone. The long femur bone was dislocated from the proximal hip joint and the distal knee joint by transecting all ligament and tendons at both joints until it became mobilized. Bone was then dissected and placed in a 50-mL tube containing sterile PBS with 1% Penicillin/Streptomycin. Under a sterile tissue culture hood, bone was placed in a 10-cm tissue culture dish containing 10 mL of sterile PBS. The remaining muscles and connective tissues covering the long bone as well as the periosteum were removed using a scalpel. After removing all residual tissues, bones were further rinsed with PBS and placed in a new tissue culture plate containing fresh 10 mL PBS. The bone epiphyses were cut off and the bone marrow was flushed out using a needle and a syringe. Flushing step was repeated several times, each time with fresh PBS until all bone marrow has been flushed out. Bones were then placed in a new tissue culture dish with fresh 10 mL PBS and it was cut in half lengthwise and then cut into 1 – 2 mm long using a scalpel. After cutting bones into

small pieces, they were placed in fresh PBS for a brief wash. Next, four digestion cycle have been performed on the bone pieces to isolate osteoblasts as follows; (**Digest 1**) was done by incubating the bone pieces in 8 ml of warmed collagenase solution (filtered 1% collagenase type I in PBS) for 1 hour in the 37 °C room on a rocker set at 5 RPM. 1 hour after incubation, the entire solution was aspirated and transferred in a new tube, bone pieces in the old tube were rinsed with 5 ml of HBSS three times with aspirating the solution to the new tube in every time. Collagenase with the HBSS aspirates in the new tube was centrifuged for 5 minutes at 500 g until a pellet was obtained, then the pellet was resuspended with MEM Alpha (1X) Minimum Essential Medium supplemented with 15% FBS and 1% Penicillin/Streptomycin, and then plated in a six-well tissue culture plate with 5 ml medium. Another 8 mL of the collagenase solution were added to the bone pieces to further digest them for 1 h to get to the second digest cycle. For **digest cycle 2, 3, and 4** the same procedure from digest cycle 1 was repeated. After completing digest cycle 4, bone pieces were places in another six-well tissue culture plate with 5 ml of MEM Alpha (1X) Minimum Essential Medium supplemented with 15% FBS and 1% Penicillin/Streptomycin per well and maintained in a tissue culture incubator at 37°C, 5%CO₂, 3%O₂. Medium was changed every 3 days, and 7 days post plating, when all the wells reached ~ 90% confluence, cells were trypsinized with 0.25 EDTA trypsin solution and harvested then plated into a new T-150 flask at a density of 6 X 10⁵ cells/flask for further expansion. Cells were never frozen and were used at the second passage for further experiments.

4.2.7 Morphological and Immunofluorescence Phenotypic Characterization of the Isolated Primary Cells

Primary cells are usually isolated from a heterogeneous cellular population, however, there is a

very high chance that these isolated primary cells are contaminated with other cellular populations. To ensure the homogeneity within the isolated cellular population, these cells must undergo phenotypic characterizations steps. Morphology and Immunofluorescence phenotypic characterization are some of the most commonly used methods to characterize isolated primary cells.

4.2.7.1 Morphological Characterization of the Isolated Primary Cells

For morphological characterization, the three different cell types in the culture dishes were fixed in 2.5% glutaraldehyde in 0.1 M cacodylate for 20 min. They were then rinsed with PBS for 5 min, then they were incubated in 1 % osmium tetroxide for 20 min, then dehydrated in a graded series of alcohol (cold 30%, cold 70%, 95% and 100%), and subsequently samples were let to dry overnight under a chemical hood. Cells were then visualized under a normal light microscopy, and pictures at low (10 X) and high (40 X) magnifications were taken.

4.2.7.2 Immunofluorescence Phenotypic Characterization of the Isolated Primary Cells

For Immunofluorescence characterization, large coverslips were autoclaved for sterilization, and then placed in sterile six-well tissue culture plates. The three different cell types were separately cultured (each cell type in a separate plate) over the cover slips for 2 days at a density of 5×10^3 per well and maintained in a tissue culture incubator at 37°C, 5%CO₂, 3%O₂. Every cell type was maintained in culture with 5 mL of the relevant medium type, MEM supplemented with 15% FBS, 1X Penicillin/Streptomycin, non-essential amino acids, and sodium pyruvate, DMEM/F-12 supplemented with 10% FBS and 1% P/S, and MEM Alpha (1X) Minimum Essential Medium supplemented with 15% FBS and 1% Penicillin/Streptomycin, for primary dermal fibroblasts,

ligament fibroblasts, and bone osteoblasts respectively. When cells reached 50 – 70 % confluent, the culture medium was aspirated from every well and cells were gently rinsed twice with PBS at room temperature. Cells were then fixed with 2 mL of 100X absolute methanol for 5 minutes, followed by three washes with PBS. Cells were then Permeabilized with 1 mL of 0.1 % Triton X-100 in PBS for 15 minutes, followed by three washes with PBS. Cells were then blocked with 10% goat serum in PBS for 1 hour at room temperature, following by three washes with PBS. Every cell type was incubated for 2 hours with two positive IgG monoclonal unconjugated primary antibodies and one negative IgG monoclonal unconjugated primary antibody (negative control). Dermal fibroblasts were incubated with IgG monoclonal unconjugated Anti-TE-7 antibody (1:250), IgG monoclonal unconjugated Anti-Vimentin antibody (1:500) (the two positive antibodies), and with IgG monoclonal unconjugated Anti-tenomodulin antibody (1:100) as a negative control; ligament fibroblasts were incubated with IgG monoclonal unconjugated Anti-SCXA antibody (1:1000), IgG monoclonal unconjugated Anti-tenomodulin antibody (1:100) (the two positives antibodies), and IgG monoclonal unconjugated Anti-TE-7 antibody (1:250) as a negative control; and bone osteoblast were incubated with IgG monoclonal unconjugated Anti-Alkaline Phosphatase (1:100), IgG3 monoclonal unconjugated Anti-Osteocalcin antibody (1:100) (the two positive antibodies), and IgG monoclonal unconjugated Anti-SCXA antibody (1:1000) as a negative control. All antibodies were diluted using the same blocking solution of 10% goat serum in PBS. Post incubation, cells were washed three times with PBS and incubated with the secondary antibodies for another 2 hours at dark. All cells were incubated with the secondary antibody IgG polyclonal Goat Anti-Rabbit IgG H&L (Alexa Fluor® 488) (1:500), except for the cells incubated with Anti-Osteocalcin primary antibody, which were incubated with the secondary antibody IgG polyclonal Goat Anti-Mouse IgG H&L (Alexa Fluor® 488) (1:500). After incubation with the

secondary antibodies for 2 hours, cells were washed three times with PBS away from light, then incubated with DAPI (4',6-Diamidino-2-Phenylindole, Dihydrochloride) at a concentration (1:3000). Cells were then washed 1 time with PBS and coverslips were mounted on microscope slides on anti-fade mounting medium. Nail polish was applied at the edge of every cover slip to keep the samples hydrated. All samples were visualized using an inverted fluorescence microscope (Zeiss LSM 880) using Zen Software. To quantify the fluorescence data, all images were processed through Image J software. For every antibody, the intensity in six images were measured, averaged and values were plotted as % of antibody expression.

4.2.8 LIVE/DEAD Viability Assay

All scaffolds were sterilized prior to cell seeding. To sterilize PLGA microsphere scaffolds, they were submerged in 70% ethanol for 20 minutes followed by submerging in sterile PBS to remove any ethanol residuals. Next, scaffolds were exposed to UV light for 30 minutes each side. To sterilize both the uniaxial and uniaxial-growth factors as well as the coaxial and coaxial-growth factors electrospun nanofiber scaffolds, they were placed inside of the cell culture hood and exposed to UV light for 30 minutes each side. To incorporate BMP-2 in PLGA microsphere scaffolds, scaffolds were either surface absorbed with 10 μ l of BMP-2 (1 μ g/ scaffold), or injected with 100 μ l of gelatin-mTG/BMP-2 (1 μ g/ scaffold). Scaffolds injected with gelatin-mTG were further incubated at 37°C to allow for complete gelation. Four different experimental groups were included to assess the viability of every cell type as follows; dermal fibroblasts were seeded on coaxial PLGA-Gelatin-PDGF-BB, PLGA-Gelatin, and uniaxial PLGA-PDGF-BB, PLGA electrospun nanofiber scaffolds; ligament fibroblasts were seeded on coaxial PLGA-Gelatin-IGF-I, PLGA-Gelatin, and uniaxial PLGA-IGF-I, PLGA electrospun nanofiber scaffolds; and primary

osteoblasts were seeded on PLGA-gelatin-mTG/BMP-2, PLGA-gelatin-mTG, PLGA/BMP-2, and PLGA microsphere scaffolds. All cells were seeded at a density of 1×10^5 cells/ scaffold and scaffolds were placed in low binding 24-well plates in triplicate. Cells were allowed to attach for 1.5 h in the cell culture incubator at 37 °C prior to the addition of 2 ml of the relevant medium for every cell type. All cells were maintained in a tissue culture incubator at 37°C, 5%CO₂, 3%O₂. After 3 and 7 days, scaffolds were harvested, washed with PBS twice and assessed for LIVE/DEAD assay, which was used to qualitatively determine cell viability based on a green fluorescent probe that recognizes intracellular esterase activity, calcein AM, and a red fluorescent probe that recognizes damaged plasma membranes, ethidium homodimer-1 (EthD-1). To perform the assay, all scaffolds were incubated with 2 mL of the prepared EthD-1/calcein solution at a concentration of 2 µl/ mL EthD-1, and 0.5 µl/ mL calcein AM in PBS for 1 hour. Next, scaffolds were washed twice with PBS and visualized using an inverted fluorescence microscope (Zeiss LSM 880) using Zen Software.

4.2.9 Proliferation Assay

The capability of all scaffolds to support the growth and proliferation of the different cell types were assessed using the Cell Titer 96® AQueous One Solution Cell Proliferation Assay according to the manufacturer's instructions. All scaffolds underwent the same sterilization technique as described in the previous experiment, and the same seeding density was applied to all scaffolds for all cell types having the same experimental groups. After day 3 and 7, scaffolds were removed from their wells and placed in new wells after two washes with PBS. Next, scaffolds were incubated with a cocktail of the relevant medium type premixed with MTS solution at a ratio of (1:5) for 3 hours at 37 °C. 500 µl of sodium dodecyl sulfate was added to each well to stop the

reaction and the absorbance at 490 nm was measured with a spectrophotometric plate reader (TECAN, Crailsheim, Germany).

4.2.10 Statistical Analysis

Data are presented as mean \pm standard deviation (SD). All statistical analyses were performed using the Statistical Software Prism GraphPad (Version 5) using two-way Analysis of Variance (ANOVA) with a Tukey test for Post Hoc parameter comparisons. Statistical significance was set at $p < 0.05$.

4.3.Results:

4.3.1. Morphological and Immunofluorescence Phenotypic of the Isolated Primary Cells

The three different cell types were morphologically characterized or by immunofluorescence to ensure the homogeneity in our cellular population. To morphologically characterize them, all cells were fixed and visualized under a normal light microscopy at two different magnifications high (40 X) and low (10 X). Both cell types isolated from skin and ligament exhibited a spindle and elongated cytoplasm structure with relatively long cytoplasmic processes of 3 - 7 μm and 5 – 11 μm in length for both dermal and ligament respectively as measured in Image J. These cells displayed a thicker central part of the body and two narrow peripheral processes with smooth lateral edges, which suggest their fibroblastic phenotype (Figure 4.1, 4.2). Cells isolated from long bones appeared flattened and slightly slender in shape and displayed sparse and relatively-short cytoplasmic processes (2-5 μm) in length when compared to the isolated fibroblasts (Figure 4.3). These maintained their slenderer shape during culture but they became smaller and packed when they reach confluence. These findings suggest that the isolated cells are the cells of interest, but

further characterization of these cells is indeed required to ensure the exact phenotype of every cell type.

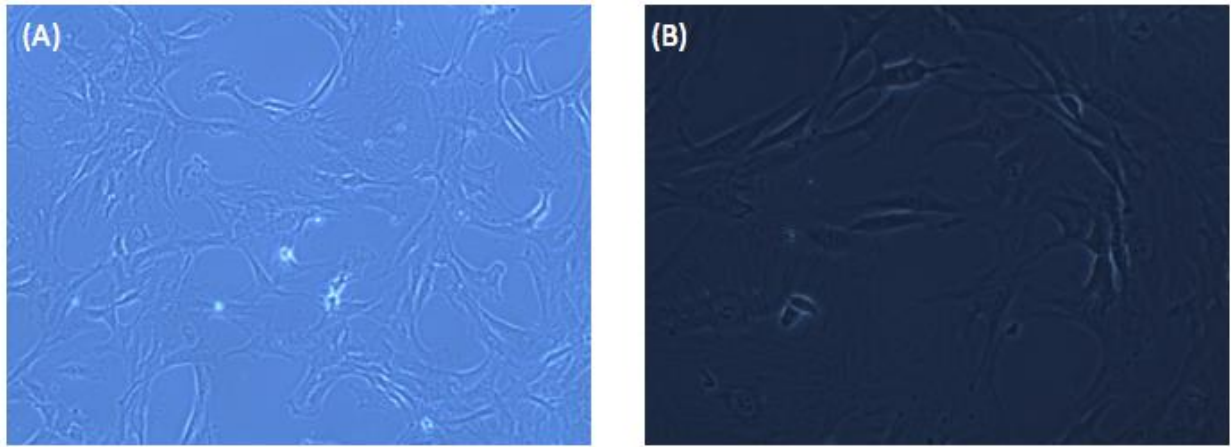


Figure 4.1 Morphological characterization of primary dermal fibroblasts (A) Primary Dermal Fibroblasts (10X), (B) Primary Dermal Fibroblasts (40X)

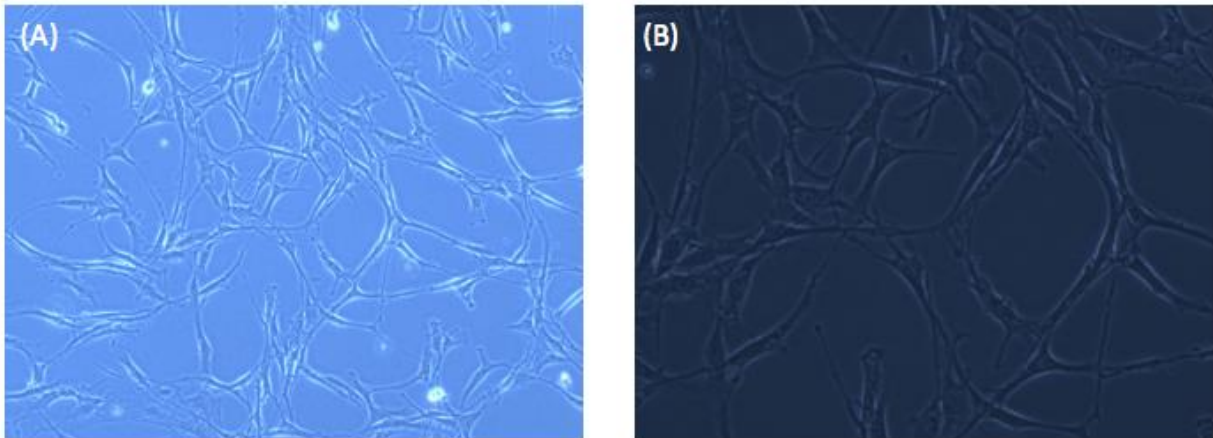


Figure 4.2 Morphological characterization of primary ligament fibroblasts (A) Primary Ligament Fibroblasts (10X), (B) Primary Ligament Fibroblasts (40X)

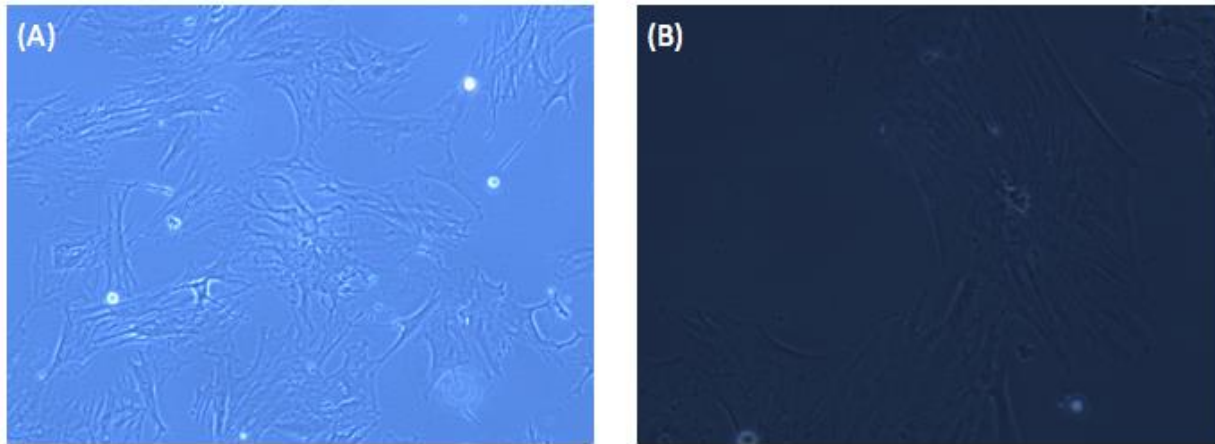


Figure 4.3 Morphological characterization of primary osteoblasts (A) Primary Osteoblasts (10X), (B) Primary Osteoblasts (40X)

Next, cells were stained for specific markers that are known to be expressed by them. Dermal fibroblasts were stained against two positive markers TE-7 and Vimentin, and negatively stained against Alkaline Phosphatase. Similarly, ligament fibroblasts were stained against two positive markers that are known to be expressed by ligament fibroblast, SCXA and tenomodulin, and negatively stained against TE-7. Primary osteoblasts are known to express Alkaline Phosphatase and Osteocalcin, which were used as positive markers to stain osteoblasts, however, SCXA was used as the negative control for this last cell type. Our data revealed that all the three different cell types were specific to all markers and showed 100% positive expression for every specific marker (Figure 4.4, 4.5, 4.6). All cell types were stained negative and showed no expression at all for all the negative control markers, except for ligament fibroblasts, which showed a very slight expression for the dermal fibroblastic specific marker TE-7, indicating that TE-7 is not 100% specific for dermal fibroblasts. Our data indicate that all the isolated primary cells are specific to their origin and can be used for further analysis.

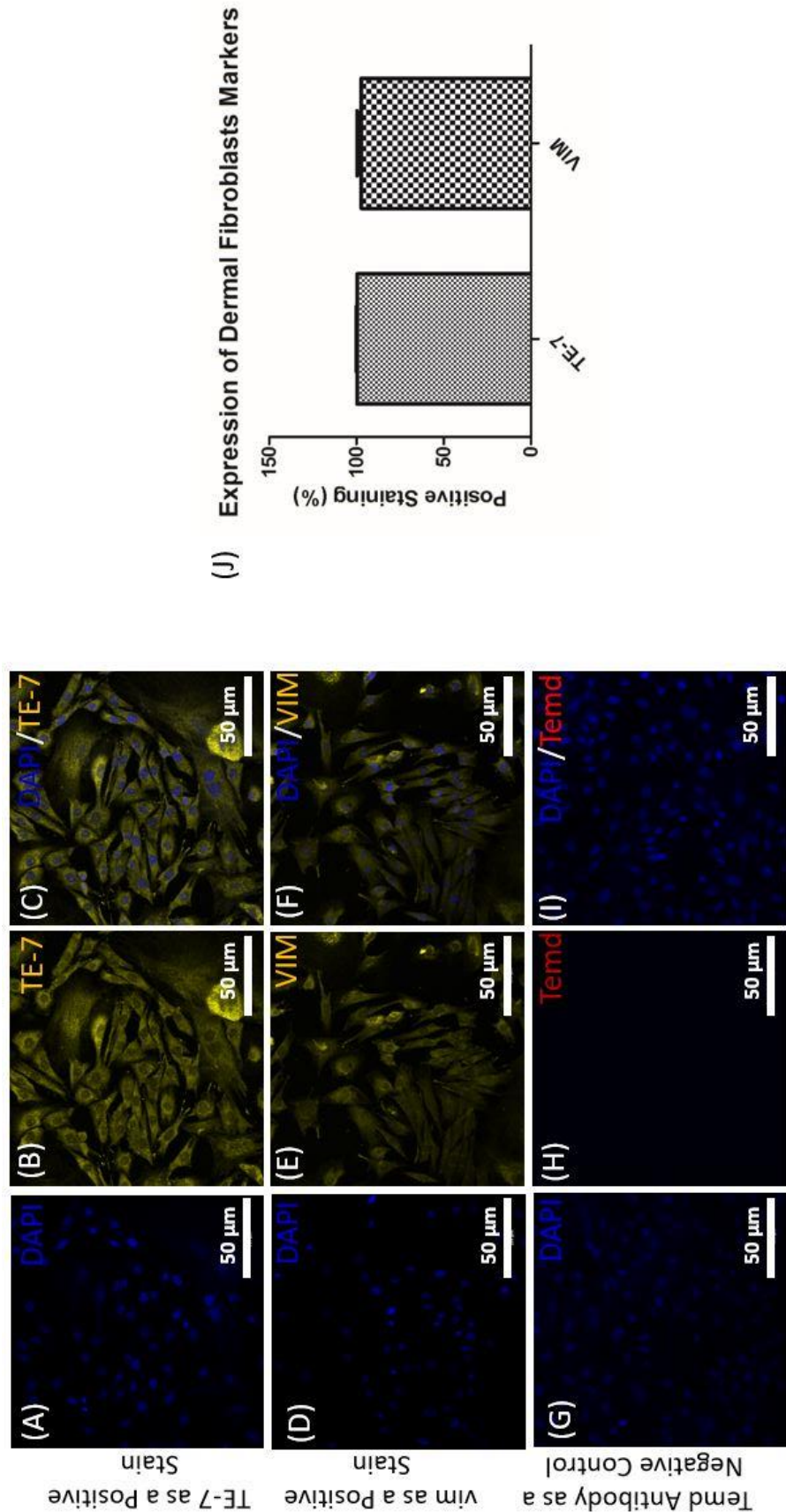


Figure 4.4 Expression of dermal fibroblastic markers by immunofluorescence (A) DAPI channel, (B) TE-7 expression, (C) merged between DAPI and TE-7 expression, (D) DAPI channel, (E) VIM expression, (F) merged between DAPI and VIM, (G) DAPI channel, (H) Temd expression, (I) merged between DAPI and Temd, and (J) TE-7 and VIM expression levels.

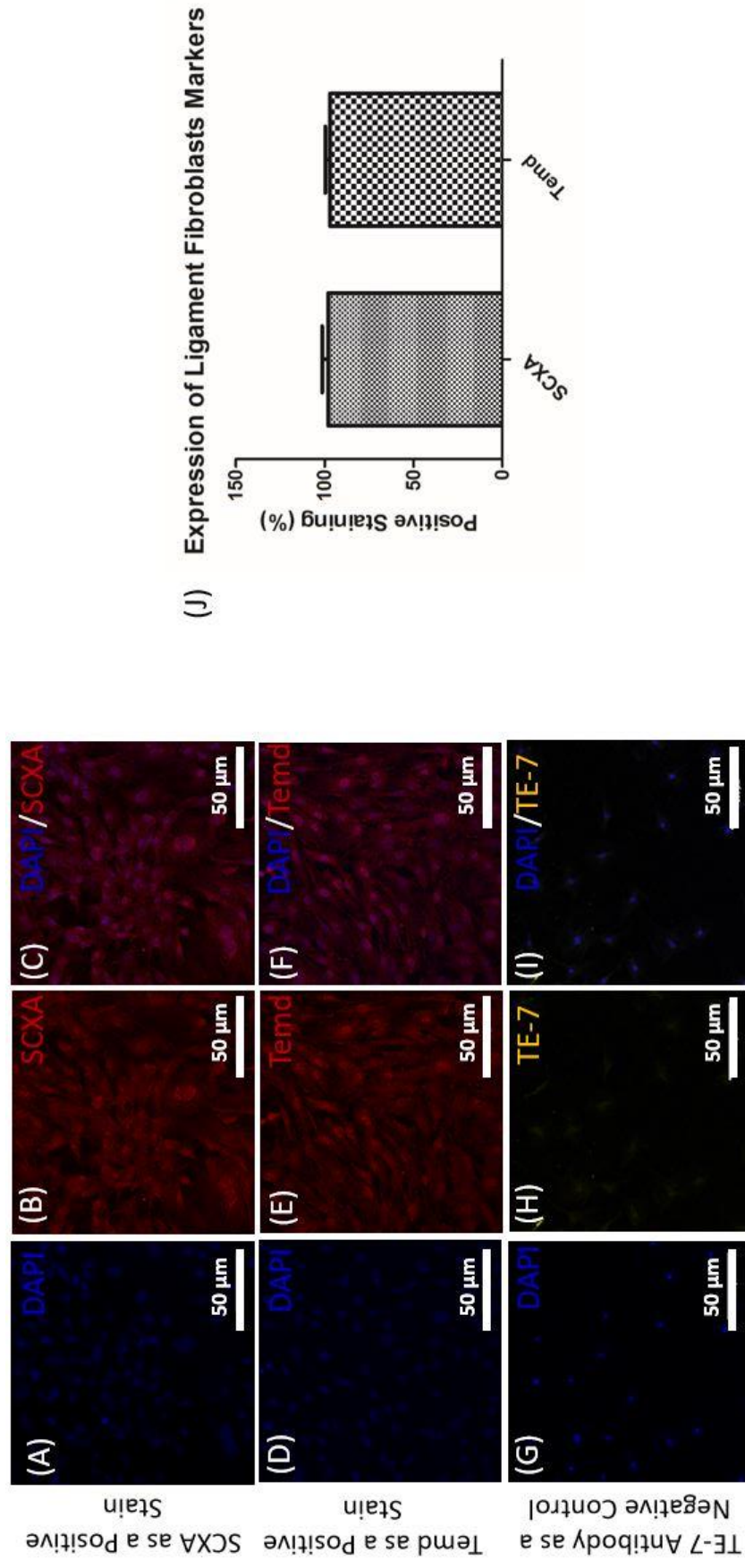


Figure 4.5 Expression of ligament fibroblastic markers by Immunofluorescence (A) DAPI channel, (B) SCXA expression, (C) merged between DAPI and SCXA expression, (D) DAPI channel, (E) Temd expression, (F) merged between DAPI and Temd, (G) DAPI channel, (H) TE-7 expression, (I) merged between DAPI and TE-7, and (J) SCXA and Temd expression levels.

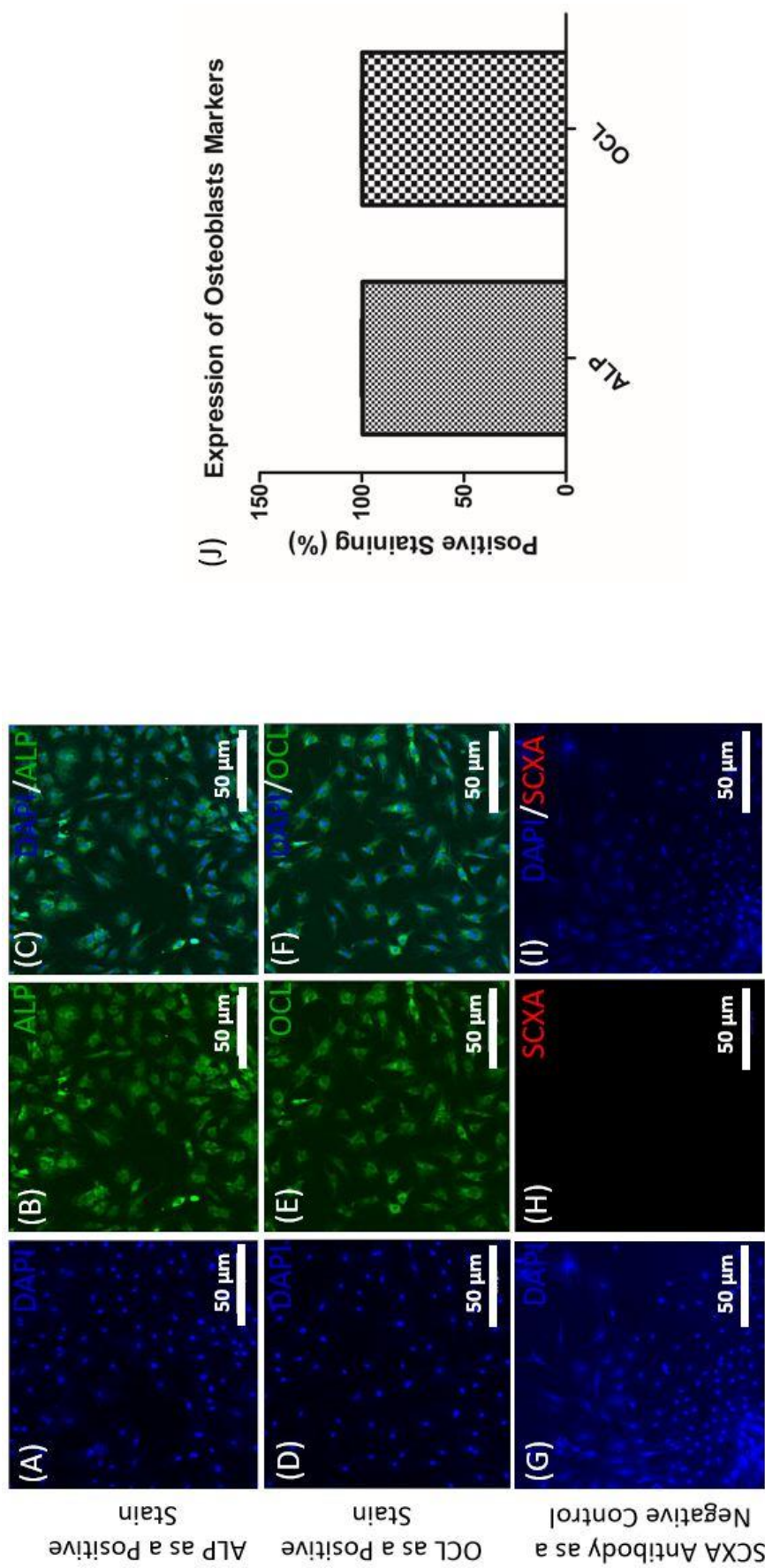


Figure 4.6 Expression of osteoblastic markers by Immunofluorescence (A) DAPI channel, (B) ALP expression, (C) merged between DAPI and ALP expression, (D) DAPI channel, (E) OCL expression, (F) merged between DAPI and OCL, (G) DAPI channel, (H) SCXA expression, (I) merged between DAPI and SCXA, and (J) ALP and OCL expression levels.

4.3.2. LIVE/DEAD Viability and Proliferation Assays

LIVE/DEAD and MTS proliferation assays were performed on the three different cell types cultured in different scaffolds either with or without growth factor on day 3 and 7 to qualitatively determine the capability of these substrate to support the viability of the different cells as well as to quantitatively examine the effect of the growth factors incorporation methods (coaxial Vs uniaxial, or gelation incorporation Vs. surface absorption) and releasing profiles (minimal burst release Vs. rapid burst release) on the cell proliferation. As shown in (Figure 4.7, Figure 4.8, Figure 4.9), all scaffolds supported the viability and the proliferation of primary dermal fibroblasts and dead cells were not evidence, as cells displayed a robust and healthy morphology. In general, cells cultured on coaxial PLGA-Gelatin-PDGF-BB and uniaxial PLGA-PDGF-BB showed a significant increase in cell viability and proliferation in both days 3 and 7 when compared to PLGA-Gelatin and PLGA electrospun nanofiber scaffolds without PDGF-BB (Figure 4.8, Figure 4.9). When cultured on PLGA-Gelatin and PLGA nanofiber scaffolds, dermal fibroblasts showed a significant increase in cell viability and proliferation on the coaxial PLGA-Gelatin when compared to the uniaxial PLGA nanofiber scaffolds at both days 3 and 7 (Figure 4.7). When cultured on coaxial PLGA-Gelatin-PDGF-BB and uniaxial PLGA-PDGF-BB, dermal fibroblasts showed a relatively similar viability and cell growth in both time points 3 and 7 days with no significant difference (Figure 4.8 A, B, E, F, Figure 4.9).

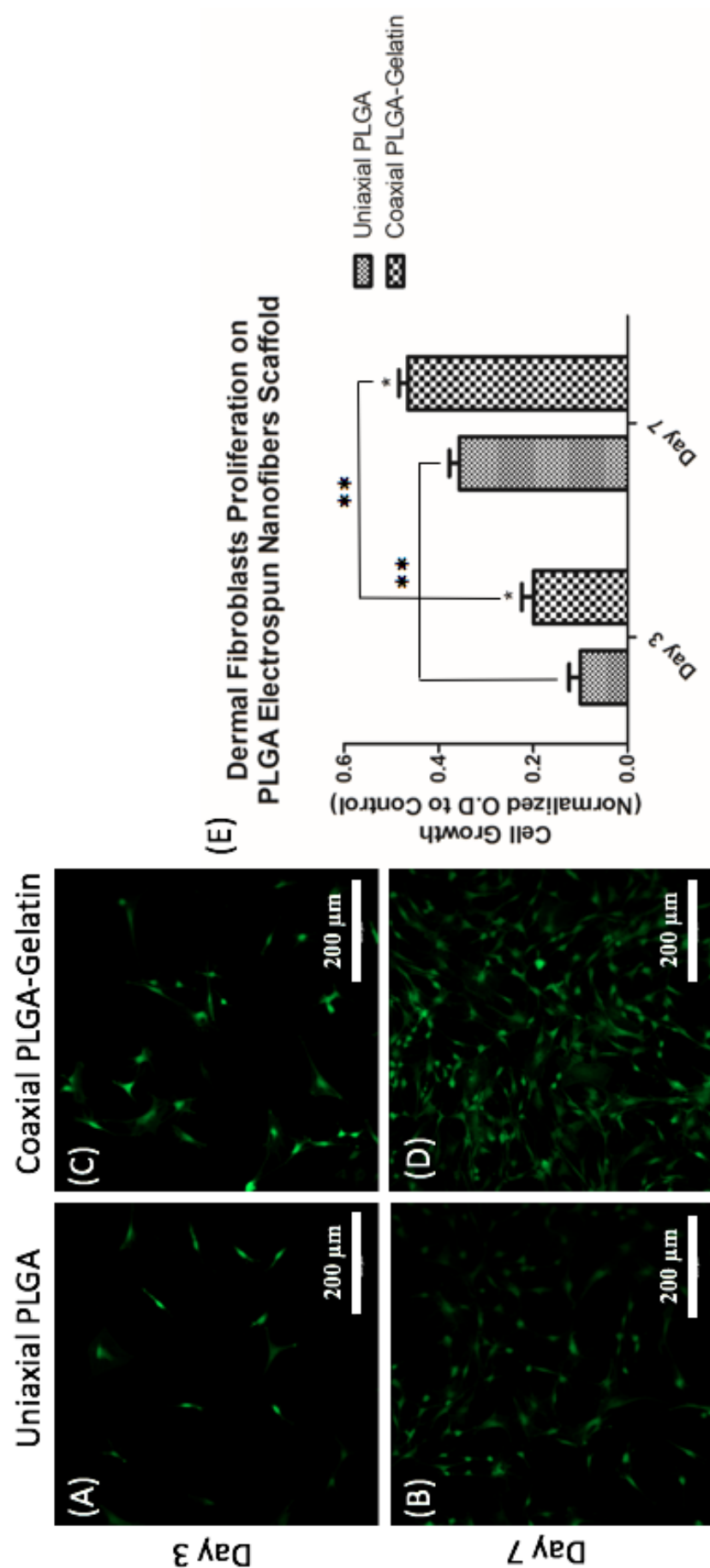


Figure 4.7 Viability and proliferation of dermal fibroblasts on different PLGA nanofibers scaffolds
 (A) Uniaxial PLGA at day 3, (B) Uniaxial PLGA at day 7, (C) Coaxial PLGA at day 3, (D) Coaxial PLGA-Gelatin at day 7, and (E) proliferation of primary dermal fibroblasts cultured on Uniaxial PLGA, and Coaxial PLGA-Gelatin. $n=3$ $P < 0.05^*$, $P < 0.01^{**}$, $P < 0.001^{***}$

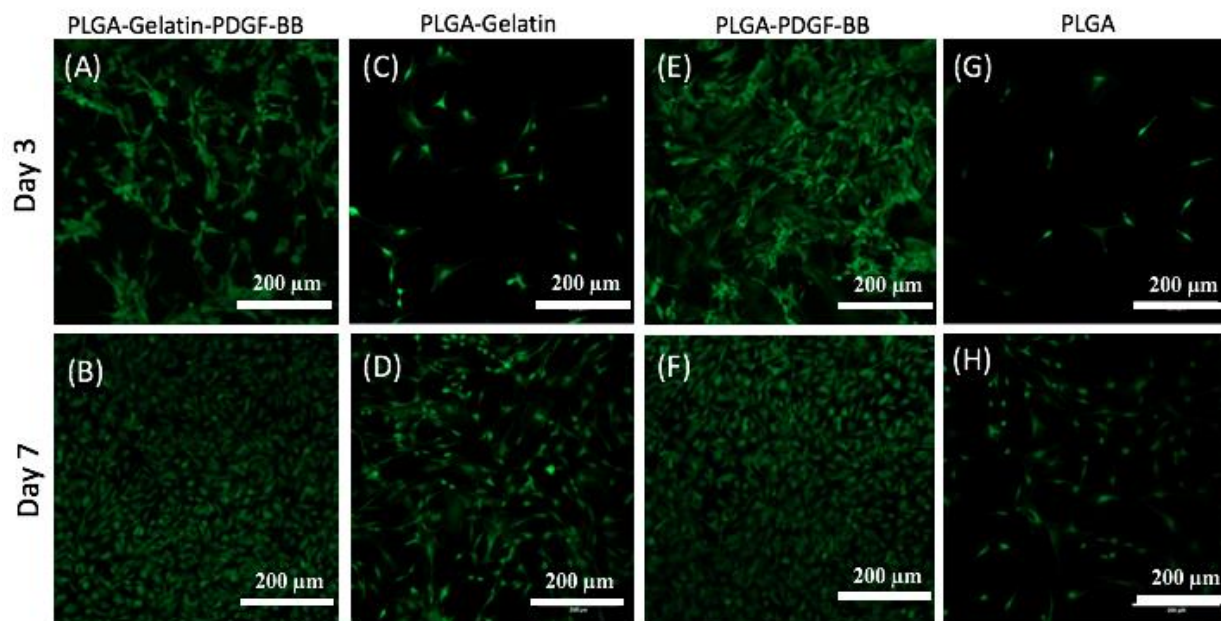


Figure 4.8 Viability of dermal fibroblasts on different PLGA coaxial or uniaxial electrospun nanofibers scaffolds (A) PLGA-Gelatin-PDGF-BB at day 3, (B) PLGA-Gelatin-PDGF-BB at day 7, (C) PLGA-Gelatin at day 3, (D) PLGA-Gelatin at day 7, (E) PLGA/PDGF-BB at day 3, (F) PLGA/PDGF-BB at day 7, (G) PLGA at day 3, (H) PLGA at day 7.

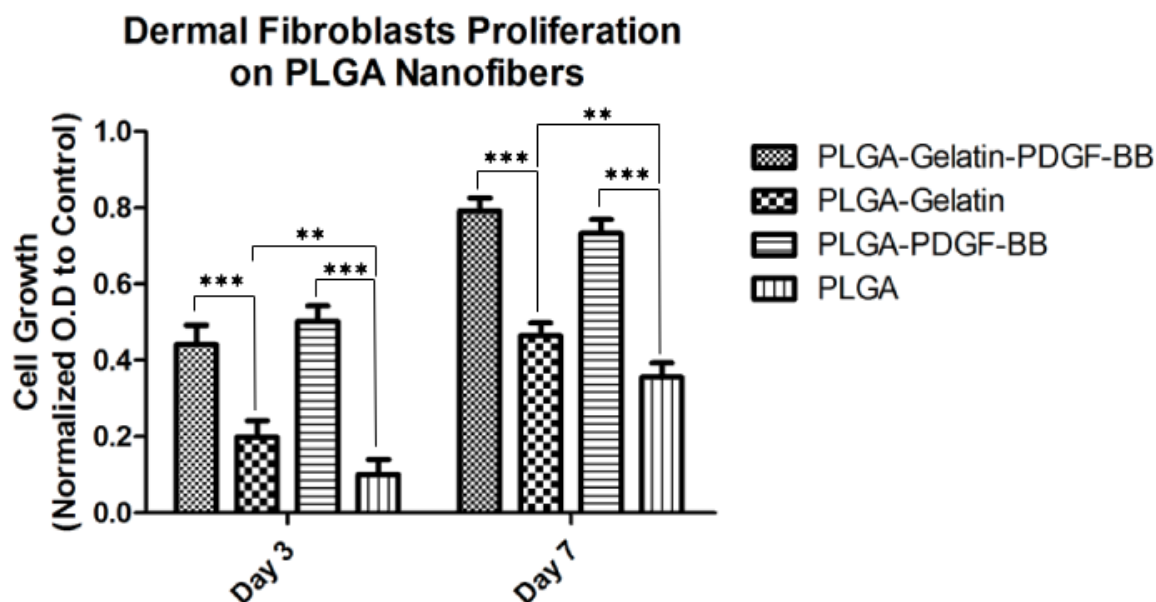


Figure 4.9 Proliferation Assay. Primary Dermal fibroblasts were cultured on PLGA-Gelatin PDGF-BB, PLGA-Gelatin (negative control), PLGA-PDGF-BB (positive control), PLGA (negative control), then assayed for cell proliferation on day 3 and 7. $n=3$ $P < 0.05^*$, $P < 0.01^{**}$, $P < 0.001^{***}$

The behaviors of ligament fibroblasts cultured on the same scaffolds but with the presence of IGF-I, was relatively similar to the behavior of dermal fibroblasts with no significant difference (Figure 4.10, Figure 4.11, Figure 12), where viability and proliferation have been supported by these substrates, and cells showed significantly higher proliferation and viability with the presence of IGF-I when compared to the scaffold that don't contain IGF-I in the coaxial and uniaxial cases. As shown in (Figure 4.13, Figure 4.14, Figure 15) Osteoblasts cultured on PLGA-Gelatin-mTG/BMP-2 and PLGA/BMP-2 showed a significant increase in cell viability and proliferation in both days 3 and 7 when compared to PLGA-Gelatin-mTG and PLGA-Gelatin free. When cultured on the PLGA-Gelatin-mTG and PLGA-Gelatin-mTG free, osteoblasts showed a significant increase in cell viability and proliferation on PLGA-Gelatin-mTG when compared to the PLGA-Gelatin-mTG free in both time points day 3 and 7 (Figure 4.13). When cultured on PLGA-Gelatin-mTG/BMP-2 and PLGA/BMP-2, osteoblasts showed a significant increase in cell viability and proliferation on the PLGA/BMP-2 group in day 3 when compared to the PLGA-Gelatin-mTG/BMP-2 group (Figure 4.14 A, B, E, F, and Figure 4.15). In day 7, osteoblasts showed a significant increase in cell viability and proliferation on PLGA-Gelatin-mTG/BMP-2 scaffolds when compared to PLGA/BMP-2 scaffolds.

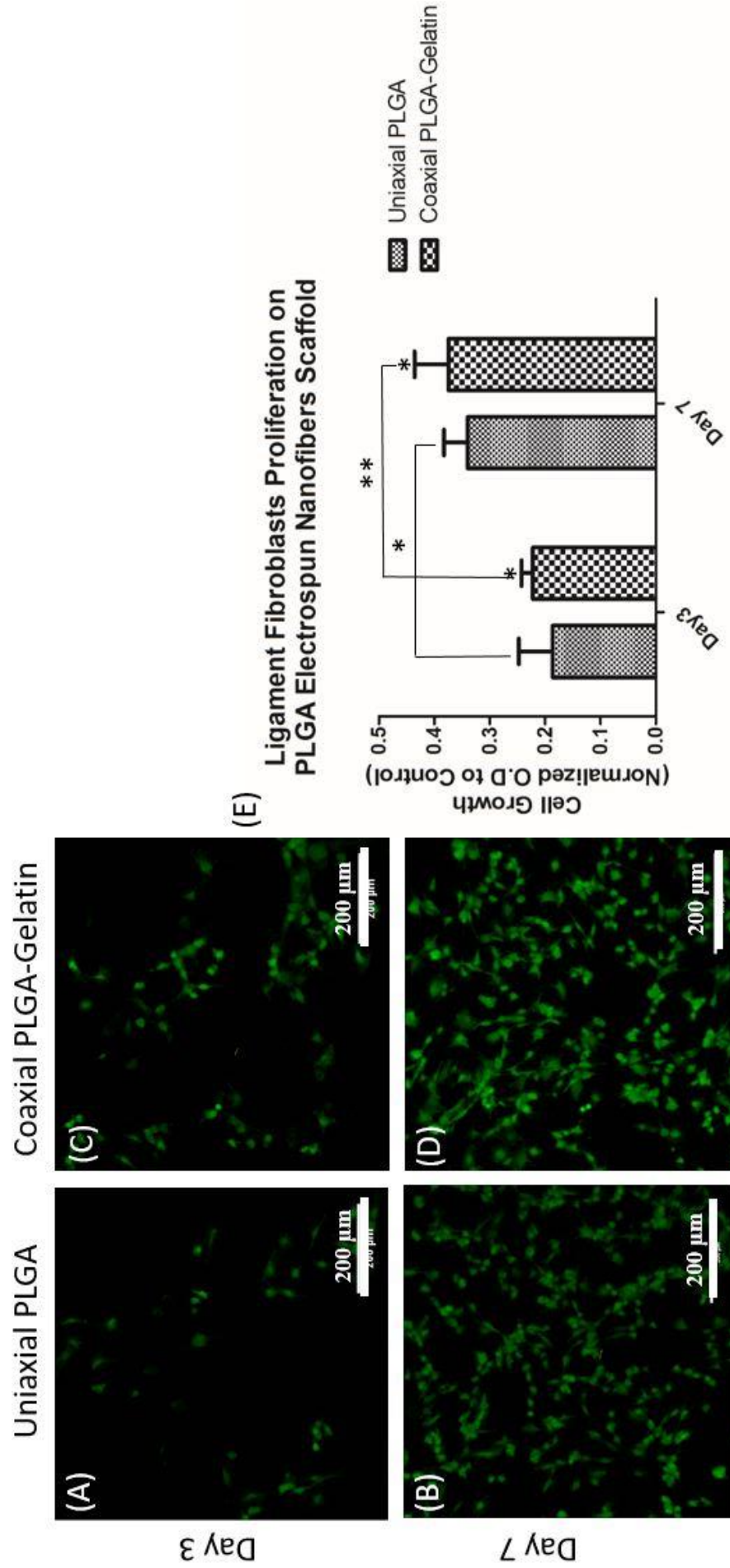


Figure 4.10 Viability and proliferation of ligament fibroblasts on different PLGA nanofibers scaffolds (A) Uniaxial PLGA at day 3, (B) Uniaxial PLGA at day 7, (C) Coaxial PLGA at day 3, (D) Coaxial PLGA-Gelatin at day7, and (E) proliferation of primary ligament fibroblasts cultured on Uniaxial PLGA, and Coaxial PLGA-Gelatin. $n=3$ $P < 0.05^*$, $P < 0.0^{**}$, $P < 0.001^{***}$

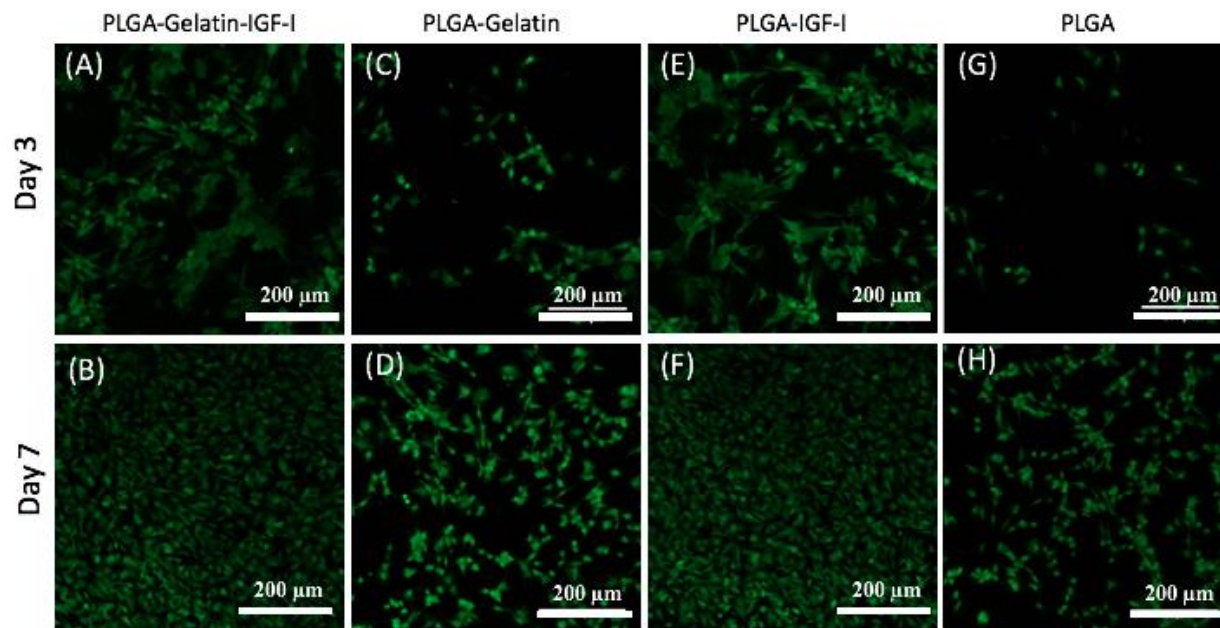


Figure 4.11 Viability of ligament fibroblasts on different PLGA coaxial or uniaxial electrospun nanofibers scaffolds (A) PLGA-Gelatin-IGF-I at day 3, (B) PLGA-Gelatin-IGF-I at day 7, (C) PLGA-Gelatin at day 3, (D) PLGA-Gelatin at day 7, (E) PLGA-IGF-I at day 3, (F) PLGA-IGF-I at day 7, (G) PLGA at day 3, (H) PLGA at day 7.

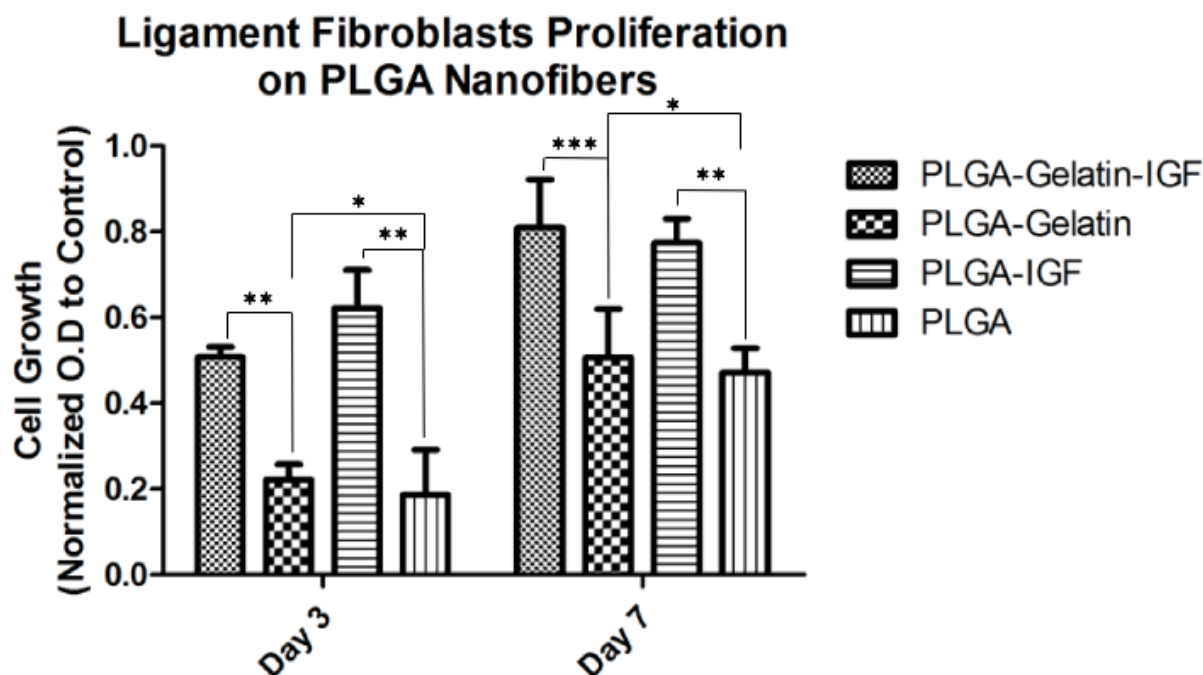


Figure 4.12 Proliferation Assay. Primary ligament fibroblasts were cultured on PLGA-Gelatin IGF-I, PLGA-Gelatin (negative control), PLGA-IGF-I (positive control), PLGA (negative control), then assayed for cell proliferation on day 3 and 7. $n = 3$ $P < 0.05^*$, $P < 0.01^{**}$, $P < 0.001^{***}$

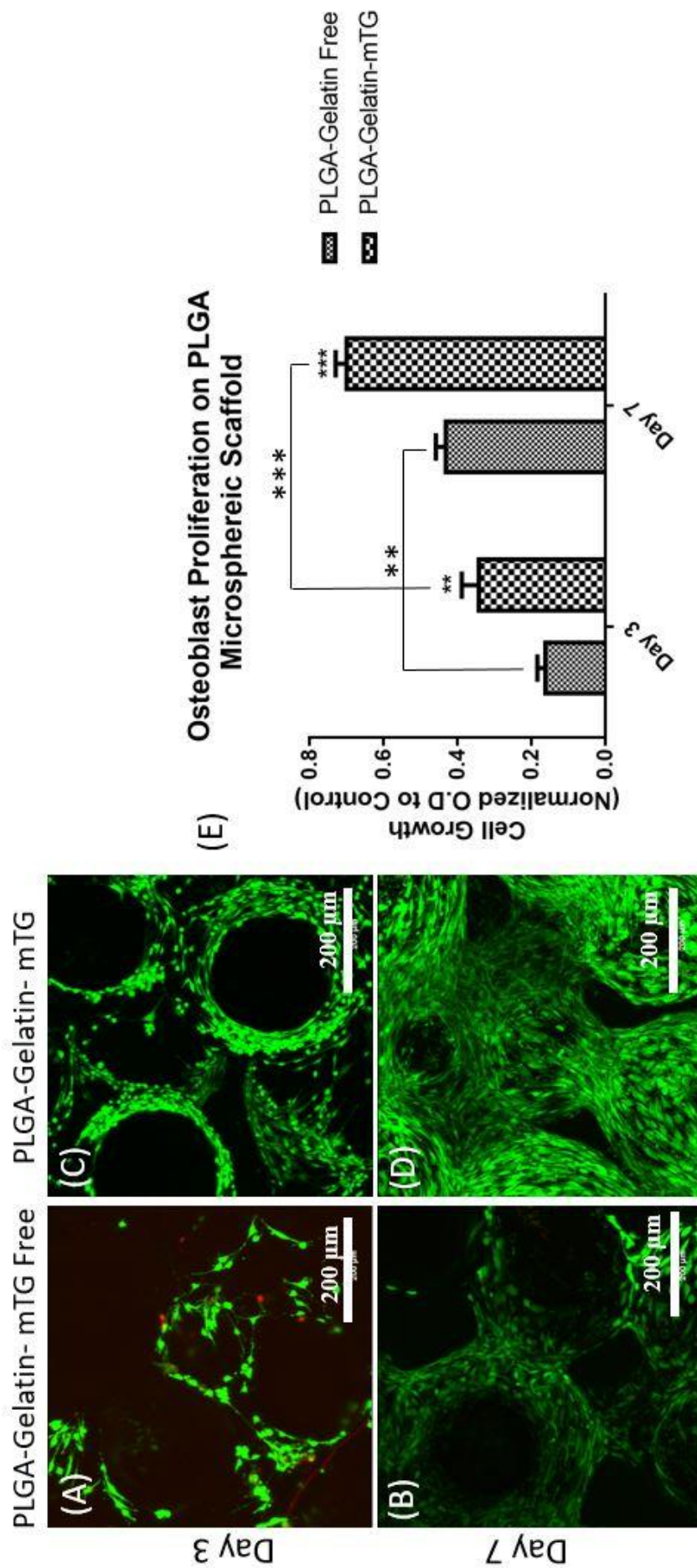


Figure 4.13 Viability and proliferation of osteoblasts on different PLGA microspheres scaffolds (A) PLGA-Gelatin-mTG free at day 3, (B) PLGA-Gelatin-mTG free at day 7, (C) PLGA-Gelatin-mTG at day 3, (D) PLGA-Gelatin-mTG at day 7, and (E) proliferation of primary osteoblasts cultured on PLGA-Gelatin-mTG free, and PLGA-Gelatin-mTG. $n = 3$ $P < 0.05^*$, $P < 0.001^{***}$

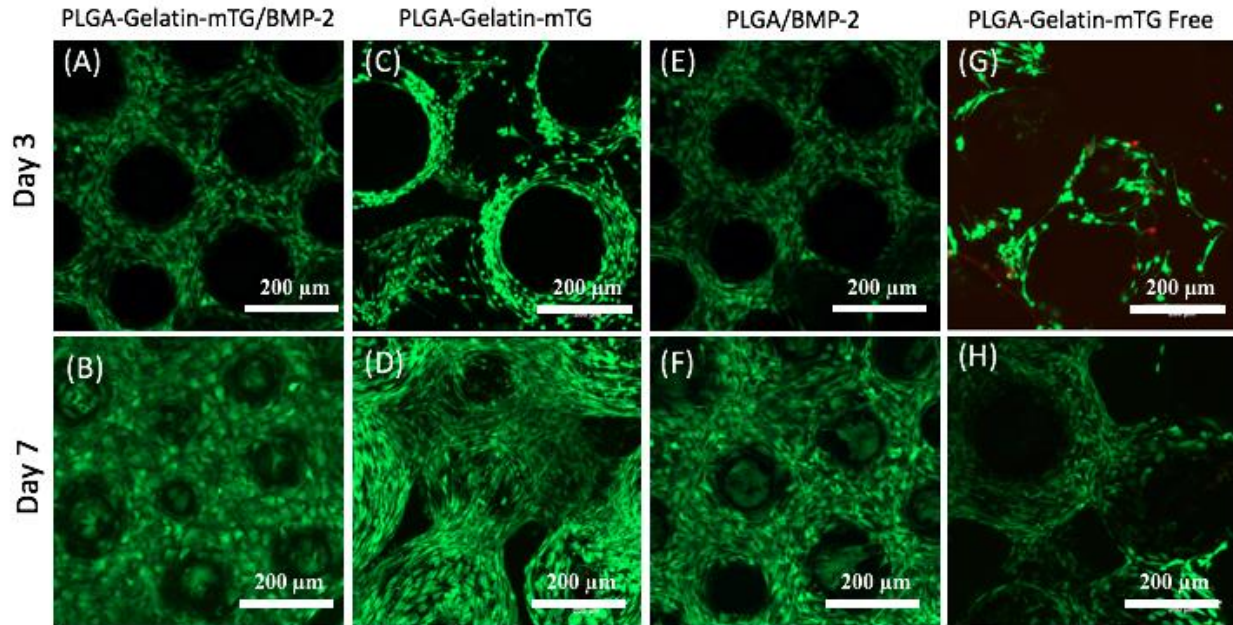


Figure 4.14 Viability of osteoblasts on different PLGA microsphere scaffolds (A) PLGA-Gelatin-mTG/BMP-2 at day 3, (B) PLGA-Gelatin-mTG/BMP-2 at day 7, (C) PLGA-Gelatin-mTG at day 3, (D) PLGA-Gelatin-mTG at day 7, (E) PLGA/BMP-2 at day 3, (F) PLGA/BMP-2 at day 7, (G) PLGA-Gelatin-mTG Free at day 3, (H) PLGA-Gelatin-mTG Free at day 7.

Osteoblasts Proliferation on PLGA Microsphere Scaffold

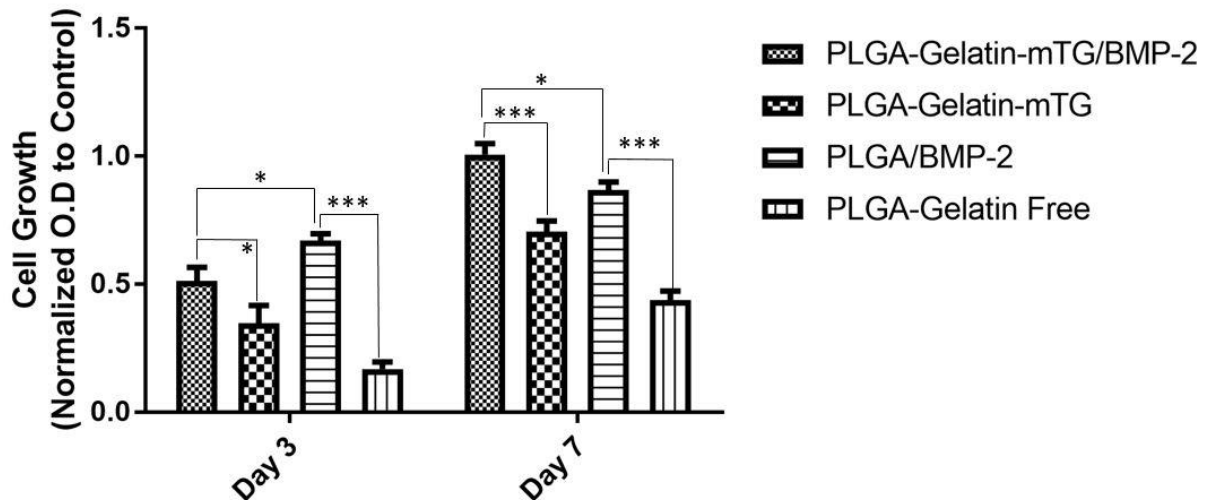


Figure 4.15 Proliferation Assay. Primary osteoblasts were cultured on PLGA-Gelatin-mTG/BMP-2, PLGA-Gelatin-mTG (negative control), PLGA/BMP-2 (positive control), PLGA-Gelatin-mTG Free (negative control), then assayed for cell proliferation on day 3 and 7. $n = 3$ $P < 0.05^*$, $P < 0.01^{**}$, $P < 0.001^{***}$

4.4.Discussion:

The capability of the three different phases within the integrated graft system to support cellular viability and proliferation as well as the effect of the different growth factors incorporation methods have been evaluated on the three-different isolated primary cells; dermal fibroblast, ligament fibroblasts, and osteoblasts.

The three different cells were successfully isolated and characterized by morphology and immunofluorescence against specific markers in order to confirm their phenotype after they have been isolated from a heterogeneous environment to ensure the homogeneity in our cellular population. We initially morphologically characterized every cell type by observing the shape, size, and structure of the cell. Both cell types isolated from skin and ligament exhibited a spindle and elongated cytoplasm structure with relatively long cytoplasmic processes of 3 - 7 μm and 5 – 11 μm in length for both dermal and ligament respectively as measured in Image J. These cells displayed a thicker central part of the body and two narrow peripheral processes with smooth lateral edges, which suggest their fibroblastic phenotype. Cells isolated from long bones appeared flattened and slightly slender in shape and displayed sparse and relatively short cytoplasmic processes 2-5 μm in length when compared to the isolated fibroblasts (Figure 4.3). Osteoblasts maintained their slender shape during culture, but they became smaller and packed when they reach confluence. Our morphological observations to the three different cell types correspond with previously conducted morphological studies that morphologically characterized both fibroblasts and osteoblasts [20, 21].

Further characterizations have been conducted with immunofluorescence in order to verify the cells' phenotype. Every cell type was stained against two positive markers that are known to be expressed by them along with a negative marker as a control. Our data revealed that all the three different cell types were specific to all markers and showed 100% positive expression for every specific marker as indicated by Image J when conducting the image pixel analysis (Figure 4.4, 4.5, 4.6). All cell types were stained negative and showed no expression at all for all the negative control markers, except for ligament fibroblasts, which showed a very slight expression for the dermal fibroblastic specific marker TE-7. This corresponds with other several previous studies that TE-7 could potentially be expressed in other fibroblasts from different anatomical locations such as lung and muscle fibroblasts [27, 29]. Thus, our data suggest that ligament fibroblasts can be one of the TE-7 expressing cells since it was slightly stained in its cytoplasm. Our cell characterization results indicate that all the three different cell types are specific to the origin they were isolated from and that they can be used to conduct further studies with confident.

LIVE/DEAD and MTS proliferation assays were performed on the three different cell types cultured in different scaffolds either with or without growth factor on day 3 and 7 to qualitatively determine the capability of these substrate to support the viability of the different cells as well as to quantitatively examine the effect of the growth factors incorporation methods (coaxial Vs uniaxial, or gelatin incorporation Vs. surface absorption) and releasing profiles (minimal burst release Vs. rapid burst release) on the cell proliferation.

As shown in (Figure 4.7, Figure 4.8, Figure 9), all scaffolds supported the viability and the proliferation of primary dermal fibroblasts, and dead cells were not evidence, as cells displayed a

robust and healthy morphology. In general, cells cultured on PLGA-Gelatin-PDGF-BB and PLGA-PDGF-BB showed a significant increase in cell viability and proliferation in both days 3 and 7 when compared to PLGA-Gelatin and PLGA electrospun nanofiber scaffolds without PDGF-BB (Figure 4.8, Figure 4.9). This corresponds with a previously conducted study that PDGF-BB has the ability to support dermal fibroblasts growth by stimulating them to rapidly proliferate [64]. When cultured on PLGA-Gelatin and PLGA nanofiber scaffolds, dermal fibroblasts showed a significant increase in cell viability and proliferation on the coaxial PLGA-Gelatin when compared to the uniaxial PLGA nanofiber scaffolds at both days 3 and 7 (Figure 4.7). This could have been due to the fact the coaxial nanofibers have less PLGA content than the uniaxial, which might have caused the hydrophilicity in the coaxial nanofibers to increase, resulting in enhanced cellular attachment and therapy, proliferation. In addition, the presence of gelatin in the core-shell of the scaffold have been shown to enhance cell proliferation because gelatin inherits all the necessary arginine-glycineaspartic acid (RGD) sequences that allows for enhanced cell adhesion, which is the reason for the increase in the cell number in the PLGA-Gelatin group [81]. When cultured on coaxial PLGA-Gelatin-PDGF-BB and uniaxial PLGA-PDGF-BB, dermal fibroblasts showed a relatively similar viability and cell proliferation in both time points 3 and 7 days with no significant difference (Figure 4.8 A, B, E, F, Figure 4.9). This does not seem to correlate with the data of PLGA-Gelatin and PLGA alone, where the viability and proliferation were significantly higher in the coaxial PLGA-Gelatin scaffolds when compared to uniaxial PLGA alone in both time points in the case of no growth factors. However, we believe that having no significant difference in cell proliferation at the two-time points might have been due to the effect of the burst release of the growth factor from the uniaxial nanofiber scaffolds, which caused a rapid cell proliferation that could level up in a timely manner with the proliferation

of the cells seeded on the coaxial fibers.

The behaviors of ligament fibroblasts cultured on coaxial PLGA-Gelatin and uniaxial PLGA with or without IGF-I was relatively similar to the behavior of dermal fibroblasts (Figure 4.10, Figure 4.11, Figure 12), where viability and proliferation have been supported by these substrates, and cells showed significantly higher proliferation and viability with the presence of IGF-I when compared to the scaffolds that don't contain IGF-I in the coaxial and uniaxial cases. Several groups have previously demonstrated the positive effect of IGF-I in enhancing the metabolic activities of ligament fibroblast, stimulating them to rapidly proliferate. This, however, explains the reason for the rapid proliferation of ligament fibroblasts seeded on PLGA/IGF-I nanofingers scaffolds when compared to PLGA nanofibers scaffold with no growth factors [73]. Although no significant difference in cell growth was found between PLGA-Gelatin and PLGA alone, ligament fibroblasts seeded on PLGA-Gelatin had a relatively higher proliferation when compared to PLGA, which further confirms that the presence of gelatin in the core-shell enhances the cellular performance. Data from both cell types indicate that the presence of gelatin in the core-shell of the fiber enhanced cell viability and proliferation.

As shown in (Figure 4.13, Figure 4.14, Figure 4.15) Osteoblasts cultured on PLGA-Gelatin-mTG/BMP-2 and PLGA/BMP-2 showed a significant increase in cell viability and proliferation in both days 3 and 7 when compared to PLGA-Gelatin-mTG and PLGA-Gelatin free. This implies that BMP-2 has positive effects on primary osteoblasts, stimulating them to rapidly proliferate as previously mentioned [79]. When cultured on the PLGA-Gelatin-mTG and PLGA-Gelatin-mTG free, osteoblasts showed a significant increase in cell viability and proliferation on PLGA-Gelatin-

mTG when compared to the PLGA-Gelatin-mTG free in both time points day 3 and 7 (Figure 4.13). This indicates that the presence of gelatin did not negatively affect cellular viability or proliferation and thus, enhanced the overall cellular performance and increased the scaffold biocompatibility.

When cultured on PLGA-Gelatin-mTG/BMP-2 and PLGA/BMP-2, osteoblasts showed a significant increase in cell viability and proliferation on the PLGA/BMP-2 group in day 3 when compared to the PLGA-Gelatin-mTG/BMP-2 group (Figure 4.14 A, B, E, F, and Figure 4.15). In day 7, osteoblasts showed a significant increase in cell viability and proliferation on PLGA-Gelatin-mTG/BMP-2 scaffolds when compared to PLGA/BMP-2 scaffolds. Because of the high burst release of the surface adsorbed BMP-2, osteoblasts showed a significantly higher proliferation within the first three days in the surface adsorbed group when compared to the retained BMP-2 group. Surface absorbed PLGA with BMP-2 is known to exhibit a high initial burst release, followed by a complete release of the protein within the first 48 hours [83]. However, it is believed that the complete release of BMP-2 in the growth medium stimulated osteoblasts to rapidly proliferate, which correlates with the high cell growth of osteoblasts seeded on the surface absorbed with BMP-2 group at day 3. During the experiment, mediums from all groups were removed and replaced with freshly new medium after day 3. However, since all the BMP-2 in the surface adsorbed groups was released to the medium within the first ~ 48 h, it was removed with the medium change. This, however, caused osteoblasts cultured on the retained BMP-2 groups to constantly maintain their proliferation over time, and osteoblasts cultured on the surface adsorbed scaffold to decrease in proliferation due to the lack of BMP-2. This can be correlated with our ALP findings from the previous chapter (Figure 3.3), where cultured MC3T3 cells had lower ALP

activities when seeded on PLGA-Gelatin-mTG/BMP-2 group in comparison to the surface absorbed PLGA with BMP-2 group on the 7th day of the experiment, but significantly higher ALP activities on day 14 on PLGA-Gelatin-mTG/BMP-2 group when compared to the other groups, indicating that the retention of BMP-2 in the gelatin hydrogel does not affect the osteoinductivity of BMP-2. These findings demonstrate the gelatin-mTG/BMP-2 embedded PLGA microspheres have the potential to stimulate osteoblasts proliferation for longer times due to the immobilization of BMP-2.

Based on the overall findings of the proliferation and viability studies performed on the three different cell types on the different relevant scaffolds, we decided to further continue conducting the next set of experiments using the PLGA-Gelatin-Growth factors electrospun nanofiber scaffolds for the support of dermal and ligament fibroblasts culture, and PLGA-Gelatin-mTG/BMP-2 for the support of osteoblasts culture.

4.5.Conclusion:

In conclusion, the isolated primary cells, dermal fibroblasts, ligament fibroblasts and osteoblasts were specific to all markers and showed 100% positive expression for every specific marker, indicating that these cells are specific to the origin they were isolated from. Ligament fibroblasts showed low expression of the specific dermal osteoblasts marker TE-7, indicating that this marker is not completely specific to dermal fibroblasts. Viability and proliferation of both dermal and ligament fibroblasts were shown to be enhanced on the coaxial electrospun PLGA-Gelatin nanofiber scaffolds when compared to the uniaxial PLGA alone at the two time points due to the presence of gelatin at the core-shell of the fiber, which enhanced cell adhesion and therapy cell proliferation. PDGF-BB and IGF-I were shown to enhance the proliferation of dermal and ligament fibroblasts respectively. Cell proliferation was shown to be affected by the different incorporation methods of growth factors within the scaffolds. In the case of no growth factors, both cells showed significant increase in cell growth on PLGA-Gelatin scaffolds when compared to the uniaxial PLGA alone. However, due to the effect of the burst release associated with the uniaxial PLGA nanofiber scaffolds, no significant difference was noticed in cell growth of both cell types seeded on PLGA-Gelatin or uniaxial PLGA alone, in the case of growth factors. Osteoblasts proliferation and viability were enhanced on PLGA-Gelatin-mTG scaffold when compared to PLGA-Gelatin-mTG free at both time points. Due to the burst release of BMP-2, osteoblasts showed a significantly higher proliferation on the surface absorbed PLGA with BMP-2 when compared to PLGA-Gelatin-mTG/BMP-2 at day 3, and significantly higher on PLGA-Gelatin-mTG/BMP-2 when compared to PLGA/BMP-2 at day 7. These findings indicate that osteoblasts proliferation was affected by the different growth factors incorporation methods. Based on these results, its anticipated that PLGA-Gelatin-mTG/BMP-2 microsphere scaffolds and PLGA

coaxial electrospun nanofiber scaffold (w/growth factors) will have the potential to serve as suitable substrates for further experiments.

4.6.References:

1. edited by Cato T. Laurencin, Lakshmi S. Nair Nanotechnology and Tissue Engineering: The Scaffold
2. COMPONENTS OF TISSUE ENGINEERING Cell Sources, <http://aibolita.com/sundries/23305-components-of-tissue-engineering-cell-sources.html>
3. Thangapazham RL, Darling TN, Meyerle J. Alteration of skin properties with autologous dermal fibroblasts. *Int J Mol Sci.* 2014 May 13;15(5):8407-27. doi: 10.3390/ijms15058407.
4. "WoundandHealing"(http://www.skincience.com/_int/_en/topic/topic_sousrub.aspx?tc=SKIN_SCIENCE_ROOT%5EPROTECTING_SENSING_REPAIRING%5EWOUND_AND_HEALING&cur=WOUNDND_HEALING.) Skin Science. L'Oreal.
5. Weiss, R.A. Autologous cell therapy: Will it replace dermal fillers? *Fac. Plast. Surg. Clin. N. Am.* 2013, 21, 299–304.
6. Greaves, N.S.; Ashcroft, K.J.; Baguneid, M.; Bayat, A. Current understanding of molecular and cellular mechanisms in fibroplasia and angiogenesis during acute wound healing. *J. Dermatol. Sci.* 2013, 72, 206–217.
7. http://www.hopkinsmedicine.org/neurology_neurosurgery/centers_clinics/cutaneous_nerve_lab/physicians/biopsy_procedure.html
8. A. Hoffmann and G. Gross, “Tendon and ligament engineering in the adult organism: mesenchymal stem cells and genetherapeutic approaches,” *International Orthopaedics*, vol. 31, no. 6, pp. 791–797, 2007.


9. S. L. Y. Woo, K. Hildebrand, N. Watanabe, J. A. Fenwick, C. D. Papageorgiou, and J. H. C. Wang, "Tissue engineering of ligament and tendon healing," *Clinical Orthopaedics and Related Research*, no. 367, pp. S312–S323, 1999
10. J. A. Cooper Jr., L. O. Bailey, J. N. Carter et al., "Evaluation of the anterior cruciate ligament, medial collateral ligament, 6 Stem Cells International achilles tendon and patellar tendon as cell sources for tissueengineered ligament," *Biomaterials*, vol. 27, no. 13, pp. 2747– 2754, 2006.
11. [Z. Ge, J. C. H. Goh, and E. H. Lee, "Selection of cell source for ligament tissue engineering," *Cell Transplantation*, vol. 14, no. 8, pp. 573–583, 2005.
12. Brune, A. Borel, T.W. Gilbert, J.P. Franceschi, S.F. Badylak and P. Sommer. IN VITRO COMPARISON OF HUMAN FIBROBLASTS FROM INTACT AND RUPTURED ACL FOR USE IN TISSUE ENGINEERING T. Brune et al. *European Cells and Materials* Vol. 14. 2007
13. Pittenger MF, Mackay AM, Beck SC, Jaiswal RK, Douglas R, Mosca JD, Moorman MA, Simonetti DW, Craig S, Marshak DR. (1999). "Multilineage potential of adult human mesenchymal stem cells". *Science*. 284: 143-7. doi:10.1126/science.284.5411.143 PMID 10102814.
14. <https://www.nature.com/subjects/osteoblasts>
15. Bilezikian JP, Raisz LG, Martin TJ, editors. *Principles of Bone Biology*, 3rd ed. New York: Academic Press; 2008.
16. Jaba Mitra, Garima Tripathi, Ashutosh Sharma, Bikramjit Basu. Scaffolds for bone tissue engineering: role of surface patterning on osteoblast response. *RSC Adv.*, 2013,3, 11073-11094

17. Sethu SN, Namashivayam S, Devendran S, Nagarajan S, Tsai WB, Narashiman S, Ramachandran M, Ambigapathi MNanoceramics on osteoblast proliferation and differentiation in bone tissue engineering. *Int J Biol Macromol*. 2017 May;98:67-74. doi: 10.1016/j.ijbiomac.2017.01.089. Epub 2017 Jan 24.
18. Andrada Serafim, Romain Mallet, Florence Pascaretti-Grizon, Izabela-Cristina Stancu, and Daniel Chappard, "Osteoblast-Like Cell Behavior on Porous Scaffolds Based on Poly(styrene) Fibers," *BioMed Research International*, vol. 2014, Article ID 609319, 6 pages, 2014. doi:10.1155/2014/609319
19. <https://www.webmd.com/cancer/bone-biopsy#2>
20. M. ABERCROMBIE. The Cells Fibroblasts. *J. clin. Path.*, 31, Suppl. (Roy. Coll. Path.), 12, 1-6
21. Yang RS¹, Liu TK, Tsai KS, Lin-Shiau SY, Lu KS. Morphological and immunocytochemical characterization of osteoblast cultures from long bones of neonatal rats. *Arch Histol Cytol*. 1992 Oct;55(4):415-22.
22. Gavin, AL; Hoebe, K; Duong, B; Ota, T; Martin, C; Beutler, B; Nemazee, D (22 December 2006). "Adjuvant-enhanced antibody responses in the absence of toll-like receptor signaling.". *Science*. 314 (5807):19368. PMC 1868398 . PMID 17185603. doi:10.1126/science.1135299.
23. Sorrell, J.M., Baber, M.A., Caplan, A.I., 2007. Clonal characterization of fibroblasts in the superficial layer of the adult human dermis. *Cell Tissue Res*. 327, 499–510.
24. Fang Cheng, Yue Shen, Ponnuswamy Mohanasundaram, Michelle Lindström, Johanna Ivaska, Tor Ny, and John E. Eriksson Vimentin coordinates fibroblast proliferation and keratinocyte differentiation in wound healing via TGF- β -Slug

signaling PNAS 2016 113 (30) E4320-E4327; published ahead of print July 8, 2016, doi:10.1073/pnas.1519197113

25. Menko AS, et al. (2014) A central role for vimentin in regulating repair function during healing of the lens epithelium. *Mol Biol Cell* 25(6):776–790.
26. Pilling, D., Fan, T., Huang, D., Kaul, B. and Gomer, R. H. (2009). Identification of markers that distinguish monocyte-derived fibrocytes from monocytes, macrophages, and fibroblasts. *PLoS ONE* 4, e7475.
27. Stewart, J. D., Masi, T. L., Cumming, A. E., Molnar, G. M., Wentworth, B. M., Sampath, K., McPherson, J. M. and Yaeger, P. C. (2003). Characterization of proliferating human skeletal muscle-derived cells in vitro: differential modulation of myoblast markers by TGF- β 2. *J. Cell. Physiol.* 196, 70-7
28. "Fibroblast". *Genetics Home Reference*. U.S. National Library of Medicine. 2014-05-05. Retrieved 2014-05-10.
29. Goodpaster T, Legesse-Miller A, Hameed MR, Aisner SC, Randolph-Habecker J, Collier HA. An immunohistochemical method for identifying fibroblasts in formalin-fixed, paraffin-embedded tissue. *J Histochem Cytochem.* 2008 Apr;56(4):347-58. Epub 2007 Dec 10.
30. (Haynes, B.F., et al. (1984). *J. Exp. Med.* 159(4):1149-1168).
31. Cserjesi P, Brown D, Ligon KL, Lyons GE, Copeland NG, Gilbert DJ, Jenkins NA, Olson EN (April 1995). "Scleraxis: a basic helix-loop-helix protein that prefigures skeletal formation during mouse embryogenesis". *Development.* 121 (4): 1099–1110. PMID 7743923.

32. Analysis of the tendon cell fate using Scleraxis, a specific marker for tendons and ligaments
Ronen Schweitzer, Jay H. Chyung, Lewis C. Murtaugh, Ava E. Brent, Vicki Rosen, Eric N. Olson, Andrew Lassar, Clifford J. Tabin *Development* 2001 128: 3855-3866;
33. Murchison, N.D., Price, B.A., Conner, D.A., Keene, D.R., Olson, E.N., Tabin, C.J., and Schweitzer, R. Regulation of tendon differentiation by scleraxis distinguishes force-transmitting tendons from muscle-anchoring tendons. *Development* 134, 2697, 2007.
34. Alberton, P., Popov, C., Pragert, M., Kohler, J., Shukunami, C., Schieker, M., and Docheva, D. Conversion of human bone marrow-derived mesenchymal stem cells into tendon progenitor cells by ectopic expression of scleraxis. *Stem Cells Dev* 21, 846, 2012
35. Rothrauff BB, Yang G, Tuan RS. Tendon resident cells-functions and features in section I-developmental biology and physiology of tendons. In: Gomes ME, Reis RL, Rodrigues M.T., editors. *Tendon regeneration*. Elsevier Inc.; 2015. p. 41—76
36. Thayer PS, Verbridge SS, Dahlgren LA, Kakar S, Guelcher SA, Goldstein AS. 2016. Fiber/collagen composites for ligament tissue engineering: influence of elastic moduli of sparse aligned fibers on mesenchymal stem cells. *J Biomed Mater Res Part A* 2016;104A:1894–1901.
37. Sugimoto Y, Takimoto A, Akiyama H, Kist R, Scherer G, Nakamura T, et al. Scx+/Sox9+ progenitors contribute to the establishment of the junction between cartilage and tendon/ligament. *Development* 2013;140(11):2280—8
38. ChisaShukunami, AkiTakimoto, MiwaOroYujiHiraki. *Scleraxis* positively regulates the expression of *tenomodulin*, a differentiation marker of tenocytes. 1 October 2006, Pages 234-247

39. Dex S, Lin D, Shukunami C, Docheva D (August 2016). "Tenogenic modulating insider factor: Systematic assessment on the functions of tenomodulin gene". *Gene*. 587 (1): 1–17. PMID 27129941. doi:10.1016/j.gene.2016.04.051
40. Shukunami C, Oshima Y, Hiraki Y (February 2001). "Molecular cloning of tenomodulin, a novel chondromodulin-I related gene". *Biochemical and Biophysical Research Communications*. 280 (5): 1323–7. PMID 11162673. doi:10.1006/bbrc.2001.4271.
41. Docheva D, Hunziker EB, Fässler R, Brandau O (January 2005). "Tenomodulin is necessary for tenocyte proliferation and tendon maturation". *Molecular and Cellular Biology*. 25 (2): 699–705. PMC 543433 . PMID 15632070. doi:10.1128/mcb.25.2.699-705.2005.
42. Komiyama Y, Ohba S, Shimohata N, Nakajima K, Hojo H, Yano F, Takato T, Docheva D, Shukunami C, Hiraki Y, Chung UI (2013). "Tenomodulin expression in the periodontal ligament enhances cellular adhesion". *PloS One*. 8 (4): e60203. PMC 3622668  . PMID 23593173. doi:10.1371/journal.pone.0060203.
43. D. Docheva, E.B. Hunziker, R. Fassler, O.Brandau Tenomodulin is necessary for tenocyte proliferation and tendon maturation *Mol. Cell. Biol.*, 25 (2005), pp. 699-705
44. Y. Oshima, K. Sato, F. Tashiro, J.I. Miyazaki, K. Nishida, Y. Hiraki, Y. Tano, C. Shukunami Anti-angiogenic action of the C-terminal domain of tenomodulin that shares homology with chondromodulin-II. *Cell Sci.* (2004), pp. 2731-2744
45. Bilezikian, J. P., Raisz, L. G. & Martin, T. J. Principles of bone biology (Elsevier, Amsterdam; London, 2008).
46. Whyte, M. P. Physiological role of alkaline phosphatase explored in hypophosphatasia. *Ann N Y Acad Sci* 1192, 190-200 (2010).

47. Farley, J. R., Hall, S. L., Tanner, M. A. & Wergedal, J. E. Specific activity of skeletal alkaline phosphatase in human osteoblast-line cells regulated by phosphate, phosphate esters, and phosphate analogs and release of alkaline phosphatase activity inversely regulated by calcium. *J Bone Miner Res* 9, 497-508 (1994).
48. Harris, H. The human alkaline phosphatases: what we know and what we don't know. *Clin Chim Acta* 186, 133-150 (1990).
49. Stigbrand, T. Present status and future trends of human alkaline phosphatases. *Prog Clin Biol Res* 166, 3-14 (1984).
50. Price, P. A. Role of vitamin-K-dependent proteins in bone metabolism. *Annu Rev Nutr* 8, 565-583 (1988).
51. Martin, I., et al., *Trends Biotechnol* (2004) 22, 80.
52. Taek Gyoung Kim, Heungsoo Shin, and Dong Woo Lim, *Biomimetic Scaffolds for Tissue Engineering*
53. Guven S, Chen P, Inci F, Tasoglu S, Erkmen B, et al. (2015) Multiscale assembly for tissue engineering and regenerative medicine. *Trends in Biotechnology* 33: 269-279.
54. *biomaterials and scaffold for tissue engineering (biomematic)*
55. L. J. Chen and M. Wang, "Production and evaluation of biodegradable composites based on PHB-PHV copolymer," *Biomaterials*, vol. 23, no. 13, pp. 2631–2639, 2002. View at Publisher · View at Google Scholar · View at Scopus
56. Peter x Ma *Biomimetic Materials for Tissue Engineering*
57. Lee, J.; Tae, G.; Kim, Y.H.; Park, I.S.; Kim, S.H. The effect of gelatin incorporation into electrospunpoly(L-lactide-co-epsilon-caprolactone) fibers on mechanical properties and cytocompatibility. *Biomaterials*

2008, 29, 1872–1879. [CrossRef] [PubMed]

58. Mota, A.; Sahebghadam Lotfi, A.; Barzin, J.; Hatam, M.; Adibi, B.; Khalaj, Z.; Massumi, M. Human bone marrow mesenchymal stem cell behaviors on PCL/gelatin nanofibrous scaffolds modified with a collagen IV-derived RGD-containing peptide. *Cell J.* 2014, 16, 1–10.
59. Cross M., Dexter T. M. 1991. Growth factors in development, transformation, and tumorigenesis. *Cell* 64, 271–280. doi:10.1016/0092-8674(91)90638-F (doi:10.1016/0092-8674(91)90638-F) [PubMed] [Cross Ref]
60. Zhang BJ, Han ZW, Duan K, Mu YD, Weng J. *J Biomed Mater Res A.* 2017 Sep 7. doi: 10.1002/jbm.a.36210. [Epub ahead of print] PMID:28884494
61. Nocini PF, Menchini Fabris GB, Gelpi F, Lotti J, Favero V, Zanotti G, Jurlaro A, Roskopf I, Lotti T, Barone A, Castegnaro G, De Santis D. *J Biol Regul Homeost Agents.* 2017 Apr-Jun;31(2 Suppl. 2):1-13.
62. Reckenbeil J, Kraus D, Stark H, Rath-Deschner B, Jäger A, Wenghoefer M, Winter J, Götz W. *Arch Oral Biol.* 2017 Jan;73:142-150. doi: 10.1016/j.archoralbio.2016.10.010. Epub 2016 Oct 15. PMID:27769028
63. Goodpaster T, Legesse-Miller A, Hameed MR et al. An immunohistochemical method for identifying fibroblasts in formalin-fixed, paraffin-embedded tissue. *J Histochem Cytochem* 2008; 56:347–358.
64. Palsson, B. *Tissue Engineering* (Pearson Education, 2009).
65. Bennett SA, Birnboim HC. Receptor-mediated and protein kinase-dependent growth enhancement of primary human fibroblasts by platelet activating factor. *Mol Carcinog* 1997;20(4): 366–75.

66. Lorenz HP, Longaker MT. Wound healing: repair biology and wound and scar treatment.
In: Mathes SJ, editor. Plastic surgery. 2nd edition. Philadelphia: Saunders; 2006. p. 209–34.
67. Pierce GF, Mustoe TA, Altmann BW, et al. The role of platelet-derived growth factor in wound healing. *J Cell Biochem* 1991; 45:319–26.
68. Robson MC, Phillips LG, Thomason A, et al. Recombinant human platelet-derived growth factor-BB for the treatment of chronic pressure ulcers. *Ann Plast Surg* 1992; 29:193–201.
69. Pierce GF, Tarpley JE, Allman RM, et al. Tissue repair processes in healing chronic pressure ulcers treated with recombinant platelet-derived growth factor BB. *Am J Pathol* 1994; 145:1399–410.
70. Salmon WD, Daughaday WH (1957). "A hormonally controlled serum factor which stimulates sulfate incorporation by cartilage in vitro". *J Lab Clin Med.* 49 (6): 825–36. PMID 13429201.
71. Keating GM (2008). "Mecasermin". *BioDrugs.* 22 (3): 177–88. PMID 18481900. doi:10.2165/00063030-200822030-00004.
72. Levine ME, Suarez JA, Brandhorst S, Balasubramanian P, Cheng CW, Madia F, Fontana L, Mirisola MG, Guevara-Aguirre J, Wan J, Passarino G, Kennedy BK, Wei M, Cohen P, Crimmins EM, Longo VD (2002). "Low protein intake is associated with a major reduction in IGF-1, cancer, and overall mortality in the 65 and younger but not older population". *Cell Metabolism.* 19(3): 407–417. PMC 3988204 . PMID 24606898. doi:10.1016/j.cmet.2014.02.006.
73. P. G. Murphy, B. J. Loitz, C. B. Frank, and D. A. Hart, "Influence of exogenous growth factors on the synthesis and secretion of collagen types I and III by explants of normal and

- healing rabbit ligaments,” *Biochemistry and Cell Biology*, vol. 72, no. 9-10, pp. 403–409, 1994.
74. Insulin-like growth factor I accelerates functional recovery from Achilles tendon injury in a rat model. *Kurtz CA, Loebig TG, Anderson DD, DeMeo PJ, Campbell PG* *Am J Sports Med.* 1999 May-Jun; 27(3):363-9.
 75. A. K. Letson and L. E. Dahners, “The effect of combinations of growth factors on ligament healing,” *Clinical Orthopaedics and Related Research*, no. 308, pp. 207–212, 1994.
 76. Yu, Y., Mu, J., Fan, Z. et al. *Histochem Cell Biol* (2012) 137: 513.
<https://doi.org/10.1007/s00418-011-0908-x>
 77. Urist, M. R. Bone: formation by autoinduction. *Science* 150, 893-899 (1965).
 78. Bilezikian, J. P., Raisz, L. G. & Martin, T. J. *Principles of bone biology* (Elsevier, Amsterdam; London, 2008).
 79. T. Katagiri, A. Yamaguchi, M. Komaki et al., “Bone morphogenetic protein-2 converts the differentiation pathway of C2C12 myoblasts into the osteoblast lineage,” *The Journal of Cell Biology*, vol. 127, no. 6, pp. 1755–1766, 1994.
 80. Bone morphogenetic proteins: Relationship between molecular structure and their osteogenic activity. September–December 2014, Pages 127-13
 81. Norouzi M, Shabani I, Ahvaz HH, Soleimani M.J *Biomed Mater Res A*. 2015 Jul;103(7):2225-35. doi: 10.1002/jbm.a.35355. Epub 2014 Nov 4. PLGA/gelatin hybrid nanofibrous scaffolds encapsulating EGF for skin regeneration.
 82. Tang G, Zhang H, Zhao Y, Zhang Y, Li X, Yuan XJ *Biomater Sci Polym Ed*. 2012;23(17):2241-57. doi: 10.1163/156856211X614185. Epub 2012 May 11.

Preparation of PLGA scaffolds with graded pores by using a gelatin-microsphere template as porogen.

83. Patel, Zarana S. et al. "Biodegradable Gelatin Microparticles as Delivery Systems for the Controlled Release of Bone Morphogenetic Protein-2." *Acta biomaterialia* 4.5 (2008): 1126–1138. *PMC*. Web. 3 Nov. 2017.

CHAPTER 5

DEVELOPMENT AND CHARACTERIZATION OF A TRI-CULTURE SYSTEM AND EVALUATING THE CAPABILITY OF THE INTEGRATED GRAFT SYSTEM TO SUPPORT HETEROGENIC CELLULAR INTERACTIONS

5.7.Introduction

The human body is known for its limited regenerative capacity [1]. Bone and skin, for instance, can self-regenerate upon injury to a certain extent depending on how severe the damage is, however, if self-repair mechanisms are overstrained, in case of non-unions or critical size defects, these tissues loss the ability to repair themselves, leading to the existence of an empty defect or the formation of a scar tissue that lacks all the necessary functional and biological properties [2, 3, 4].

One of the grand challenges in the modern medicine is the limited availability of subsequent functional impairment to these lost or damaged tissues; for example, to address the current challenges of restoring the function of damaged/injured organ or tissue, the use of biological grafts such as autograft, defined as the transplantation of a tissue within an individual from a donor site to the injury site, or allograft, defined as the transplantation of a tissue or a whole organ from another individual or a cadaver, is considered as the only viable strategy [5]. Despite the fact that the use of biological grafts led to improving the quality of lives to many individuals, serious drawbacks such as the poor biocompatibility and integration of allografts to the host tissues, and the limited availability along with the high price demand of autograft limit their clinical use, which led to the necessity of finding alternatives that mostly focus on regenerating the damaged tissues rather than repairing or replacing them [6].

Tissue engineering, which has been defined as the application of biological, chemical, and engineering principles toward the repair restoration, regeneration of tissues using biomaterial, cells, and factors alone or in combination, evolved of this necessity. Significant efforts have been made in the past few decades towards regenerating single tissues both in vitro and in vivo using the tissue engineering approaches [7]. By utilizing the tissue engineering approaches, tissue-specific scaffolds for almost every single tissue within the lower and the upper extremities such as bone [8-17], ligament [17-21], cartilage [22], muscle [23] and skin [22] have been created with great potential. Despite the fact that tissue engineering demonstrated many approaches that led to understanding the feasibility toward repairing or regenerating single targeted tissues, they do not address the grand challenges associated with engineering complex tissues such as organ systems or an entire limb.

Limitations of the current biological and engineering approaches towards complex tissue regeneration made it clear that a paradigm shift is required to successfully create translational technologies that can address the grand clinical challenges [24]. Developing a new interdisciplinary approach that utilizes the most advanced technologies currently available in different fields such as developmental biology, bioengineering, biomaterials science, stem cell biology, and clinical medicine along with a full understanding of the human's self-regenerative capacity may hold the key toward complex tissue regeneration [24, 25]. The efforts of scientists from these various fields led to the emergence of a new paradigm we term "Regenerative Engineering," which has been defined as "the Convergence of Advanced Materials Sciences, Stem Cell Sciences, Physics, Developmental Biology and Clinical Translation for the regeneration of complex tissues and organ systems." Regenerative Engineering has elements of regenerative

medicine, tissue engineering, and morphogenesis but is distinct from these individual disciplines in that it is less applicable to spot the repair of injured tissues and elements and primarily focuses on the integration and the subsequent response of stem cells to biomaterials and regeneration of the interfaces between different tissue types [26]. This new field is proposed to regenerate damaged complex tissues, with addressing grand challenges such as the regeneration of a total knee or a whole limb through the utilization of the classical top-down tissue engineering approaches in combination with bottom-up strategies used in regenerative biology in addition to the knowledge from other discipline such as advanced materials science and engineering and developmental biology [27].

The top-down approach is built on the integration of well-established elements of classical tissue engineering such as biomaterials, cells with high regenerating ability, and biologically active factors such as growth factors or small molecules [27]. The bottom-up approach calls on developmental and regenerative biology, where intact tissues are self-assembled from highly proliferative and differentiated cell layers, similarly to those cells found within the blastema in the urodele amphibians [27]. This opens the chance to discuss the unique ability of the urodele amphibians in regenerating a totally amputated limb. Distance from humans, who don't possess the ability to regenerate amputated limbs, urodele amphibians have a remarkably high regenerative capability to regenerate a severely damaged or amputated limb any time during their life time through a process known as “Epimorphic Regeneration” [28]. This unique ability to completely regrow severed limb loss in urodele amphibians has established a field of intense study to understand the characteristics of a regenerative limb [29]. Amphibians rely on their regeneration on the formation of what is referred to as blastema (a cluster of highly proliferative differentiated

cells) that plays a crucial role in establishing the regeneration process [29]. Briefly, following amputation, a cascade of events sequentially takes place starting from the formation of the wound epidermal, to the formation of blastema and the proliferation of the cells within the blastema followed by patterning of the forming tissues until a newly intact limb is regenerated [29]. We simply cannot use the same approach that the amphibians use due to the fact that our biology is completely different from the biology of the amphibians, which adds up another translational challenge; however, studying their regenerative capacity must be part of the arsenal we use to achieve our grand challenge [29].

The Regenerative engineering strategy in overcoming the barriers to regeneration in vertebrates is to harness the amphibians in humans through (1) the lessons learned from their regenerative process, which has the potential to inform us and provide us with hints in what is required for a regenerative limb to successfully regenerate, (2) in addition to developing novel engineering-based translational strategies using the top-bottom and bottom-up approaches. One lesson that we can learn from the regenerative process in the amphibian is that during limb regeneration, all tissues within the limb, including the skin interact together to reform simultaneously until a newly intact limb is regenerated. This lesson taken from the regenerative process in the amphibians has provided us with insight, that tissue formation during limb regeneration is a simultaneous process and is required for a regenerative limb to successfully regenerate. Knowing that limb regeneration is a simultaneous process, the next horizon in the field of regenerative engineering resides in how to simultaneously form these tissues and assemble them into intact multi-tissue units and facilitate their integration to the host in vivo [27].

A great deal of advances has been accomplished in the past few years to regenerate multi-tissue units along with their interfaces through the utilization of the regenerative engineering approaches, such as bone-to-ligament interface [30], bone-to-tendon interface [31], tendon-to-muscle interface [32] as well as bone-to-cartilage interface [33]. However, these current advances in the field of regenerative engineering, at the musculoskeletal level, would not have been accomplished without the effort made in several very initial proof-of-concept studies that have been carried out attempting to study the interactions between different tissue-relevant and/or interface-relevant cells in three-dimensional heterogenic cellular environments. These preliminary studies led to understanding the feasibility toward tissue/interface relevant cell-cell interactions and their role in initiating interfaces between several musculoskeletal tissues. For example, Sapalazzi et al. was the first who studied the interaction between primary osteoblasts and ligament fibroblast in a three-dimensional substrate with location-specific topographies based on the hypothesis that co-culturing both cells in a substrate with tissue-specific phases will result in the formation of a fibrocartilage-like tissue at the contact site without modulating the phenotype of both cells at either site [30]. This one initial novel preliminary study clarified many concepts and demonstrated the feasibility towards multi-tissue regeneration and tissues interfaces. However, providing a well-engineered three-dimensional framework to study the interactions between the different tissue/interface relevant cells, especially those found within the limb may hold the key towards limb regeneration.

In this aim, a tri-culture system has been developed in order to determine a growth medium that would best sustain the viability and proliferation of the three different cell types, dermal fibroblasts, ligament fibroblasts and osteoblasts in a tri-culture environment. In addition, the

capability of the integrated graft system to sustain the biological properties of the three different cell types such as cell viability, proliferation, and phenotype in the heterogenic cellular environment has been evaluated. Furthermore, cell localization in their respective phases, as well as cell migration between the three different phases within the integrated graft system, have been examined by immunofluorescence.

5.2 Materials and Methods:

Poly(lactide-co-glycolide) PLGA 85:15 (PLGA) (MW ~ 94,000 kDa) was purchased from (Absorbable Polymers, Birmingham, AL, USA), Hexafluoro-2-propanol (HFIP) was purchased from (Acros Organics, USA), Gelatin Type A from Pork (Porcine skin) was purchased from (MP Biomedical, OH, USA), Microbial Transglutaminase (mTG) was Purchased from (Ajinomoto, Japan), Dichloromethane (DCM) was purchased from (Fisher Scientific, USA), PDGF-BB, IGF-I and BMP-2 growth factors were purchased from (Fisher Scientific, USA), Dulbecco's Phosphate-Buffered Saline (PBS) of pH 7.4, MEM Alpha (1X) Minimum Essential Medium, DMEM/F-12 (1:1) (Dulbecco's Modified Eagle Medium/Nutrient Mixture F-12), Antibiotic-Antimycotic (100X), Trypsin-EDTA (0.25%) phenol red, Fetal Bovine Serum, Qualified, Penicillin-Streptomycin (10,000 U/mL), and Hank's balanced salt solution (HBSS) were purchased from Gibco (Grand Island, NY), primary antibodies, IgG monoclonal unconjugated Anti-Alkaline Phosphatase (ab108337), IgG3 monoclonal unconjugated Anti-Osteocalcin antibody (ab13420), IgG monoclonal unconjugated Anti-SCXA antibody (ab58655), IgG monoclonal unconjugated Anti-tenomodulin antibody (ab203676), IgG monoclonal unconjugated Anti-TE-7 antibody (ab197896), IgG monoclonal unconjugated Anti-Vimentin antibody (ab92547), and the compatible secondary antibodies, IgG polyclonal Goat Anti-Rabbit IgG H&L (Alexa Fluor® 488) (ab150077), and IgG polyclonal Goat Anti-Mouse IgG H&L (Alexa Fluor® 488)(ab150113) were purchased from (Abcam, MA, USA), DAPI (4',6-Diamidino-2-Phenylindole, Dihydrochloride), and anti-fade mounting medium, LIVE/DEAD™ Viability/Cytotoxicity Kit were purchased from (Invitrogen, USA), and CellTiter 96® Aqueous One Solution Cell Proliferation Assay (MTS) was purchased from (Promega Inc, USA), Polydimethylsiloxane was purchased from (Fisher Scientific Inc. , USA).

5.2.1 Tri-Culture Design Concept

The capability of the integrated graft system to sustain the viability, proliferation and the heterogeneity of the three different cell types was evaluated. However, this has been accomplished by seeding the three different cell types within the integrated graft system, each in its relevant phase and maintaining them in culture for predetermined time points and conducting the appropriate set of experiment. Prior to this, knowing the suitable growth medium that would best sustain the growth of the three different cell populations in a tri-culture environment was essential in order to ensure maintaining the viability of the cell populations. In order to determine the best suitable medium, a tri-culture model has been developed. The concept behind the idea was to establish an appropriate environment that can be employed to culture three different cell populations and have them share the same medium while they are physically separated under the same symmetrical conditions. This was done by separating the well of a 24-well plate into three different chambers, in which each chamber could be used to culture a different cell population. This was accomplished by placing a prefabricated Polydimethylsiloxane (PDMS) segment that separated the well into three different chambers. By separating the well into three different chambers, every cell population could be cultured in a different chamber within the same well, in which one cellular population could be seeded in one chamber, another cellular population could be seeded in the other next chamber, and a third cellular population could be seeded in the next third chamber within the same well. Culturing three different and physically separated cellular populations within the same well while sharing the same medium is an optimal setup for initiating cell-cell interactions in order to study the behavior of the single cell population in a tri culture environment. The tri-culture model served as a suitable tool that could be utilized in order to study the behavior of the single cell population in a tri-culture environment.

5.2.2 Mold Design, Development and Three-Dimensional Printing

A mold was first designed and 3D printed in order to be used for fabricating the PDMS segment. The mold consisted on two parts, a disc and a plate that served as a carrier for the disk. The two parts were first 3D designed using the SolidWorks 3D CAD software. The disc had a diameter of (17 mm) and a thickness of (5 mm) with an internal gap distance of (2 mm). The plate had a length of (13 mm), and a width of (8 mm) and a height of (2 mm) with an internal hole diameter of (17 mm). For 3D printing, both parts were 3D printed using (MakerBot Replicator, Makerbot, USA). Briefly, PLA filament plastic was loaded into the 3D printer syringe and it was heated to 50 °C to melt the polymer. Both parts were 3D printed with a syringe nozzle of 200 um and printing velocity of 5 mm/s within a laminar flow-cabinet. Parts were then harvest and stored.

5.2.3 Polydimethylsiloxane Segments Fabrication

To fabricate the polydimethylsiloxane (PDMS) segment, PDMS elastomer was mixed with a curing agent at a ratio of (10:1) elastomer to curing agent. The solution was mixed thoroughly for 5 minutes to ensure homogeneity between the elastomer and the curing agent. The mixture was then placed in a desiccator until almost all bubbles were removed. To fabricate the PDMS segment, the 3D printed disc was inserted into the holes within the plate, followed by pouring the PDMS elastomer into the mold. The mold containing PDMS elastomer was then placed at 37 °C for 24 hours for the PDMS elastomer to completely cure. After it is cured, the PDMS segments were removed from the mold, and stored at the desiccator for later use

5.2.4 Testing the Functionality of the Tri-Culture System

Testing the functionality of the PDMS segments was compromised into two steps:

5.2.4.1 Liquids Penetration

PDMS segments were placed into the well of a 24-well plate N=3/ time point. After placing the segments, the well was separated into three different chambers. 150 μ l of PBS was added to the first chamber, 150 μ l of a red dye was added to the second chamber, and 150 μ l of a blue dye was added to the third chamber within the same well. The plates were incubated at 37 °C. At predetermined time points, 3 and 7 days, the penetration of the three liquids to the other chambers was examined.

5.2.4.2 Cell Migration

PDMS segments were autoclaved and exposed to UV light for 30 minutes each side for sterilization. The segments were then placed into the well of a 24-well plate N=3/ time points. After placing the segments, the well was separated into three different chambers. For cell seeding, the three different cell types were trypsinized with 0.25 trypsin EDTA and centrifuged to obtain a pellet. After centrifugation, the pellet was disturbed and every chamber was seeded with a different cell type at a concentration of 5×10^3 cells/chamber and 1 ml of MEM Alpha (1X) Minimum Essential Medium supplemented with 15% FBS and 1% Penicillin/Streptomycin was added to each well and plates were incubated in a tissue culture incubator at 37°C, 5%CO₂, 3%O₂. At predetermined time points, 3 and 7 days, the plates were removed from the tissue culture incubator, the PDMS segments were removed and cell migration was observed using a normal light microscopy.

5.2.5 Fabrication of PLGA-Gelatin Coaxial Nanofiber Scaffolds

As described previously, PLGA (85:15) granules were dissolved in HFIP at 16 % wt and stirred

overnight at room temperature to prepare the (shell solution) of nanofibers. To prepare the core solution, gelatin powder type A was dissolved in HFIP at 4% wt and stirred overnight at room temperature. At the day of electrospinning, both growth factors were reconstituted at a concentration of 1 mg/ml, and 81 μ l of the reconstitution of either PDGF-BB and IGF-I were added to 1.5 ml of gelatin solutions and stirred for 15 minutes to allow the growth factor to homogenize with the gelatin solution. In the case of coaxial nanofibers with no growth factors, gelatin solution was used alone in the core-shell. An electrospinning pump (NE 300 SYRINGE pumps, USA) was used in order to fabricate the coaxial PLGA-Gelatin nanofibers. The setting to prepare the coaxial scaffolds consisted of two coaxial syringe pumps with different flow rates. In this study, the PLGA solution was used to form the outer shell and the gelatin-growth factors or free of growth factors solutions were used to form the inner core. PLGA solution and either gelatin-growth factors or free of growth factors solution were loaded into two separate 10 ml syringes and connected to the coaxial needles, a 16 G (ID = 1.6 mm) outer needle and a 22 G (ID = 0.7 mm) inner needle, respectively, and then concentrically placed. The electrospinning parameters were as follows: (applied voltage: 10 kV; 1.5 mL/h for the sheath flow rate and 0.75 mL/h for the core flow rate). The tip of the needle was placed 10 cm away from the collector. The electrospinning process lasted for 1.5 h. Coaxial electrospun nanofibers were peeled from the collector and stored under vacuumed desiccator for 24 hours to insure complete evaporation of solvent.

5.2.6 Fabrication of PLGA Microspheres

As previously described, single emulsion solvent evaporation technique was used to fabricate PLGA microspheres. PLGA granules were dissolved at 12.5% wt in Dichloromethane (DCM) in glassy vials. Vials were vortexed for 1 h at a speed of 550 RPM until clear, homogeneous, and

viscous solution was obtained. Next, PLGA solution was added via a thin stream into 1% PVA solution in a 1000 ml beaker and it was let to stir at (300 RPM) overnight to allow the solvent to evaporate. After that, microspheres were collected, filtered, air dried and then they were stored in -20 °C for 24 h to freeze any residual water particle inside of the microspheres. Next, microspheres were freeze dried for 48 h and were then sieved to obtain the desired particle size range 300 – 600 μm .

5.2.7 Incorporation of BMP-2 in Gelatin-mTG Hydrogel

Gelatin gel formation was initiated by mTG addition. For hydrogel preparation, 3% wt gelatin powder type A was dissolved in preheated phosphate-buffered saline (PBS) at 50 °C and it was let to stir on a stirrer plate for 15 minutes at 500 RPM to completely dissolve the powder. The mTG solution was prepared by dissolving 10% wt mTG in preheated PBS at 50 °C, then it was let to stir on a stirrer plate for 15 minutes at 500 RPM. As soon as both gelatin and mTG completely dissolved in PBS, the temperature of the stirrer plate was adjusted to 37 °C and they were let to stir for another 15 minutes to allow for the temperature drop. Next, to initiate the cross-linking reaction between gelatin and mTG for the hydrogel preparation, mTG solution was mixed with the 3% wt gelatin solution at a ratio of 1:11.5 under stirrer speed of 500 RPM at 37 °C. The mixture was let to stir for 5 minutes until a semi-viscus solution is fabricated and ready to be injected. BMP-2 incorporation was done by adding 1 μg of BMP-2 in 100 μl of gelatin-mTG solution and mix them gently.

5.2.8 Fabrications of PLGA Microsphere Scaffolds Incorporated Gelatin-mTG/BMP-2

To fabricate the three-dimensional scaffolds and use it to either incorporate gelatin-mTG/BMP-2 or gelatin-mTG hydrogels within it, PLGA microspheres were poured into a 10mm x 10 mm and

5 mm X 5 mm stainless steel molds and heated for 90 °C for 90 minutes. These parameters allowed the microspheres to fuse together forming the 3D scaffolds. After 90 minutes, the stainless-steel mold was removed from the oven and allowed to cool to room temperature for 2 hours. Next, scaffolds were removed and the semi-viscous gelatin-mTG/BMP-2 hydrogel was injected inside of the microsphere scaffold using an insulin syringe until all porosity were filled and it was allowed to gel at 37 °C for 1 hours.

5.2.9 Primary Cells Isolations:

6-8 weeks old (150 – 200 g) Lewis rats were obtained from (Charles River Laboratories, CT, USA) and used for all primary cell isolations. All the animal experiments were approved by the Institutional Animal Care and Use Committee (IACUC) at the University of Connecticut Health Center, CT, Farmington, USA.

5.2.9.1 Primary Dermal Fibroblasts Isolation and in Culture Maintenance:

Dermal fibroblasts were isolated and maintained in culture using the same method described in section 4.2.6.1.

5.2.9.2 Primary Ligament Fibroblasts Isolation and in Culture Maintenance:

Ligament fibroblasts were isolated and maintained in culture using the same method described in section 4.2.6.2.

5.2.9.3 Primary Bone Osteoblasts Isolation and in Culture Maintenance:

Bone osteoblasts were isolated and maintained in culture using the same method described in section 4.2.6.3.

5.2.10 In vitro Tri-culture study for the Determination of a Heterogenic Culture Medium:

The growth of the different cell types in the different mediums and medium composition in the single and the tri-culture environment was assessed using the Cell Titer 96® AQueous One Solution Cell Proliferation Assay according to the manufacturer's instructions. All scaffolds were sterilized prior to cell seeding. To sterilize PLGA microsphere scaffolds, they were submerged in 70% ethanol for 20 minutes followed by submerging in sterile PBS to remove any ethanol residuals. Next, scaffolds were exposed to UV light for 30 minutes each side. To sterilize PLGA-Gelatin coaxial electrospun nanofiber scaffolds, they were placed inside of the cell culture hood and exposed to UV light for 30 minutes each side. Finally, to sterilize the PDMS segments, they were autoclaved and exposed to UV light for 30 minutes each side. The three different cell types were trypsinized with 0.25 EDTA trypsin and centrifuged to get a pellet. After centrifugation, the cell pellet was disturbed and used for cell seeding. Dermal and ligament fibroblasts were seeded on 5 mm X 5 mm PLGA-Gelatin coaxial electrospun nanofiber scaffolds at a density of 5×10^4 cells/scaffold, and osteoblasts were seeded on 5 mm X 5 mm PLGA-Gelatin-mTG microsphere scaffolds at a density of 5×10^4 cells/scaffold. For the single culture environment, pre-seeded scaffolds were placed in low-binding 24-well plates and every scaffold was maintained in culture in 1 ml of three different mediums, and four different medium composition as follows: (1) MEM supplemented with 15% FBS, 1X Penicillin/Streptomycin, non-essential amino acids, and sodium pyruvate, (2), DMEM/F-12 supplemented with 10% FBS and 1% P/S (3), MEM Alpha (1X) Minimum Essential Medium supplemented with 15% FBS and 1% Penicillin/Streptomycin (4), [2:1:1] (5), [1:2:1] (6), [1:1:2] and (7) [1:1:1] respectively with an N=3/ medium type for every scaffold. For the tri-culture environment, PDMS segments were placed in low-binding 24-well plates, in which every well was separated into three different chambers. Every chamber was

occupied with a different scaffold pre-seeded with a different cell type. In every well, dermal fibroblasts pre-seeded PLGA-Gelatin coaxial electrospun nanofiber scaffold was placed in the first chamber, ligament fibroblasts pre-seeded PLGA-Gelatin coaxial electrospun nanofiber scaffold was placed in the second chamber, and osteoblasts pre-seeded PLGA-Gelatin-mTG scaffold was placed in the next third chamber of the same well with an N=3/ medium type for every scaffold. All scaffolds were maintained in 1 ml of the same mediums and medium compositions of the single culture environment. All scaffolds from the single and tri-culture environment were maintained in a tissue culture incubator at 37°C, 5%CO₂, 3%O₂. After day 3 and 7, scaffolds were removed from their wells or chambers and placed in new wells after two washes with PBS. Next, scaffolds were incubated with a cocktail of the relevant medium type premixed with MTS solution at a ratio of (1:5) for 3 hours at 37 C. 500 µL of sodium dodecyl sulfate was added to each well to stop the reaction and the absorbance at 490 nm was measured with a spectrophotometric plate reader (TECAN, Crailsheim, Germany).

5.2.11 *In Vitro* Evaluations of the Integrated Graft System

5.2.11.1 LIVE/DEAD Assay

All scaffolds were sterilized prior to cell seeding. To sterilize PLGA microsphere scaffolds, they were submerged in 70% ethanol for 20 minutes followed by submerging in sterile PBS to remove any ethanol residuals. Next, scaffolds were exposed to UV light for 30 minutes each side. To sterilize PLGA-Gelatin/growth factors coaxial electrospun nanofiber scaffolds, they were placed inside of the cell culture hood and exposed to UV light for 30 minutes each side. To incorporate BMP-2 in PLGA microsphere scaffolds, scaffolds were injected with 100 µl of gelatin-mTG/BMP-2 (1µg/ scaffold). Scaffolds injected with gelatin-mTG/BMP-2 were further incubated at 37C to

allow for complete gelation. Dermal and fibroblasts were seeded on 1 cm X 2 cm PLGA-Gelatin-PDGF-BB coaxial electrospun nanofiber scaffolds (Phase A), ligament fibroblasts were seeded on 1 cm X 1 cm PLGA-Gelatin-IGF-I coaxial electrospun nanofiber scaffolds (Phase B), and osteoblasts were seeded on 10 mm X 10 mm PLGA-Gelatin-mTG/BMP-2 cylindrical microsphere scaffolds (Phase C). All cells were seeded at a density of 1×10^5 cells/ scaffold and scaffolds were placed in low binding 24-well plates in triplicate. Cells were allowed to attach for 1.5 h in the cell culture incubator at 37 °C prior to the addition of 2 ml of the relevant medium for every cell type. All scaffolds were maintained in a tissue culture incubator at 37°C, 5%CO₂, 3%O₂ with an N=3/ scaffold. At day 2, all scaffolds were harvested, washed twice with PBS and assessed for construction of the integrated graft system, in which Phase B was placed on top of Phase C and both Phases C and B were wrapped up by Phase A. The grafts were then sutured to fix the phases and placed in fresh low-binding 24-well plate with 2 ml of MEM Alpha (1X) Minimum Essential Medium supplemented with 15% FBS and 1% Penicillin/Streptomycin for every well and were maintained in a tissue culture incubator at 37°C, 5%CO₂, 3%O₂. After 3 and 7 days of the graft construction, grafts were harvested, washed with PBS twice, the phases were then separated and every phase was assessed for LIVE/DEAD assay, which was used to qualitatively determine cell viability based on a green fluorescent probe that recognizes intracellular esterase activity, calcein AM, and a red fluorescent probe that recognizes damaged plasma membranes, ethidium homodimer-1 (EthD-1). To perform the assay, every separated phase was incubated with 2 mL of the prepared EthD-1/calcein solution at a concentration of 2 ul/ mL EthD-1, and 0.5 ul/ mL calcein AM in PBS for 1 hour. Next, phases were washed twice with PBS and visualized using an inverted fluorescence microscope (Zeiss LSM 880) using Zen Software.

5.2.11.2 Proliferation Assay

The capability of the integrated graft system to sustain the proliferation of the different cell types in the tri-culture environment was assessed using the Cell Titer 96® AQueous One Solution Cell Proliferation Assay according to the manufacturer's instructions. All phases underwent the same sterilization technique as described in the previous experiment, and the same seeding density was applied to all phases for all cell types having the same experimental groups and conditions. At day 2, all phases were assembled as described previously, and after culturing the graft for 3 and 7 days post graft construction, grafts were harvested, washed with PBS twice, the phases were then separated and every phase was incubated separately with a cocktail of MEM Alpha (1X) Minimum Essential Medium supplemented with 15% FBS and 1% Penicillin/Streptomycin premixed with MTS solution at a ratio of (1:5) for 3 hours at 37 C. 500 µL of sodium dodecyl sulfate was added to each well to stop the reaction and the absorbance at 490 nm was measured with a spectrophotometric plate reader (TECAN, Crailsheim, Germany).

5.2.11.3 Cell Localization and Phenotypic Maintenance of the Three Different Cellular Populations Within the Integrated Graft System:

To determine the localization and the phenotypic maintenance of three different cell types on the relevant phases within the integrated graft system in the heterogenic cellular environment, all phases were subjected to Immunofluorescence analysis. Briefly, all phases underwent the same sterilization technique as described in the previous experiment, and the same seeding density was applied to all phases for all cell types having the same experimental groups and conditions. At day 2, all phases were assembled as described previously, and after culturing the graft for 3 and 7 days post graft construction, grafts were harvested, washed with PBS twice, and they were then

separated. Post separation, the three different phases were subjected to Immunofluorescence analysis at room temperature as follows: all phases were placed separately in different wells in 24-well plate and 2 mL of 100X absolute methanol was added to each well to fix cells cultured on the phases for 5 minutes, followed by three washes with PBS. Cells within the phases were then Permeabilized with 1 mL of 0.1 % Triton X-100 in PBS for 15 minutes, followed by three washes with PBS. Cells were then blocked with 10% goat serum in PBS for 1 hour at room temperature, followed by three washes with PBS. Next, Phase A was incubated with IgG monoclonal unconjugated Anti-Vimentin antibody (1:500); Phase B was incubated with IgG monoclonal unconjugated Anti-SCXA antibody (1:1000); and Phase C was incubated with IgG monoclonal unconjugated Anti-Alkaline Phosphatase (1:100) for 2 hours. All antibodies were diluted using the same blocking solution of 10% goat serum in PBS. Post incubation, cells were washed three times with PBS and incubated with the secondary antibodies for another 2 hours at dark. All cells were incubated with the secondary antibody IgG polyclonal Goat Anti-Rabbit IgG H&L (Alexa Fluor® 488) (1:500). After incubation with the secondary antibodies for 2 hours, cells were washed three times with PBS away from light, then incubated with DAPI (4',6-Diamidino-2-Phenylindole, Dihydrochloride) at a concentration (1:3000). Cells were then washed 1 time with PBS and all phases were visualized using an inverted fluorescence microscope (Zeiss LSM 880) using Zen Software.

5.2.11.4 Cell Migration within the Integrated Graft System:

To examine the cell migration within the different phases, all phases underwent the same sterilization technique as described in the previous experiment, and the same seeding density was applied to all phases for all cell types having the same experimental groups and conditions. At day

2, all phases were assembled as described previously, and after culturing the graft for 3 and 7 days post graft construction, grafts were harvested, washed with PBS twice, and they were then separated. Post separation, the three different phases were subjected to the same Immunofluorescence analysis described in the previous experiment with varying in the type of antibodies used for incubations. Briefly, to examine the migration of ligament fibroblasts to Phase A, Phase A was incubated with the IgG monoclonal unconjugated Anti-SCXA antibody (1:1000); to examine the migration of dermal fibroblasts to Phase B, Phase B was incubated with IgG monoclonal unconjugated Anti-Vimentin antibody (1:500); to examine the migration of osteoblasts to Phase B, Phase B was incubated with IgG monoclonal unconjugated Anti-Alkaline Phosphatase (1:100); and to examine the migration of ligament fibroblasts to Phase C, Phase C was incubated with IgG monoclonal unconjugated Anti-SCXA antibody (1:1000). All phases underwent the same incubation times and were subjected to incubation with the same secondary antibody. After incubation with the secondary antibodies for 2 hours, cells were washed, incubated with DAPI and visualized under fluorescence microscope following the same procedure as described previously.

5.2.12 Statistical Analysis

Data are presented as mean \pm standard deviation (SD). All statistical analyses were performed using the Statistical Software Prism GraphPad (Version 5) using two-way Analysis of Variance (ANOVA) with a Tukey test for Post Hoc parameter comparisons. Statistical significance was set at $p < 0.05$.

5.3 Results:

5.3.1 Development and Testing the Functionality of the Tri-Culture Model:

The mold was successfully designed and 3D printed as shown in (Figure 5.1 A, B). This mold was essential in order to be able to fabricate the PDMS segments that were further used to establish our tri-culture model. As shown in the (Figure 5.1 A, B), the mold consisted of two different parts, a disc and a plate. The plate however, served as a platform that housed the disc in the provided holes to prevent the PDMS from leaking from the sides of the disc during the pouring process of the elastomer into the mold. When the PDMS was poured into the mold, no leakage was observed indicating that the disc is well fitted into the holes. After pouring the PDMS into the mold, it was incubated at 37 °C for 24 h for the PDMS to cure in order to allow for the formation of the PDMS segments. After they cured, the PDMS segments were removed from the mold and placed inside of the well of the 24-well plate and they perfectly fitted the well, indicating that the dimensions used in the design were accurate. By placing the PDMS segment to the well, the well was separated into three different chambers, in which each chamber could be used to culture a different cell population (Figure 5.1 D).

To examine the liquids penetration, different water-based dyes were added to different chambers after placing the PDMS segment into the well of the 24-well plate in which, a red dye was placed in the first chamber, a blue dye was placed in the other chamber and PBS was placed in the next third chamber and the liquid penetration was examined after 3 and 7 days of incubation at 37 °C. No liquid penetration was observed at the two-time points, indicating that the PDMS segments are well fitted into the wells and that they are acting as real physical barrier between the three different chambers (Figure 5.4). To examine the cell migration between the chambers, different cell types

were seeded in the three chambers and cultured for 3 and 7 days and the cell migration was observed after every time point under a normal light microscopy. No evidence for cellular migration between the chambers was seen after the removal of the PDMS segments from the wells in the two different time points (Figure 5.5, 5.6).

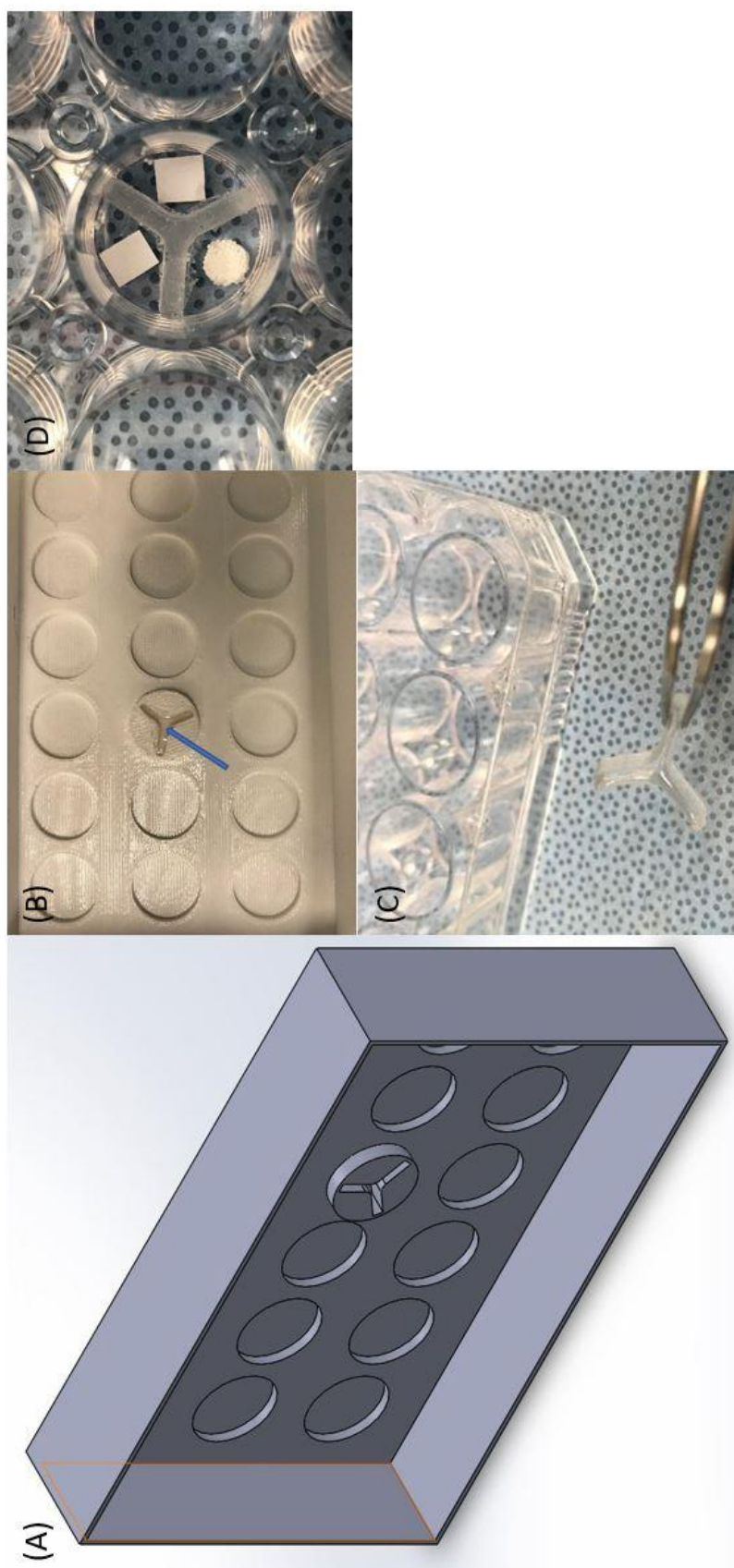


Figure 5.1. A three-dimensional representation of the mold used for the devolvement of the tri-culture model. (A) 3D view of the mold design showing the disc inserted in the provided hole, (B) the actual 3D printed mold and the PDMS elastomer filling the cavity within the disc, (C) the morphology of the cured PDMS segment after incubation at 37 C, and (D) the PDMS segment placed inside of the well of the 24-well plate and separating the well into three different chambers, the three different phases are shown occupying the different chambers. Blue arrow indicates the PDMS elastomer.

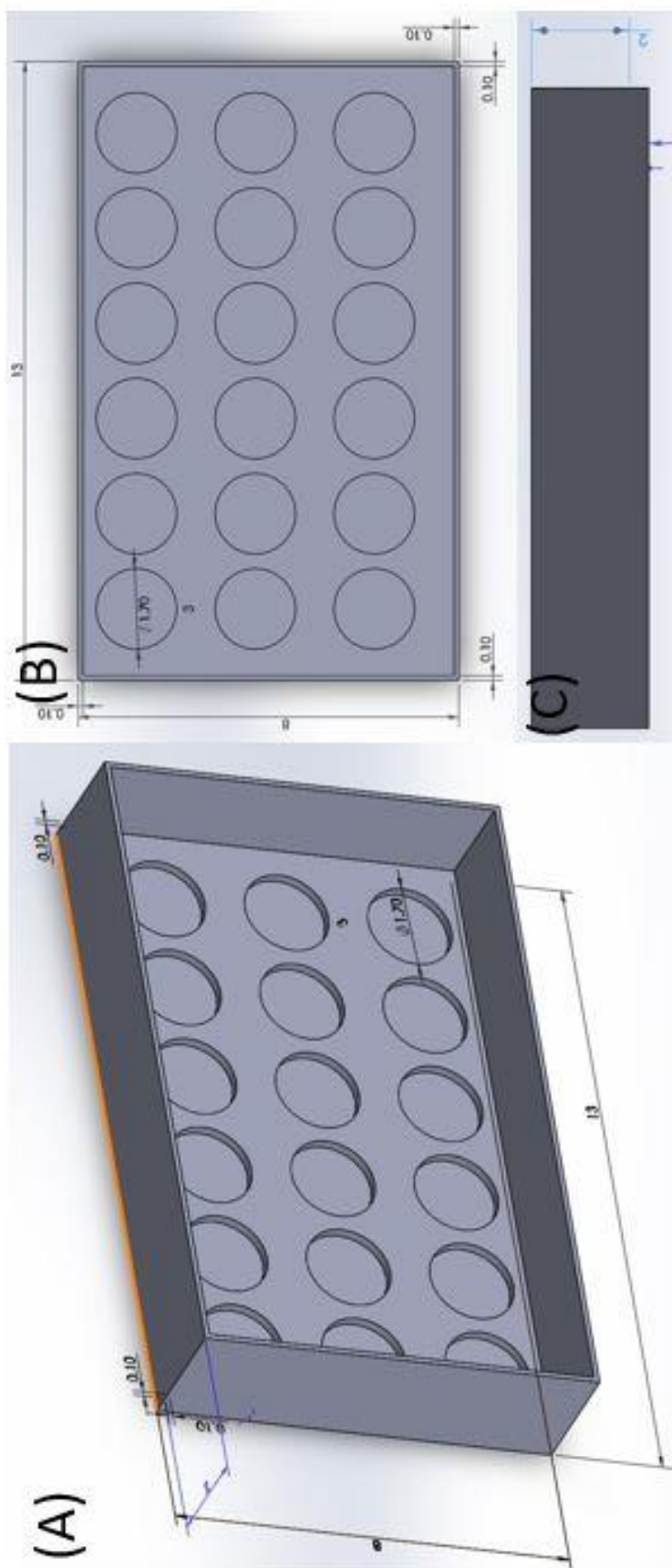


Figure 5.2. Dimensions of the plate that was used as the platform for the disc. (A) 3D view showing the dimensions of the plate from different planes, (B) top view showing the width 8 mm and the length 13 mm of the plate, and (C) side view Showing the height of the plate 2 mm.

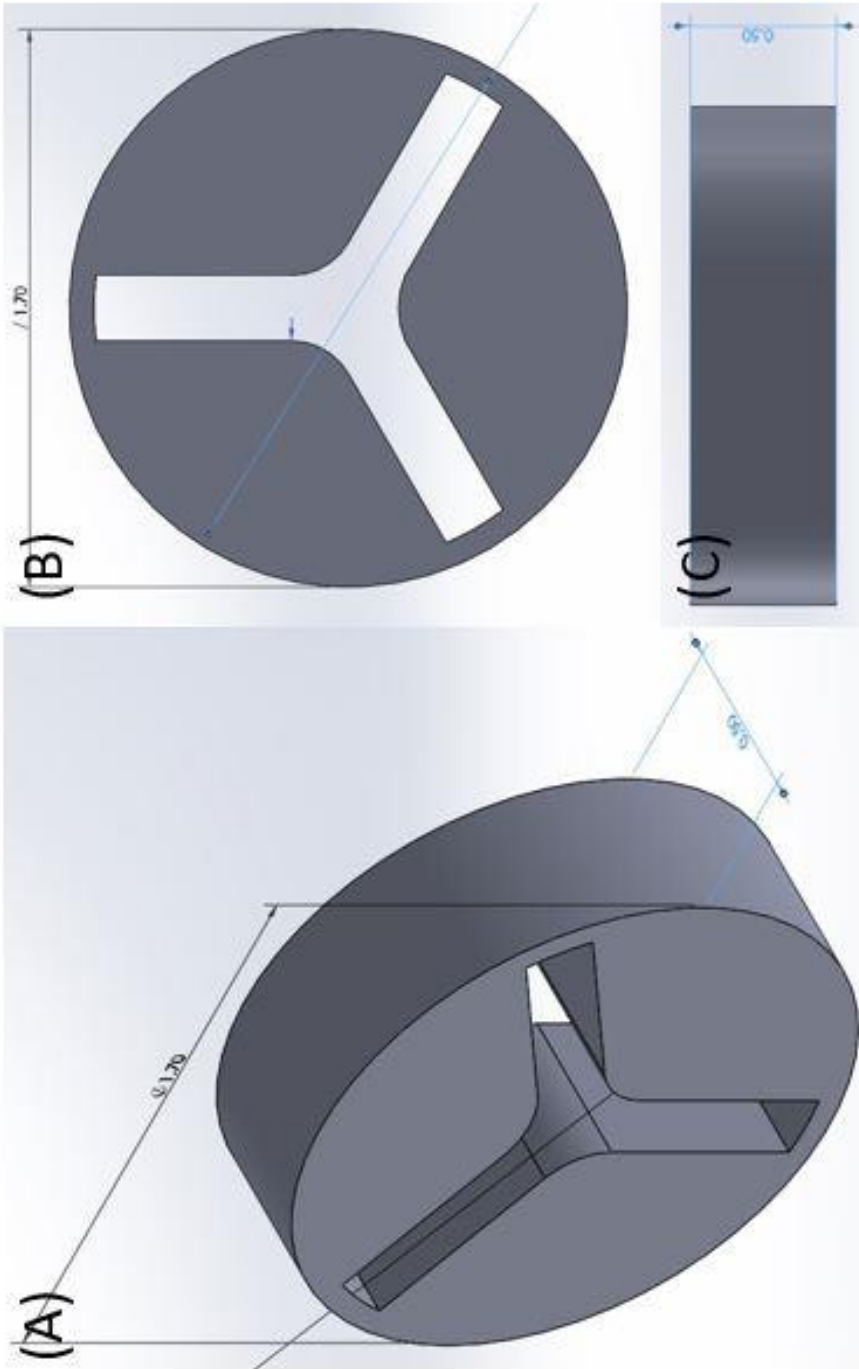


Figure 5.3. Dimensions of the disc. (A) 3D view showing the dimensions of the disc from different planes, (B) top view showing the diameter of the disc 17 mm, and (C) side view Showing the thickness of the disc 5 mm.

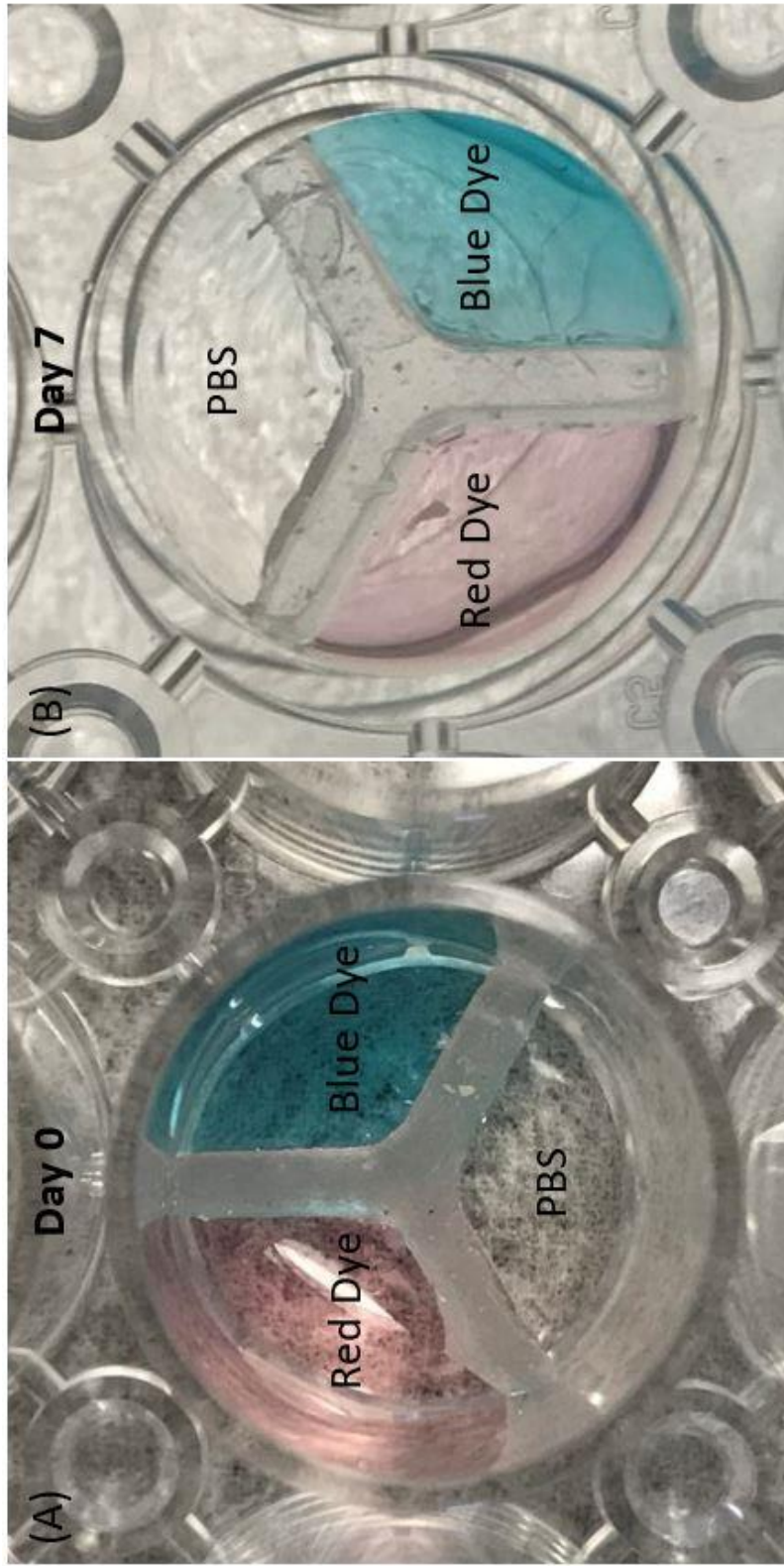


Figure 5.4. Three different water-based dyes were added to the different chambers to examine the permeability of these dyes to the neighboring chambers. (A) top view of the well showing the three different dyes, each in a different chamber at day 0, and (B) bottom view of the same well showing no evidence for water penetration after incubation at 37 C for 7 days.

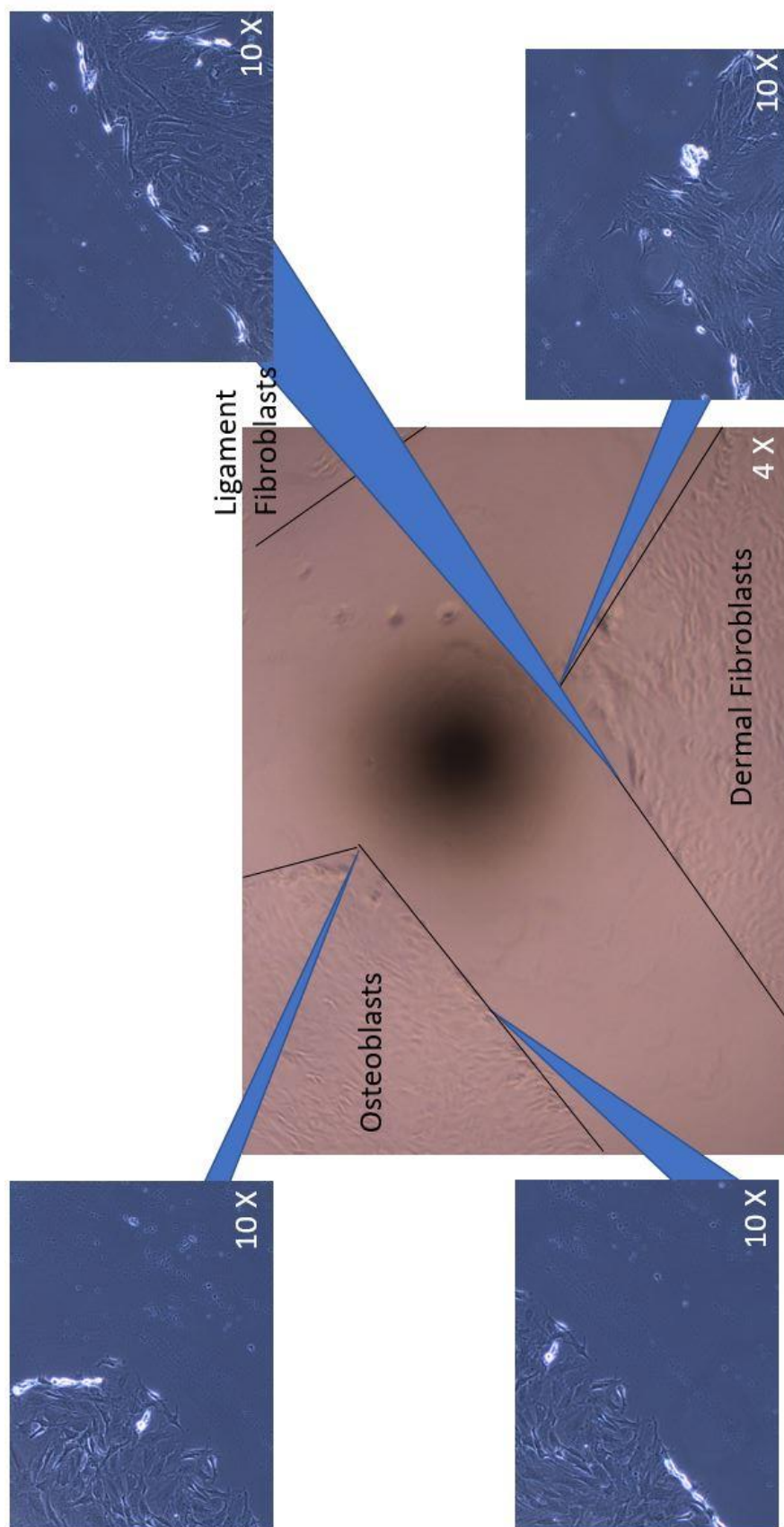


Figure 5.5. Three different cell types, dermal fibroblasts, ligament fibroblasts and osteoblasts were seeded and cultured in the well of a 24-well plate, each in a different chamber after placing the PDMS segment to examine cell migration to the neighboring chambers. At day 3, the PDMS segment was removed and different wells were visualized under a normal light microscopy to examine the cell migration, as seen in the figure, no evidence for cell migration was observed between the neighboring chambers after Day 3. Scale bars 4X and 10 X.

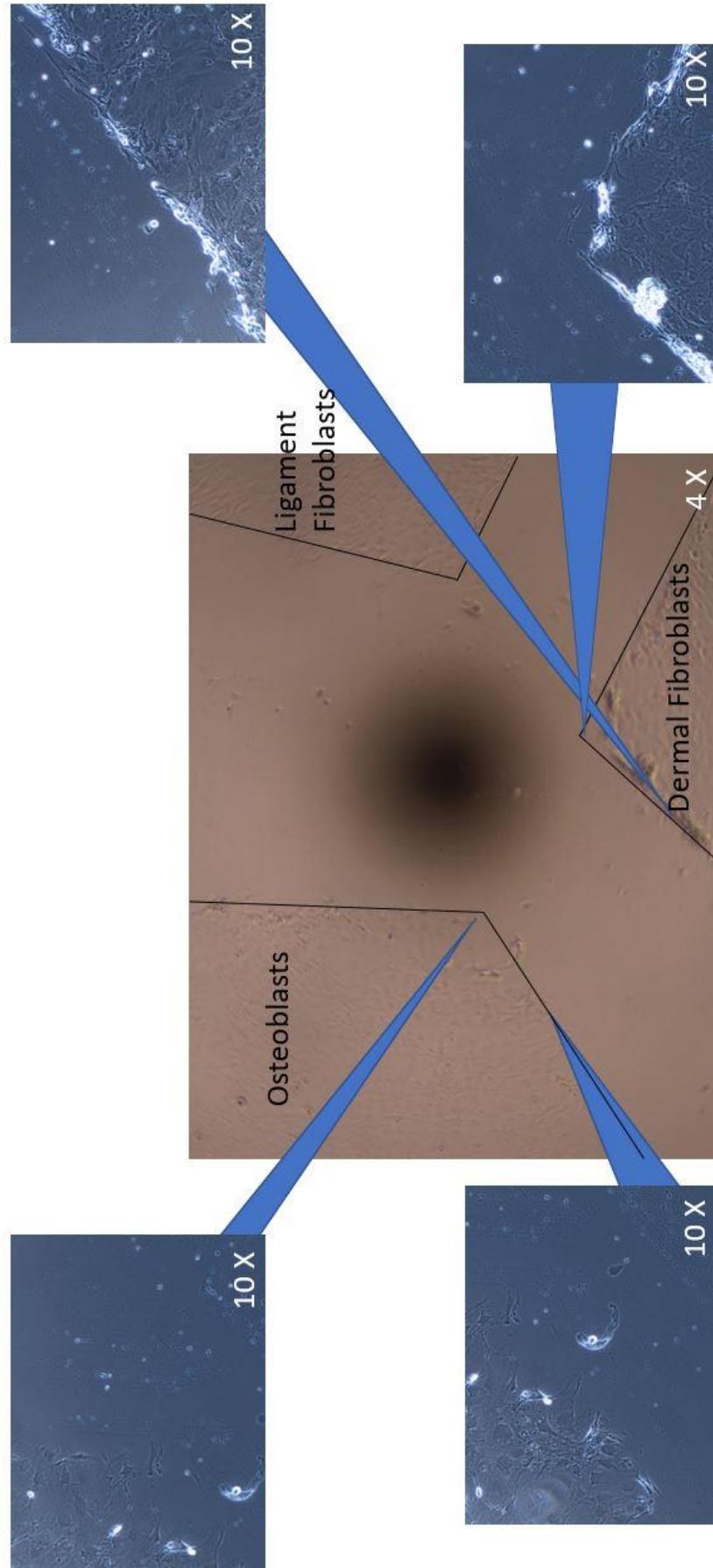


Figure 5.6. Three different cell types, dermal fibroblasts, ligament fibroblasts and osteoblasts were seeded and cultured in the well of a 24-well plate, each in a different chamber after placing the PDMS segment to examine cell migration to the neighboring chambers. At day 7, the PDMS segment was removed and different wells were visualized under a normal light microscopy to examine the cell migration, as seen in the figure, no evidence for cell migration was observed between the neighboring chambers after Day 7. Scale bars 4X and 10 X.

5.3.2. In vitro Tri-Culture Study for the Determination of a Heterogenic Culture Medium

To examine the most suitable growth medium that would best sustain the growth of the three different cell types both in the single and tri-culture environment, cells were seeded in their relevant phases and assayed for proliferation after 3 and 7 days post culture. Regardless of the medium type, all the three different cell types had significantly higher proliferation rates in the tri-culture environment in comparison to their proliferation rates when cultured alone in the single culture environment (Figure 5.7, 5.8, 5.9, 5.10).

To make the comparison understandable and much easier, we calculated the increase in the fold number between day 3 and day 7 for all cell types cultured in all different medium and medium compositions in the single and tri-culture environment (Figure 5.7). In the single culture environment, dermal fibroblasts had the highest fold number when cultured in the (LF) medium (0.54 folds) when compared to all the other mediums, and in the tri-culture environment, dermal fibroblasts had the highest fold number when cultured in the [1:2:1] medium composition (2.21 folds) in comparison to all the other mediums (Figure 5.7, 5.8). When comparing the behavior of ligament fibroblasts and osteoblasts, both ligament fibroblasts and osteoblasts had the highest fold number in the single and tri-culture environment when cultured in the (OB) medium when compared to all the other mediums (Figure 5.7, 5.9, 5.10). However, the increase in fold numbers of ligament fibroblasts cultured in (OB) medium in the single and tri-culture environment were (0.5, 0.66 folds) respectively (Figure 5.7, 5.9), and the increase in fold numbers of osteoblasts cultured in (OB) medium in the single and tri-culture environment were (1.14, 1.23 folds) respectively (Figure 5.7, 5.10).

Cell Type	Osteoblasts (OB) Medium		Dermal Fibroblasts (DF) Medium		Ligament Fibroblasts (LF) Medium		Different Compositions of OB, DF, and LF Growth Mediums			
	MEM Alpha (1X) Minimum Essential Medium supplemented with 15% FBS and 1% Penicillin/Streptomycin		MEM supplemented with 15% FBS, 1X Penicillin/Streptomycin, non-essential amino acids, and sodium pyruvate		DMEM/F-12 supplemented with 10% FBS and 1% P/S		[2:1:1]	[1:2:1]	[1:1:2]	[1:1:1]
Dermal Fibroblasts	SC / TC		SC / TC		SC / TC		SC / TC	SC / TC	SC / TC	SC / TC
	0.4 / 1.42		0.44 / 1.0		0.54 / 1.2		0.5 / 1.53	0.39 / 2.21	0.32 / 1.73	0.52 / 1.71
Ligament Fibroblasts	0.5 / 0.66		0.33 / 0.49		0.15 / 0.35		0.1 / 0.19	0.05 / 0.4	0.017 / 0.31	0.17 / 0.36
Osteoblasts	1.14 / 1.23		0.2 / 0.71		0.17 / 0.57		0.27 / 0.38	0.08 / 0.18	0.17 / 0.2	0.89 / 0.44

Figure 5.7. The three different cell types were seeded in their relevant phases and each phase was cultured in different mediums and medium compositions in a single and a tri-culture environment in order to determine the medium that would best sustain their growth in the tri-culture environment. Numbers indicate the increase in fold between day 3 and 7.

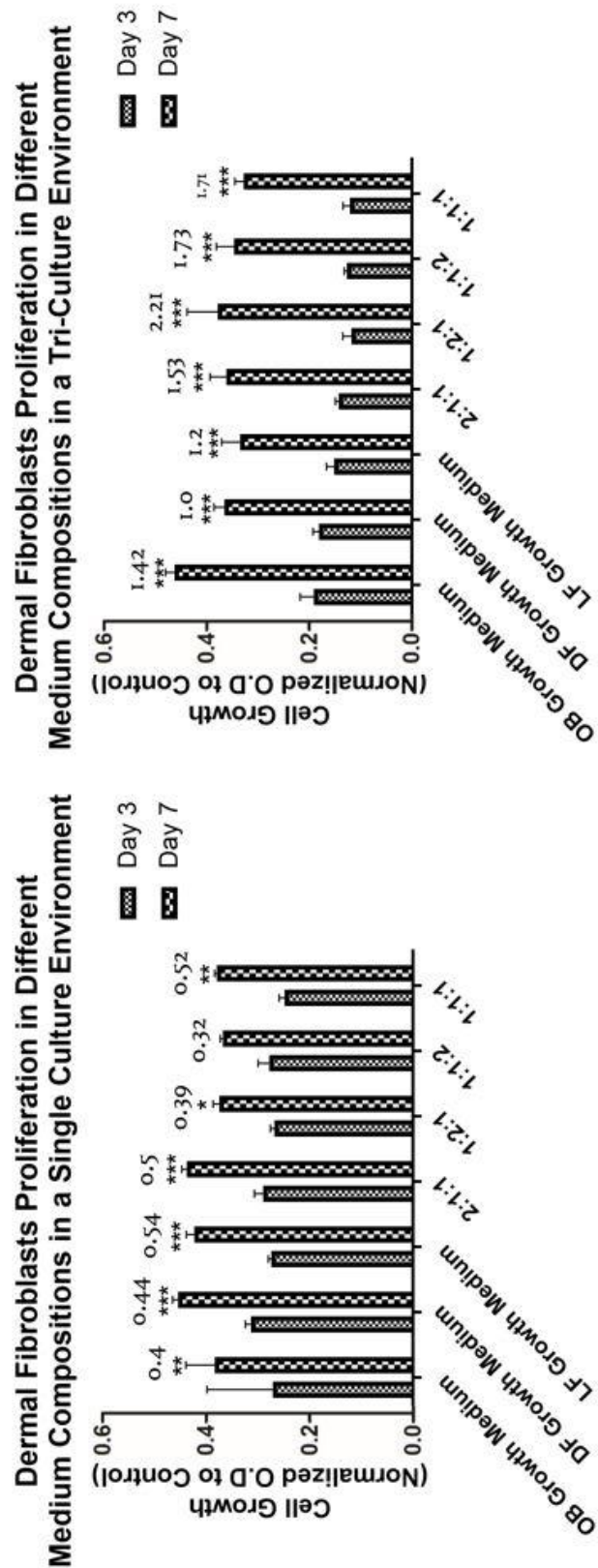


Figure 5.8. Proliferation Assay. Dermal fibroblasts cultured in different medium and medium compositions in a single and tri-culture environment. Numbers on top of the bars indicate the increase in fold between day 3 and 7. n= 3 P < 0.05*, P < 0.0**, P < 0.001***

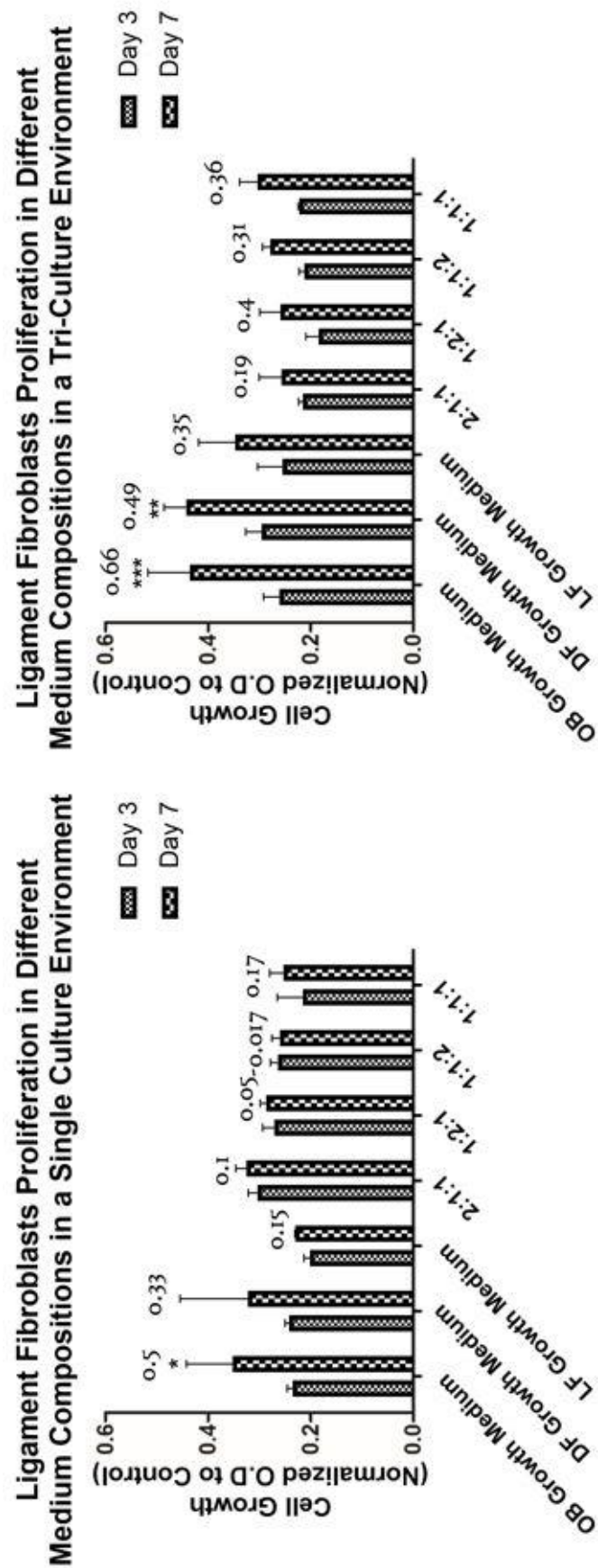


Figure 5.9. Proliferation Assay Ligament fibroblasts cultured in different medium and medium compositions in a single and tri-culture environment. Numbers on top of the bars indicate the increase in fold between day 3 and 7. $n=3$ $P < 0.05^*$, $P < 0.001^{***}$, $P < 0.0001^{****}$

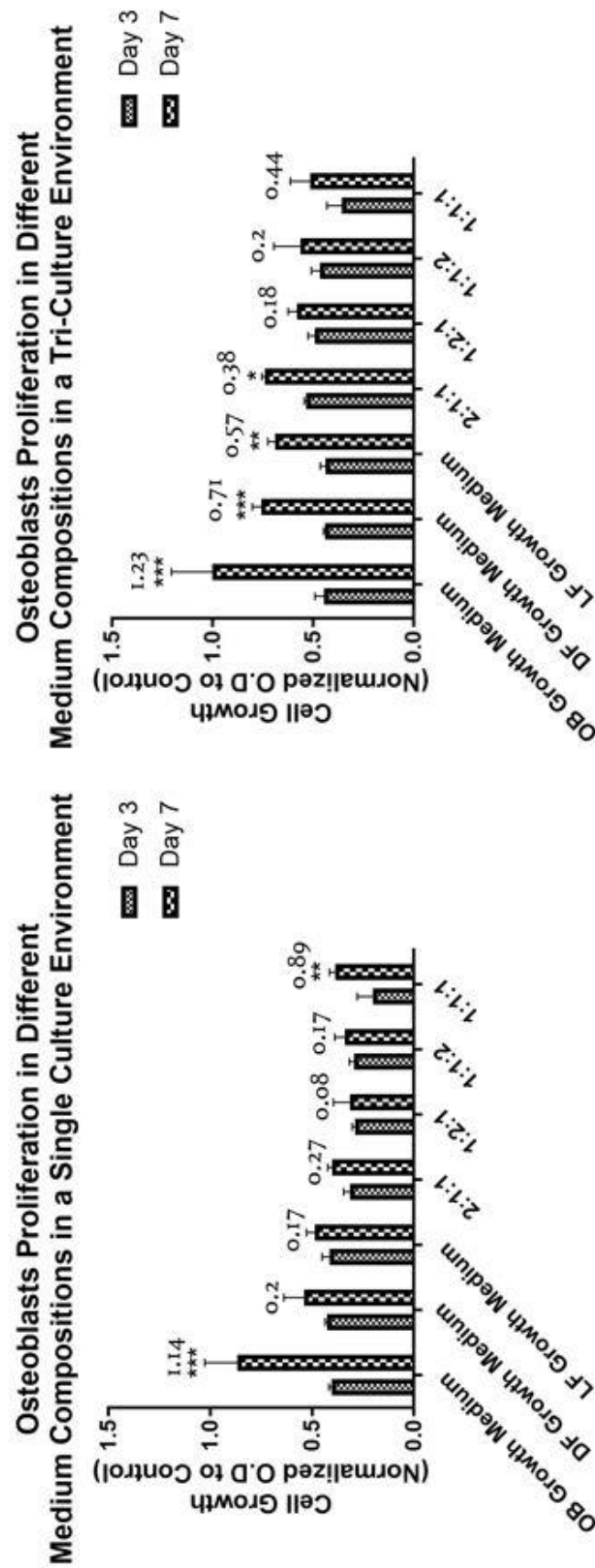


Figure 5.10. Proliferation Assay. Osteoblasts cultured in different medium and medium compositions in a single and tri-culture environment. Numbers on top of the bars indicate the increase in fold between day 3 and 7. $n=3$ $P < 0.05^*$, $P < 0.01^{**}$, $P < 0.001^{***}$

5.3.3. LIVE/DEAD and Proliferation Assays

LIVE/DEAD and MTS proliferation assays were performed on the three different phases on day 3 and 7 to qualitatively and quantitatively determine capability of the integrated graft system to sustain the viability and proliferation of the three different cell types seeded in their relevant phases. Our integrated graft system supported the viability and the proliferation of primary dermal fibroblasts, ligament fibroblasts and osteoblasts and dead cells were not evidence, as cells displayed a robust and healthy morphology. At day 3, both dermal and ligament fibroblasts showed more of a flattened morphology when compared to day 7, where they were intact and displayed more of a slender shape cytoplasm (Figure 5.11). The three different cell types showed significant increase in proliferation rates between the two different time points 3 and 7 (Figure 5.12). Although the difference was not statistically significant, osteoblasts showed higher proliferation trend in comparison to both dermal and ligament fibroblasts in day 3. This could have been due to the fact that microsphere scaffolds possess higher surface area than the electrospun nanofiber scaffold, which by its turn gave more space for osteoblasts to grow. In day 7, both dermal fibroblast and osteoblasts showed higher proliferation trends when compared to ligament fibroblasts, but not statistically significant.

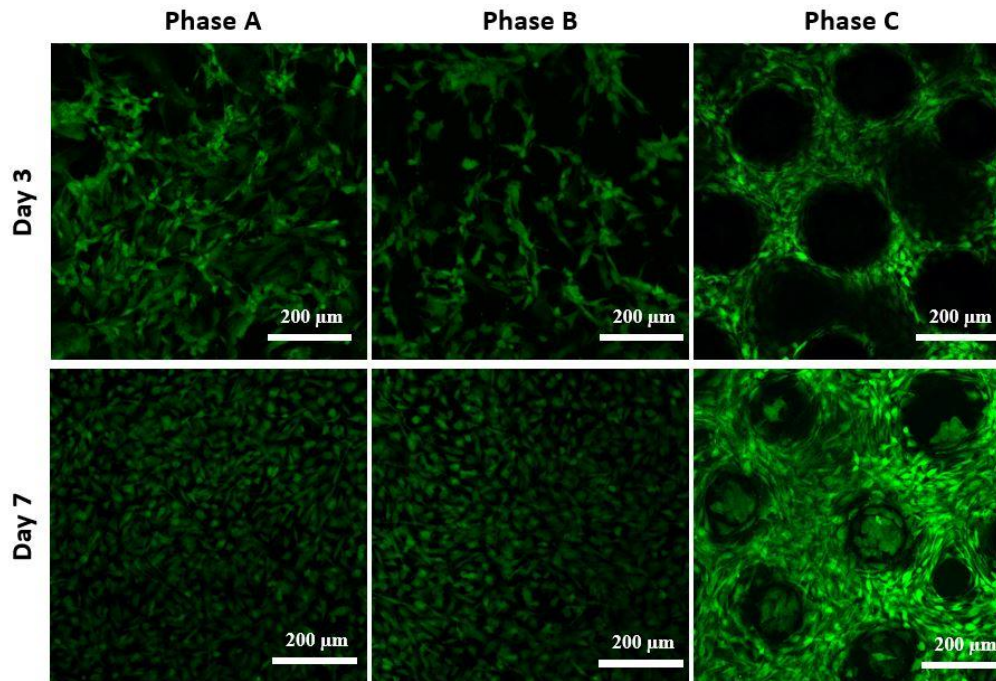


Figure 5.11 Viability Assay. Dermal fibroblasts, ligament fibroblasts and osteoblasts were seeded in phases A, B and C respectively and cultured for 2 days. 2 days post initial culture, they were assembled in which, Phase B was placed on top of Phase C and both phases were covered by Phase A and cultured for further 3 and 7 days. After 3 and 7 days, phases were separated and assayed for cell Viability using LIVE/DEAD assay. $n=3$ $P < 0.05^*$, $P < 0.0^{**}$, $P < 0.001^{***}$

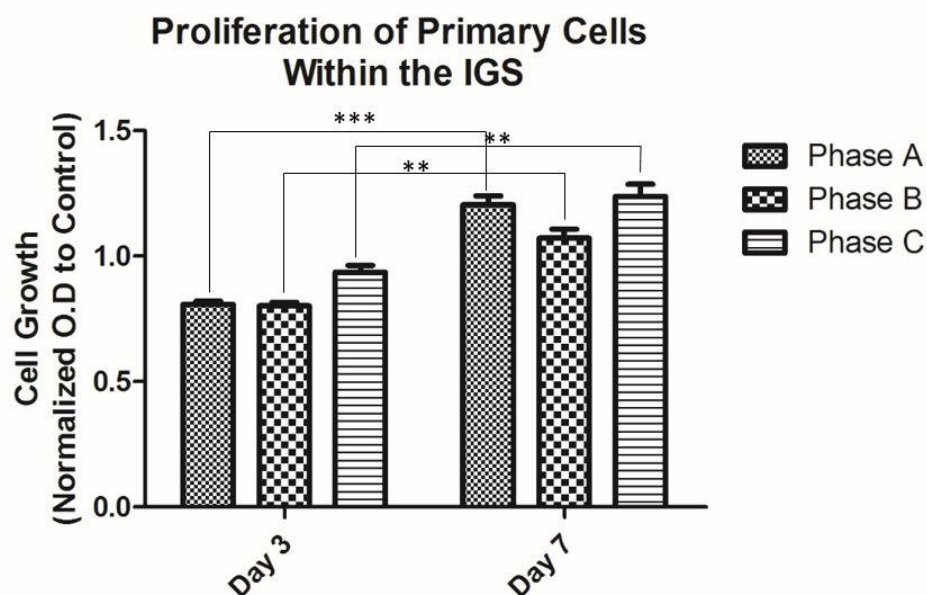


Figure 5.12 Proliferation Assay. Dermal fibroblasts, ligament fibroblasts and osteoblasts were seeded in phases A, B and C respectively and cultured for 2 days. 2 days post initial culture, they were assembled in which, Phase B was placed on top of Phase C and both phases were covered by Phase A and cultured for further 3 and 7 days. After 3 and 7 days, phases were separated and assayed for cell proliferation. $n=3$ $P < 0.05^*$, $P < 0.0^{**}$, $P < 0.001^{***}$

5.3.4. Localization, Migration and Phenotypic Maintenance:

The capability of the integrated graft system to sustain the localization and phenotypic maintenance of the three different cell types in their respective phases have been evaluated by immunofluorescence using cell-specific marker. In addition, cell migration within the phases has been examined too with immunofluorescence. As shown in in (Figure 5.13), fluorescence microscopy data revealed that the three different cell types, dermal fibroblasts, ligament fibroblasts and osteoblasts were indeed localized primarily at their respective phases at the two-time points. After 7 days of culture, the three different cell types were still localized and proliferated in their respective phases. Cell migration was observed between all the phases, where both ligament fibroblasts and osteoblasts migrated between Phases B and C in both days 3 and 7, with an increase in the number of the migrated cells at day 7 as seen in (Figure 5.13). Migration of both ligament and dermal fibroblasts between Phases A and B was evidenced too based on the immunofluorescence data, however, migration of these two cell types within these phases was only observed at day 7, with no migration observed at day 3.

The three different phases were immuno-stained with cell-specific markers, where Phase A was stained with the IgG monoclonal unconjugated Anti-Vimentin, and Phase B was stained with the IgG monoclonal unconjugated Anti-SCXA antibody, and Phase C was stained with the IgG monoclonal unconjugated Anti-Alkaline Phosphatase antibody in order to examine the maintenance of the phenotype of the three different cell types in the heterogenic cellular population. As seen in (Figure 3.15) all cells within their respective phases have been positively stained against all the specific markers used for immunostaining after culturing them in a heterogenic cellular population for 3 and 7 days, indicating that the IGS supported the phenotypic maintenance of these cells.

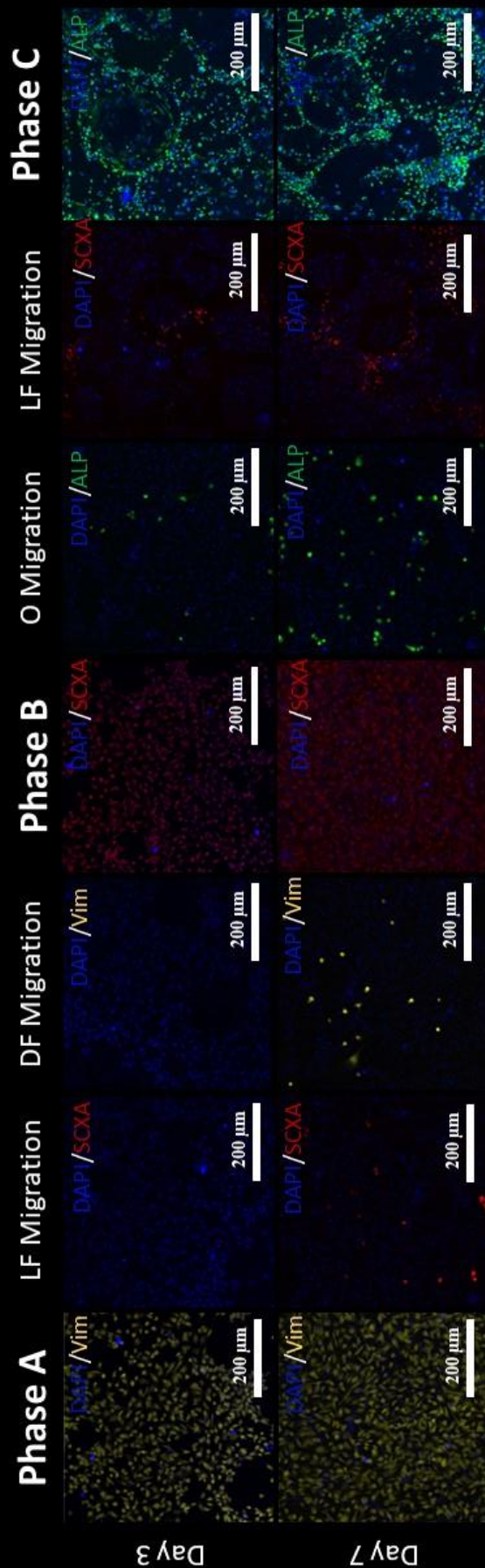


Figure 5.13 Immunofluorescence Staining. The three different phases within the IGS were immunostained with cell-specific markers to examine the localization and phenotypic maintenance of the cells cultured within every phase. Cell migration between the phases was examined too by immunostaining. As seen in the figure, the three different cell types remained localized in their relevant phases and the IGS maintained the phenotype of the three different cell types within the graft for 7 days. Cell migration between all phases was observed after 3 and 7 days. However, no cell migration was observed between Phase A and B after 3 days.

5.4. Discussion:

The capability of the integrated graft system to sustain the viability, proliferation, localization and phenotypic maintenance of the three different cell types in the heterogenic cellular population was evaluated. However, this would not have been appropriately accomplished without optimizing what growth medium would best support the growth of the three different cell types in the heterogenic environment. It is very well known from the literature that cell growth can strongly be influenced by the surrounding external environment [34]. For example, cells cultured in a co-culture environment tend to behave differently than when they are cultured in a single culture environment [34]. In a single culture environment, cells tend to normally proliferate if they are provided with the appropriate growth medium. On the other hand, cells cultured with different cellular populations tend to behave differently due to the cell-cell interactions initiated in the co-culture environment, thus, resulting in either an increase or decrease in cell proliferation [34]. Yet there is increasing evidence that the choice of growth media can contribute to the increase or decrease in cell proliferation in the co-culture environment [34]. Therefore, an early optimization of the most suitable growth medium is essential to ensure sustaining the best level of viability and cell proliferation in the co-culture environment.

In this study, to determine the best suitable medium, a tri-culture model has been developed by conducting very simple procedures that consisted of designing and three-dimensional printing of a mold, that was further used to fabricate PDMS segments that were used for the establishment of the tri-culture system. Three-dimensional (3D) printing has emerged as a unique technology that can be employed by disparate fields to several different needs [35]. This technology is utilized to produce a variety of complex and functional structures with complex geometries using less

material than the traditional manufacturing methods in a timely manner. 3D printing applications cover various sectors from education to industry and more recently in tissue engineering for the production of biomimetic scaffolds with precise geometry [35]. In this study, 3D printing technology was employed to produce a mold that could be further utilized to fabricate PDMS segments for the establishment of a tri-culture model. However, the mold was successfully designed, and 3D printed as shown in (Figure 5.1 A, B). PDMS is an elastomer which through very simple molding procedure can be shaped into a wide variety of different structures depending on the applications needs [36]. It is transparent, biocompatible, and permeable to gas, which explains the strong interest of the scientific community in using this material to fabricate microfluidic devices for cell biological studies as well as to fabricate segments, boundaries or monolayers for co-culturing studies [36].

As shown in the (Figure 5.1 A, B), the mold consisted of two different parts, a disc, and a plate. The plate, however, served as a platform that housed the disc in the provided holes to prevent the PDMS from leaking from the sides of the disc during the pouring process of the elastomer into the mold. When the PDMS was poured into the mold, no leakage was observed indicating that the disc is well fitted into the holes. After pouring the PDMS into the mold, it was incubated at 37 °C for 24 h for the PDMS to cure in order to allow for the formation of the PDMS segments. PDMS elastomer has the ability to cure at various temperatures ranging from 25 °C to 150 °C. However; the curing time largely depends on the incubation temperature, where the higher the temperature, the faster it cures. For example, PDMS elastomers incubated at 150 °C take up to ~ 10 minutes to cure, while elastomers incubated at 37 °C can take up to 24 h to completely cure. Due to the fact that the mold was printed from a plastic material, we had to incubate it at 37 °C to prevent the

mold from melting [37]. After they cured, the PDMS segments were removed from the mold and placed inside of the well of the 24-well plate, and they perfectly fitted the well, indicating that the dimensions used in the design were accurate. When designing the mold, dimensions were carefully taken into considerations to ensure the perfect fit of the PDMS segments into the wells of the 24-well plate. By placing the PDMS segment to the well, the well was separated into three different chambers, in which each chamber could be used to culture a different cell population (Figure 5.1 D). During the design process, the height of the disc (5 mm) had to be quarter the total height of the well of the 24-well plate (20 mm), and that is in order to facilitate the medium exchange between the three different cell types when establishing the tri-culture after placing the PDMS segments into the well (Figure 5.1 D). One elegant property inherited by PDMS is the stickiness observed on its surface after it cures, this property, in particular, supported the integration of the PDMS segments into the walls and the surface of the TCP when they were placed inside of the well of the 24-well plate [36]. Since the PDMS segments are mobile and not physically fixed into the wells of the 24-well plate, we needed to investigate two important factors that had to be met in order to mark the success of the tri-culture model, (1) when culturing cells into the different chambers, cells have to stay and only proliferate within the chamber they are seeded into and not migrate to the other neighboring chambers, and (2) when adding different liquids into the different chambers, they have to remain held within the chamber they are added into and not penetrate to the other chambers. This second point, however, is very important in cases where different reagents such as MTS, Picogreen, etc. need to be added into the different chambers for running assays to study the behavior of the single cell population in the tri-culture environment.

To examine the liquids penetration, different water-based dyes were added to different chambers after placing the PDMS segment into the well of the 24-well plate in which, a red dye was placed in the first chamber, a blue dye was placed in the other chamber, and PBS was placed in the next third chamber, and the liquid penetration was examined after 3 and 7 days of incubation at 37 °C. No liquid penetration was observed at the two-time points indicating that the PDMS segments are well fitted into the wells and that they are acting as real physical barriers between the three different chambers (Figure 5.4). Water molecules are very small, 0.27 nm in size, however, if these very small water molecules could not penetrate from the sides nor underneath the PDMS segments, cells which are ~ 10 um in diameter, should not migrate at all. Although this fact was stated, we still needed to examine the cell migration between the chambers [38]. To do so, different cell types were seeded in the three chambers and cultured for 3 and 7 days and the cell migration was observed after every time point under a normal light microscopy. No evidence for cellular migration between the chambers was seen after the removal of the PDMS segment from the wells in the two different time points (Figure 5.5, 5.6). In a study by Yang et al. the migration speed of cultured endothelial cells has been investigated by placing a PDMS monolayer blocker at the middle of a cell culture dish that separated the dish into two different chambers. Both chambers were seeded with the same endothelial cell population and were cultured for pretrimmed time points [39]. However, after removing the PDMS blocker, no evidence of cell migration was found. These observations suggest that PDMS have the potential to serve as a physical barrier for co-culturing or/and tri-culturing purposes. Based on our findings, we could prove the functionality of our tri-culture model and its ability to serve as a valuable system for studying the behavior of the single cell population in a tri-culture environment. Our tri-culture model has emerged to be unique, simple and functional.

The tri-culture model was further used in order to examine the most suitable growth medium that would best sustain the proliferation of the three different cell types both in the single and tri-culture environment. To do so, cells were seeded in their relevant phases and assayed for proliferation after 3 and 7 days post culture. Using our synthetic tri-culture model, we were able to study the proliferative abilities of the three different cell types cultured alone, or in a tri-culture environment by exposing them to different mediums and medium compositions.

Interestingly and regardless the medium type, all the three different cell types had significantly higher proliferation rates in the tri-culture environment in comparison to their proliferation rates when cultured alone in the single culture environment (Figure 5.7). The significant increase in cell proliferation of the three different cell types in the tri-culture environment when compared to the single culture environment could be attributed to the secretion of an array of different endogenous growth factors and cytokines by the both fibroblasts and osteoblasts that could potentially upregulated the proliferation of the three different cell types in the tri-culture environment. Fibroblasts play an essential role in wound healing by endogenously producing an array of growth factors and cytokines that are essential for collagen synthesis as well as maintaining cell viability and growth [40]. Osteoblasts are also known to produce a number of growth factors and cytokines that are known to encourage cellular proliferation and differentiation. A list of all the endogenous growth factors secreted by both fibroblasts and osteoblasts stimulating cellular behaviors can be seen in (Table 1). A number of studies have explained the biological responses of dermal fibroblasts co-cultured with osteoblasts, and ligament fibroblasts co-cultured with osteoblasts, but no study to date has evaluated the biological responses of the three cultured together [41,30]. Dermal fibroblasts have shown to enhance the biological responses of primary osteoblasts such as

proliferation when co-cultured together [41], similarly to ligament fibroblasts which have been proven to maintain the proliferation of osteoblasts in a co-culture environment. These findings demonstrate the strong relationship of both fibroblasts to primary osteoblasts, and that their presence in culture along with osteoblasts can positively influence the biological responses of osteoblasts. In contrast, findings from our study indicate that not only the presence of fibroblasts can enhance the biological responses of osteoblasts, but also the presence of osteoblasts can potentially enhance the biological properties of fibroblasts, thus, implying the strong relationship between fibroblasts and osteoblasts. However, further studies are indeed required in order to validate these findings.

To make the comparison of our findings from the tri-culture experiment understandable and much easier, we calculate the increase in the fold number between day 3 and day 7 for all cell types cultured in all different mediums and medium compositions in the single and tri-culture environment (Figure 5.7). In the single culture environment, dermal fibroblasts had the highest fold number when cultured in the (LF) medium (0.54 folds) when compared to all the other mediums, and in the tri-culture environment, dermal fibroblasts had the highest fold number when cultured in the [1:2:1] medium composition (2.21 folds) in comparison to all the other mediums (Figure 5.7, 5.8). When comparing the behavior of ligament fibroblasts and osteoblasts, both ligament fibroblasts and osteoblasts had the highest fold number in the single and tri-culture environment when cultured in the (OB) medium when compared to their proliferation in all the other mediums (Figure 5.7, 5.9, 5.10). However, the increase in fold numbers of ligament fibroblasts cultured in (OB) medium in the single and tri-culture environment were (0.5, 0.66 folds) respectively (Figure 5.7, 5.9), and the increase in fold numbers of osteoblasts cultured in (OB)

Growth Factors Secreted Cells	Endogenous Secreted Growth Factors	Dermal Fibroblasts Response to Endogenously Secreted Growth Factors	Ligament Fibroblasts Response to Endogenously Secreted Growth Factors	Osteoblasts Response to Endogenously Secreted Growth Factors
Dermal Fibroblasts	TGF- β 1	Promotes cell growth, proliferation, and increase collagen synthesis.	Promotes cell growth, proliferation, and increase collagen synthesis.	Stimulates cell proliferation, and collagen synthesis.
	PDGF-BB	Stimulates IGF-I production, cell proliferation, and has a role in tissue remodeling.	Stimulates IGF-I production, cell proliferation, and has a role in tissue remodeling.	Increases cell metabolic activities, stimulates cell proliferation, increases collagen production.
	bFGF	Promotes cell proliferation, and collagen synthesis.	Promotes cell proliferation, and collagen synthesis.	Stimulates cell proliferation, and increases collagen synthesis.
	IGF-I	Increases metabolic activities, supports cell proliferation, and aid in collagen synthesis.	Increases metabolic activities, supports cell proliferation, and aid in collagen synthesis.	Stimulates proliferation of cells Capable of synthesizing collagen.
Ligament Fibroblasts	TGF- β 1	Stimulates extensive cell proliferation and stratification.	Stimulates extensive cell proliferation, and aid in collagen synthesis.	Stimulates cell proliferation, and collagen synthesis.
	PDGF-BB	Stimulates cell proliferation and migration In vivo.	Increases cell metabolic activities, stimulates cell proliferation, increases collagen production.	Increases cell metabolic activities, stimulates cell proliferation, increases collagen production.
	bFGF	Stimulates cell proliferation, and VEGF and HGF production.	Stimulates cell proliferation, and increases collagen synthesis.	Stimulates cell proliferation, and increases collagen synthesis.
	IGF-I	Stimulates cell proliferation	Stimulates proliferation of cells Capable of synthesizing collagen.	Stimulates proliferation of cells Capable of synthesizing collagen.
Osteoblasts	TGF- β 1	Stimulates extensive cell proliferation and stratification.	Promotes cell growth, proliferation, and increase collagen synthesis.	Stimulates proliferation of cells
	PDGF-BB	Stimulates cell proliferation and migration In vivo.	Stimulates IGF-I production, cell proliferation, and has a role in tissue remodeling.	Stimulates proliferation of cells
	bFGF	Stimulates cell proliferation, and VEGF and HGF production.	Promotes cell proliferation, and collagen synthesis.	Stimulates proliferation of cells
	IGF-I	Stimulates cell proliferation	Increases metabolic activities, supports cell proliferation, and aid in collagen synthesis.	Stimulates proliferation of cells

Table 1: A list of *in vitro* **Endogenously** secreted growth factors by dermal fibroblasts, ligament fibroblasts and osteoblasts and the *in vitro* responses of the three cell types to the secreted growth factors [56-61].

medium in the single and tri-culture environment were (1.14, 1.23 folds) respectively (Figure 5.7, 5.10). Since both ligament fibroblasts and osteoblasts showed the best cell proliferation in the (OB) medium, and since dermal fibroblasts also showed a relatively good proliferation in (OB) medium (1.42 folds), we suggest that (OB) medium would be the growth medium that can best sustain the viability and proliferation of all the three different cell types when cultured in the heterogenic cellular population within the integrated graft system.

The scaffold design for this study includes different phases with variation in morphology, composition and cell type with a specific intention of supporting multiple cell types. The current integrated graft system is based on the synthetic biodegradable polymer (PLGA 85:15) and the naturally derived biomaterial (gelatin), where Phase A is fabricated from PLGA-Gelatin-PDGF-BB coaxial electrospun nanofibers to support dermal fibroblasts culture, Phase B is fabricated from PLGA-Gelatin-IGF-I coaxial electrospun nanofibers to support ligament fibroblasts culture, and Phase C is fabricated from PLGA-Gelatin-mTG/ BMP-2 to support osteoblasts culture. However, due to the morphological, compositional complexity found within the system, viability, proliferation, localization and phenotypic maintenance of the three different cell types in the heterogenic environment had to be evaluated over time in order to examine the capability of our complex integrated graft system to sustain these cellular biological properties.

Based on our findings from the proliferation and viability assays conducted after 3 and 7 days, the integrated graft system could sustain the viability and proliferation of the three different cell types, each in its respective phase. In general, cellular proliferation of osteoblasts and dermal fibroblasts were higher than ligament fibroblasts. Spalazzi et al. have reported that co-culturing ligament

fibroblasts and osteoblasts result in an increase in cell proliferation of both cell types over time. Although they both continuously proliferated over time, it was found that ligament fibroblasts had higher proliferation rates in the co-culture environment when compared to osteoblast and this is most likely due to the difference in proliferation rates between fibroblasts and osteoblasts [30]. In our case the proliferation rate of osteoblast was higher in comparison to ligament fibroblasts, but not statistically significant. Conclusions cannot be made that whether the presence of dermal fibroblasts had influenced the proliferation of osteoblasts, resulting in an increase in osteoblasts cell proliferation, therefore, further experiments are still needed in order to study the contributions and the direct influence of dermal fibroblasts on osteoblasts. Although several studies have reported the potential of dermal fibroblasts differentiation into the osteogenic tendency, very limited number of studies has reported their influence on osteoblasts proliferation in a co-culture environment [42].

Our immunofluorescence data revealed that the three different cellular populations were mainly localized and continued to proliferate in their respective phases at both time points 3 and 7 days. In addition, cell migration was observed between all the phases at both time points. However, cell migration between Phases A and B was only observed at day 7, with no cell migration observed at day 3 at all.

The three different phases were immuno-stained with cell-specific markers in order to examine the phenotypic maintenance of the three different cell types in the three-dimensional heterogenic cellular environment. As seen in (Figure 3.15) all cells within their respective phases have been positively stained against all the specific markers used for immunostaining after culturing them in

the heterogenic cellular environment for 3 and 7 days, indicating that the IGS could sustain the phenotype of these cells for up to 7 days.

It has been reported that interaction of osteoblasts and ligament fibroblasts in a monolayer co-culture model resulted in modulation in cellular phenotype along with decrease in osteoblasts alkaline phosphate activity and expression of type II collagen as well as an increase in mineralization potential of fibroblasts at the contact site, but resulted in phenotypic maintenance of both cells at either site. In addition, it was shown that co-culture of fibroblasts with osteoblasts resulted in an increase in cell proliferation, tissue-specific extracellular matrix production in comparison to the monoculture of either cell [30]. These observations suggest that both osteoblasts and ligament fibroblasts have the potential to maintain their phenotype, proliferation, and the production of tissue-specific extracellular matrix proteins in a co-culture environment. While ligament fibroblasts have the potential to maintain their phenotype in a co-culture system, dermal fibroblasts find difficulties maintaining their phenotype in heterogenic cellular populations, specifically when co-cultured with osteoblasts [42]. Dermal fibroblasts are mesenchymal stem cells by nature; they can directly be converted or reprogrammed into another differentiated lineage without passing an intermediate pluripotent Stage [42]. These conversions include direct conversion of dermal fibroblasts into cardiomyocytes (43, 44), neurons (45–47), chondrocytes (48), and hepatocytes (49, 50), as well as of human fibroblasts into cardiomyocytes (51,52), neurons (46, 53), hematopoietic cells (52) and osteoblasts [42].

Although dermal fibroblasts do not typically express markers of osteoblastic differentiation, they have previously been shown to undergo osteoinduction when stimulated with bone morphogenetic

proteins (BMPs) [55]. These observations suggest that the surrounding external environment can largely influence dermal fibroblasts by triggering them to modulate their phenotype and differentiate into other tendencies. Although BMP-2 was incorporated within Phase C, which could have been able to affect the phenotype of dermal fibroblast, dermal fibroblasts could maintain their phenotype in the heterogenic environment for up to 7 days. These findings demonstrate the capability of the IGS to sustain the phenotype of the three different cell types in the heterogenic cellular environment. The ability of the IGS to sustain the phenotype of the three different cell types in the heterogenic cellular environment can be attributed to many factors that include but not limited to, (1) providing the appropriate 3D synthetic matrix for every cell type that could potentially support the phenotypic maintenance, and (2) delivering growth factors that are known to encourage cellular proliferation locally. These factors might have aided in the maintenance of the phenotype of the three different cell types in the heterogenic cellular environment.

To our knowledge, this is the first reported study that focuses on designing a single scaffold system to study the heterogenic cellular interactions of dermal, ligament fibroblasts and osteoblasts as well as their potential to form tissues simultaneously. This integrated graft system is designed to provide structurally, compositionally and chemically suitable environment that could sustain the viability, proliferation and heterogenic cellular interaction of dermal fibroblasts, ligament fibroblast, and osteoblasts. Our promising results demonstrate the feasibility of heterogenic cellular interactions on a single scaffold, and the potential of the integrated graft system to support multiple tissue regeneration simultaneously *in vivo*.

The capability of the integrated graft system to sustain the viability, proliferation, and phenotype of the three different cell types in the heterogenic cellular environment can be further investigated for a longer time to examine the graft's capability to sustain the biological properties of the three different cell types in a longer timeframe. In addition, the direct effect of dermal fibroblast on osteoblasts and ligament fibroblasts shall be investigated.

5.5. Conclusion:

In conclusion, a tri-culture model has been successfully designed, developed, evaluated and utilized in order to determine the growth medium that would best support the viability and proliferation of the three different cell types in the heterogenic cellular environment. The tri-culture experiment findings suggest that (OB) medium “MEM Alpha (1X) Minimum Essential Medium supplemented with 15% FBS and 1% Penicillin/Streptomycin” would be a suitable growth medium that can best sustain the viability and proliferation of all the three different cell types when cultured in the heterogenic cellular environment within the integrated graft system. The integrated graft system has been shown to support the viability, proliferation, localization, and phenotypic maintenance of the distinct cellular population in the heterogenic environment for up to 7 days. While additional studies are needed to further characterize the system to confirm its efficacy, the presented work suggests the feasibility of heterogenic cellular interactions on a single scaffold, and the potential of the integrated graft system to support multiple tissue regeneration simultaneously in vivo.

5.6. References

1. Murphy MB, Monviva K, Caplan AI. Mesenchymal stem cells: Environmentally responsive therapeutics for regenerative medicine. *Experimental and Molecular Medicine*. 2013
2. <https://www.woundcarecenters.org/article/wound-basics/different-types-of-wounds>
3. <http://www.woundsource.com/blog/difference-between-acute-and-chronic-wounds>
4. Laurencin CT, Nair LS. Regenerative engineering: approaches to limb regeneration and other grand challenges. *Regenerative Engineering and Translational Medicine*. 2015; 1:13.
5. The Quest toward limb regeneration: a regenerative engineering approach Cato T. Laurencin Lakshmi S. Nair *Regenerative Biomaterials*, Volume 3, Issue 2, 1 June 2016, Pages 123–125
6. Chiarello E, Cadossi M, Tedesco G, Capra P, Calamelli C, Shehu A, Giannini S. *Aging Clin Exp Res*. 2013 Oct;25 Suppl 1: S101-3. doi: 10.1007/s40520-013-0088-8. Epub 2013 Sep 18
7. Laurencin CT, Ambrosio AA, Borden MD., et al. Annual review of biomedical engineering. In: Yarmush MI, editor. (ed). *Annual Reviews*. Palo Alto, 1999, 19–46
8. Laurencin CT, Khan Y, Kofron M, El-Amin S, Botchwey E, Yu X, Cooper JA Jr. The ABJS Nicolas Andry Award: Tissue engineering of bone and ligament: A 15-year perspective. *Clin OrthopRelat Res* 2006; 447:221–236.
9. Jabbarzadeh E, Nair LS, Khan YM, Deng M, Laurencin CT. Apatite nano-crystalline surface modification of poly(lactide-co-glycolide) sintered microsphere scaffolds for bone tissue engineering: Implications for protein adsorption. *J Biomater Sci Polymer Ed* 2007; 18:1141–1152.

10. Cushnie E, Khan Y, Laurencin CT. Amorphous hydroxyapatite-sintered polymeric scaffolds for bone tissue regeneration: Physical characterization studies. *J Biomed Mater Res* 2008; 84:54–62.
11. Khan Y, Cushnie E, Laurencin CT. In situ synthesized ceramic-polymer composites for bone tissue engineering: Bioactivity and degradation studies. *J Mat Sci* 2007; 42:4183–4190.
12. Khan Y, Yaszemski MJ, Mikos AG, Laurencin CT. Tissue engineering of bone: Material and matrix considerations. *J Bone Joint Surg* 2008; 90:36–42.
13. Jiang T, Khan Y, Nair LS, Abdel-Fattah WI, Laurencin CT. Functionalization of chitosan/poly (lactic acid-glycolic acid) sintered microsphere scaffolds via surface heparinization for bone tissue engineering. *J Biomed Mater Res A* 2010; 93:1193–1208.
14. Cushnie E, Khan Y, Laurencin CT. Tissue engineered matrices as functional delivery systems: Adsorption and release of bioactive proteins from degradable composite scaffolds. *J Biomed Mater Res A* 2010; 94:568–575.
15. Kofron MD, Cooper JA Jr, Kumbar SG, Laurencin CT. Novel tubular composite matrix for bone repair. *J Biomed Mater Res A* 2007; 82:415–425.
16. Kofron MD, Laurencin CT. Development of a calcium phosphate coprecipitate/poly(lactide-co-glycolide) DNA delivery system: release kinetics and cellular transfection studies. *Biomaterials* 2004; 25:2637–2643.
17. Lu HH, Kofron MD, El-Amin SF, Attawia MA, Laurencin CT. In vitro bone formation using muscle-derived cells: A new paradigm for bone tissue engineering using polymer-bone morphogenetic protein matrices. *Biochem Biophys Res Commun* 2003; 305:882–889.

18. Cooper JA, Lu HH, Ko FK, Freeman JW, Laurencin CT. Fiber-based tissue-engineered scaffold for ligament replacement: Design considerations and in vitro evaluation. *Biomaterials* 2005; 26:1523–1532
19. Lu HH, Cooper JA, Jr, Manuel S, Freeman JW, Attawia MA, KoFK, Laurencin CT. Anterior cruciate ligament regeneration using braided biodegradable scaffolds: In vitro optimization studies. *Biomaterials* 2005;26:4805–4816.
20. Cooper JA Jr, Bailey LO, Carter JN, Castiglioni CE, Kofron MD, KoFK, Laurencin CT. Evaluation of the anterior cruciate ligament, medial collateral ligament, achilles tendon and patellar tendon as cell sources for tissue-engineered ligament. *Biomaterials* 2006; 27:2747–2754.
21. Cooper JA, Jr, Sahota JS, Gorum WJ II, Carter J, Doty SB, Laurencin CT. Biomimetic tissue-engineered anterior cruciate ligament replacement. *Proc Natl Acad Sci USA* 2007; 104:3049–3054.
22. Kumbar SG, Nukavarapu SP, James R, Nair LS, Laurencin CT. Electrospun poly(lactic acid-co-glycolic acid) scaffolds for skin tissue engineering. *Biomaterials* 2008;29:4100–4107
23. Karalaki M, Fili S, Philippou A, Koutsilieris M. Muscle regeneration: cellular and molecular events. *In Vivo*. 2009 Sep-Oct;23(5):779-96.
24. Laurencin, Cato T., and Lakshmi S. Nair. “The Quest toward Limb Regeneration: A Regenerative Engineering Approach.” *Regenerative Biomaterials* 3.2 (2016): 123–125. *PMC*. Web. 4 Nov. 2017.

25. Yun, Maximina H. “Changes in Regenerative Capacity through Lifespan.” Ed. Francesc Cebrià. *International Journal of Molecular Sciences* 16.10 (2015): 25392–25432. *PMC*. Web. 4 Nov. 2017.
26. Laurencin CT, Kahn Y, Regenerative Engineering,
27. 2010 Panel on the biomaterials grand challenges. *Reichert WM, Ratner BD, Anderson J, Coury A, Hoffman AS, Laurencin CT, Tirrell D J Biomed Mater Res A*. 2011 Feb; 96(2):275-87.
28. The axolotl model for regeneration and aging research: a mini-review. *McCusker C, Gardiner DM Gerontology*. 2011; 57(6):565-71.
29. Towards a functional analysis of limb regeneration. *Gardiner DM, Carlson MR, Roy S Semin Cell Dev Biol*. 1999 Aug; 10(4):385-93.
30. Spalazzi JP¹, Dagher E, Doty SB, Guo XE, Rodeo SA, Lu HH. In vivo evaluation of a multiphased scaffold designed for orthopaedic interface tissue engineering and soft tissue-to-bone integration. *J Biomed Mater Res A*. 2008 Jul;86(1):1-12. doi: 10.1002/jbm.a.32073.
31. Calcium-phosphate matrix with or without TGF- β 3 improves tendon-bone healing after rotator cuff repair. *Kovacevic D, Fox AJ, Bedi A, Ying L, Deng XH, Warren RF, Rodeo SA Am J Sports Med*. 2011 Apr; 39(4):811-9.
32. Kostrominova TY, Calve S, Arruda EM, Larkin LM. Ultrastructure of myotendinous junctions in tendon-skeletal muscle constructs engineered in vitro. *Histol Histopathol*. 2009; 24:541–550.

33. Munoz-Pinto DJ, McMahon RE, Kanzelberger MA, Jimenez-Vergara AC, Grunlan MA, Hahn MS. Inorganic-organic hybrid scaffolds for osteochondral regeneration. *J Biomed Mater Res A*. 2010 Jul;94(1):112-21. doi: 10.1002/jbm.a.32695.
34. Sidney LE, Branch MJ², Dua HS², Hopkinson A Effect of culture medium on propagation and phenotype of corneal stroma-derived stem cells. *Cytotherapy*. 2015 Dec;17(12):1706-22. doi: 10.1016/j.jcyt.2015.08.003. Epub 2015 Oct 9.
35. Gu, Bon Kang et al. “3-Dimensional Bioprinting for Tissue Engineering Applications.” *Biomaterials Research* 20 (2016): 12. *PMC*. Web. 1 Nov. 2017.
36. Velte-Casquillas, Guilhem et al. “Microfluidic Tools for Cell Biological Research.” *Nano today* 5.1 (2010): 28–47. *PMC*. Web. 1 Nov. 2017.
37. <http://blogs.rsc.org/chipsandtips/2006/10/23/rapid-curing-of-pdms-for-microfluidic-applications/>
38. <http://kirschner.med.harvard.edu/files/bionumbers/fundamentalBioNumbersHandout.pdf>
39. Cines, D. B. *et al.* Endothelial cells in physiology and in the pathophysiology of vascular disorders. *Blood* 91, 3527–3561 (1998).
40. Mishra P, Banerjee D, Ben-Baruch A (2011) Chemokines at the crossroads of tumor-fibroblast interactions that promote malignancy. *Journal of leukocyte biology* 89: 31–39. pmid:20628066
41. Hee CK, Jonikas MA, Nicoll SB. Influence of three-dimensional scaffold on the expression of osteogenic differentiation markers by human dermal fibroblasts. *Biomaterials*. 2006 Feb;27(6):875-84. Epub 2005 Aug 15.
42. Yamamoto K¹, Kishida T², Sato Y¹, Nishioka K², Ejima A², Fujiwara H³, Kubo T³, Yamamoto T⁴, Kanamura N⁴, Mazda O⁵ Direct conversion of human fibroblasts into

- functional osteoblasts by defined factors. *Proc Natl Acad Sci U S A*. 2015 May 12;112(19):6152-7. doi: 10.1073/pnas.1420713112. Epub 2015 Apr 27
43. 16. Ieda M, et al. (2010) Direct reprogramming of fibroblasts into functional cardiomyocytes by defined factors. *Cell* 142(3):375–386.
 44. Inagawa K, Ieda M (2013) Direct reprogramming of mouse fibroblasts into cardiac myocytes. *J Cardiovasc Transl Res* 6(1):37–45.
 45. Han DW, et al. (2012) Direct reprogramming of fibroblasts into neural stem cells by defined factors. *Cell Stem Cell* 10(4):465–472.
 46. Kim J, Ambasudhan R, Ding S (2012) Direct lineage reprogramming to neural cells. *Curr Opin Neurobiol* 22(5):778–784.
 47. Thier M, et al. (2012) Direct conversion of fibroblasts into stably expandable neural stem cells. *Cell Stem Cell* 10(4):473–479.
 48. Hiramatsu K, et al. (2011) Generation of hyaline cartilaginous tissue from mouse adult dermal fibroblast culture by defined factors. *J Clin Invest* 121(2):640–657.
 49. Huang P, et al. (2011) Induction of functional hepatocyte-like cells from mouse fibroblasts by defined factors. *Nature* 475(7356):386–389.
 50. Sekiya S, Suzuki A (2011) Direct conversion of mouse fibroblasts to hepatocyte-like cells by defined factors. *Nature* 475(7356):390–393.
 51. Nam YJ, et al. (2013) Reprogramming of human fibroblasts toward a cardiac fate. *Proc Natl Acad Sci USA* 110(14):5588–5593.
 52. Wada R, et al. (2013) Induction of human cardiomyocyte-like cells from fibroblasts by defined factors. *Proc Natl Acad Sci USA* 110(31):12667–12672.

53. Pang ZP, et al. (2011) Induction of human neuronal cells by defined transcription factors. *Nature* 476(7359):220–223.
54. Szabo E, et al. (2010) Direct conversion of human fibroblasts to multilineage blood progenitors. *Nature* 468(7323):521–526.
55. Hee CK, Nicoll SB. Endogenous bone morphogenetic proteins mediate 1 α , 25-dihydroxyvitamin D (3)-induced expression of osteoblast differentiation markers in human dermal fibroblasts. *J Orthop Res.* 2009 Feb;27(2):162-8. doi: 10.1002/jor.20728.
56. Growth Factors and Cytokines in Bone Cell Metabolism Ernesto Canalis, Thomas L. McCarthy, Michael Centrella *Annual Review of Medicine* 1991 42:1, 17-24
57. Molloy T, Wang Y, Murrell G. The roles of growth factors in tendon and ligament healing. *Sports Med.* 2003;33(5):381-94.
58. Clark RA, McCoy GA, Folkvord JM, McPherson JM. TGF-beta 1 stimulates cultured human fibroblasts to proliferate and produce tissue-like fibroplasia: a fibronectin matrix-dependent event. *J Cell Physiol.* 1997 Jan;170(1):69-80.
59. Yu A, Matsuda Y, Takeda A, Uchinuma E, Kuroyanagi Y. Effect of EGF and bFGF on fibroblast proliferation and angiogenic cytokine production from cultured dermal substitutes. *J Biomater Sci Polym Ed.* 2012;23(10):1315-24. doi: 10.1163/092050611X580463. Epub 2012 May 8.
60. Daskalaki, Andriani. *Medical Advancements in Aging and Regenerative Technologies: Clinical Tools.*
61. Kerstin J Rolfe, Alison D Cambrey, Janette Richardson, Laurie M Irvine, Adriaan O Grobbelaar, Claire Linge. Dermal fibroblasts derived from fetal and postnatal

humans exhibit distinct responses to insulin like growth factors. *BMC Developmental Biology* 2007;7:124

CHAPTER 6

FUTURE DIRECTION

6.1. Conclusion and Future work.

The present study demonstrated the feasibility of the integrated graft system to sustain heterogenic cellular interactions for a short period of time. However, future work will focus on increasing the culture duration of the integrated graft system for up to 35 days to facilitate evaluating the production of the tissues-specific extracellular matrix proteins and the expression of cell-specific genes within the distinct phases. In addition, cell localization in every phase as well as cells migration within the different phases will be evaluated through cell tracking experiments by pre-labeling the three different cells. Furthermore, the graft's capability to sustain cell viability, proliferation, and phenotype of the three cell types will be examined for a prolonged period of time. Interaction between ligament fibroblasts and osteoblasts, dermal fibroblasts and osteoblasts, as well as between osteoblasts and both fibroblasts will be evaluated using the appropriate set of experiments in a co-culture and tri-culture environment in order to further understand their capabilities, interactions and biological responses in respect of each other. All the aforementioned experiments will be conducted with or without the presence of growth factor to examine whether the presence of growth factor have a significant impact on sustaining the phenotype of the cells in the heterogenic cellular environment. Lastly, the *in vivo* response to the integrated graft system will be examined after optimizing the optimal *in vitro* condition in order to investigate the potential of skin, ligament and bone to in vivo form simultaneously.